Investigating the genetic basis of sleep using *forward genetics*



Mathilde C. C. Guillaumin

Christ Church
University of Oxford

A thesis submitted for the degree of
Doctor of Philosophy

Trinity 2018

ABSTRACT

The alternation between waking and sleep is regulated by the internal circadian clock and sleep-wake history, and is also influenced by the external environment. Although our understanding of the circadian aspect of sleep regulation has increased, the mechanisms underlying sleep homeostasis are still largely unknown. Independent of the circadian clock, only a limited number of genes have been associated with specific sleep-wake properties. Forward genetics provides an unbiased approach, which seeks to identify genes involved in specific biological processes. This project has focused on the Sleepy6 mouse line which was obtained via a forward genetics sleep screen. This model has a mutation in synaptobrevin 2, which results in a decreased sleep duration. We aimed to further characterise the sleep phenotype of this line, at a molecular and behavioural level, to gain novel insights into the regulation of sleep. Using molecular techniques to evaluate neurotransmitter levels and gene expression, we found no significant differences in the neurotransmitter pathways investigated. Behavioural assays highlighted hyperactivity, with a mild learning deficit. Electrophysiology recordings from the motor (M1) and visual (V1) cortical areas revealed that Sleepy6 homozygous mice have reduced amounts of rapid-eye movement sleep (REMS) and a strong decrease in the amplitude of electroencephalography (EEG) and local field potential (LFP) signals, especially during non-REMS when traces are reminiscent of the burst suppression patterns often observed during anaesthesia, rather than natural sleep. At a local level, neuronal firing in Sleepy6 homozygotes ceased for seconds at a time during non-REMS, coinciding with very low-amplitude EEG and LFP traces. Sleepy6 homozygous mice also displayed a longer latency to switch between vigilance states. Finally, the successful adaption of an elaborated version of the "two-process" model of sleep regulation to recordings performed in mice suggests that sleep pressure decreases at a slower rate in Sleepy6 homozygotes. This result should be interpreted in light of the above findings, as the model relies on power in the slow-wave (0.5-4 Hz) range during non-REMS, which is affected by the very low-amplitude oscillations observed in this state in Sleepy6 homozygotes. This combination of *in vivo* and computational work using the Sleepy6 line provides new insights into the mechanisms that underlie sleep architecture and the alternation between vigilance states. It also has the potential to further our understanding of the mechanisms underpinning the generation of slow-waves and anaesthesia.

TABLE OF CONTENTS

ABSTRACT **1**

ACKNOWLEDGEMENTS **11**

TABLE OF FIGURES **12**

ABBREVIATIONS **16**

CHAPTER 1: General introduction **21**

1. THE REGULATION OF SLEEP **21**

A. THE CIRCADIAN SYSTEM **23**

B. THE HOMEOSTATIC PROCESS **24**

C. CELLULAR & NETWORK MECHANISMS OF SLEEP OSCILLATIONS **27**

D. PROPOSED FUNCTIONS OF SLEEP **30**

E. NEUROANATOMY OF SLEEP/WAKE REGULATION **33**

I. WAKE-PROMOTING PATHWAYS. 35

II. NREM SLEEP PROMOTING PATHWAYS 37

III. REM SLEEP PROMOTING PATHWAYS 38

IV. THE CIRCADIAN REGULATION OF SLEEP AND WAKE 39

V. NON-MAMMALIAN MODELS 41

2. FORWARD GENETICS **43**

3. THE *SLEEPY6* LINE **46**

4. MATHEMATICAL MODELLING: ANOTHER APPROACH TO STUDYING SLEEP/WAKE REGULATION **53**

5. AIMS OF THE PROJECT 55

CHAPTER 2: Molecular analysis 57

1. INTRODUCTION 57

A. SNARE PROTEINS AND NEUROTRANSMITTER SYSTEMS 57

B. *SLEEPY6* MICE, ADHD AND NEUROTRANSMITTER PATHWAYS 59

C. EFFECTS OF NEUROTRANSMITTERS ON SLEEP AND WAKEFULNESS 59

D. HYPOTHESES 61

2. MATERIALS AND METHODS 61

A. *SLEEPY6* GENOTYPING PROTOCOL 61

I. GENOMIC DNA (GDNA) EXTRACTION 61

II. RUNNING OF THE QPCR 62

III. INTERPRETATION OF THE RESULTS 64

B. SETTING UP OF THE HIGH-PERFORMANCE LIQUID CHROMATOGRAPHY (HPLC) 65

I. APPARATUS USED 65

II. MOBILE PHASE 66

III. STANDARDS 67

IV. DISSECTIONS OF BRAIN SAMPLES 67

V. PREPARATION OF BRAIN SAMPLES 68

VI. RUNS ON THE HPLC COLUMN 69

C. RT-QPCR 69

I. RNA EXTRACTIONS 69

II. CDNA SYNTHESIS 70

III. CHOICE OF THE GENES AND PRIMER DESIGN 71

IV. qPCR REACTIONS 72

D. DATA ANALYSIS 75

3. RESULTS 76

A. BREEDING OUTCOMES 76

B. HPLC 76

C. qPCRs 80

4. DISCUSSION 83

A. BEYOND SEROTONERGIC AND DOPAMINERGIC PATHWAYS 83

B. ADENOSINE AS A CORRELATE TO EVALUATE SLEEP NEED IN *SLEEPY6* MICE? 84

C. APPETITE-REGULATING HORMONES AND SLEEP ARCHITECTURE 85

D. A POSSIBLE ALTERATION IN GLIOTRANSMISSION 86

E. LIMITATIONS 86

CHAPTER 3: Behavioural characterisation of *Sleepy6* mice 88

1. INTRODUCTION 88

2. MATERIALS AND METHODS 91

A. ANIMALS AND HOUSING CONDITIONS 91

B. NOVEL OBJECT RECOGNITION TASK 93

C. OBJECT-IN-PLACE RECOGNITION TASK 94

D. VIDEO ANALYSIS 95

E. DATA ANALYSIS 96

F. DISSECTIONS FOR *cFOS* AND *ARC* EXPRESSION MEASUREMENTS 96

G. RNA EXTRACTIONS, cDNA SYNTHESIS AND RTqPCR 97

3. RESULTS 98

A. PILOT COHORT 98

I. NOVEL OBJECT RECOGNITION TASK 98

II. OBJECT-IN-PLACE RECOGNITION TASK 99

B. MAIN EXPERIMENT 100

I. NOVEL-OBJECT RECOGNITION TASK 100

II. OBJECT-IN-PLACE RECOGNITION TASK 101

C. TOTAL TIME OF INTERACTION WITH OBJECTS 103

D. LOCOMOTOR ACTIVITY 104

I. DISTANCE TRAVELLED 104

II. TOTAL TIME OF MOBILITY 106

III. AVERAGE SPEED WHILE MOBILE 106

E. QPCR 107

I. PILOT COHORT 108

II. MAIN EXPERIMENT 109

4. DISCUSSION 111

A. SUMMARY OF FINDINGS 111

B. SNARE PROTEINS, ATTENTION AND ADHD 112

C. LIMITATIONS 114

CHAPTER 4: Electrophysiology recordings in *Sleepy6* mice 116

1. INTRODUCTION 116

2. MATERIALS AND METHODS 119

A. ANIMALS AND HOUSING CONDITIONS. 119

B. EEG AND LAMINAR PROBE IMPLANTATION SURGERIES 120
C. RECORDINGS 124
D. DATA ANALYSIS 124
E. SLEEP DEPRIVATION 126
F. AUDITORY STIMULATION 127
G. PERFUSIONS AND MICRO-LESIONS 127
H. HISTOLOGY 128
I. STATISTICAL ANALYSIS 128

3. RESULTS 128

A. POSITION OF LAMINAR PROBES 128
B. SLEEP ARCHITECTURE IN *SLEEPY6* HOMOZYGOTES AND WT LITTERMATE CONTROLS 129
C. SPECTRAL ANALYSIS ACROSS VIGILANCE STATES AND DERIVATIONS 134
D. REPONSES TO SLEEP DEPRIVATION IN *SLEEPY6* HOMOZYGOUS MICE 138
E. CHANGES IN SIGNALS ACROSS REM SLEEP EPISODES 144
F. RESPONSES TO AUDITORY STIMULATION 147

4. DISCUSSION 150

A. INCREASED SLEEP EFFICIENCY OR CHRONIC SLEEP DEPRIVATION? 150
B. AN IMPAIRMENT IN THE "SLEEP SWITCH"? 151
C. NEURONAL SILENCE AND VESICULAR RELEASE. 152
D. REMS AND BODY TEMPERATURE 154
E. LIMITATIONS 155
F. FURTHER INVESTIGATION OF SLEEP HOMEOSTASIS IN *SLEEPY6* MICE. 155

CHAPTER 5: Computational modelling of sleep-wake regulation in C57BL/6J and *Sleepy6* mice 157

1. INTRODUCTION 157

A. PROCESSES UNDERLYING THE REGULATION OF SLEEP/WAKE ARCHITECTURE 158

B. HISTORY OF THE TWO-PROCESS MODEL OF SLEEP 159

C. CONTRIBUTION OF THE MODEL TO OUR UNDERSTANDING OF SLEEP/WAKE REGULATION. 160

D. INITIAL AIMS OF THE STUDY 162

E. ADAPTING SLEEP MODELLING TO *SLEEPY6* MICE 162

2. MATERIALS AND METHODS 163

A. ANIMALS. 163

I. INITIAL STUDY COHORT 163

II. *SLEEPY6* COHORT 165

B. SURGICAL PROCEDURE 165

C. DATA ACQUISITION AND SIGNAL PROCESSING 165

I. INITIAL COHORT 165

II. *SLEEPY6* COHORT 166

D. SCORING OF VIGILANCE STATES. 166

E. CALCULATION OF EEG SLOW-WAVE ACTIVITY 166

F. SELECTION OF NREMS EPISODES. 168

G. DESCRIPTION OF THE MODEL. 169

H. IMPLEMENTATION OF THE EQUATIONS AND DEFINING PARAMETER VALUES 173

I. OPTIMISATION/ESTIMATION PROCESS OF THE PARAMETERS 176

J. STEP-BY-STEP OPTIMISATION APPROACH. 178

K. CALCULATION OF THE ERROR TO EVALUATE HOW WELL THE MODEL PREDICTS THE DATA. 179

L. STATISTICAL ANALYSIS. 180

3. RESULTS 180

A. RESULTS FROM THE INITIAL STUDY COHORT (WILD-TYPE C57BL/6J MICE) 180

I. SLEEP-WAKE ARCHITECTURE IN THE REGULAR-WHEEL (RW) GROUP. 180

II. ACCURACY OF THE ELABORATED MODEL IN PREDICTING INTRA-EPISODIC DYNAMICS OF SWA. 183

III. REGIONAL DIFFERENCES IN PARAMETER VALUES 186

IV. INFLUENCE OF THE LIGHT PHASE ON THE PERFORMANCE OF THE MODEL. 188

V. IMPACT OF WAKING BEHAVIOUR ON THE PERFORMANCE OF THE MODEL. 190

VI. IMPACT OF WAKING EXPERIENCE ON THE EEG 194

B. RESULTS FROM *SLEEPY6* MICE 201

4. DISCUSSION 206

A. EVALUATION OF THE PERFORMANCE OF THE MODEL IN C57BL/6J MICE. 206

B. DIFFERENCES BETWEEN CORTICAL REGIONS IN THE DYNAMICS OF PROCESS S. 207

C. EFFECT OF LIGHTING CONDITIONS. 208

D. IMPACT OF WAKE EXPERIENCES ON MODEL PREDICTIONS. 209

E. LIMITATIONS OF THE PRESENT MODELLING WORK 210

F. CONCLUSIONS OF THE MODELLING WORK USING C57BL/6J MICE. 211

G. CONCLUSIONS REGARDING THE *SLEEPY6* RESULTS 212

CHAPTER 6: General discussion 214

1. SUMMARY OF THE RESULTS OBTAINED 214

A. MOLECULAR FINDINGS 214

B. DIFFERENCES OCCURRING AT A CELLULAR LEVEL 215

C. LEARNING AND MEMORY IN *SLEEPY6* MICE 216

D. FINDINGS OBTAINED FROM MATHEMATICAL MODELLING 216

2. MODEL PARAMETERS AND SLEEP/WAKE ARCHITECTURE OF THE *SLEEPY6* MICE 217

3. EEG POWER, SLEEP PRESSURE IN *SLEEPY6* AND OTHER MOUSE LINES: WHAT CAN IT TELL US? 218

4. THE *SLEEPY6* MUTATION, SLEEP AND MEMORY. 220

A. EXOCYTOSIS AND COGNITION 220

B. THE ROLES OF NREMS AND REMS IN LEARNING AND MEMORY AND THEIR RELEVANCE TO THE *SLEEPY6* LINE 221

C. SWA AND MEMORY 222

5. AN IMPAIRMENT OF THE SLEEP SWITCH? 223

A. SWITCHING BETWEEN NATURALLY-OCCURRING VIGILANCE STATES 223

B. SWITCHING BETWEEN ANAESTHESIA AND WAKE 227

6. *SLEEPY6* MICE: A GOOD MODEL TO STUDY THE SLEEP HOMEOSTAT? 229

7. LIMITATIONS 231

8. CONCLUSION 232

ANNEXES 234

1. ANNEX 1 – BIOSYNTHESIS AND CATABOLISM PATHWAYS OF SEROTONIN 234

2. ANNEX 2 – BIOSYNTHESIS AND CATABOLISM PATHWAYS OF DOPAMINE 235

REFERENCES 236

ACKNOWLEDGEMENTS

I would like to express my sincere thanks to my supervisors, Prof. Vladyslav Vyazovskiy, Prof. Stuart N. Peirson and Dr Patrick Nolan for their guidance and encouragements. Thank you for allowing me to enter the wonderful world of research, for challenging me and always inspiring me to go further forward! I would also like to thank Prof. David Dupret for reminding me that science is first meant to be enjoyed.

Cristina Blanco Duque, Martin Kahn, Lukas Krone, Laura McKillop, Tomoko Yamagata and Linus Milinski – I wish I could name you all – I cannot thank you enough for your help in the lab (regardless of the time of day), the intellectually challenging discussions, your support and maybe most importantly, for making these past 3 years so enjoyable in many respects. Thank you for making me want to run to the lab every morning! I would never have dared believe that being a doctoral student could prove so fulfilling and exciting.

A very special thanks to Michael C.N. Urbasch and Sarah Leung. I am not sure on which roads I would be walking today without your help. You set me back on the right track, and there are no words to express my gratitude for this. You helped me fight back a long-term illness while continuing my PhD; I didn't even think that would be possible. Ultimately, thank you for reminding me that "the world is my oyster"!

I would like to thank all who helped me for various aspects of my project: Prof. Peter Achermann and Dr Maarten de Vos for your comments and advice on the modelling work; Dr Gareth Banks for your help on the *Sleepy6* molecular work; Prof. Trevor Sharp and Dr Judith Schweimer for allowing me to perform the chromatography experiments within your lab; Prof. David Bannerman and Dr Eric Tam for your advice on the behaviour experiments; Dr Steven Hughes, Dr Jessica Rodgers and Dr Laurence Brown for helping me find my way through the lab in many occasions. A special thanks to Maylis Guillaumin for drawing the *Sleepy6* mouse!

Finally, thank you to those of you, friends and family, who supported me over these past years. Again, I cannot name you all. I wish I was worthier of all your friendships, affection, support and patience.

I dedicate my thesis to my mother, Dr Guyonne Loyer, who passed away shortly after my viva. There are so many things I could thank her for, but importantly, she never failed to believe in my abilities, and she encouraged me to pursue my deepest aspirations.

TABLE OF FIGURES

Figure 1: The two-process model of sleep regulation. 22

Figure 2: Changes in EEG spectra during state transitions 28

Figure 3: The synaptic homeostasis hypothesis 31

Figure 4: Neuronal pathways regulating wake (A), NREM sleep (B) and REM sleep (C) 35

Figure 5: Upstream and downstream pathways of the circadian pacemaker 40

Figure 6: Breeding protocol for detection of recessive mutations 45

Figure 7: Summary of the known phenotypes of Sleepy6 homozygous mice 47

Figure 8: Molecular model of vesicle exocytosis 48

Figure 9: *VAMP2* gene expression levels across various tissues 50

Figure 10: Presence of variants in the human *VAMP2* gene 52

Figure 11: Complementary DNA sequence of the mouse *Vamp2* gene 63

Figure 12: Allelic discrimination plot obtained at the end of the PCR 64

Figure 13: High performance liquid chromatography set up 65

Figure 14: Evaluation of the reliability of housekeeping gene expression 74

Figure 15: Examples of chromatograms 78

Figure 16: HPLC results 79

Figure 17: RT-qPCR results 81

Figure 18: Experimental set up for the novel object recognition 94

Figure 19: Brain section of a WT animal showing the hippocampus. 97

Figure 20: Performance for the novel object recognition task 99

Figure 21: Performance for the object-in-place recognition task 100

Figure 22: Performance for the novel object recognition task (larger cohort) 101

Figure 23: Performance for the object-in-place recognition task (larger cohort) 102

Figure 24: Total time spent interacting with any of the objects 103

Figure 25: Total distance travelled by the mice 105

Figure 26: Total time of mobility of the mice 106

Figure 27: Average speed of the mice (while mobile) 107

Figure 28: Expression of the immediate early genes c-Fos (a, b) and Arc (c, d) 108

Figure 29: Expression of c-Fos (a, b) and Arc (c, d) in the larger cohort 110

Figure 30: Normalised expression of c-Fos (a,b,e,f) and Arc (c,d,g,h) 111

Figure 31: EEG and laminar probe designs. 122

Figure 32: Characteristic frontal and occipital EEG and EMG traces 126

Figure 33: Auditory experiment design 127

Figure 34: Image of a silicon probe implantation site 129

Figure 35: LFP and EMG variances from a baseline day 130

Figure 36: Total time in each vigilance state across 24h 131

Figure 37: Amount of time spent in each vigilance state during the light and dark phases 131

Figure 38: Number of episodes in each vigilance state during the light and dark phases 132

Figure 39: Distribution of NREMS episodes (a) and REMS episodes (b) according to their duration 134

Figure 40: Absolute EEG and LFP spectra in NREM, REM and Wake 135

Figure 41: Sample EEG, LFP and multi-unit activity (MUA) recordings in NREMS 137

Figure 42: Distribution of vigilance states across 24h 139

Figure 43: Slow-wave activity (SWA) levels across 48h and 2h 141

Figure 44: SWA levels during baseline and following sleep deprivation. 142

Figure 45: NREM spectra over the 6h following sleep deprivation 143

Figure 46: REMS LFP, frontal EEG, occipital EEG and EMG traces 144

Figure 47: Evaluation of the evolution of peak frequency across REMS episodes. 145

Figure 48: Evolution of peak frequency across REMS episodes 146

Figure 49: Average spectrum at the transition from NREM to REM sleep 147

Figure 50: Effect of auditory stimulation on vigilance states 148

Figure 51: Power density spectra in WT and Sleepy6 homozygous (HOM) mice in the occipital EEG derivation before, during and after an 8-s sound 149

Figure 52: Examples of a regular wheel (RW) and a complex wheel (CW) 164

Figure 53: Definition of rapid-eye movement sleep (REMS) and wake trigger functions. 172

Figure 54: Illustration of the optimisation process. 176

Figure 55: Distribution of vigilance states and power density spectra. 181

Figure 56: Evaluation of long wake bouts (LWB) durations. 182

Figure 57: EEG SWA levels are shown across 48h (a) and 2h (b) 184

Figure 58: Evaluation of the fit between data and simulations. 185

Figure 59: Parameters values in the occipital and frontal EEG derivation in WT C57BL/6J mice with access to a regular wheel. 187

Figure 60: Parameter values in the regular- and complex-wheel groups 188

Figure 61: Evaluation of the absolute and real values of the error between data and simulations 189

Figure 62: Accuracy of the model's predictions following long wake bouts. 191

Figure 63: Correlations between wake bout durations and predicted & empirical SWA. 194

Figure 64: Impact of long wake bouts on EEG spectra. 195

Figure 65: Wheel-running activity in the normal- and complex-wheel groups. 197

Figure 66: Effect of empirical SWA on the model's predictions. 199

Figure 67: Correlations between time spent running, SWA and model predictions 200

Figure 68: Empirical and simulated EEG SWA levels in WT and Sleepy6 homozygous mice. 202

Figure 69: Evaluating model parameters in WT and Sleepy6 mutant mice 204

Figure 70: Comparison of the values obtained for the parameters gc, rs, S_U in the frontal EEG, occipital EEG and LFP in Sleepy6 wild-types (WT) and homozygotes (HOM) 205

Figure 71: Enlarged hypnogram from a WT (left panel) and a sodium-leak-channel mutant mouse $Nalcn^{Drl/+}$ (right panel) at zeitgeber time 7. 224

Figure 72: Illustration of a hypothetical impairment in the sleep switch 226

ABBREVIATIONS

5-HIAA: 5-hydroxyindoleacetic acid

5-HT: serotonin/serotonergic

ADHD: attention deficit hyperactivity disorder

ALDH: aldehyde dehydrogenase

ARC: activity-regulated cytoskeleton-associated protein

ATP: adenosine triphosphate

BF: basal forebrain

BL: baseline

cDNA: complementary DNA

Ch: cholinergic

CI: confidence interval

COMT: catechol-O-methyltransferase

CW: complex wheel

D: dark

DA: dopamine/dopaminergic

DMH: dorsomedial hypothalamic nucleus

DOPAC: 3,4-dihydroxyphenylacetic acid

DPGi: dorsal paragigantocellular reticular nucleus

DR: dorsal raphe nucleus

Drl: *Dreamless*

EEG: electroencephalogram

EMG: electromyogram

ENU: N-ethyl-N-nitrosourea

EW: exploratory wakefulness

FB: fan-shaped body

fc_R: fall constant of REMT

fc_W: fall constant of WT

Fro: frontal derivation

GABA: gamma-aminobutyric acid

gc: gain constant

gDNA: genomic DNA

GiA: alpha gigantocellular reticular nucleus

GiV: ventral gigantocellular reticular nucleus

Gm: glutamate/glutamatergic

HA: histamine/histaminergic

HOM/Hom: homozygote (generally designating *Sleepy6* homozygous mice)

HPLC: high performance liquid chromatography

HVA: homovanillic acid

IEG: immediate early gene

KO: knock-out

L: light

LC: locus coeruleus

LDT: laterodorsal tegmental nucleus

LED: light-emitting diode

LFP: local field potential

LH: lateral hypothalamus

LPGi: lateral paragigantocellular nucleus

LPT: lateral pontine tegmentum

LTC: light-tight ventilated chamber

LTP: long-term potentiation

LWB: long wake bout

MAO: monoamine oxidase

MnPO: median preoptic nucleus

MUA: multi-unit activity

NA: noradrenaline/noradrenergic

NALCN: sodium leak channel, non-selective

NI: nucleus incertus

NOR: novel object recognition task

NR = NREM(S): non-rapid eye movement (sleep)

Occ: occipital derivation

OIP: object-in-place task

OSA: 1-octanesulphonic acid sodium salt

PB: parabrachial nucleus

PBS: phosphate-buffered saline

PC: precoeruleus area

PCA: perchloric acid

PCR: polymerase chain reaction

PFA: parafomaldehyde

PGO: pons, lateral geniculate nucleus and occipital cortex

PH: posterior hypothalamus

PPT: pedunculopontine tegmental nucleus

qPCR: quantitative polymerase chain reaction

QTL: quantitative trait locus

rc: rise constant

R = REM(S): rapid eye movement (sleep)

REMT: rapid eye movement sleep trigger

RRP: readily-releasable pool

rs: rise rate of Process S

RT-qPCR: reverse transcription quantitative polymerase chain reaction

RW: regular running wheel

S: homeostatic process or 'Process S'

S_0: initial level of Process S

SCN: suprachiasmatic nucleus

SD: sleep deprivation

SEM: standard error of the mean

SERT: serotonin transporter

SHY: synaptic homeostasis hypothesis

Sim: simulation

SLD: sublaterodorsal nucleus

Slp: *Sleepy*

SNAP-25: synaptosome-associated protein of 25 kDa

SNARE: soluble *N*-ethylmaleimide-sensitive factor attachment protein receptor

SPZ: subparaventricular zone

STD: standard deviation

STX1A: Syntaxin 1A

S_U: upper asymptote of Process S

SWA: slow-wave activity

SWA_L: lower asymptote of SWA

SWA_0: initial level of SWA

t_a: advance of REMT

t_{aw}: advance of WT

TDT: Tucker-Davis Technologies (Inc.)

TH: tyrosine hydroxylase

TMD: transmembrane domain

TMN : tuberomammillary nucleus

t_p: prolongation of REMT

TPH: tryptophan hydroxylase

t_{pw}: prolongation of WT

ts: time step (= 4 s)

VAMP2: vesicle-associated membrane protein 2, also known as synaptobrevin 2

vlPAG: ventrolateral periaqueductal grey matter

VLPO: ventro-lateral preoptic nucleus

vPAG: ventral periaqueductal grey matter

W: wake

WT: wake trigger / wild-type

ZT: zeitgeber time (ZT 0 = light onset in a light-dark cycle).

CHAPTER 1: General introduction

1. THE REGULATION OF SLEEP

Life on Earth has evolved under marked environmental oscillations, with dramatic changes in light levels, temperature and food availability between night and day, leading to important consequences for both physiology and behaviour (Rajaratnam and Arendt, 2001). The alternation between periods of rest and activity is one of the most recognised 24h rhythms, also termed circadian rhythm (from the Latin "*circa": around, "diem": day*). The ability to anticipate rhythmic changes in one's environment has generally been acknowledged to provide a selective advantage (Hughes et al., 2015). Unlike diurnal rhythms that are simply driven by the light-dark cycle, circadian rhythms are internally generated and can persist in constant conditions (i.e. in the absence of environmental cues).

As human beings, we spend about a third of our time asleep, which supports the idea that sleep is undoubtedly a major physiological process. Some hypothesise that it originally served one primordial function. Yet, if such a primary function existed, there is still no consensus between scientists on its nature. Thus, sleep remains in many respects an enigma (Krueger et al., 2016). Sleep is tightly regulated, and its occurrence and architecture is mainly determined by two processes: a circadian process, which depends on the internal circadian clock whose master pacemaker is located in the suprachiasmatic nuclei (SCN) in the hypothalamus, and a homeostatic process which reflects prior sleep-wake history (Fisher et al., 2013). The interaction between the circadian and homeostatic processes to regulate sleep propensity and

sleep duration has been formalised in the 'two-process model' of sleep in 1982 (Borbély, 1982), presented in Figure 1.

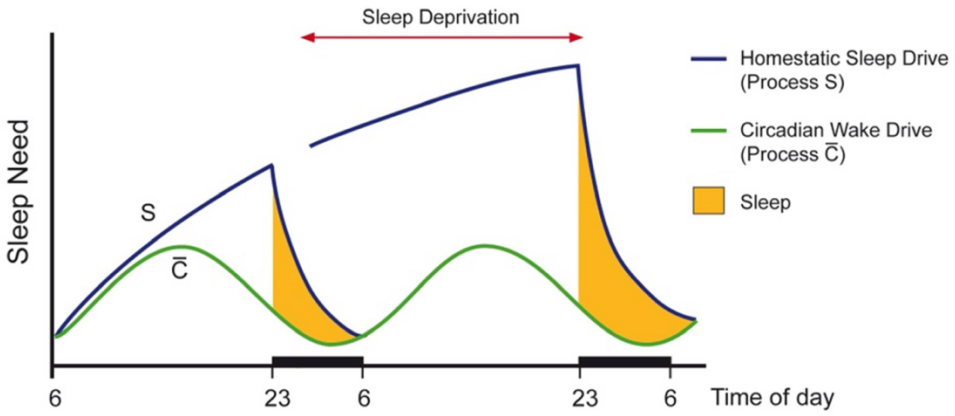


Figure 1: The two-process model of sleep regulation. The model relies on the interaction between the homeostatic and circadian processes to predict sleep propensity and sleep duration. Figure taken from Fisher, Guillaumin & Vyazovskiy (2016a).

The regulation of the alternation between sleep and wake is also influenced by the external environment. Different neurotransmitter systems and neural networks are involved, with intricate connections between sleep-promoting and wake-promoting neuronal populations (Fisher et al., 2013; Tobler, 1995). It has also been argued that the regulation of sleep relies not on two, but three main systems: the homeostatic system necessary for the regulation of sleep duration and intensity, the circadian system regulating sleep/wake timing across the 24-h day, and an ultradian system governing rapid-eye movement sleep (REMS)/non-REMS (NREMS) alternation within sleep (Rosenwasser, 2009).

In humans, a typical night of sleep is structured around 5 NREMS-REMS cycles, with each cycle consisting in an initial descent through NREMS stages (1 to 4) and a rapid ascension to REMS (which is marked by muscle atonia), possibly followed by a brief arousal. Most of us will then

naturally wake up from REMS (Foster and Wulff, 2005; Merica and Fortune, 2004). This sleep/wake architecture varies dramatically across species.

A. The circadian system

Major advances have occurred over the past decades in our understanding of the circadian system. Firstly, evidence has allowed the identification of the master circadian pacemaker in the suprachiasmatic nucleus (SCN) in the anterior hypothalamus (Klein et al., 1991). The SCN innervates several brain regions which are also involved in sleep-wake alternation, such as the ventrolateral preoptic nucleus (VLPO) (Saper et al., 2001) and the median preoptic nucleus (MnPO), which will be described further below. The SCN is composed of numerous clock cells and coordinates the timing of secondary oscillators throughout the body (Reppert and Weaver, 2002). The circadian system is primarily entrained by the light/dark cycle (photoentrainment). At the level of the eye, the entrainment to light relies on retinal photoreceptors: the rods and cones (which also mediate vision), but also photosensitive retinal ganglion cells which express the blue-light sensitive photopigment melanopsin (Foster, 1998; Hankins et al., 2008; Provencio et al., 2000). This photic input is transmitted to the SCN via the retino-hypothalamic tract (RHT) and is used to entrain the SCN clock to local time (Hughes et al., 2015).

The circadian core oscillator includes two main interlocking transcriptional and translational positive/negative feedback loops. In mammals, the central loop consists of the transcription factors CLOCK and BMAL1, which are the positive elements of the circadian loop and which form a heterodimer that drives the transcription of the repressor genes Period (PER 1,2) and Cryptochrome (CRY 1, 2). PER1-2 and CRY1-2 then interact and translocate to the nucleus where they limit their own expression by inhibiting BMAL1-CLOCK transcriptional activity (Curtis et al., 2014; Reppert and Weaver, 2002). Additional steps are added to this basic loop.

For instance, CLOCK and BMAL1 activate the expression of *Rev-Erbα*; the REV-ERBα protein then acts via Rev-Erb/ROR response elements to repress the transcription of *Bmal1* (Preitner et al., 2002). Alongside the genes involved in this core clock machinery, many other clock-controlled genes are involved in the regulation of physiological processes, such as body temperature (Buhr and Takahashi, 2013). Clock genes are expressed in peripheral tissues too, and independent peripheral clocks are present throughout the body, synchronised by the central pacemaker in the SCN via various mechanisms such as metabolic factors or temperature (Buhr and Takahashi, 2013).

The hormone melatonin, which is primarily secreted by the pineal gland during the dark phase of a light/dark cycle, can serve as a biological marker of night time, and its levels can be used to determine the circadian phase (Pandi-Perumal et al., 2006). Circadian signals to the paraventricular nucleus of the hypothalamus have been shown to regulate the daily melatonin rhythm (Scammell et al., 2017).

The processes underlying the generation and regulation of circadian rhythms are increasingly well-understood. Despite these advances, the mechanisms by which the circadian system interacts with the homeostatic process are still largely unknown. The independence of the two processes also remains a matter of controversy.

B. The homeostatic process

The homeostatic process, also termed as Process S, is dependent on preceding sleep-wake history: it increases with time spent awake and decreases during sleep. Sleep propensity, or the "need for sleep", can be quantified by the levels of slow-wave activity (0.5-4Hz, SWA) detected from the electroencephalogram (EEG). In mammals, the primary method used to distinguish vigilance states (wake, NREM sleep, and REM sleep) are EEG recordings visualised alongside

electromyogram recordings (EMG). Wake is defined by a low-amplitude, high-frequency EEG signal along with a high or phasic EMG, while REM sleep is also characterised by a low-amplitude, fast-oscillation EEG signal – with a prevalence of theta waves (5-10 Hz) – but with a very low-amplitude EMG signal (absence of muscle tone). NREM sleep, on the other hand, is characterised by an overall absence of movement and the EEG is dominated by the presence of high-amplitude slow waves (delta waves, 0.5-4Hz), which span across the entire cortical surface (Massimini et al., 2004). In both animals and humans, it has been shown that the levels of EEG SWA are correlated with preceding time spent asleep and awake. Indeed, SWA levels show a global decline during sleep, while at the beginning of a NREMS episode such levels depend on the prior waking bout (Achermann and Borbély, 2003; Borbély et al., 1981; Dijk et al., 1990). 'Local sleep' has also been described, with slow-waves being recorded in specific regions while the animal is behaviourally awake (Vyazovskiy et al., 2011a).

It is important to note that the EEG traits of sleep and wake vary across the animal kingdom, and for example, reptiles show a higher EEG amplitude in wake than in sleep states – opposite to what we observe in mammals; this shows that EEG signature cannot be used as a universal characteristic of sleep (Allada and Siegel, 2008). Although this is still discussed, it is generally acknowledged that REMS does not occur in reptiles and amphibians (Allada and Siegel, 2008; Ayala-Guerrero and Huitrón-Reséndiz, 1991; Flanigan, 1973; Hobson et al., 1968). Additionally, some species (e.g. cetaceans) have the ability to sleep unihemispherically, i.e. sleep one brain hemisphere at a time (Konadhode et al., 2016; Oleksenko et al., 1992).

Although the idea that Process S increases with time spent awake has rarely been challenged overall, various 'refinements' have been proposed. For instance, a recent study suggested that sleep pressure increases mainly during waking dominated by high theta-activity (Vassalli and Franken, 2017). Another study in *Drosophila* has shown that the various populations of wake-promoting neurons have differential effects on sleep pressure build-up, with a cholinergic group

of neurons which would mainly trigger an increase in sleep need, while another octopaminergic group would inhibit it, and a third dopaminergic group would have more ambiguous effects on sleep pressure thus not fulfilling the criteria of sleep homeostasis (Seidner et al., 2015). Interestingly, the authors of this latter study report that activation of neuronal circuits that do contribute to sleep homeostasis also facilitate learning and memory following sleep deprivation (Seidner et al., 2015).

As mentioned above, whether the circadian and homeostatic processes are independent has long been – and is still – debated (Franken and Dijk, 2009). In support of their independence, it has indeed been shown that lesions to the SCN didn't affect the homeostatic regulation of sleep such that, for instance, only the timing but not the total time of a sleep rebound following sleep deprivation is altered (Mistlberger et al., 1983; Tobler et al., 1983). It was shown that the sleep-propensity rhythm peaks shortly after the core body temperature reaches its lowest point within its 24-h rhythm, but that SWA is largely independent from the endogenous circadian phase and depends mainly on sleep/wake history; this means that the circadian rhythm in the propensity to initiate sleep does not vary concomitantly with SWA at sleep onset (Dijk and Czeisler, 1995). On the other hand, REMS and sleep spindles (7-15 Hz) within NREMS are strongly modulated by the endogenous circadian phase (Dijk and Czeisler, 1995). Importantly, REMS is also homeostatically regulated with selective REMS deprivation leading to a rebound in the following sleep bout (Endo et al., 1997; Roffwarg et al., 1966). Yet the fur seal for instance, displays sleep patterns very similar to terrestrial mammals when on land, but when at sea, it shows unihemispheric sleep with reduced REMS time, and no REMS rebound occurs once the animals return to land (Lvamin et al., 1996). However, in most cases, as REMS pressure builds up, SWA during NREMS decreases (Endo et al., 1997). Conversely, SWA has an inhibitory action on REMS, and therefore there seems to be a mutual inhibitory interaction between REMS propensity and SWA (Endo et al., 1997). Finally, it is worth noting that the amount of REMS is

particularly high in neonates and subsequently decreases by about 80% throughout lifetime (as opposed to a 25% decrease in NREMS time) (Roffwarg et al., 1966).

Importantly, inter-individual variability in sleep regulation has been noted (Rusterholz et al., 2010), and it has also been shown that the dynamics of sleep homeostasis and of SWA occur at a local level with regional differences being observed (Rusterholz and Achermann, 2011; Zavada et al., 2009). Finally, several candidate 'sleep homeostat' molecules – of which the levels would reflect the increase and decrease in sleep pressure – have been proposed, such as prostaglandin D2, adenosine, or a molecule similar to an adrenergic alpha2 agonist (Zhang et al., 2015).

C. Cellular & network mechanisms of sleep oscillations

The changes in extracellular field potentials that are observable in EEG recordings reflect the synchronised electrical activity of large numbers of neurons in the cortex (Brown et al., 2012). Various phenomena contribute to the EEG waves: mostly synaptic current from apical dendrites of pyramidal neurons, but also membrane charges and neuronal firing (Buzsáki and Draguhn, 2004). Fast-frequency, low amplitude EEG signals are characteristic of wake and REM sleep, reflecting the synchronisation in the activity of only small areas. Lower frequency rhythms reflect synchronicity over more widespread areas. The various EEG rhythms are thought to reflect higher-order brain functions (e.g. memory, attention), allowing the synchronisation of various cortical and subcortical regions (Brown et al., 2012; Buzsáki and Draguhn, 2004). Each vigilance state displays characteristic EEG features, as shown in Figure 2.

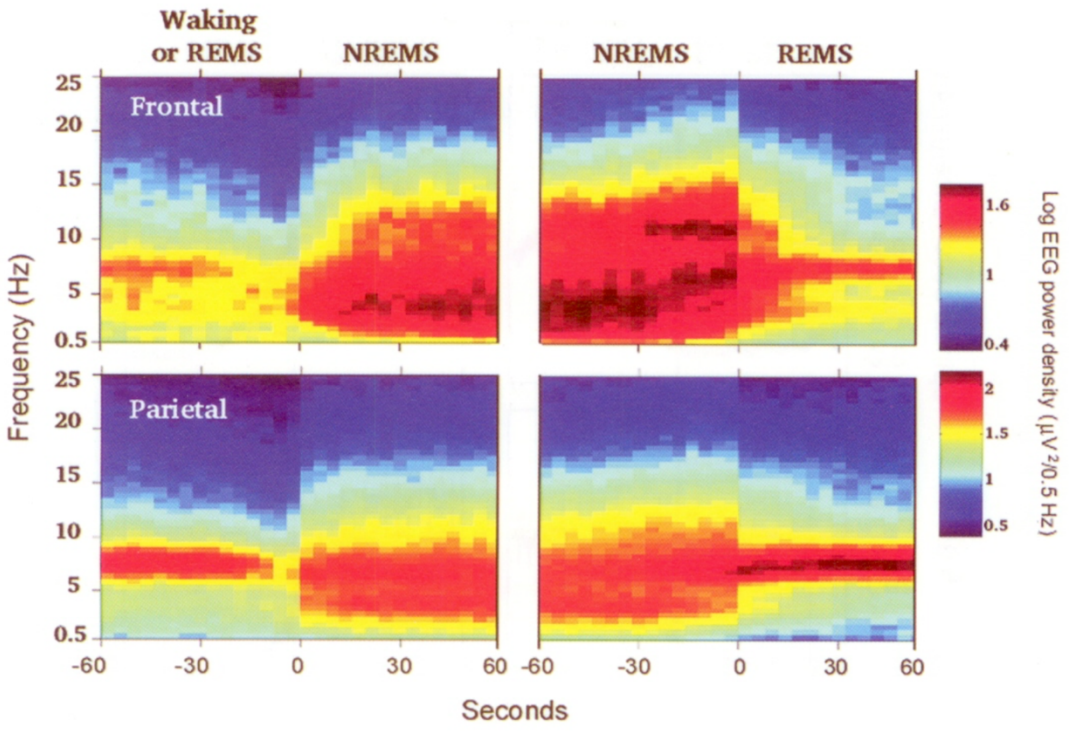


Figure 2: Changes in EEG spectra during state transitions from waking/REM sleep (REMS) to NREM sleep (NREMS) and from NREMS to REMS, in the frontal and parietal derivations during baseline conditions. EEG recordings were performed in mice. Figure taken from (Vyazovskiy et al., 2004) .

- **Wakefulness**. The EEG during quiet waking is marked by low-amplitude gamma (30-120 Hz) and beta (15-30 Hz) oscillations. Gamma rhythms have been shown to generate in the neocortex, although subcortical inputs play a role, and networks of fast-spiking gamma-aminobutyric acid (GABA)-ergic interneurons within the cortex, projecting to glutamatergic neurons, are believed to be at the basis of gamma rhythm generation (Brown et al., 2012). Beta oscillations are alternatively considered slow gamma oscillations, subharmonics of gamma waves, or an altogether distinct phenomenon (Kopell et al., 2000). Alpha rhythms (8-14 Hz) are often observed during quiet wakefulness, in particular in occipital and parietal cortical regions, and stem from interactions between neuronal networks in the thalamus, neocortex and brain stem (Hughes and Crunelli, 2005). Theta rhythms (5-10 Hz) are mainly observed during active waking, and during REM sleep; they have been shown to play a role in spatial

navigation and episodic memory formation, while also facilitating synaptic plasticity, possibly by their impact on pyramidal cell firing (Buzsáki and Draguhn, 2004).

- **NREM sleep**. When transitioning to NREM sleep, the EEG displays large amplitude slow waves, due to the reduced firing of neurons within the ascending reticular activating system. A very slow cortical oscillation (0.5-1 Hz), described as a travelling wave from prefrontal to posterior cortical areas, was characterised by Steriade et al. and has been shown to allow the synchronisation of cortical and thalamic neuronal activity, leading to the occurrence of delta rhythms (0.5-4 Hz) and spindles (7-15 Hz) (Brown et al., 2012; Massimini et al., 2004; Steriade, 2006). Delta oscillations result from a decrease in excitatory inputs leading to hyperpolarisation of thalamic pyramidal cells, and to firing bursts occurring at 1-4 Hz, with silent periods in between the bursts (Brown et al., 2012). Spindles are thought to be generated in the thalamic GABAergic reticular and perigeniculate nuclei (Fuentealba and Steriade, 2005; Steriade and McCarley, 2005). In humans, spindles mainly occur during stage 2 of NREM sleep and decline in deeper sleep states (Brown et al., 2012). Finally, sharp-wave ripple complexes (100-400 Hz) can be recorded in the hippocampus during both NREM sleep and quiet wakefulness (Brown et al., 2012) and have been associated with memory replay and consolidation (Girardeau et al., 2009; Roumis and Frank, 2015).
- **REM sleep**. Theta waves are a characteristic feature of REM sleep, and reflect synchronous oscillations occurring in membrane currents of local dendrites and synapses (Buzsáki, 2002; Robinson et al., 1977). It has been proposed that hippocampal theta rhythms are generated via rhythmic inputs coming from the medial septum and other regions (Buzsáki, 2002; Shirvalkar and Bahar, 2009), and that theta waves observed during REM sleep are generated by distinct mechanisms to those occurring during waking (Tafti et al., 2003). In addition to theta waves, synchronised electrical

field potentials in the pons, lateral geniculate nucleus and occipital cortex (PGO) occur either as low-amplitude bursts during REM episodes, or as high-amplitude single events immediately preceding REM. Those PGO events have been proposed as being the source of dreaming episodes (Steriade and McCarley, 2005).

D. Proposed functions of sleep

An interesting and usually widely-accepted hypothesis is that sleep originally served one primordial function and that additional 'opportunistic' mechanisms were added during later evolutionary stages, such that sleep now serves many functions (Krueger et al., 2016). Although, as mentioned above, there is no consensus on what the initial 'primordial' function of sleep is, many roles have been proposed (Krueger et al., 2016). These functions include:

- **Connectivity** (Krueger, 2010). Slow-wave sleep would provide an optimal state for memory consolidation (Rasch and Born, 2013), while also facilitating processes necessary for sustained attention during wakefulness (Kirszenblat and van Swinderen, 2015). Various hypotheses exist on how this could occur. One of them is the synaptic homeostasis hypothesis (SHY) (Tononi and Cirelli, 2003); its authors propose that 'sleep is the price the brain pays for plasticity', whereby there would be selective synaptic downscaling during sleep – with only the most relevant circuits surviving and being strengthened – and an increase in net synaptic strength during waking (Tononi and Cirelli, 2014, 2016) – see Figure 3. This would allow us to consolidate already formed memories while we are asleep while disposing of 'noise', and allow the brain to learn and form new memories during the next waking episode (Tononi and Cirelli, 2016). In essence, sleep would allow an increase in signal-to-noise ratios via selective synaptic down-selection, thus enabling memory consolidation (Tononi and Cirelli, 2016).

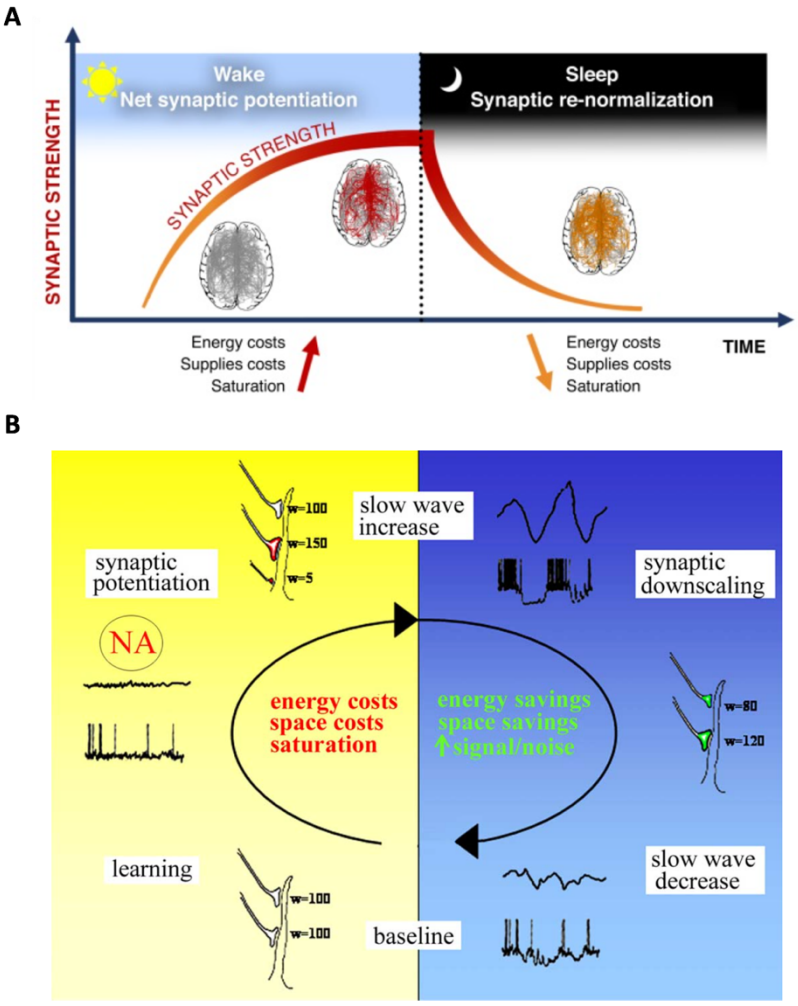


Figure 3: The synaptic homeostasis hypothesis. ***A)*** *Illustration of the increase in synaptic strength proposed during wake and the subsequent synaptic renormalization occurring during sleep.* ***B)*** *During waking new synapses form and older synapses are strengthened while a subject interacts with his environment, learns and forms new memories. During subsequent sleep, non-essential synapses are removed or weakened and the 'fittest' ones are strengthened. Panel A taken from Cirelli (2017) and panel B taken from Tononi & Cirelli (2006). NA: noradrenaline; the authors propose that high levels of noradrenaline facilitate information storage.*

Alternative hypotheses have been proposed, with studies arguing that there is synaptic strengthening while we are asleep which accounts for the cognitive benefits of sleep (Puentes-Mestril and Aton, 2017). Importantly, the role of sleep in memory consolidation has been shown to be conserved across distant species, from humans to invertebrates, such as honeybees (Zwaka et al., 2015).

- **Immune function**. This assumption is based on the increased need for sleep during various illnesses and infectious diseases (Toth et al., 1993). A more recent study highlighted the reciprocal relationship between sleep and immunity and suggested that, among other processes, sleep could influence immune function via the production of cytokines that occur during sleep (Bryant et al., 2004). That sleep serves an immune function is therefore backed by compelling evidence, but it would not explain, however, why loss of responsiveness to the environment is necessary during sleep – which suggests that the immune function of sleep was not its initial role.
- **Energy conservation**. A reduction in caloric use would enable the body to replenish its energy stores, which are substantially lowered during waking. Here as well, such a function does not account for the loss of responsiveness observed during sleep. Additionally, the calorie savings allowed by falling asleep are relatively small, with sleep deprivation (5 h of sleep per night over 5 days) increasing energy expenditure by only around 5%, representing about 110 kCal (Markwald et al., 2013).
- **Restoration of brain energy metabolism**. This idea that NREMS would be essential to replenish cerebral glycogen stores depleted during wakefulness was presented in 1995 (Benington and Heller, 1995). It is supported by positron emission tomography showing a reduced glucose consumption by the brain during NREMS, while the consumption in REMS is similar to, or above, that in wake (Buchsbaum et al., 1989). This 'energy hypothesis' of sleep has since been re-evaluated, and although some of its original predictions have been shown to be too simplistic, the evidence overall supports the fact that wakefulness does indeed represent an energetic challenge for the brain (Scharf et al., 2008).
- **Glymphatic function**. An increase in connective flow from the brain to the general circulation during sleep has been proposed to enable the "wash-out" of

neurotransmitters (that escaped reuptake), toxins and other by-products of brain activity generated during wakefulness (Cantor, 2015; Xie et al., 2013a). A 60% increase in cortical interstitial space during sleep was reported, allowing an efficient convective clearance (Xie et al., 2013a). However, the 'glymphatic pathway' remains controversial, both in terms of mechanisms involved and the role of the glia itself in waste clearance (Bacyinski et al., 2017). Some more recent studies have proposed a revised concept, with a perivascular fluid system that would also allow waste clearance, while better taking into account cerebrovascular physiology (Abbott et al., 2018).

Although more functions have been proposed, the few described here emphasize the fact that sleep is now vital for various body functions (Vassalli and Dijk, 2009) and disrupted sleep will therefore impact health in many ways (metabolic disorders such as obesity, immune defence dysfunction, cognitive impairment, compromised mental health, increased risk of cancer etc.) (Foster and Wulff, 2005; Krueger et al., 2016).

E. Neuroanatomy of sleep/wake regulation

Although much is yet to be discovered, the neuronal circuits that may play a role in sleep/wake regulation have been extensively studied. Functions related to the sleep homeostat have been traditionally associated with circuits within the preoptic area, while circadian functions have been linked to the anterior hypothalamus and ultradian NREMS/REMS alternations have been proposed to rely on rostral brainstem systems (Rosenwasser, 2009).

Others have however proposed that the hypothalamus contains the sleep homeostat, with candidate populations of sleep-active neurons in the anterior hypothalamus and wake-active neurons in the posterior lateral hypothalamus (Qiu et al., 2015). These different pathways are therefore further described here.

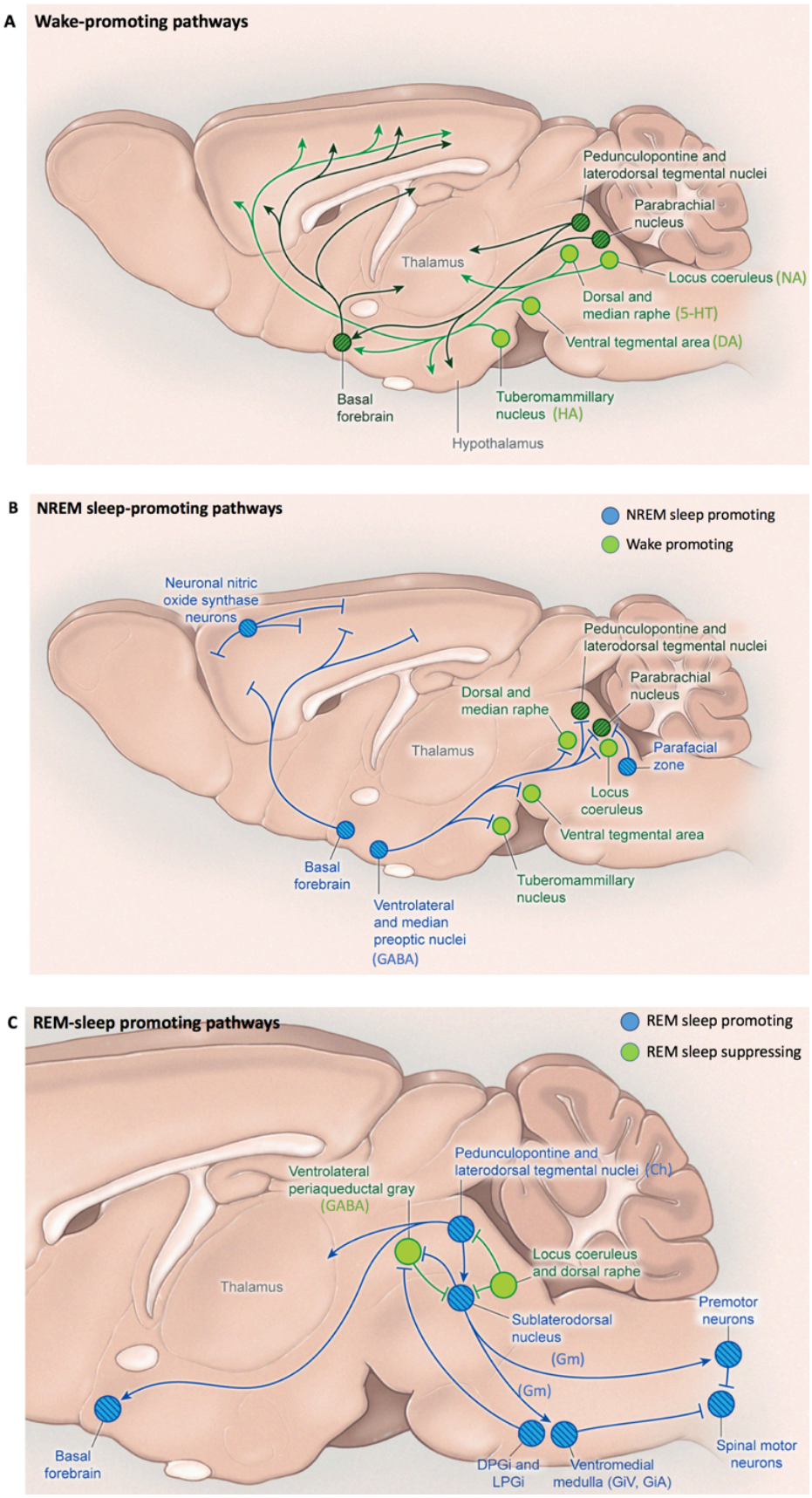

A Wake-promoting pathways
Pedunculopontine and laterodorsal tegmental nuclei
Parabrachial nucleus
Thalamus
Locus coeruleus (NA)
Dorsal and median raphe (5-HT)
Ventral tegmental area (DA)
Basal forebrain
Tuberomammillary nucleus (HA)
Hypothalamus
B NREM sleep-promoting pathways
NREM sleep promoting
Wake promoting
Neuronal nitric oxide synthase neurons
Pedunculopontine and laterodorsal tegmental nuclei
Parabrachial nucleus
Dorsal and median raphe
Thalamus
Parafacial zone
Locus coeruleus
Ventral tegmental area
Basal forebrain
Tuberomammillary nucleus
Ventrolateral and median preoptic nuclei (GABA)
C REM-sleep promoting pathways
REM sleep promoting
REM sleep suppressing
Ventrolateral periaqueductal gray (GABA)
Pedunculopontine and laterodorsal tegmental nuclei (Ch)
Locus coeruleus and dorsal raphe
Thalamus
Sublaterodorsal nucleus
Premotor neurons
(Gm)
(Gm)
Basal forebrain
Spinal motor neurons
DPGi and LPGi
Ventromedial medulla (GiV, GiA)

Figure 4: Neuronal pathways regulating wake (A), NREM sleep (B) and REM sleep (C). ***A)*** *Monoaminergic neurons (shown in light green) in the rostral brainstem and caudal hypothalamus send projections to the cortex, hypothalamus and thalamus. The parabrachial nucleus, pedunculopontine and laterodorsal tegmental nuclei and basal forebrain (all shown in dark green with hatching) have also been shown to be wake-promoting regions.* ***B)*** *Neurons in the ventrolateral preoptic area and median preoptic nucleus exert a sleep-promoting effect by inhibiting wake-promoting neurons in the caudal hypothalamus and brainstem. The basal forebrain also contains sleep-active neurons that project to the cortex. It was also proposed that GABAergic neurons of the parafacial zone promote sleep through their inhibiting action on the parabrachial nucleus. The cortex also contains NREM sleep-active neurons such as the neuronal nitric oxide synthase neurons.* ***C)*** *The sublaterodorsal nucleus (SLD) projects to the ventromedial medulla and spinal cord, which then hyperpolarize motor neurons, thus playing a major role in the muscle atonia observed during REM sleep. The pedunculopontine and laterodorsal tegmental nuclei are also REM sleep promoting. The SLD is the target of inhibitory projections that are active during wake and NREM sleep. The SLD may in return inhibit the ventrolateral periaqueductal grey area during REM sleep. Ch: cholinergic neurons, DA: dopaminergic, DPGi: dorsal paragigantocellular reticular nucleus GABA: GABAergic, GiV: ventral gigantocellular reticular nucleus, GiA: alpha gigantocellular reticular nucleus, Gm: glutamatergic, HA: histaminergic, LPGi: lateral paragigantocellular nucleus, NA: noradrenergic neurons, 5-HT: serotonergic neurons. Figure and legends adapted from Scammell et al. (2017).*

i. Wake-promoting pathways.

The pathways which have been found to promote wakefulness include ascending connections through the paramedian region of the midbrain which then separate between the dorsal pathway toward the thalamus, and an extensive ventral pathway that innervates all the way to the cortex via the hypothalamus and basal forebrain (Figure 4 A). Although Figure 4 A presents the arousal pathways as an ensemble of discrete nuclei and brain entities, it is important to note that they have many inter-connections and similar target regions (Scammell et al., 2017). One of the wake-promoting regions is the locus coeruleus which is essential for high levels of arousal in situations of stress or in the presence of salient stimuli (Scammell et al., 2017). Serotonergic neurons in the median raphe nuclei are also wake promoting, and photoactivation of 5-HT neurons has been shown to double the amount of wake while fragmenting NREM sleep (Ito et al., 2013). The basal forebrain (BF) also plays an essential role in promoting arousal and appears necessary for cortical activation; however its role varies depending on the type of neurons considered, with BF cholinergic neurons promoting fast cortical activity – but it is not entirely certain how essential for wakefulness these neurons are – while GABAergic BF neurons increase

wake when activated (Scammell et al., 2017). The parabrachial nucleus also appears essential for regulating arousal and plays an important role in relaying sensory signals to the forebrain (Fuller et al., 2011).

There is also evidence of a wake-promoting role for histamine, and that tuberomammillary nucleus (TMN) histaminergic neurons are inhibited by inputs from the ventrolateral preoptic nucleus (VLPO), which is known to promote sleep, while their activation leads to arousal and hyperactivity (Ma et al., 2018). Relaxin-3, a neuropeptide recently discovered (Bathgate et al., 2002), is synthesised in regions of the midbrain and pons, among which the nucleus incertus (NI) (Ma et al., 2018). It was recently shown that activation of NI neurons increased wakefulness and locomotion during the natural active phase, with NI GABA and relaxin-3 signalling likely playing a role in NI-mediated effects on arousal (Ma et al., 2017).

Finally, orexin neurons, which play a role in various systems, including reward, energy homeostasis, stress and emotions, also play an essential part in wake promotion (Inutsuka and Yamanaka, 2013). A large body of evidence supports the role of orexin neurons in stabilising waking and sleep states, with orexin signalling – rather than other co-transmitters – being crucial for this behavioural-state stabilisation (Ma et al., 2018). Loss of orexin peptides or receptors in mice leads to narcolepsy-like traits, and a null-mutation of the orexin-2 receptor gene leads to inheritable narcolepsy in dogs (Lin et al., 1999; Ma et al., 2018). Orexin neurons excite all the wake-promoting brain regions described above and shown in Figure 4 A (Scammell et al., 2017). Their stimulation increases the probability for mice to transition from a sleep state to wakefulness (Adamantidis et al., 2007), and activates downstream wake-promoting regions (Carter et al., 2009). Conversely, inhibition of orexin neurons favours NREM sleep (Tsunematsu et al., 2011). Finally, loss of orexin function has been linked to narcolepsy (Chemelli et al., 1999; Peyron et al., 2000; Thannickal et al., 2000). It was proposed that the orexin/glutamate system

receives negative feedback from wake-promoting areas, allowing them to play their role in the regulation of arousal and wakefulness (Schöne and Burdakov, 2017).

ii. NREM sleep promoting pathways

Essential populations of NREM sleep-active neurons have been identified in the VLPO (Sherin et al., 1996) and median preoptic nucleus (MnPO) of the hypothalamus (Gong et al., 2004); they exert GABA-mediated and galaninergic inhibitory control over arousal-promoting cell groups (Szymusiak and McGinty, 2008) – see Figure 4 B. The VLPO and MnPO have been extensively studied as candidate NREM sleep-promoting regions, however the precise neuronal populations underlying this function is not entirely understood (Scammell et al., 2017). Given that the VLPO contains a population of neurons excited by adenosine, and another population that does not respond to it, it was suggested that the adenosine-responsive neurons play a role in the homeostatic response to sleep pressure, while the non-responsive neurons would play a role in sleep consolidation once a sleep episode has been initiated (Gallopin et al., 2005). It has also been proposed that VLPO and MnPO neurons mediate the homeostatic response observed following sleep restriction, although the fact that these neuronal populations increase firing in response to sleep pressure cannot be considered sufficient evidence to prove that they drive the sleep homeostat as such (Qiu et al., 2015).

Sleep-active neurons have been identified in the basal forebrain (Hassani et al., 2009a), and may exert their sleep-promoting action by inhibiting the wake-promoting neurons also present in the basal forebrain (Xu et al., 2015). Sleep-active neurons have also been found in the cortex, where the numbers of active cells from a neuronal nitric oxide synthase-producing subpopulation of GABAergic interneurons during sleep has been shown to be proportional to sleep intensity (Gerashchenko et al., 2008). Finally, given that the VLPO sends inhibitory

projections to many wake-promoting regions in the brain, and conversely receives inhibitory projections from many of these regions, it was proposed that this mutual inhibition constitute a 'sleep switch' (Saper et al., 2010). It was shown that natural sleep induces changes in high-frequency oscillations (measurements from local field potentials) in the first 10 to 20 s of NREM sleep, before delta power builds up; those changes can be detected in the thalamus before they occur in the neocortex (Baker et al., 2014). Once delta oscillations are established during a NREM sleep episode, the authors went on to show that there is a 90° phase advance in the thalamic nuclei compared to neocortical regions. This supports the idea that the central medial thalamus is a "control switch" or hub that regulates cortical arousal and sleep (Baker et al., 2014; Glenn and Steriade, 1982; Picchioni et al., 2014).

iii. REM sleep promoting pathways

Pedunculopontine and laterdorsal tegmental nuclei neurons in the pons have traditionally been considered essential for REM sleep generation, but a shift has occurred recently, with these regions now no longer considered central elements of REM sleep regulation, but only modulators (Scammell et al., 2017). Indeed, the sublaterodorsal nucleus (SLD), another region of the pons, has been identified as central to obtain muscle atonia during REM sleep (alongside neurons in the ventromedial medulla (Luppi et al., 2012)), as well as being crucial – via its links with nearby regions – in generating REM sleep (Scammell et al., 2017). It has also been shown that during wakefulness, GABAergic and glycinergic interneurons located in the brainstem and spinal cord receive inhibiting inputs from the locus coeruleus, and that this inhibition ceases during REM sleep, allowing the muscle atonia associated with this state (McGregor and Siegel, 2010).

However, the pons has also been reported to contain REM sleep-suppressing neuronal populations, including monoaminergic neurons in the locus coeruleus and the dorsal raphe nuclei, as well as in the ventrolateral periaqueductal grey matter (vlPAG) and the lateral pontine tegmentum (LPT) – as shown in Figure 4 C. It was then proposed that mutual inhibition between the vlPAG/LPT and SLD would form the basis of a 'REM sleep switch' (Lu et al., 2006). Additionally, regions in the preoptic area and LH and PH may help generate and regulate REM sleep (Hassani et al., 2009b; Lu et al., 2002).

Regarding transitions to and from REM sleep more specifically, it was proposed that these are regulated by an interaction between cholinergic 'REM-on' neurons and aminergic 'REM-off' neurons, both located in the brainstem (Merica and Fortune, 2004). Given that transitions directly from wakefulness to REMS do not usually occur in healthy individuals, it has been proposed that REMS-promoting neurons are strongly inhibited during wake (Hayashi et al., 2015). Interestingly, it was also proposed that the cells regulating REMS/NREMS transitions may have emerged form populations initially regulating sleep/wake cycles (Hayashi et al., 2015).

iv. The circadian regulation of sleep and wake

The circadian system is known to synchronise the sleep/wake cycle with the light-dark cycle, to which it is entrained by mechanisms described earlier (see 1.A). The SCN is composed of two neuronal populations, which form the ventrolateral 'core' and dorsomedial 'shell', and which are neurochemically distinct (Bedont and Blackshaw, 2015). The fact that the SCN is able to sustain circadian oscillations in the absence of external cues is still an area of investigation, but the communication between the core and shell neurons has been shown to be crucial for network synchrony (Buhr et al., 2010). The inter-relationship between membrane electrical

activity, intracellular signalling cascades and transcriptional/translational regulation in the nucleus also play a crucial role in the circadian timing system and to drive rhythmic firing patterns in the SCN (Colwell, 2011). The mechanisms and pathways through which the SCN promotes wake at different times of day is not fully understood, but the SCN heavily projects to the subparaventricular zone (SPZ), and also moderately projects to the paraventricular nucleus, dorsomedial hypothalamic nucleus (DMH), ventromedial nucleus, lateral hypothalamus (LH) and medial preoptic area (Brown and Piggins, 2007; Scammell et al., 2017) – see Figure 5.

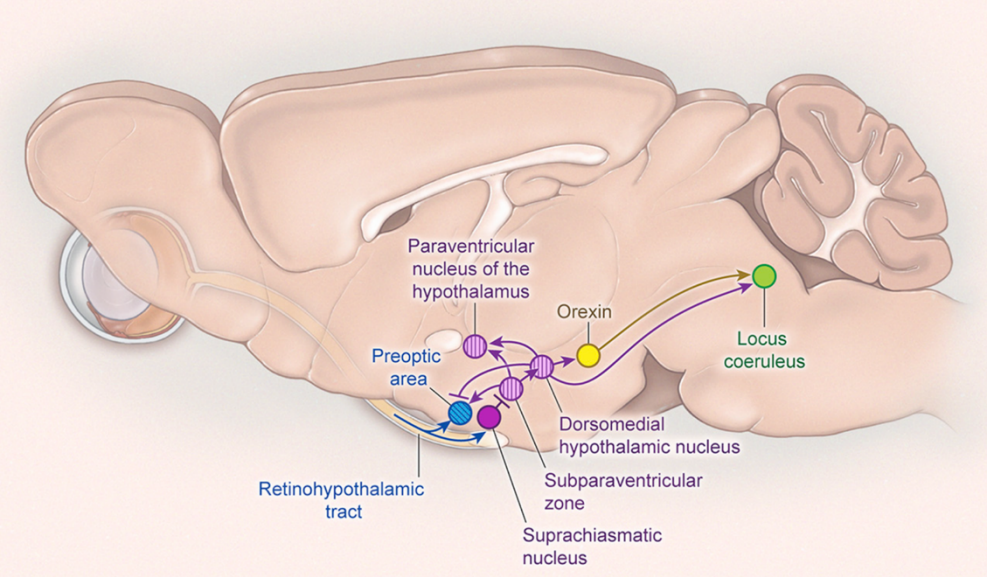


Figure 5: Upstream and downstream pathways of the circadian pacemaker in the suprachiasmatic nucleus (SCN). The SCN can entrain to the light/dark cycle by direct inputs from the eye via the retinohypothalamic tract. The SCN mainly projects to the subparaventricular zone that relays SCN signals to other nuclei which receive only limited direct projections from the SCN. The dorsomedial hypothalamic nucleus regulates wakefulness by sending excitatory projection to orexin cells in the lateral hypothalamic area and to the wake-promoting locus coeruleus, while sending inhibitory projections to the sleep-promoting preoptic area. Figure taken from Scammell et al. (2017).

The SPZ has been proposed as a candidate area for the circadian regulation of endocrine function, sleep/wake rhythms (promoting arousal during the active phase and sleep during the rest phase) and possibly REMS variations; it was suggested that not only does it relay SCN signals to other areas of the body, but it could also serve as an integrator of non-SCN circadian inputs (Vujovic et al., 2015). In particular, the ventral SPZ projects to the DMH, via which it may

play a role in sleep/wake regulation (Chou et al., 2003). It has been suggested that the DMH alternatively promotes wake and sleep at adequate times according to the circadian signals it integrates, and via its excitatory projections to orexin neurons and the locus coeruleus and inhibitory projections to the preoptic area (Scammell et al., 2017). A study showed that a local clock in mouse histaminergic neurons in the TMN played a role in the regulation of the sleep-wake cycle (Yu et al., 2014). Those neurons are silent during sleep periods and become active following wake onset. Deleting the clock gene *Bmal1* in those cells did not impact circadian rhythms (assessed by wheel-running) but led to an increased sleep fragmentation, a decrease in SWA in NREMS sleep, more numerous NREM-to-REM transitions, altered recovery following sleep deprivation. The authors propose that these effects are mediated by a BMAL1-dependent suppression of histaminergic tone during the day that allows timely occurrence of sleep and waking episodes (Yu et al., 2014). This illustrated how the circadian and homeostatic processes are interlinked at many levels. Finally, sleep centres have been shown to feedback on the circadian pacemaker in the SCN, showing further links between the homeostatic and circadian aspects of sleep regulation (Colwell and Michel, 2003).

v. Non-mammalian models

Studies in flies have highlighted a glutamatergic wake-promoting and a cholinergic sleep-promoting microcircuits (located in the fly brain's mushroom body) involved in sleep regulation: the activity of these circuits is altered by sleep deprivation, and their signalling to downstream targets is essential for the occurrence of rebound sleep following extended wake (Sitaraman et al., 2015).

Other studies in flies have also reported the existence of sleep-promoting neurons which would serve as the effector arm of the sleep homeostat (Donlea et al., 2014). These neurons project to

the dorsal fan-shaped body (FB) of the fly brain, and molecular processes occurring in this population of neurons would allow sleep pressure to be transduced into increased sleep via the increased electrical membrane excitability of dorsal FB neurons. The authors of the study suggested that given that the generation of spikes is a threshold process, even a minimal increase in membrane excitability could be sufficient to make an effective on/off sleep switch. This increased excitability would be limited to a small population of neurons and thus not contradict the general "down" state of reduced neuronal activity that usually accompanies NREMS (Donlea et al., 2014). The same authors went on to show that state transitions from sleep to wake could occur via switching the sleep–promoting dorsal FB neurons from an active to a quiescent state, with dopamine being the neuromodulator operating the switch (Pimentel et al., 2016).

This summary illustrates that given the number of brain areas involved in sleep/wake regulation, as well as the number of neurotransmitters which also play a role, sleep abnormalities are a frequent comorbidity of psychiatric disorders and neurodegenerative disorder and improving sleep can reduce the symptoms of such diseases (Wulff et al., 2010).

Finally, as illustrated above, more and more is known regarding the neuroanatomy of sleep/wake regulation, however, at a molecular level, although much is known about the mechanisms underlying the circadian clock (see 1.A), much less is known about the specific genes and molecular mechanisms underlying the homeostatic regulation of sleep. It is generally acknowledged that sleep mechanisms are polygenic in nature, but specific genes involved remain poorly described (Tafti and Franken, 2002). A forward genetics approach may therefore provide additional insights in pathways involved in the homeostatic aspect of sleep regulation that may not have been suspected before.

2. FORWARD GENETICS

There are two primary approaches to try and understand the relationship between genes and behaviours or traits: *reverse genetics* and *forward genetics*. Reverse genetics start from a given gene of interest, and aim to understand the effects on phenotype of modifications in this gene. Forward genetics, on the other hand, is a phenotype-driven approach and can be performed in two main ways: either by quantitative trait locus (QTL) analysis, or by mutagenesis screens. In the latter methodology, random mutations are induced and animals are screened for particular phenotypes – without *a priori* knowledge on the gene involved in the phenotypic alterations observed (the underlying mutation is only subsequently identified) (Acevedo-Arozena et al., 2008). The forward-genetics approach is therefore non-biased as no initial assumptions are made on genes that could be involved in a particular phenotype (Justice et al., 1999) – in our case, sleep. New pathways that may never have been suspected to play a role may therefore be identified. For this reason, forward genetics provides a powerful tool.

Although, large-scale phenotypic screens in the mouse have been limited by space and financial constraints, those difficulties have been reduced thanks to the use of the chemical mutagen N-ethyl-N-nitrosourea, also known as ENU, and the combination of systematic screening protocols with automated technologies (Nolan et al., 2002). This technique led to the development of various mouse mutants with different phenotypes of interest, with some lines specifically displaying abnormal sleep.

ENU is generally administered intraperitoneally in adult male mice. It acts by transferring ethyl groups to some nucleophilic nitrogen or oxygen sites present on each of the deoxyribonucleotides, resulting in mispairing and base-pair substitution and leading to point mutations during DNA replication if not repaired, which are inheritable if occurring in sperm cells (Justice et al., 1999). In most cases a nucleotide substitution is observed and in some rare

cases, point or small deletions occur; these mutations mostly happen at A-T base pairs. A minimum dose of ENU is necessary, below which ENU treatment is ineffectual as cell DNA repair mechanisms are still able to cope with the number of mutations induced (Favor, 1998). Reversely, too high a dose results in impairments in fertility and general health, resulting in reduced chances for animals to pass on the mutations to the next generation (Acevedo-Arozena et al., 2008).

Two points are important to note:

- the probability that a given gene will be mutated is directly linked to the gene size, with larger genes having therefore higher chances of being mutated with an ENU protocol. As an example, it was estimated that the mutation rate is around 1 in 1.01 million base pairs (MBp) with functional mutations being slightly less frequent (1 in 1.82 MBp) (Quwailid et al., 2004).
- a first-generation individual mouse is estimated to contain around 30 to 50 potential functional mutations. Therefore, residual non-specific mutations may remain for a few generations; this can be a confounding factor as it cannot be entirely excluded that when a given mutation is identified, another mutation in a mouse's genome – not yet identified – may also contribute to the altered phenotype observed. However, this is generally considered a low risk as the mutation load is approximately halved with every next generation (Acevedo-Arozena et al., 2008).

The successive crosses necessary to detect recessive mutations are illustrated in Figure 6. Dominant mutations are much less frequent, but present the advantage to require only the generation G1.

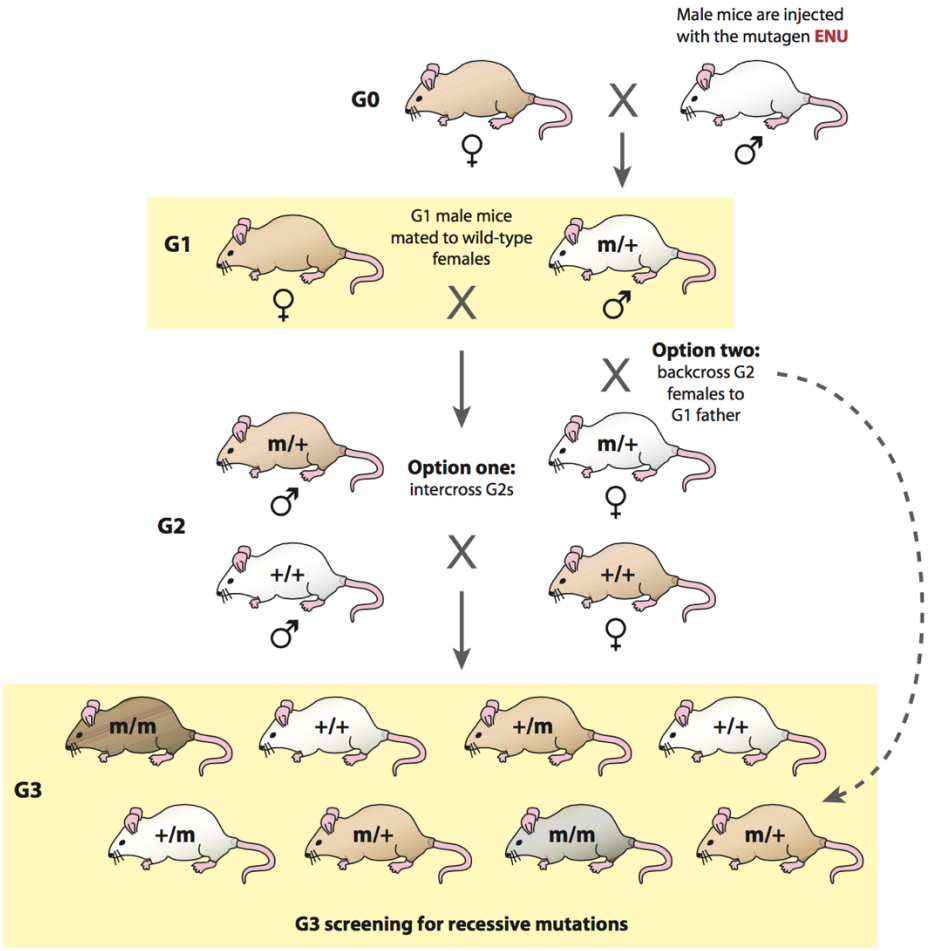


Figure 6: Breeding protocol for detection of recessive mutations following the treatment of a male (G0) with N-ethyl-N-nitrosourea (ENU). Figure taken from Acevedo-Arozena et al. (2008).

Following identification of a phenodeviant mouse, the penetrance and inheritability of the mutation (that is still unidentified at this stage) needs to be tested. Mutations can eventually be identified via extensive mapping and positional cloning work.

ENU screens have already proven powerful tools, and have allowed the identification of genes involved in sleep regulation (Funato et al., 2016).

3. THE *SLEEPY6* LINE

This thesis focuses on a detailed characterisation of mechanisms underlying sleep disruption in the *Sleepy6* mouse line, which was obtained via such an ENU-based protocol. Mice were initially screened at MRC Harwell for numerous phenotypes of interest, including sleep abnormalities. Video monitoring and wheel-running activity showed that *Sleepy6* homozygous mice (i.e. homozygous for the *Sleepy6* mutation described below) have a strong sleep phenotype and present with a reduced amount of sleep in both the dark and light phases as compared to wild-type littermate controls. This was assessed by monitoring activity using video-tracking during 'baseline' conditions (12h:12h light-dark cycle) and when the mice were exposed to light pulses (to test for abnormalities in light-induced sleep). Additionally, wheel-running monitoring under various light-dark cycles (12h:12h light-dark; constant light; constant darkness) revealed no marked circadian phenotype in the *Sleepy6* homozygotes (Heise, 2015). These animals however did display other deviant phenotypes such as impaired innate behaviours (absence of nest building or marble burying), along with a possible deficit in attention as shown by various behavioural tests (Heise, 2015). Moreover, pilot EEG recordings revealed reduced amounts of REM sleep during the light phase.

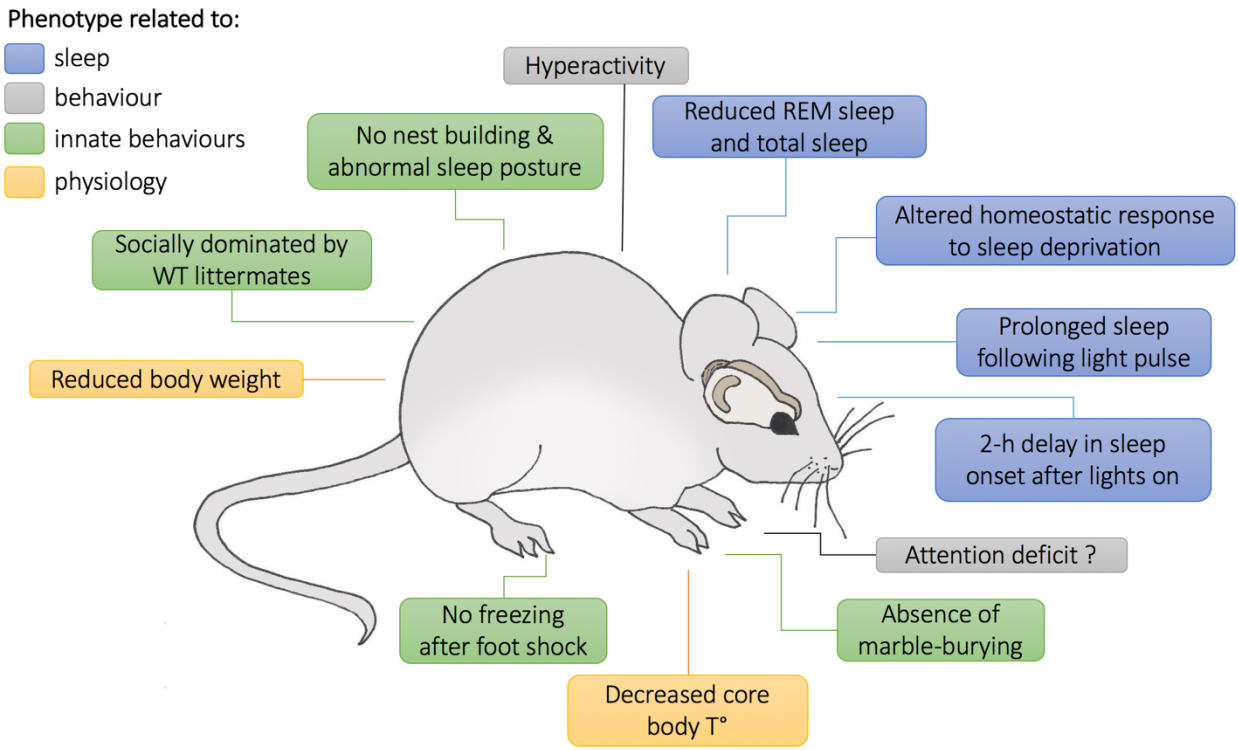


Figure 7: Summary of the known phenotypes of Sleepy6 homozygous mice, as compared to their wild-type (WT) littermates. REM = rapid eye movement, T° = temperature. Background image by Maylis Guillaumin.

It was shown that the *Sleepy6* line possesses a recessive mutation in the gene of the vesicle-associated membrane protein 2 (VAMP2 – also known as synaptobrevin 2), which belongs to the **s**oluble **N**-ethylmaleimide-sensitive factor **a**ttachement protein **re**ceptor (SNARE) protein family. It is well known that SNARE proteins are core components of the membrane recognition and fusion machinery (Chen and Scheller, 2001; Südhof, 1995). It was originally proposed that 3 proteins would form the SNARE complex: one vesicle membrane protein (v-SNARE or VAMP) and two proteins attached to the target membrane (t-SNAREs, called Syntaxin and SNAP-25), although very early on, it was also suggested that specificity in membrane trafficking may be enabled by the differential distribution of v-SNARE proteins and t-SNARE proteins among different vesicles and target cells or compartments (Söllner et al., 1993). Since then, many isoforms and homologous proteins have been identified, which are distributed differentially

across the brain and periphery, some serving synaptic functions and others not (Benagiano et al., 2011).

Specifically, the SNARE complex, which consists of the synaptic vesicle protein VAMP2 and of the presynaptic membrane proteins SNAP-25 (synaptosome-associated protein of 25kDa) and syntaxin 1A, plays a key role in exocytosis at synapses: as shown in Figure 8 it allows the fusion of the vesicle with the plasma membrane, leading to the release of neurotransmitters (Chen and Scheller, 2001; Schoch et al., 2001).

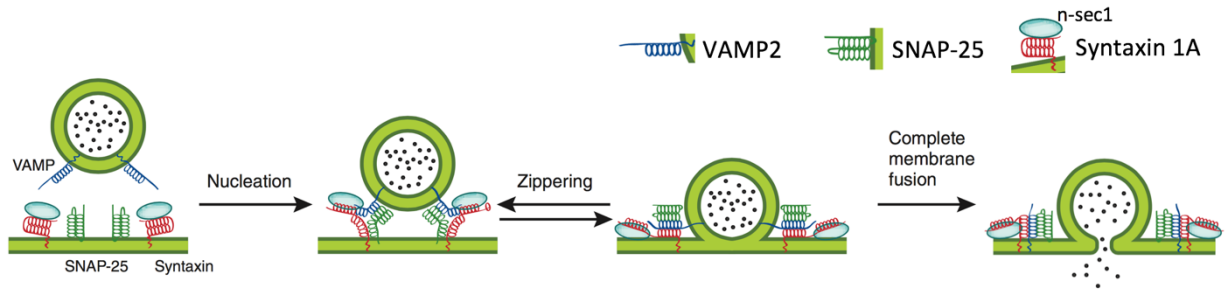


Figure 8: Molecular model of vesicle exocytosis, showing the interaction of the vesicle-associated membrane protein 2 (VAMP2) with syntaxin 1A and SNAP-25 (synaptosome-associated protein of 25kDA), both of which are located on the membrane with which the vesicle will fuse (presynaptic membrane in the case of synaptic release). Figure adapted from Scheller (2013).

To allow efficient neurotransmitter release, vesicles need to dock to the pre-synaptic membrane and form a readily-releasable pool (RRP) of vesicles that can fuse when an action potential reaches the nerve terminal, thereby promoting the influx of extracellular calcium ions and triggering fusion mechanisms (Rosenmund and Stevens, 1996). Synaptotagmins serve as Ca^{2+}-sensors to allow release (at slow or fast rates, depending on the specific synaptotagmin involved), while also preventing spontaneous fusion; it has also been shown that they would be essential to maintain the RRP of vesicles at synapses (Bacaj et al., 2015).

The *VAMP2* gene is expressed throughout the body (see Figure 9), but mainly in the brain. Its function is not limited to neurotransmitter release as it also plays a role in endocrine function,

for instance insulin release in pancreatic cells (Regazzi et al., 1995) or renal function (Mendez et al., 2011).

The mutation present in the *Sleepy6* line is a missense mutation (codon ATC becomes AAC), leading to an amino-acid change (Ile102Asn – the hydrophobic amino acid isoleucine becomes the even less water-soluble amide asparagine) in the C-terminal region of VAMP2 in the transmembrane domain of the protein. VAMP2 has been reported to contain α-helices in its SNARE motives, linker regions and its transmembrane domain (TMD) (Stein et al., 2009). It was shown that stabilising helices (via introduction of leucine residues) in the TMD of VAMP2 impaired exocytosis, while on the contrary, destabilising those helices (via introduction of valine or isoleucine residues) accelerates fusion pore expansion; the authors concluded that the TMD of VAMP2 catalyses the membrane fusion process thanks to its conformational flexibility (Dhara et al., 2016). The mutation occurring in *Sleepy6* homozygous mice could have important effects, as it replaces a 'destabilising' isoleucine with asparagine. However, protein conformation prediction work showed that α-helices could be predicted with high confidence in the TMD of the mutant form of VAMP2 of the *Sleepy6* line, and that the protein should still be able to integrate in the vesicular membrane (Heise, 2015). It is therefore difficult to make *a priori* assumptions on how the mutation will affect vesicular release, as it induces a destabilising amino acid change in the TMD, but computational conformation predictions do not point towards a strong impact. Preliminary findings obtained at MRC Harwell suggest that docking of the vesicles occurs, but that fusion itself may be impaired (Heise, 2015).

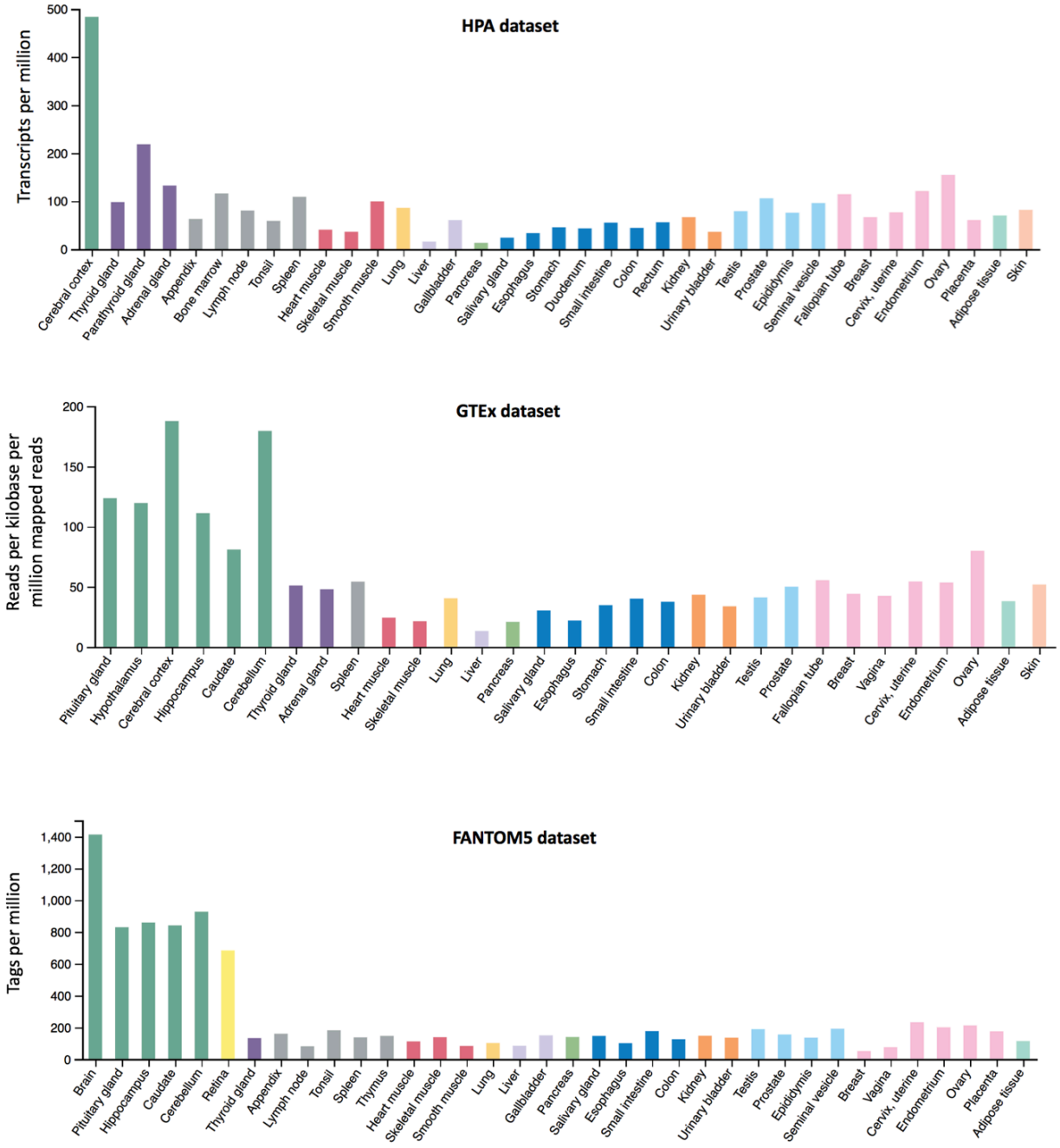


Figure 9: VAMP2 gene expression levels across various tissues (samples of human origin), as reported by 3 projects (HPA, GTEx, FANTOM5). Relative levels are concordant across the datasets, with the higher levels consistently reported in brain structures. Figure adapted from https://www.proteinatlas.org/ENSG00000220205-VAMP2/tissue#top

The findings regarding hyperactivity and a deficit in attention in the *Sleepy6* mouse line are of particular interest in regard to a recent study showing links between mutations in the genes of the SNARE proteins (including VAMP2) and attention-deficit/hyperactivity disorder (ADHD) in males (Gao et al., 2015). For instance, VAMP2 Ins/Del polymorphisms have shown associations with ADHD in human populations (Kenar et al., 2014). A National Centre for Biotechnology Information (NCBI) database search revealed no known variants in human populations at the exact orthologous site where the mutation occurs in *Sleepy6* mice (Figure 10). However, many variants occur near this mutation site (shown as red bars in Figure 10), although no associated phenotypic consequences are provided for the closest 3 variants. Variants in the *VAMP2* gene have been associated with various psychiatric disorders, such as bipolar disorder and ADHD, but the associations are not always clear (Abou Jamra et al., 2008; Kenar et al., 2014). This will be further discussed in subsequent chapters, in light of the findings obtained.

Further experiments are necessary to understand how this mutation may affect the interactions between the proteins of the SNARE complex (Poirier et al., 1998; Stein et al., 2009). In particular, as SNARE proteins are found throughout the brain, it is puzzling that this mutant exhibits a relatively restricted behavioural phenotype. This is all the more striking as *Vamp2* knockouts (KO) die immediately after birth (Schoch et al., 2001), which would suggest that *Vamp2* mutants should show a profound phenotype, far from what is observed in the *Sleepy6* line.

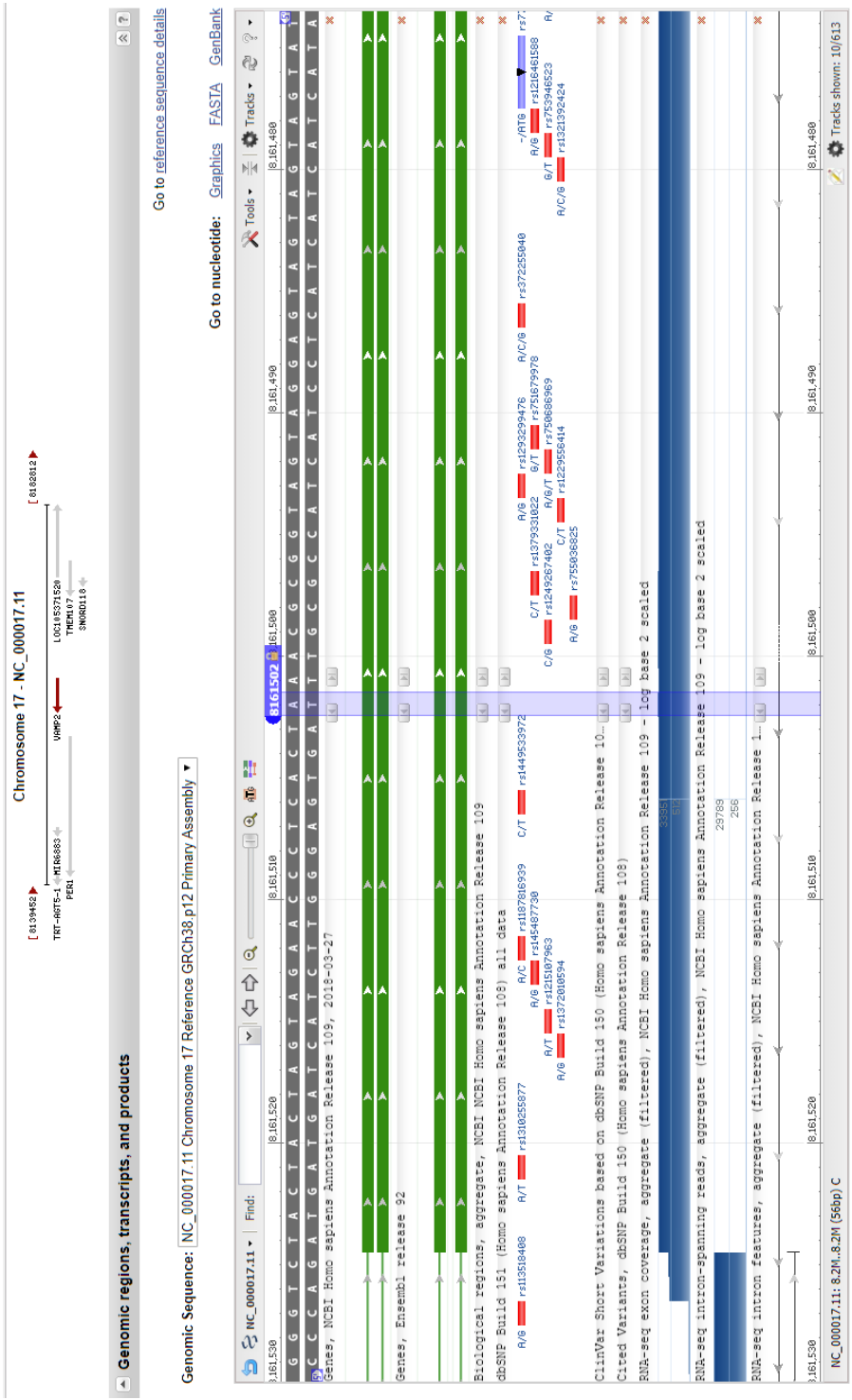


*Figure 10: Presence of variants in the human VAMP2 gene on chromosome 17 around the orthologous site of the point mutation occurring in the Vamp2 gene in Sleepy6 mice (highlighted in blue). In the Sleepy6 mutation, the T is replaced with an A leading to an amino acid change from isoleucine to asparagine. Note that in mice the original codon is ATC while in human it is ATT; both code for isoleucine. The Sleepy6 mutation modifies the codon to A**A**C, which codes for asparagine; in humans, the exact same mutation would lead to AAT which also codes for asparagine. Data taken from https://www.ncbi.nlm.nih.gov/gene/6844*

As *Sleepy6* homozygous mice showed no obvious circadian phenotype, but a strong sleep phenotype, we hypothesised that this line will provide a good model to study the mechanisms underlying sleep homeostasis. We chose to investigate this further using not only an *in vivo* approach – to try and understand the molecular and cellular mechanisms that could be altered, but also a computational approach, as this would give us some more indications of which aspect of the sleep homeostat may be affected.

4. MATHEMATICAL MODELLING: ANOTHER APPROACH TO STUDYING SLEEP/WAKE REGULATION

As introduced in paragraph 1, the regulation of sleep by the interaction of the circadian and homeostatic processes was formalised in 1982 by A. Borbély in the so called "two-process" model (Borbély, 1982). The model assumed that sleep pressure increased as a saturating exponential function of time awake, and decreased with time asleep, while the drive to remain awake followed circadian variations (Figure 1). The levels of Process S (the homeostatic process) were derived from slow-wave activity (SWA) levels during NREMS following periods of wake of varying lengths, while the levels of Process C (the circadian process) were initially arbitrary (only later on, upper and lower thresholds of sleep pressure which varied with circadian time were introduced (Daan et al., 1984)). The model was extended further to predict intra-episodic dynamics of SWA during NREMS episodes – this approach is also known as the 'elaborated' two-process model (Achermann et al., 1993).

A later version of the model simulated the ultradian rhythms of sleep/wake architecture, in particular the NREMS-REMS transitions, without the necessity to add a third process: starting from the two-process model of sleep it introduced the homeostatic drive for sleep and circadian

drive for wake as ultradian-rhythm generators, whereby arousal states (wake and REMS treated identically) would feedback to the circadian and homeostatic drives to generate ultradian variations (Phillips et al., 2013). Using this model, the authors were able to predict both normal state architecture and the state-specific rebounds associated with total or selective sleep deprivation (Phillips et al., 2013). The history of the two-process model will be further developed in Chapter 5.

It is important to note that although the two-process model has been widely used and referred to, many other mathematical models also aiming to replicate or predict sleep/wake architecture have been proposed (Achermann and Borbély, 2003):

- **Variations of the two-process model**. This was the case of the 'three-process model' which added for instance a third 'sleep inertia' process (Process W), so that the model could predict subjective alertness and cognitive throughput in humans (Folkard and Åkerstedt, 1991; Jewett and Kronauer, 1999). Another study introduced Process Z – to 'replace' Process S – to characterise local variations in SWA (as opposed to global variations that are usually reflected in Process S) (Zavada et al., 2009).
- **Distinct approaches.** Others took altogether different approaches such as the 'limit cycle reciprocal interaction model', directly derived from physiological data, which aimed to replicate NREM-REM cycles using self-excitatory and self-inhibitory reciprocal interactions between cell populations (McCarley and Hobson, 1975; McCarley and Massaquoi, 1986).
- **Combined models.** Other studies combined several models such as the 'composite model of sleep regulation' which merged the elaborated two-process model, the limit cycle reciprocal interaction model and also adding sleep inertia (Process W mentioned above) (Achermann and Borbély, 1992). The authors thus showed that various modelling approaches are not mutually exclusive and can be integrated together.

All of these models have been developed using data recorded either in humans (Achermann et al., 1993; Borbély, 1982; Zavada et al., 2009) or animals – such as the mouse (Franken et al., 2001; Huber et al., 2000a), the rat (Borbély et al., 1989; Franken et al., 1991; Vyazovskiy et al., 2007) or the guinea pig (Tobler et al., 1992).

Importantly, not only do mathematical approaches allow us to predict the outcomes of experiments, but via their ability to replicate sleep-wake architecture, they allow the experimenter to evaluate parameters such as the rates of increase or decrease of sleep pressure in a species, or in a particular strain of mice (Huber et al., 2000a). Furthermore, it can provide information on how those dynamics may differ across brain areas (Rusterholz and Achermann, 2011). Indeed, as mentioned above, regional differences can be observed in SWA dynamics and therefore in sleep homeostasis. In the novel modelling approach that will be presented in Chapter 5, we have therefore also chosen to address regional differences in the dynamics of Process S.

5. AIMS OF THE PROJECT

The present DPhil work aimed to try and contribute to the current understanding of the mechanisms underlying the abnormal sleep phenotype in the *Sleepy6* mutant mice, knowing the mutation causing this phenotype. More specifically, the project aimed to address the three following questions:

a) Investigate the molecular, neuronal and cellular correlates of the sleep phenotype observed in the *Sleepy6* mouse line. This was addressed using chromatography techniques to evaluate the levels of key neurotransmitters and their metabolites, as well as other quantitative molecular approaches to investigate the levels of expression of

genes involved in some key neurotransmitter pathways. Additionally, electrophysiology recordings were performed, providing us with further information regarding time spent in each vigilance state and the global differences associated with each state between the *Sleepy6* mutants and their wild-type littermates. Electrophysiology recordings also allowed us to look at neuronal activity, at a local level, across waking and sleep.

b) Gain a broader understanding of the spectrum of abnormal phenotypes also present in the *Sleepy6* animals, which may occur as a consequence of sleep disruption. This second aim was addressed using behavioural testing to assess learning and memory in *Sleepy6* mice.

c) Adapt an elaborated version of the two-process model to mouse data, while addressing regional differences in SWA dynamics. Ultimately, this modelling approach was applied to recordings performed in *Sleepy6* homozygotes to gain further insights into the alterations in their sleep homeostat.

CHAPTER 2: Molecular analysis

1. INTRODUCTION

Whilst VAMP2 is expressed throughout the brain, the specific mechanisms by which the *Sleepy6* mutation gives rise to changes in sleep are unclear. Given the key role played by VAMP2 in membrane fusion and vesicular release (Chen and Scheller, 2001; Schoch et al., 2001), it is important to determine if the *Sleepy6* mutation results in major differences in neurotransmitter levels – and their metabolites – within the brain. Neurotransmitter levels can be measured *in vivo* using microdialysis, or from tissue samples using high performance liquid chromatography (Chefer et al., 2009; Hambrecht-Wiedbusch et al., 2014; Justice, 1993; Schmidt et al., 1990).

A. SNARE proteins and neurotransmitter systems

As SNARE protein complexes have been shown to be modulated by neurotransmitters (Fisher and Braun, 2000), it cannot be excluded that reversely, a disruption in vesicular release could lead to compensatory effects within the biosynthesis pathways of neurotransmitters, or on the reuptake and catabolic pathways. Indeed, neurotransmitter release relies on two presynaptic cycles: the synaptic vesicle cycle (targeting, docking, fusion, endocytosis and recycling of vesicles) and the neurotransmitter cycle (biosynthesis, storage, reuptake and degradation of neurotransmitters); and importantly, those two cycles – one of which involves VAMP2 - are interdependent and partially overlap (Fon and Edwards, 2001). Additionally, those cycles involve processes tightly influenced by various proteins, which in turn affect each other. For instance, it has been shown that synuclein proteins have an impact on monoamine biosynthesis

and vesicular release/reuptake, while also interacting with SNARE proteins such as SNAP-25 (Oaks and Sidhu, 2011). We therefore aimed to investigate the levels of expression of genes coding for proteins involved in the biosynthesis and trafficking pathways of neurotransmitters.

However, the large number of neurotransmitters – and even more so of the genes involved in their synthesis, transport and degradation – required to target our analysis towards one to two pathways at first. Several observations led down the route of a possible impairment in the serotonergic system. It has been shown that VAMP2 interacts with the serotonin transporter (SERT)(Müller et al., 2014), and it is known that SERT plays a key role in the homeostasis of serotonin in the brain, determining the magnitude and the duration of serotonergic signalling (Zahniser and Doolen, 2001).

Additionally, the range of behaviours affected in *Sleepy6* homozygotes paralleled those affected in SERT knock-out mice (Murphy and Lesch, 2008), but the effect were generally opposite (Table 1). These observations therefore supported possible alterations in the serotonergic system in *Sleepy6* Homozygotes. SERT-overexpressing mice, consistently with those results, show decreased anxiety-like behaviours (Jennings et al., 2006).

Table 1: Comparison of phenotypes observed in Sleepy6 homozygotes and SERT knock-out mice.

***Sleepy6* homozygotes**	**SERT mutants**
Hyperactive during the dark phase	Decreased exploratory activity (hypoactive)
Reduced REM sleep	Increased REM sleep
Decreased body weight	Increased body weight
Decreased baseline body temperature	Increased baseline body temperature
Reduced amount of sleep	Increased anxiety-like behaviour
No marble burying, no nest building	Increased learned fear (depression)
Sleepy6 dominated by WT males	Under-aggressive
Possible attention-deficit.	SERT (Slc6a4) is a candidate gene for autism spectrum disorder (ASD)(Page et al., 2009)
SERT mutants' phenotypes derived from Murphy & Lesch (2008).	

B. *Sleepy6* mice, ADHD and neurotransmitter pathways

As can be seen in Table 1, *Sleepy6* homozygotes are hyperactive and may show a possible attention deficit; both features remind of attention-deficit hyperactivity disorder (ADHD). Interestingly, it has been reported that ADHD is associated with variants in genes coding for proteins involved in the synthesis, reuptake and breakdown of 5-HT, and result in alterations of serotonin availability and metabolism (Oades, 2010). Similarly however, studies have shown an involvement of the dopaminergic synthesis and reuptake pathway in ADHD (Buitelaar et al., 2011; Forssberg et al., 2006), as well as other catecholamines (Prince, 2008). Indeed, ADHD has traditionally been treated with psychostimulants (e.g. Methylphenidate) acting on catecholaminergic pathways, in particular dopaminergic and noradrenergic ones (Engert and Pruessner, 2008; Oades, 2010; Prince, 2008).

C. Effects of neurotransmitters on sleep and wakefulness

The sleep phenotype of *Sleepy6* mice can also provide valuable insights into the possible neurotransmitter pathways that our study could initially focus on. Yet, the effects of various neurotransmitters on sleep and wakefulness are complex and vary across brain regions (Szabadi, 2006; Watson et al., 2010) – see also Chapter 1, section 1.E. For example, while GABA-mimetic drugs can be sleep-promoting if administered systematically, they have been shown to have opposite effects (increase wake and decrease sleep) if administered locally in the pontine reticular formation, a brain region that also contributes to the generation of REMS (Camacho-Arroyo et al., 1991; Watson et al., 2008; Xi et al., 1999).

Acetylcholine has also been shown to modulate sleep and wakefulness; for instance, hindering the breakdown of acetylcholine enhances REMS (Lydic and Baghdoyan, 2008; Watson et al., 2010). Adenosine, on the other hand, has been proposed to play a role in REMS generation;

specifically, drug-induced decreases in adenosine levels in the pontine reticular formation are associated with REMS disruption (Bjorness and Greene, 2009; Watson et al., 2010).

Serotonin is generally viewed as a wake-promoting neurotransmitter (Monti and Jantos, 2008). For instance, serotonin release has been shown to be at its highest during wake in the dorsal raphe nuclei and frontal cortex (Portas et al., 1998). However, the role of the serotonergic system in modulating sleep and wakefulness is more complex, with for example, agonists of some serotonergic receptors (e.g. $5HT_{1A}$, $5HT_{1B}$, $5HT_{2A/2C}$) having a specific REMS-suppressing effect. In a similar manner, noradrenergic cells in the locus coeruleus have shown wake-promoting and REMS-inhibiting effects; the role of norepinephrine in sleep-wake regulation is however brain-region specific (Berridge and Waterhouse, 2003; Berridge et al., 2012; Gottesmann, 2011). The fact that selective serotonin reuptake inhibitors lead, in all tested species, to a reduction in REM sleep has been considered evidence that serotonin could have an inhibitory effect on REM sleep, and the midbrain raphe nucleus has been proposed as another candidate REMS-inhibiting area (Ursin, 2002).

Finally, dopamine has been shown to increase wakefulness, and the wake-promoting effects of increased dopamine levels triggered by stimulants such as amphetamines are well documented (Boutrel and Koob, 2004; Brown, 2016). Administration of D-amphetamine leads to increased waking time and compromises both NREMS and REMS (Andersen et al., 2009). Additionally, knock-out mice for the dopamine transporter have shown increased levels of wakefulness and decreased NREMS time (Sidhu et al., 2003; Wisor et al., 2001). All these observations echo the sleep phenotype of the *Sleepy6* homozygotes, and although the underlying mechanisms may arguably be very different, it seemed important to investigate whether *Sleepy6* mice did not show striking differences in dopamine – or other neurotransmitter – levels, as well as investigate levels of expression of proteins involved in the corresponding pathways (e.g. transporter, enzymes necessary for biosynthesis, etc.).

D. Hypotheses

For the reasons discussed above, our main hypothesis remained for a possible impairment in the serotonergic pathway. We chose to analyse serotonin and its metabolite 5-hydroxyindolacetic acid (5-HIAA) using HPLC. This initial HPLC data may then help direct further investigations performed using quantitative reverse transcription PCR methods.

2. MATERIALS AND METHODS

A. *Sleepy6* genotyping protocol

A *Sleepy6* colony was generated using pairs of heterozygous males and females, which required identifying the genotype of the pups. The genotyping of the *Sleepy6* mice was based on the TaqMan dual-labeled probe method (Holland et al., 1991), where a pair of probes with fluorophore tags are designed to hybridise either to the WT *Vamp2* gene, or to the mutated version (see below and Figure 11). Depending on the fluorescent signal obtained, this allows to discriminate between WT animals (only one type of probe can bind efficiently to the target genomic DNA), homozygous animals (only the second probe binds) and heterozygous animals (both probes can bind, and a "mixed" fluorescent signal is obtained).

i. Genomic DNA (gDNA) extraction

After transferring ear notches to 1.5mL Eppendorf tubes, 100µL of 50mM NaOH were added to samples, before incubating at 95°C for 1 h in a heat block. Samples were then vortexed for 10s, before being centrifuged for 2min at 13000 rpm

10µL of 1M Tris-HCl were then added, before vortexing samples again for 10 s and centrifuging at 13000 rpm for 2min. Finally, 500µL of sterile water were added to each Eppendorf; samples were then immediately used (see below) or kept at -20°C for genotyping.

ii. Running of the qPCR

The following mix was added for each reaction (well), using a 96-well qPCR plate:

- 10µL of qPCR MasterMix (Platinum qPCR Supermix UDG – with ROX, ThermoFisher Scientific)
- 1µL of forward primer* (at 20µM)
- 1µL of reverse primer* (at 20µM)
- 1µL of VIC probe* (at 5 µM) – corresponds to mutated gene
- 1µL of FAM probe* (at 5µM) – corresponds to WT gene
- 2µL of gDNA
- 4µL of sterile water

The plate was then covered with an optically clear adhesive film and the following program was run on a qPCR machine (StepOnePlus Real-time PCR System, Applied Biosystems) using a TaqMan protocol (Genotyping – FAM/VIC protocol):

- 30s at 60°C (pre-PCR read)
- 10 min at 95°C (holding stage)
- 40 cycles of 15s at 95°C and 1 min at 60°C (cycling stage)
- 30s at 60°C (post-PCR read)

*Forward primer: 5'- CACC TCCC TCTC ACTC TTAG ATGA T – 3'

*Reverse primer: 5'- GCCT CTGG CCCC ACTC A -3'

*VIC probe (binds to mutated gene): VIC – ATC TTG GGA GTG AAC T – MGB

* FAM probe (binds to WT gene): 6-FAM – ATC TTG GGA GTG ATC TG – MGB

Primers and the complementary sequence to the probes are highlighted in the *Vamp2* mouse gene shown in Figure 11 (note that the complementary DNA – and not genomic DNA – sequence is shown, and therefore part of the forward primer sequence does not appear as it overlaps with an intron).

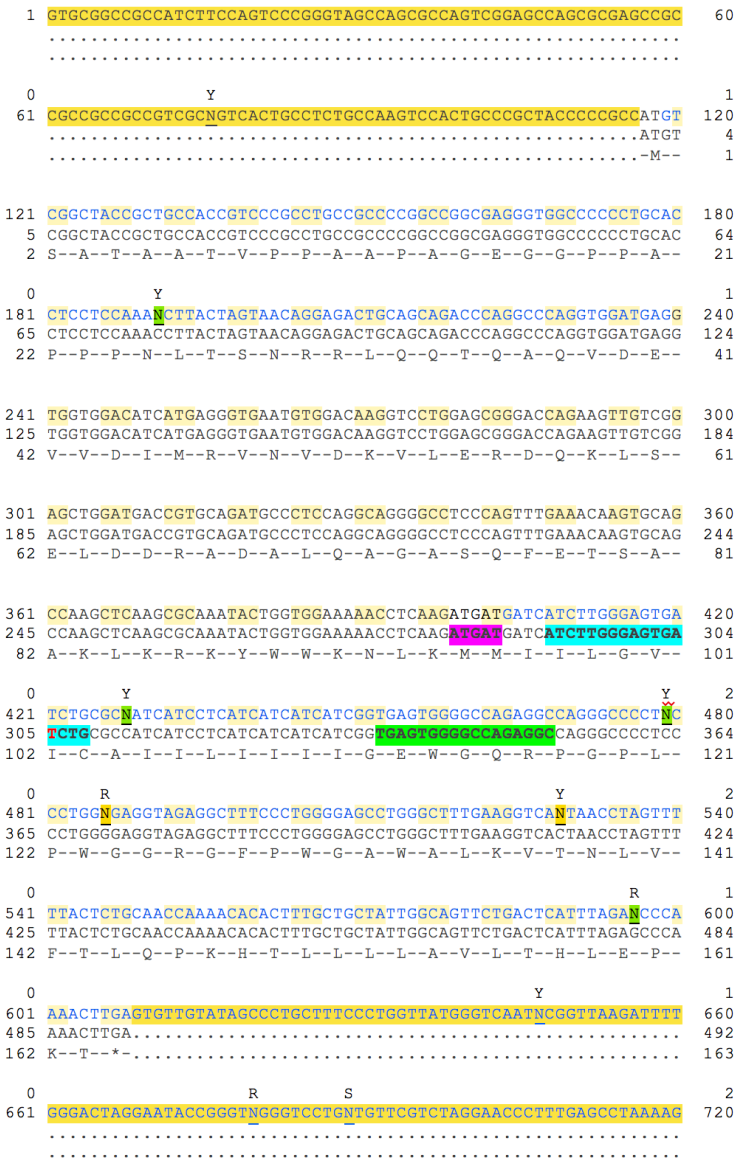


Figure 11: Complementary DNA sequence of the mouse Vamp2 gene, with part of the 3'- and 5'- untranslated regions (highlighted in ochre). The amino acid sequence is shown below the nucleotide sequences. Highlighted in pink is part of the forward primer (the rest of which is complementary to an intron region), in cyan is the region where the VIC/FAM probes bind (the nucleotide where the Sleepy6 mutation occur is shown in red) and in green is the complementary region to the reverse primer. Sequences were taken from ensembl.org

iii. Interpretation of the results

The following type of graph was obtained at the end of the qPCR programme, using the StepOne™ software (version 2.3, Applied Biosystems), allowing us to determine the genotype of each animal.

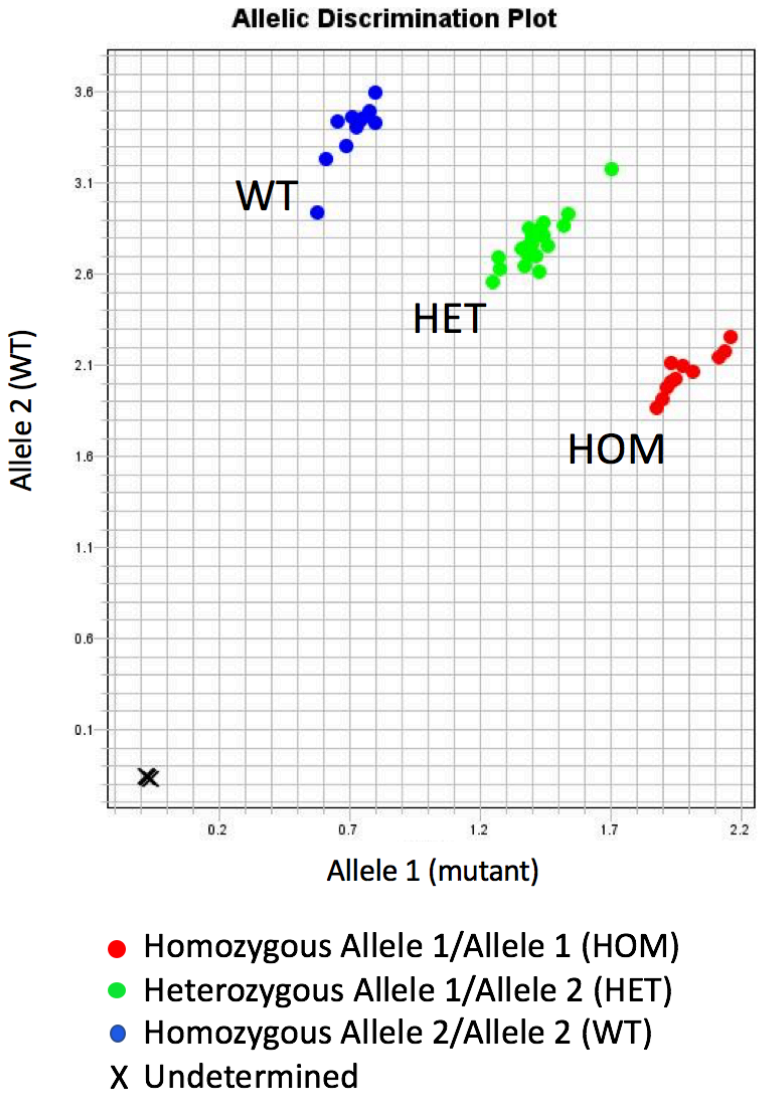


Figure 12: Allelic discrimination plot obtained at the end of the PCR. Blue dots (allele 2/allele 2) represent WT animals, red dots (allele 1/allele 1) represent animals homozygous for the Sleepy6 mutation (HOM) and green dots represent heterozygous animals (HET). Black crosses at the bottom represent negative controls (i.e. no DNA to confirm no cross-contamination of the master mix).

B. Setting up of the High-Performance Liquid Chromatography (HPLC)

HPLC is a method that allows to separate molecules within a solution, based on their chemical and electrical properties. The samples to test are injected via a high-pressure pump into a column in which they will be retained a given amount of time depending on their affinity with the mobile phase that carries the sample and the stationary phase that constitutes the inside of the column. Compounds will be detected by an electrode at various time points, leading to peaks in the chromatogram, as they elute from the column – see Figure 13.

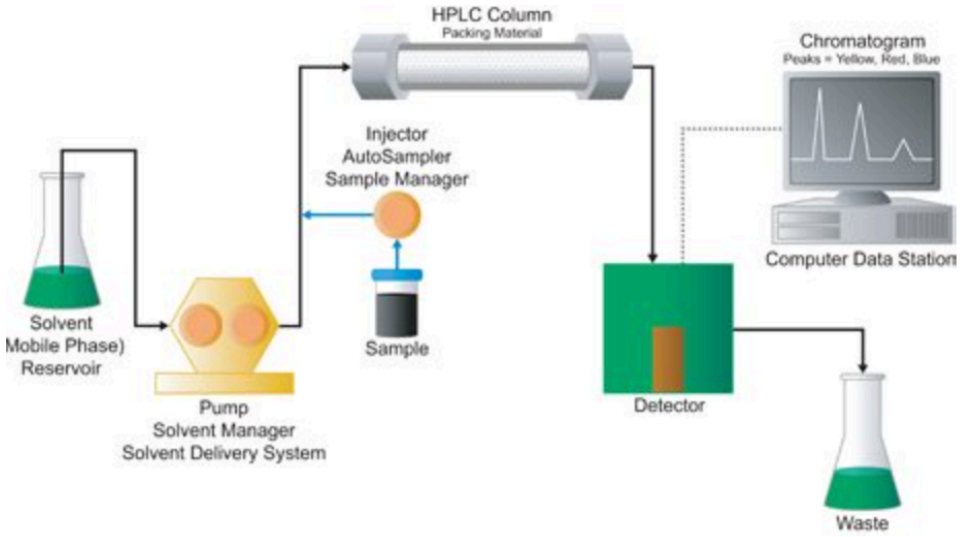


Figure 13: High performance liquid chromatography set up. Note that the set up used in the present study printed the chromatogram on paper and was not linked to a computer. Image taken from Waters.com

i. Apparatus used

Experiments were run using an HPLC pump (Jasco, *Intelligent HPLC Pump* PU-980), an amperometric detector (Bio Analytical Systems, *Amperometric Detector* LC-4C), an analyser (Bio Analytical Systems, *Liquid Chromatography* CC-4) equipped with an adequate HPLC column (4.6x100mm Analytical Column, Waters, Ireland) and glassy carbon electrode (Dual glassy

carbon working-crossflow 3mm, Alvatek Ltd, UK). The output of the HPLC was analysed using an integrator (Milton Roy, *Computing Integrator* CI 4000).

ii. Mobile phase

The mobile phase – initially optimised for the analysis of serotonin and its metabolites – was prepared with the following reagents (final concentrations indicated):

- HPLC-grade methanol: 625mL
- $NaH_2PO_4H_2O$: 0.13 M
- ethylenediaminetetraacetic acid (EDTA): 0.85 M
- 1-octanesulphonic acid sodium salt (OSA – $C_8H_{17}NaO_3S$): 0.025 mM
- Concentrated phosphoric acid: <5mL

To prepare 5 L of mobile phase, 89.694g of $NaH_2PO_4H_2O$ (MW=137.99g/mol, Alfa Aesar) were diluted in 1 L of double-distilled H_2O (ddH_20). 1.582g of EDTA (MW=372.24g/mol, VWR Int.) were added to the solution, after which 625 mL of methanol (12.5% HPLC grade, Fisher Scientific, UK) and 375 mL of ddH_20 were added. While leaving the solution to stir for a few minutes, a 10 mM stock solution of OSA (MW=216.28g/mol, HPLC grade, Fisher Scientific, UK) was prepared by diluting 216.28 mg of OSA in 100 mL of ddH_2O. An additional 2750 mL of ddH_2O and 12.5 mL of OSA stock solution were added to the HPLC mobile phase solution. The volume was filled up to 5 L with H_20 and phosphoric acid (MW=98.00g/mol, HPLC grade, Sigma-Aldrich) to adjust the pH to around 3.5 at 20°C.

The solution was filtered and degassed in 1-L aliquots at a time, prior to being used in the HPLC machine (Nitrocellulose membrane, 0.22 μm GSWP, Merck Millipore Ltd., Ireland).

iii. Standards

Six "standard" solutions were prepared at a concentration of 10^{-3} M: norepinephrine (NP – MW=319.26g/mol, Sigma-Aldrich), dopamine (DA – dopamine hydrochloride 99%, MW=189.64g/mol, Alfa Aesar, UK), 3,4-dihydroxyphenylacetic acid (DOPAC, 98%, MW=168.15g/mol, Sigma-Aldrich), serotonin or 5-hydroxytryptamine (5-HT, MW=212.68g/mol, Sigma-Aldrich), 5-hydroxyindoleacetic acid (5-HIAA, 98%, MW=191.19g/mol, Sigma-Aldrich) and homovanillic acid (HVA, MW=182.17g/mol, Sigma-Aldrich). A perchloric acid (PCA, 60%, HPLC grade, MW=100.46g/mol, Fisher Scientific, UK) stock solution at 0.092M was prepared by diluting a concentrated 60% PCA solution 1:100. This stock was subsequently stored at 4°C. Each standard stock solution was prepared by diluting the accurate solid weight in 20 mL of PCA stock solution to obtain a final 10^{-3} M concentration. All standard stock solutions were stored at 4°C and were aliquoted and diluted down to 10^{-7} M on every single day when brain samples were to be run.

In order to check the linearity of detection of the HPLC machine, a standard curve was drawn by running at least twice 50 µL of mixed standard solutions (containing equal concentrations of NP, DA, DOPAC, 5-HT, 5-HIAA, HVA) at the following concentrations: 4.10^{-7}M, 2.10^{-7}M, 10^{-7}M, 2.10^{-8}M and 10^{-8}M.

iv. Dissections of brain samples

1. Pilot study

This first batch included n=3 *Sleepy6* homozygotes and n=4 WT littermates. Immediately following neck dislocation, the brain was extracted and placed in a stainless steel sagittal brain matrix (slice width: 0.5mm). The first blade was placed in front of the optic chiasm, the second blade 1.5mm posteriorly (i.e. 2 graduations left empty between the blades) and a third blade 1.5mm further away from the 2nd blade. Brain slices were placed in phosphate-buffered saline. Samples from the cortex, hypothalamus, hippocampus and cerebellum of approximately 1 mm^3

were collected on each side of the brain and snap frozen in isopentane resting on dry-ice. Samples were subsequently stored at -20°C.

2. Final study

In this second batch of experiments, samples from n=8 WT controls and n=10 *Sleepy6* homozygotes were used. Immediately following neck dislocation, the brain was extracted and placed on a cotton pad kept on an ice-cold surface and humidified with saline solution. Two pieces of cerebellum and hypothalamus, the midbrain region, the 2 hippocampi, and 2 pieces of cortex were dissected in this order, following the method shown in "Dissection of the brain (rat and mouse)", by Prof. Dr. Michel Hammond (Science Vision, Universiteit Maastricht). Pieces weighed approximately 15-30mg, depending on the region.

v. Preparation of brain samples

On the day the samples were to be run, they were kept for about an hour on wet ice to let them thaw slowly. To be able to express the final results relative to wet tissue weight, samples were weighed, after which 200 μL of 0.092M PCA solution was added to each sample in micro tubes cooled on ice. Tissues were homogenised using a sonicator (VibraCell, VCX 500, Sonics, USA). The sonicator was set on 40% and samples were sonicated for 17 s each. Samples were subsequently centrifuged at 13,000 rpm and at 4°C for 15 minutes. Supernatants were transferred to clean test tubes kept on ice, being particularly careful not to pipet up parts of the pellet. All samples were kept on ice at all times, unless being processed.

vi. Runs on the HPLC column

As mentioned in paragraph 2.B.iii, at the beginning of each day when brain samples were to be run, standard solutions were injected first – one at a time – at a concentration of 10^{-7} M to calibrate the apparatus (i.e. to allow to infer initial concentrations in the samples depending on the height of the detection peak). Samples were injected 50 μL at a time in the HPLC. Each run lasted for 20 minutes and 50 μL of 0.093M PCA were injected between each sample, allowing at least 3 minutes for the solvent to pass through the column. In the pilot study, each sample was run at least twice to assess variability in the results. In the final study, given the satisfying stability of the results, each sample was injected once only in the HPLC column.

C. RT-qPCR

i. RNA extractions

RNA extractions were performed using the QIAGEN RNeasy Mini kit, following the manufacturer's instructions.

Prior to starting the experiments, the bench and equipment were washed with deionised water, followed by 70% ethanol, an RNase decontamination solution (RNaseZap™, Thermo Fisher Scientific Inc., UK), and finally with water again. The steps were then as follows:

- Brain samples previously stored at -20°C were kept on dry ice.
- 100μL of 'RLT' lysis buffer (with 2-mercaptoethanol) were added to each sample. The samples were then disrupted with a pestle and motor. Samples were kept on dry ice before and after being disrupted.
- An additional 500μL of RLT buffer (with 2-mercaptoethanol) were added to each sample and samples were homogenised using a 27G needle with 1mL syringe. Samples were kept on wet ice while other samples were homogenised.

- Samples were centrifuged for 3 min at 13500 rpm, at 4°C. The supernatant was then carefully pipetted into new sterile nuclease-free 1.5mL Eppendorfs.
- 600μL of 70% ethanol was added to the lysates and mixed by pipetting.
- 600μL of each sample was transferred to a MiniSpin column and centrifuged for 30s at 13500rpm at 4°C. The flow-through was discarded. This step was performed a second time to finish off the 1.2mL of each sample.
- Buffers RW1 and RPE were added to the columns as prescribed by the instruction sheet, for washing membrane-bound RNA.
- Finally the columns were placed on nuclease-free collection tubes and 50μL of nuclease-free water was added on each column membrane. Samples were centrifuged for 1 min at 13500 rpm. The flow-through was re-pipetted and placed on the membrane again to increase RNA concentrations. The samples were centrifuged one more time at 13500 rpm for 1 minute. The flow through was kept at -20°C until the cDNA synthesis was performed.
- RNA concentrations were measured using a NanoDrop (Thermo Scientific, UK).

ii. cDNA synthesis

cDNA synthesis was performed using a qScript cDNA synthesis kit (QuantaBio, USA) following the manufacturer's instruction and using the volumes (per sample) shown in Table 2. The following temperature cycle was then performed on a PCR machine:

- 5 min at 22°C
- 30 min at 42°C
- 5 min at 85°C
- hold at 4°C

Table 2: Quantities of reagents for complementary DNA synthesis depending on RNA concentrations in the samples obtained after RNA extraction. RT = reverse transcriptase.

Sample RNA concentration	c<50ng/µL	50ng/µL<c<200ng/µL	200ng/µL<c<300ng/µL	>300ng/µL
RNA	15µL	5µL	3µL	2µL
Nuclease-free H_2O	/	10µL	12µL	13µL
qScript reaction mix	4µL	4µL	4µL	4µL
qScript RT	1µL	1µL	1µL	1µL

iii. Choice of the genes and primer design

In addition to the *Vamp2* gene and the genes coding for the two main SNARE proteins it interacts with (*Stx1a* and *Snap25*), and following the HPLC results (see Results section), we chose to investigate possible differences in the serotonin and dopamine pathways between *Sleepy6* homozygotes and WT littermates.

The genes initially chosen are presented in Table 3 – with the idea to test more genes should significant differences appear. All primers were first tested by running qPCR using the method below and 4 brain samples. Initially, two forward primers and two reverse primers were designed for each gene using Primer3 (http://primer3.ut.ee) and all 4 possible pairs were tested. The qPCR products were then analysed on a gel to check the presence of a single band. The gel was prepared with 1.3 g of agarose, 100 mL of TAE 1X, 6 µL of GelRed® nucleic acid gel stain (Biotium). 5 µL of loading buffer was added to each qPCR product and 10 µL were then pipetted into the gel. Primer pairs leading to the clearest single bands at the expected length were chosen; if all pairs were successful, one of them was arbitrarily chosen.

Table 3: Genes coding for proteins involved in the serotonergic and dopaminergic pathways that were tested in Sleepy6 mice using qPCR methods.

Gene	Description	Rationale
Slc6a4	Serotonin transporter (*Sert*)	Codes for the serotonin transporter, which is involved in clearing of the synaptic cleft and reuptake of serotonin to the presynaptic neuron. Link to Ensembl.org gene description.
Slc6a3	Dopamine transporter (*Dat1*)	Codes for the dopamine transporter, which is involved in the clearing of the synaptic cleft and reuptake of dopamine to the presynaptic neuron. Link to Ensembl.org.
Tph2	Isoform 2 of tryptophan hydroxylase.	Tryptophan hydroxylase (TPH) is an enzyme which plays a major role in the biosynthesis pathway of serotonin – see Annex 1. The TPH-mediated reaction is the rate-limiting step in this pathway. *Tph2*, which codes for TPH2 – a second isoform of TPH – was selected here as it is brain-specific (it is mainly expressed in the midbrain raphe nuclei) (Chen and Miller, 2012). Link to Ensembl.org.
Th	Tyrosine hydroxylase	Tyrosine hydroxylase (TH) is involved in the biosynthesis pathway of dopamine, allowing the conversion of L-Tyrosine into L-DOPA (L-DOPA is then converted into dopamine by DOPA decarboxylase) (Cooper et al., 1996) – see Annex 2. TH is the rate-limiting enzyme in catecholamine biosynthesis (Cooper et al., 1996; Daubner et al., 2011), and it is also commonly used as a marker of dopaminergic neurons (White and Thomas, 2012). Link to Ensembl.org.

iv. qPCR reactions

The expression of the genes coding for VAMP2, STX1A, SNAP25, SERT, DAT, TH, TPH2 was thus performed, using the primer pairs indicated in Table 4.

Table 4: Genes analysed using RT-qPCR.

Protein	Gene	Function and primers used (F: forward, R: reverse).
VAMP2	*Vamp2*	Vesicle-associated-membrane protein 2. SNARE complex protein. F: 5' TGCACCTCCTCCAAACCTTA 3' ; R: 5' CCACCAGTATTTGCGCTTGA 3'
STX1A	*Stx1a*	Syntaxin 1A. SNARE complex protein. F: 5' GCCAAGGACAGCGATGAC 3'; R: 5' CAGGATGGCGCTGTGTTTC 3'
SNAP25	*Snap25*	Synaptosomal-associated protein 25. SNARE complex protein. F: 5' TGGCATCAGGACTTTGGTTATG 3'; R: 5' TACAGGGACACACACAAAGC 3'
SERT	*Slc6a4*	Solute carrier family 6, member 4. Serotonin transporter. F: 5' CCTCCTGTCTGTCATTGGCT 3' ; R: 5' CATTTCGGTGGTACTGGCC 3'
DAT	*Slc6a3*	Solute carrier family 6, member 3. Dopamine transporter. F: 5' TGGATCCACTGCAACAACAC 3' ; R: 5' GAACAATGACCAGCACCAGG 3'
TH	*Th*	Tyrosine hydroxylase. Enzyme involved in the biosynthetic pathway of dopamine (and noradrenaline). F: 5' TGAAGCCAAAATCCACCACT 3' ; R: 5' GGTCAGGGTCAAACTTGGTG 3'
TPH2	*Tph2*	Tryptophan hydroxylase 2. Enzyme involved in the biosynthetic pathway of serotonin. F: 5' GAATGAAGTTGGTGGGCTGG 3' ; R: 5' TTCCTCCGTCCAAATGCTCT 3'
ARBP	*Arbp*	Attachment region binding protein. Serves here as a housekeeping gene. F: 5' CGACCTGGAGTCCAACTAC 3'; R: 5' ATCTGCTGCATCTGCTTG 3'
GAPDH	*Gapdh*	Glyceraldehyde-3-phosphate dehydrogenase. Serves as a housekeeping gene. F: 5' TGCACCACCAACTGCTTAG 3'; R: 5' GATGCAGGGATGATGTTC 3'
B2M	*B2m*	Beta-2 microglobulin. Serves as a housekeeping gene. F:5'GCTATCCAGAAAACCCCTCAA 3';R: 5' CATGTCTCGATCCCAGTAGACGGT 3'
PSMβ2	*Psmb2*	Proteasome subunit, beta type 2. Serves as a housekeeping gene. F: 5' AAATGCGGAATGGATATGAAT 3'; R: 5' GAAGACAGTCAGCCAGGTT 3'

90 samples (from 18 animals, 5 brain regions per animal – cortex, hypothalamus, hippocampus, cerebellum, midbrain) were analysed. Each gene of interest (see above) was analysed on a separate RT-qPCR plate. Data was normalised against the geometric mean of the values from 4 housekeeping genes (B2M, PSMβ2, GAPDH and ARBP) which were tested beforehand for generating similar results in both homozygotes and wild-type animals (Figure 14).

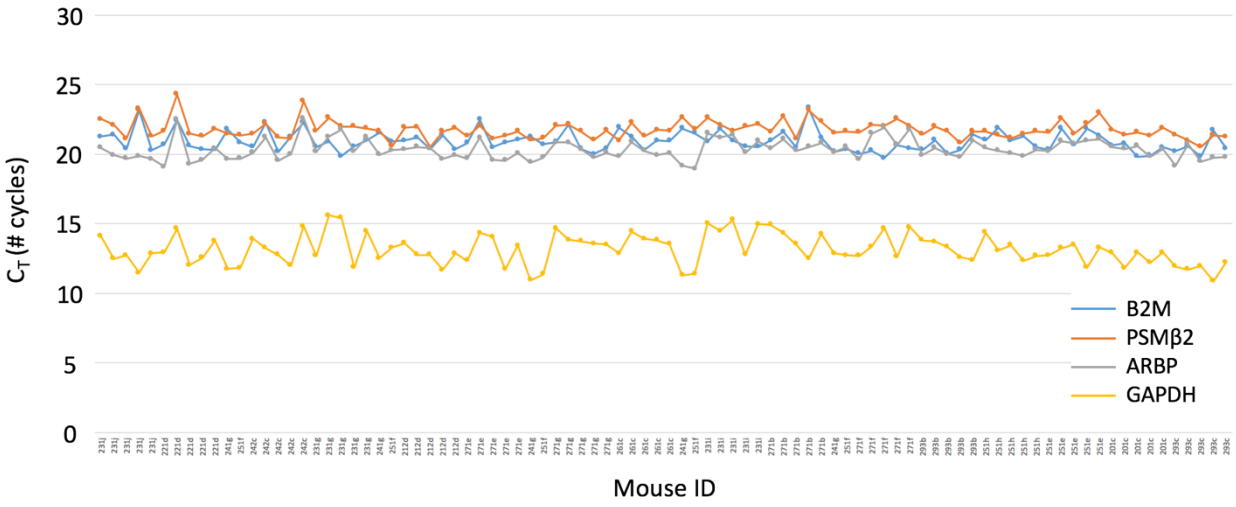


Figure 14: Evaluation of the reliability of housekeeping gene expression to serve as normalizing values. Each dot represents one sample from a given animal.

A total of 15µL was added per RT-qPCR well:

- 7.5 µL of Quantifast SYBRGreen PCR kit Master Mix (QIAGEN).
- 0.75 µL of adequate forward primer at 20 µM.
- 0.75 µL of adequate reverse primer at 20 µM.
- 6 µL of diluted cDNA (dilution: 7 volumes of nuclease-free water added to 1 volume of cDNA product).

The RT-qPCR cycle was run on a StepOnePlus real-time PCR machine (Applied Biosystems) using the StepOne software (version 2.1). The settings were as follows:

- quantitation – Comparative CT.
- SYBR Green reagents.
- Fast programme.

The PCR cycle was as follows:

- 95°C for 5 minutes
- 95°C for 10s
- 60°C for 10s

} x 40

- 76°C for 20s
- 95°C for 15s
- 60°C for 1 minute
- + 0.5°C ramp to 95°C for 15s.

D. Data analysis

Results were analysed and visualised using custom-made scripts in Matlab (The MathWorks Int., USA) and Microsoft Excel. Statistical analysis of the results was performed using SPSS software (SPSS Inc., IBM Analytics, USA). Tests used and their outcome are reported in the main text or figure legends. qPCR data was analysed in the following way: the 2^{-Ct} value was calculated for each measure, and divided by the geometric mean of the 2^{-Ct} values of the housekeeping genes.

3. RESULTS

A. Breeding outcomes

Breeding numbers, shown in Table 5, show that the *Sleepy6* homozygotes are viable, with numbers similar to WT mice. The WT ratio is 0.23, the Het ratio 0.56 and the Hom ratio is 0.21. Litter size was on average 6 pups.

Table 5: Number of mice of each genotype and sex within the Sleepy6 colony. Numbers collected over the period spanning from September 2016 to July 2018.

	WT	**HETEROZYGOTES**	**HOMOZOZYGOTES**
FEMALES	30	84	23
MALES	34	70	34
TOTAL	64	154	57

B. HPLC

As a first step, HPLC experiments were performed to explore possible differences in neurotransmitter levels between *Sleepy6* homozygotes (n=10) and wild-type control animals (n=8). The metabolites that were included in our analysis were serotonin (5-HT), 3,4-dihydroxyphenylacetic acid (DOPAC), 5-hydroxyindolacetic acid (5-HIAA) and homovanillic acid (HVA).

5-HIAA is one of the products of serotonin catabolism and its main metabolite (Cooper et al., 1996; Matsumoto et al., 1991) – see Annex 1. Serotonin is converted to 5-HIAA by the action of the enzymes monoamine oxidase (MAO) and aldehyde dehydrogenase (ALDH) (Chen et al., 2011). The levels of 5-HIAA within the cerebrospinal fluid are considered a marker of serotonergic neurons' activity (Matsumoto et al., 1991).

DOPAC and HVA are primary metabolites of dopamine – see Annex 2; after reuptake by the presynaptic neuron or by glial cells, dopamine is converted to DOPAC by the enzymes MAO and ALDH (Cooper et al., 1996; Meiser et al., 2013). Dopamine is also converted to HVA via the action of MAO and catechol-O-methyltransferase (COMT) (Cooper et al., 1996). COMT activity in the brain mainly occurs in glial cells, with no reported activity in presynaptic terminals of dopaminergic neurons (Meiser et al., 2013; Myöhänen et al., 2010). The accumulation of HVA and DOPAC in the brain have traditionally been used as a marker of the activity of dopaminergic neurons (Cooper et al., 1996).

The mobile phase used here was primarily adequate for the study of serotonin and its main metabolite 5-HIAA, as we had hypothesised a possible alteration in the serotonergic pathway, given the known interaction between VAMP2 and SERT (see Introduction). Therefore, the metabolites of which the levels could be measured were limited, as the retention time of a given analyte (the time it takes for it to elute from the injection site to the detection electrode) depends strongly on:

- its own chemical and physical properties.
- the chemical and physical properties of the mobile phase (e.g. its polarity)
- the nature of the adsorbent material within the HPLC column.

Any metabolite of which the detection peak is merged with the solvent front or which is not clearly separated from other substances cannot be analysed.

Figure 15 shows examples of chromatograms obtained after running a standard solution (see Methods) and a hippocampal sample. We were able to detect DOPAC and HVA in addition to 5-HT and 5-HIAA. Dopamine (DA), which had a short retention time with the chosen mobile phase (~ 2 min) was only detectable with standard solutions (Figure 15 a) and not with brain samples,

as it was then merged with the solvent front and the peaks of many components present in the brain samples themselves.

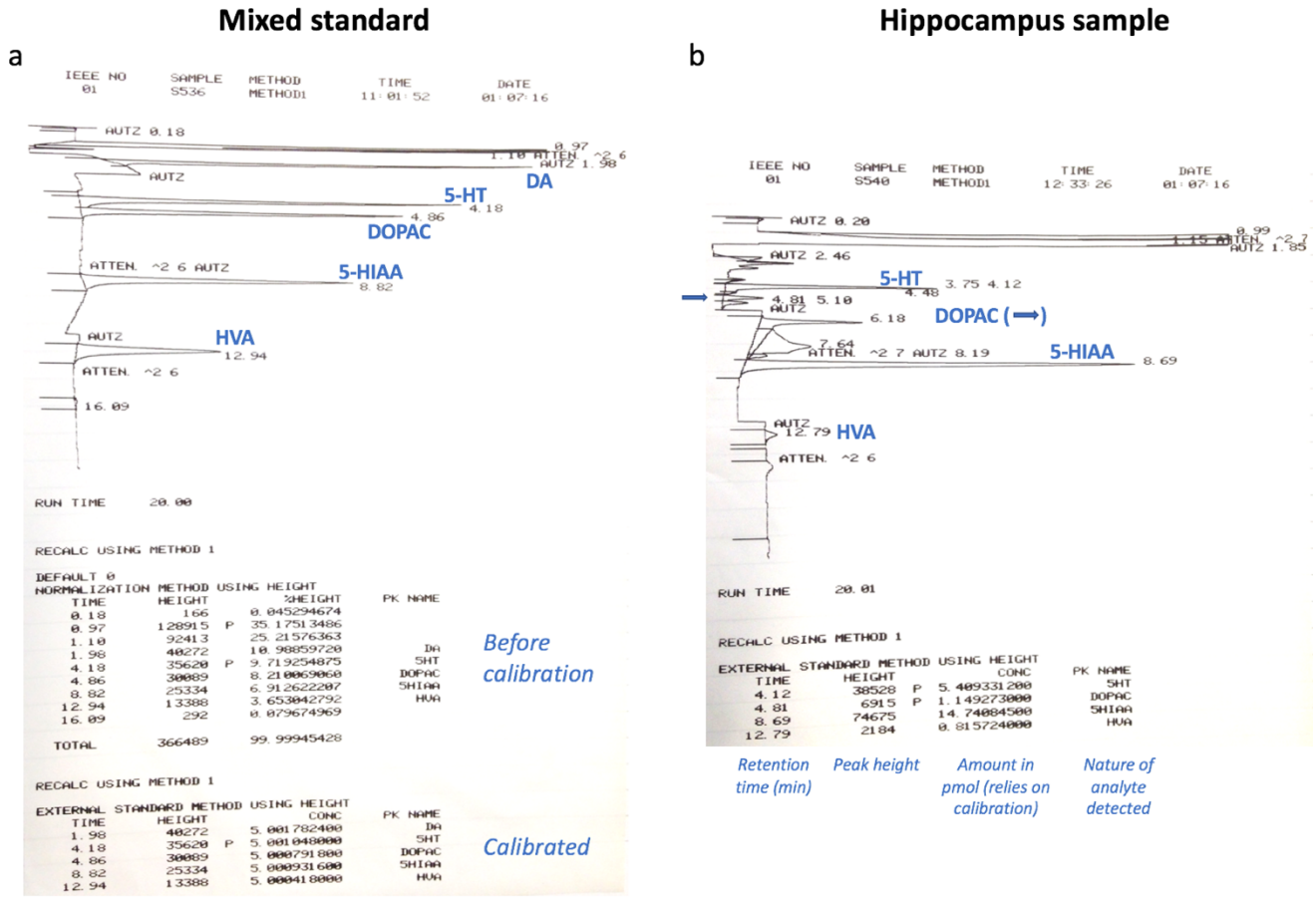


Figure 15: Examples of chromatograms obtained after running a mixed standard (a) or a hippocampus sample (b) in the HPLC apparatus. Chromatograms are printed from top to bottom (solvent front and analytes with shorter retention times at the top). The mixed standard contained dopamine (DA), serotonin (5-HT), 3,4-dihydroxyphenylacetic acid (DOPAC), 5-hydroxyindolacetic acid (5-HIAA), and homovanillic acid (HVA), all at concentration of 10^{-7} M. To simplify the analysis of brain samples, this concentration was directly converted to the equivalent quantity present in the 50 µL of solution injected, i.e. 50 x 10^{-6} x 10^{-7} =5 x 10^{-12} M = 5 pmol. As can be seen below the chromatogram from the standard, to obtain adequate values, calibration is necessary at the beginning of each day of experiments. The values to which each column corresponds is indicated at the bottom of panel b.

Results from all mice and analytes are shown in Figure 16.

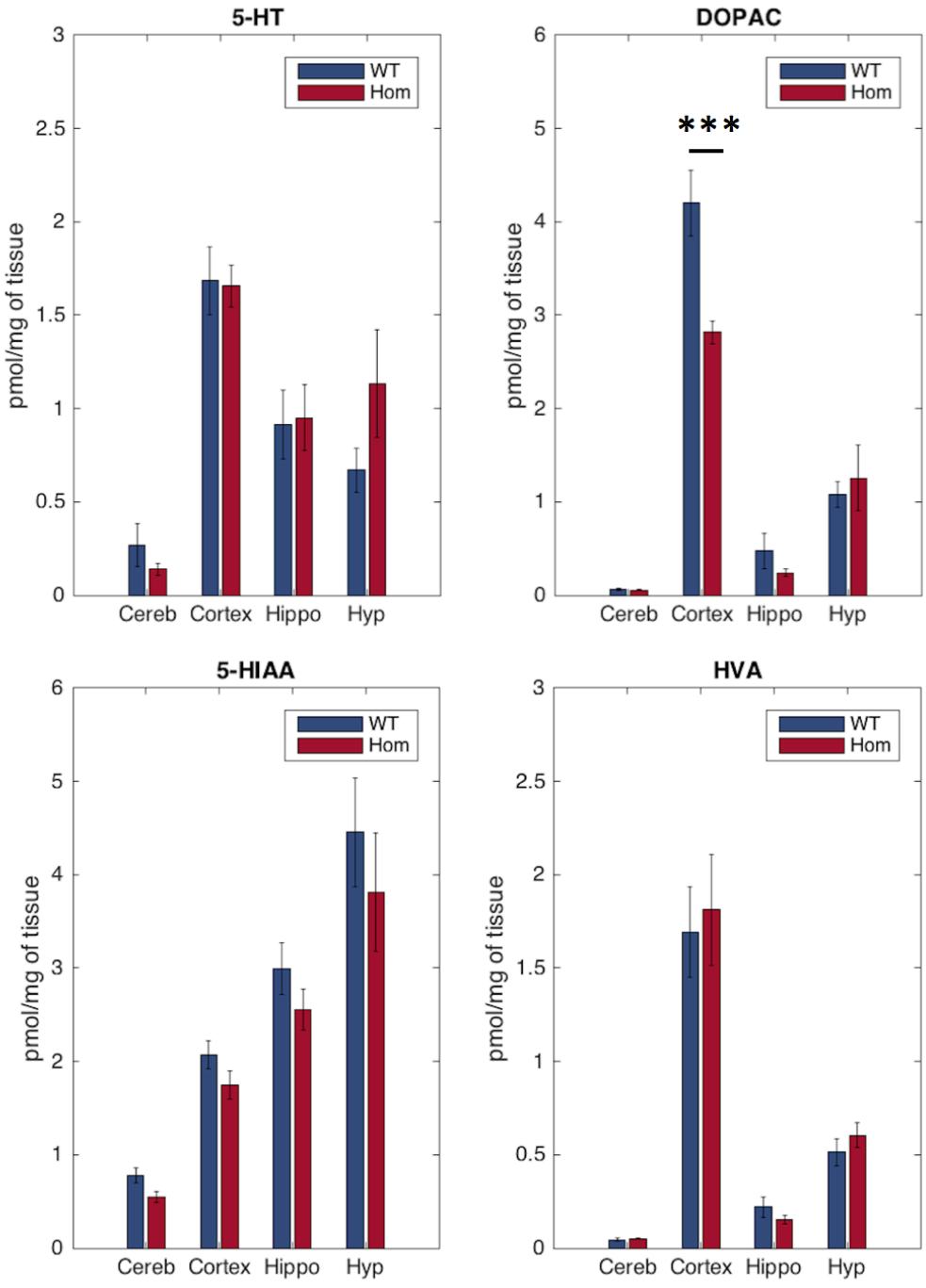


*Figure 16: HPLC results for serotonin (5-HT), 3,4-Dihydroxyphenylacetic acid (DOPAC), 5-hydroxyindolacetic acid (5-HIAA), homovanillic acid (HVA) in the cerebellum (Cereb), cortex, hippocampus (Hippo) and hypothalamus (Hyp). Results are expressed in pmol/mg as values obtained from chromatograms (pmol) are subsequently normalised against the amount of brain tissue (mg). Error bars represent the standard error of the mean (SEM). WT controls, n=8; Sleepy6 Homozygotes (Hom), n=10. ***p≤0.001. With a Bonferroni correction for multiple comparisons, the new level of significance is α=0.05/4=0.012.*

Main effects of brain regions (cortex, hypothalamus, hippocampus, cerebellum) and genotype (WT or homozygous for the VAMP2 mutation) were analysed using a two-way mixed-design ANOVA. When significant interactions were found, post-hoc independent samples t-tests were performed to investigate the effect of genotype further (but not of brain region). As the levels of metabolites are known to differ across brain regions (Wetherell et al., 1989), observing a main effect of brain region for all metabolites studied was expected; this was tested here as a control only.

- 5-HT: we only found a significant main effect of brain region ($F(3,48)=47.32$, $p<0.0001$), but not of genotype, with no significant interaction.
- DOPAC: we found significant main effects of brain region ($F(3,48)=132.66$, $p< 0.0001$) and genotype ($F(1,16)=5.28$, $p=0.035$). There was also a significant interaction of brain region*genotype ($F(3,48)=6.66$, $p=0.001$). The post-hoc independent samples t-test showed a significant difference between WT and homozygous animals in the cortex only ($t(16)=4.07$, $p=0.001$, Bonferroni correction, new alpha=0.05/4=0.0125).
- 5-HIAA: we only found a significant main effect of brain region ($F(3,48)=45.55$, $p<0.0001$), but not of genotype, with no significant interaction.
- HVA: we only found a significant main effect of brain region ($F(3,48)=60.02$, $p<0.0001$), but not of genotype, with no significant interaction.

C. qPCRs

In this set of experiments, each gene of interest was analysed separately – but all values were normalised against a set of 4 housekeeping genes (see Methods). The genes analysed are presented in Table 4. We chose genes coding for proteins interacting with VAMP2 (STX1A and SNAP25) as well as for enzymes involved in the biosynthetic pathways of serotonin and

dopamine, given our hypothesis that there could be an alteration in the serotonergic pathway, and given the preliminary results of the HPLC experiments (see Introduction and Methods). Results are presented in Figure 17.

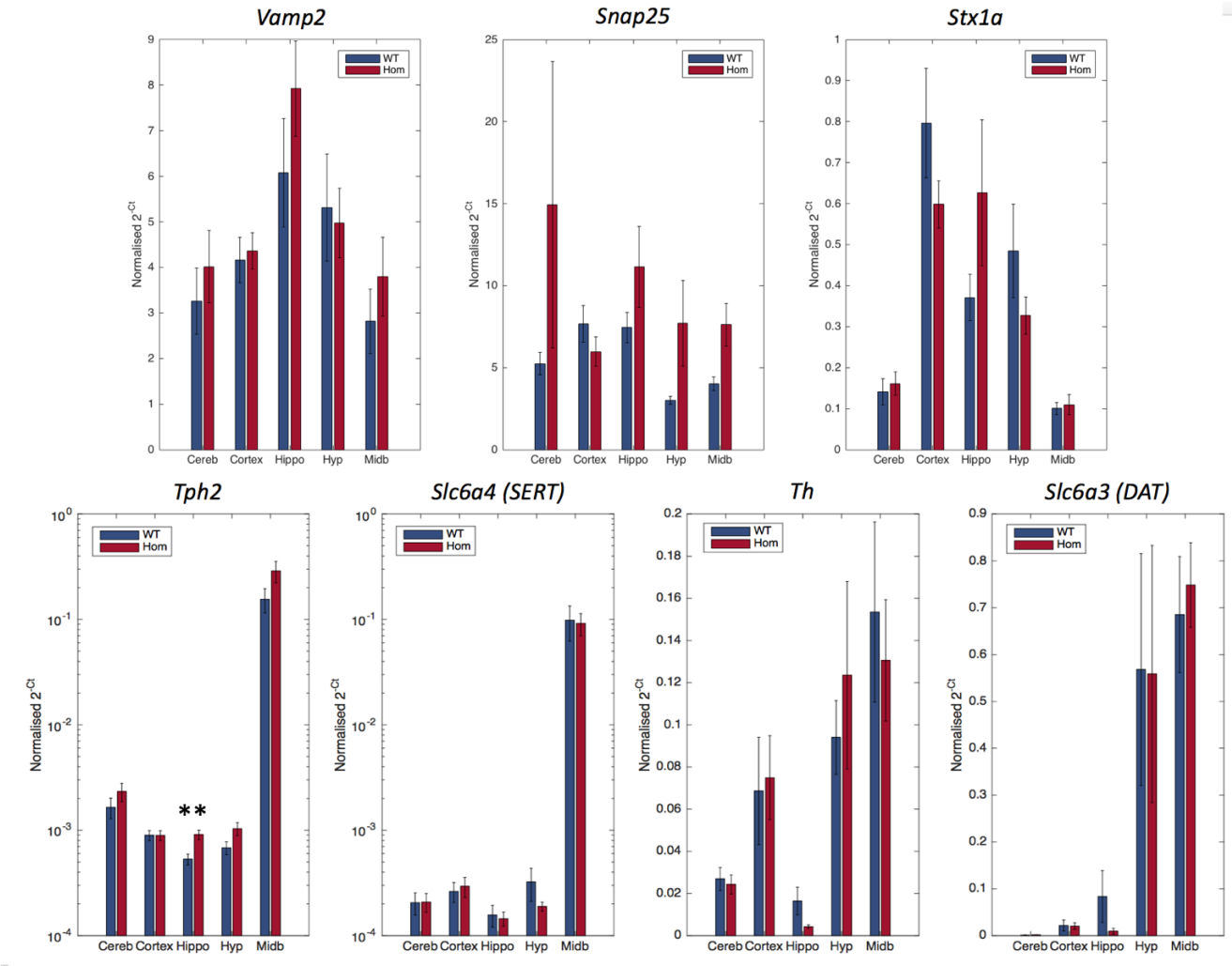


*Figure 17: RT-qPCR results for the Vamp2, Snap25, Stx1a, Tph2, Slc6a4 (SERT), Th and Slc6a3 (DAT) genes in the cerebellum (Cereb), cortex, hippocampus (Hippo), hypothalamus (Hyp) and midbrain (Midb). Error bars indicate the SEM. WT controls, n=8; Sleepy6 homozygotes (Hom), n=10. ** indicates p=0.006. Note that with a Bonferroni correction for multiple comparisons, the new level of significance is α= 0.05/5=0.01. Note that the graphs for Tph2 and SERT are presented on a log-scale.*

Main effects of brain regions (cortex, hypothalamus, hippocampus, cerebellum, but also the midbrain raphe nuclei - where serotonergic neuron bodies are located) and genotype were

analysed using a two-way mixed-design ANOVA. For all genes (except *Snap25*) a significant main effect of brain region was found. For no gene, a significant main effect of genotype was found.

For *Stx1a* and *Tph2*, a significant main interaction of brain region*genotype was found (*Stx1a*: $F(4,62)=2.55$, $p=0.048$; *Tph2*: $F(4,64)=2.60$, $p=0.044$). For *Tph2* only, a significant difference between WT and homozygous animals was found in the hippocampus ($t(16)=-3.15$, $p=0.006$). With a Bonferroni correction (new $\alpha=0.05/5=0.01$) the difference remains significant. However, *Tph2* being mainly expressed in serotonergic neuron bodies, which are located in the midbrain, finding a difference in the hippocampus is difficult to interpret. Indeed, although other studies have found an expression of *Tph2* in various brain areas such as the midbrain raphe nuclei, cortex, hippocampus, striatum and cerebellum using RT-qPCR techniques (Gutknecht et al., 2009), these authors as well as other rodent studies, using *in-situ* hybridisation, found that *Tph2* was almost exclusively expressed in the raphe nuclei, where most serotonergic neuronal bodies are (Gutknecht et al., 2009; Malek et al., 2005; Patel et al., 2004). Accordingly, we find that the levels of *Tph2* are much higher in the midbrain than in any other of the brain regions analysed here (Figure 17). Similarly, our results regarding the serotonin transporter are in accordance with the literature, which reports that SERT is exclusively expressed in the midbrain and hindbrain raphe nuclei complex (Bengel et al., 1997).

4. DISCUSSION

Given the phenotypes observed in the *Sleepy6* homozygous mice, as compared to SERT knock-out mice (Table 1), and knowing the interaction between VAMP2 and SERT (Müller et al., 2014), we hypothesised that there could be alterations in the serotonergic pathway in the *Sleepy6* homozygotes. Yet, the preliminary results obtained from HPLC and RT-qPCR experiments did not support this hypothesis. The only significant and possibly relevant difference observed between *Sleepy6* homozygous animals and their wild-type littermates was in the levels of DOPAC in the cortex (Figure 16). The negative results obtained from the HPLC and RT-qPCR protocols could either reflect that the metabolites and genes studied are not those affected in *Sleepy6* mice, or that the serotonergic and/or dopaminergic pathways are not impaired. If additional genes of interest were to be studied, using an unbiased method such as RNA sequencing should be evaluated.

A. Beyond serotonergic and dopaminergic pathways

Given that VAMP2 is widely expressed throughout the brain and is not linked to the release of a specific neurotransmitter, it is plausible that the mutation occurring in *Sleepy6* mice affects various systems. It is possible that the absence of differences in our analyses stems from a small cohort of animals correlated to small effect sizes; indeed, given the overall healthy phenotype of *Sleepy6* mice, it is likely that effects on major neurotransmitter systems – if they exist – are mild. Such a hypothesis would be plausible with the numerous links between neurotransmitter pathways and sleep-wake architecture (see Chapter 1, section 1.E) and in line with other striking phenotypes of the *Sleepy6* homozygotes.

For instance, it has been shown that GABA levels in the pontine reticular formation are positively associated with increased wakefulness and decreased sleep time (Watson et al., 2008). Additionally, decreasing levels of GABA can lead to shorter anaesthesia-induction time when using isoflurane (Vanini et al., 2008), while blocking $GABA_A$ receptors leads to longer delays for animals anesthetised with isoflurane to wake up (Flint et al., 2010). Experimental observations revealed that *Sleepy6* homozygotes need much longer to be fully anesthetised and to wake up following anaesthesia; it may therefore be of interest to investigate the GABAergic pathway in those mice.

Similarly, drugs (e.g. zolpidem, diazepam) that decrease the release of acetylcholine in the pontine reticular formation (in the rat) have also been shown to hinder REM sleep and cause an increase in EEG delta power (Hambrecht-Wiedbusch et al., 2014); given the decreased REM sleep time and increase in EEG slow frequencies (see Chapter 4) in *Sleepy6* homozygotes, an alternative hypothesis is that differences in the cholinergic pathway may occur.

B. Adenosine as a correlate to evaluate sleep need in *Sleepy6* mice?

Adenosine is a by-product of adenosine triphosphate (ATP) and its levels increase with time spent awake, and decline during natural sleep (Dworak et al., 2010). More specifically, adenosine levels have been shown to increase at different rates across brain regions during wake, possibly related to the recruitment of such regions during wakefulness and how metabolically active they are (Porkka-Heiskanen et al., 1997; Watson et al., 2010). Levels of adenosine, and more specifically its rate of release (rather than its accumulation), have been proposed to be a function of sleep need and to modulate EEG slow-wave activity (Benington and Heller, 1995). As EEG slow-wave activity is commonly used as a biomarker of sleep pressure (Borbély et al., 1981; Dijk et al., 1987), and given that *Sleepy6* homozygotes show increased

waking time compared to their wild-type littermates, it would be informative to measure adenosine levels across a 24-h day. This could highlight whether such levels accumulate or decrease at similar rates in homozygous and WT mice, and could help understand whether *Sleepy6* homozygotes sleep less because of a decreased homeostatic need for sleep.

C. Appetite-regulating hormones and sleep architecture

The initial characterisation of the *Sleepy6* homozygotes revealed a significantly reduced body weight (Heise, 2015). VAMP2 function is indeed not limited to the central nervous system and it also plays a role in endocrine and intestinal cells (Némoz-Gaillard et al., 1998), for instance in the exocytosis of glucagon-like peptide 1 from intestinal L cells (Li et al., 2014), or in insulin secretion in pancreatic islets and beta cell lines (Regazzi et al., 1995; Wheeler et al., 1996). It also plays a role in glucose uptake by enabling translocation of the glucose transporter GLUT4 to the plasma membrane (Thurmond, 2013). Interestingly, well-known metabolically-impaired mouse models such as the *ob/ob* mice (leptin-deficient and obese) and *db/db* mice (leptin-resistant and obese) show sleep abnormalities with increased NREMS time but impaired sleep consolidation (*ob/ob*) or similarly, shorter bouts of both wakefulness and NREMS and increased NREMS & REMS time (*db/db*) (Laposky et al., 2006, 2008). The authors of the latter studies argue that leptin signalling plays a crucial role in sleep regulation and architecture (Laposky et al., 2008). Strikingly, not only are all these effects opposite to those observed in *Sleepy6* mice (see Chapter 4), but a study also showed that *db/db* mice presented abnormalities in SNARE proteins in islet cells – with increased levels of SNAP25 and VAMP2 and decreased levels of STX1A (Do et al., 2014). It is therefore possible that the sleep phenotype of *Sleepy6* homozygotes is indirectly linked to the *Vamp2* mutation via the role of VAMP2 in metabolic regulation, for instance insulin secretion. Therefore, in addition to testing the pathways of common

neurotransmitters, it may be informative to investigate the levels of (and the response to) hormones such as insulin, leptin and ghrelin.

D. A possible alteration in gliotransmission

The phenotypes observed in *Sleepy6* animals could also stem from other mechanisms, such as gliotransmission, which has also been shown to modulate cortical slow oscillations (Fellin et al., 2009). Another study also showed that inhibiting the release of gliotransmitters selectively in astrocytes through a mutation in *Vamp2* (dominant-negative form – 'dnSNARE') led to a possible attenuation in sleep-pressure accumulation (Halassa et al., 2009). Those latter results may however be confounded as they relied on the assumption that the dnSNARE transgene expression is specific to astrocytes. However, a later study showed that this may not be the case, reporting widespread expression of the dnSNARE form of *Vamp2* in cortical neurons (Fujita et al., 2014).

E. Limitations

It may be argued that having found no major differences in the two pathways investigated here is a positive finding: too many alterations would raise the question of whether the *Sleepy6* line is relevant to study sleep homeostasis. However, this links to some limitations of the experiments presented here. Firstly, if small effect sizes are to be expected, the number of mice should be increased accordingly; and yet, our group sizes were limited as we were initially expecting larger effects. It was also shown that 5-HT and 5-HIAA levels undergo circadian variations (Pietraszek et al., 1992), which were not specifically controlled for in this study, although mice were culled in a similar time window.

Additionally, higher-throughput methods such as RNAseq would have provided us with a much wider and unbiased overview of which pathways may be differentially expressed: while the qPCR approach requires to select candidate pathways, transcriptomics approaches are unbiased in that they allow to look at the expression of all genes at once, and may thus point towards changes in pathways that would not have been suspected *a priori*. The choice of HPLC – followed by RT-qPCR – was initially driven by the idea to perform a pilot study, where we expected large effects, and by our knowledge of key neurotransmitter systems affecting sleep and of interactions of VAMP2. It appears, however, that we did not know as much as we first thought.

Instead, to gain further insights into the possible alterations caused by the mutation in *Vamp2* present in *Sleepy6* mice, the complementary but different approach of behaviour testing was chosen. Depending on their outcome, behavioural tests can indeed highlight specific impairments and provide clues about the specific neural pathways that could be altered, which will be discussed further in Chapter 3.

CHAPTER 3: Behavioural characterisation of *Sleepy6* mice

1. INTRODUCTION

One defining phenotypic feature of *Sleepy6* homozygous mice is a reduction of total sleep time. This raises the question of whether their decreased sleep stems from a reduced need for sleep, or reflects a chronic sleep deprivation due to an inability to initiate or maintain sleep episodes. To evaluate whether *Sleepy6* mice may indeed be chronically sleep-deprived, we wanted to evaluate their learning and memory capacity, as both are known to be critically affected by sleep deprivation (Alhola and Polo-Kantola, 2007; Patti et al., 2010; Prince and Abel, 2013).

Both NREMS and REMS have been shown to play a critical role in learning and memory processes (Ackermann and Rasch, 2014; Rasch and Born, 2015) and can impact memory acquisition, consolidation or retrieval processes (Rasch and Born, 2013; Stickgold and Walker, 2013). The exact roles of REMS and NREMS in memory and learning are still unclear and controversial, with conflicting results (Rasch and Born, 2013). REMS has traditionally been linked to memory consolidation (Horne and McGrath, 1984) and REMS deprivation has been shown to impair memory formation on complex – rather than simple – tasks such as those involving difficult mazes (Beaulieu and Godbout, 2000; Hars and Hennevin, 1983). Some results also showed a possible role for REM sleep in procedural memory processes (Smith, 1995), and accordingly, the "dual process hypothesis" assumes that REM sleep primarily serves the consolidation of non-declarative memories (i.e. that do not require conscious recollection, for

instance procedural or emotional memories) while slow-wave sleep would be necessary for declarative memories (i.e. conscious recollection of events and facts) (Ackermann and Rasch, 2014). This hypothesis is however judged simplistic by some, as if indeed experimental data support the critical role of NREMS (in particular slow-wave sleep) in declarative memory consolidation, procedural memory may also depend on NREMS – and reversely, REMS may also improve declarative memory (Diekelmann and Born, 2010). It has therefore been proposed that instead of associating NREMS/slow-wave sleep and REMS to specific types of memories, they may be differentially associated with different forms of memory processing (for instance, cellular level *versus* network level) (Cairney et al., 2015; Stickgold, 2013).

Various mechanisms by which sleep deprivation exerts deleterious effects on cognitive processes have been proposed, including the alteration of long-term potentiation (LTP) processes in the hippocampus (Calais et al., 2015; Ravassard et al., 2015). Memory impairments could also be mediated by other behavioural effects of sleep deprivation, such as decreased attention and motivation, longer reaction times, decreased exploratory behaviour or increased stress (Alhola and Polo-Kantola, 2007; Cedernaes et al., 2015; Rimmele and Tambini, 2015).

Following a forward genetics protocol, many behavioural tests can be performed to assess learning and other cognitive processes, and it is important to choose the tests depending on the question asked (Rodriguiz and Wetsel, 2006). Specific behaviour tests – depending on their outcome – can direct towards specific altered pathways. For instance, fear conditioning has been shown to be hippocampus-dependent, whereby the consolidation and acquisition of memories linked to the conditioning context are mediated by the hippocampus, while other brain structures are involved in memory storage (Sanders et al., 2003). This is of interest given that previous results from fear conditioning tests suggested that freezing behaviour was absent in *Sleepy6* homozygotes: while their wild-type littermates displayed a freezing period following a foot shock, *Sleepy6* mice immediately entered a marked hyperactive period (Heise, 2015). It is

important to bear in mind, however, that many behavioural phenotypes and abnormalities can impact the performance observed during learning and memory tasks (Rodriguiz and Wetsel, 2006).

Some preliminary results (Heise, 2015), using novel object recognition run in the home cage (which is not the norm), revealed that *Sleepy6* homozygous mice may display intact learning and memory, while spending less time interacting with the objects. On the other hand, the Y-maze task revealed that *Sleepy6* homozygotes spent a shorter amount of time in the novel arm and entered the novel arm less frequently than their wild-type littermates. Taken together, these results suggested that there may be some conserved memory processes but disturbed spatial memory, that there may be an attention deficit or a lack of exploratory activity. To further test spatial and contextual memory, we therefore chose to perform an object-in-place recognition (OIP) task. Additionally, the novel object task mentioned above (Heise, 2015) used a non-classical set-up: only one object was presented to the animals during the sample phase, and was presented again in a first test phase, then replaced by a new object in a second test phase. We chose to replicate the novel object recognition (NOR) experiments using a standard set-up (two objects presented at once –see Methods). The NOR test is particularly useful to study recognition memory in mice and can highlight impairments in short-term or long-term memory depending on the time interval separating the initial presentation of the objects and the test (Ennaceur and Delacour, 1988). However, if memory deficits are detected via this test, additional testing is required to investigate the deficit in a more detailed and specific manner (Rodriguiz and Wetsel, 2006). The OIP test is also useful for evaluating impairments in long-term and short-term memory as the delay between initial exposition and testing can be variable too; the OIP task is also a simple and useful way to evaluate contextual memory more specifically (Lesburguères et al., 2017; Mumby et al., 2002).

These two tasks are of relevance to characterise learning and memory in the *Sleepy6* mice as both rely on the innate preference for novelty, but are not inherently stressful; other simple tasks such as the Morris water maze or the contextual fear conditioning also allow to evaluate memory for novel objects and spatial context in rodents, but they also involve aversive and stressful events during training (Vogel-Ciernia and Wood, 2014).

The choice of the novel object recognition and object-in-place recognition tasks was also oriented by the will to confirm the preliminary results obtained, before making assumptions on the possible processes involved in the deficits observed. Following those two tasks, it was also decided to look at the levels of expression of some immediate early genes (*Arc* and *c-Fos*) in the hippocampus in *Sleepy6* homozygous and WT mice following exposition to new objects. Such genes have indeed been shown to be markers of neuronal activity induced by learning and memory processes (Heroux et al., 2018). *Arc*, for instance, has been linked to memory consolidation processes in particular, rather than memory acquisition (Czerniawski et al., 2011; Guzowski et al., 2000). This would therefore provide additional information on the possible underlying mechanisms of the cognitive differences observed between *Sleepy6* homozygotes and their wild-type littermates.

2. MATERIALS AND METHODS

A. Animals and housing conditions

All procedures were performed in accordance with the Animals (Scientific Procedures) Act 1986 and the University of Oxford's guidelines, under Project License 30/3371, and a personal license (PIL I8D8D5669).

Sleepy6 animals (homozygous for the *Vamp2* mutation) and wild-type littermate controls (both males and females) were used for this experiment. Animals were no younger than 8 weeks of age and no older than 6 months of age.

Animals were kept at 22±2 °C, under a 12h:12h light-dark cycle, with food and water available *ad libitum*. Mice were co-housed in groups of 2 to 6 animals, except for 8 males which were singly-house, as only males co-housed since birth could be kept together. Cages measured 25cm x 35 cm (12 cm x 35 cm for singly-housed animals), and were covered with an open wired grid. Cages were kept in light-tight ventilated chambers (LTC), fitted with multiple white LEDs (100-150 lux during the light phase, measured at the cage floor). Males and females were kept in separate chambers. Following transfer from the colony, mice were given a week to habituate to their new home cage prior to starting any experiment.

Two cohorts were used:

- a first "pilot" cohort consisted of 18 animals: 8 homozygous mice (5 males & 3 females); 9 wild-type littermate control (3 males & 6 females). The numbers of males and females of each genotype were unequal across groups as they depended on the breeding outcomes.
- a larger cohort was then subsequently used, consisting of 49 animals: 21 homozygous mice (9 males & 12 females); 28 wild-type littermate controls (14 males & 14 females).

All analyses were performed separately for each cohort and numbers were not pooled together.

The number of animals for the pilot cohort was primarily decided depending on the animals available from the newly generated colony, with the aim to create a larger cohort subsequently. The numbers in this larger cohort were decided based on an average of 10 animals per group, above or similar to the numbers frequently used in behaviour testing in the literature (Palchykova et al., 2006; Sanderson et al., 2011; Tam et al., 2016).

B. Novel object recognition task

Animals were habituated to the white arena in which testing was to be performed (20cm x 20cm x 20cm, light levels 80-100 lux, see Figure 18a), for 10 minutes on two consecutive days before the start of the behaviour testing. No objects were placed in the arena at this point.

Both the "sample" and "test" phases were performed in the first 6 h of the light phase using the white box. The sample phase consisted in exposing the animals to two identical objects for 10 minutes, after which animals were returned to their home cage. After a delay of 5 min, 1 hour or 24 hours (to evaluate both short and longer term memory), the animals were exposed to two new objects: one strictly identical in appearance to the ones from the sample phase (i.e. 3 identical objects were used in total, to avoid bias due to odour recognition), and one different. This test phase lasted for 3 minutes (see Figure 18). The position and nature of the new objects were randomised across mice, to ensure that measures would not be biased by a preference for one corner of the arena or for one type of object over the other. The objects and the arena were carefully cleaned with 70% ethanol between each phase and each animal. Objects were fixed to the floor of the arena using small hoop-and-loop stickers. Objects used were of various colours, sizes, shapes and materials (e.g. small bottles, light bulbs, hard-plastic toys, etc.) with a base area no larger than $7cm^2$. This enabled the objects to be recognised based on visual and non-visual cues. Videos were recorded using a web camera fixed 35 cm above the arena, and using an *EZ Grabber* device and software.

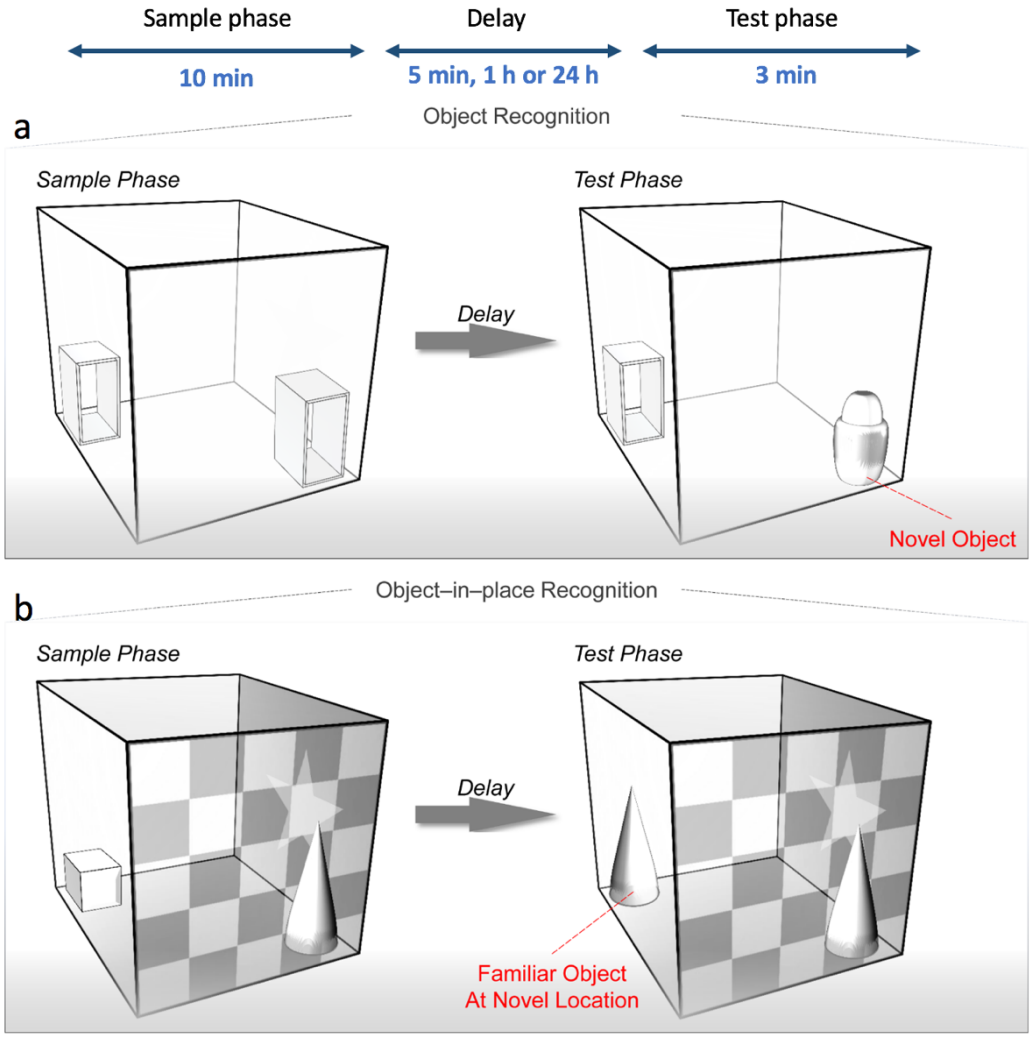


Figure 18: Experimental set up for the novel object recognition (a) and the object-in-place ("spatial recognition") tasks (b). While the object recognition box is made of entirely white & non-transparent material, the object–in-place task takes place in a box of which the four sides display different patterns. Background images by Dr Eric Tam.

C. Object-in-place recognition task

The cohorts of animals were the same as the ones used for the novel object recognition task (pilot and larger cohorts), except for one homozygous male from the pilot cohort, which showed signs of ill health during the object recognition experiment. As this animal showed no such sign

5 weeks earlier when the novel object recognition task was performed, his scores were still included in the NOR results (but not the OIP).

Animals were habituated to the object-in-place recognition arena, kept empty, for 10 minutes one day before being exposed to any objects. The arena, made in transparent acrylic, was customized by attaching on the outside distinct wall-papers, to allow for discrimination between the 4 corners: one side displayed a white star on a black background, one side displayed a checker-board pattern with alternating 4 cm x 4 cm black and white squares, one side was kept uniformly white and the last side was uniformly black with a white triangle (Figure 18 b).

Both the sample and test phases were performed in the first 6 h of the light period. The sample phase consisted in exposing the animals to two distinct objects for 10 minutes, after which animals were returned to their home cage. After a delay of 5 min, 1 h or 24 h, the animals were exposed to two new objects, both identical in appearance to one object from the sample phase, i.e. 3 identical objects were used in total, to avoid bias due to odour recognition (Figure 18 B). This test phase lasted for 3 minutes. Here as well, the position of the novel location was randomised across mice, to ensure that measures would not be biased by a preference for one corner of the arena.

The box and objects were thoroughly cleaned with 70% ethanol between each animal and phase. Videos of both the sample and test phases were recorded using an *EZ Grabber* device and software.

D. Video analysis

All videos were subsequently analysed using the ANY-maze software (Stoelting Co., Ireland), which allowed automated tracking of the animals. All tracking was however supervised, to check

that the software was able to accurately track the animal's movements. For each video file, the 20 cm x 20 cm floor of the arena was delimited, as well as the zone around each object.

E. Data analysis

Data was extracted from the ANY-maze software and subsequently analysed using Microsoft Excel and Matlab (The MathWorks Inc., USA, version R2017b).

Memory performance for the novel object recognition test was expressed as a recognition ratio, or "score", equal to: $\frac{T_{new}-T_{old}}{T_{new}+T_{old}}$, where T_{new} and T_{old} represent the time spent interacting with the new and old (familiar) object, respectively, during the 3 min of the test phase. The recognition ratio was calculated in a similar manner for the object-in-place recognition test, but T_{new} and T_{old} then represent the time spent interacting with the objects at novel *versus* familiar locations.

A score of 0 indicates that the animal shows no preference for any of the objects/locations; a positive score shows a preference for the novel object/location, whereas a negative score indicates a preference for the familiar object/location.

F. Dissections for *cFos* and *Arc* expression measurements

On the day of the dissections, for the pilot cohort, n=12 animals (3 of each sex and genotype) were exposed to two pairs of identical objects simultaneously for 10 minutes. In the second cohort, n=29 animals (16 females – 8 WT, 8 Homozygotes ; 13 males – 7 WT, 6 Homozygotes) were exposed to objects in a similar manner to those in the pilot cohort, and n=12 mice (3 of each sex and genotype) were control animals, i.e. they were not exposed to any new object prior to being culled.

All objects were unknown to the mice. The 4 objects were placed in the 4 corners of the white arena used for the NOR task. The animals were then singly-housed in clean cages for 45 minutes and culled around ZT4 by cervical-dislocation.

The brain was sliced using a stainless-steel adult mouse brain matrix with 1-mm coronal slice intervals (Zivic Instruments, USA) and blades. The matrix and blades were kept on wet ice and thoroughly cleaned between animals using an RNase decontamination solution (RNaseZap™, Thermo Fisher Scientific Inc., UK).

A sample of hippocampus was taken from an adequate slice placed in PBS (Sigma Aldrich) – see Figure 19. Hippocampus samples were placed in RNAase-free Eppendorf tubes and kept on dry ice. Samples were stored at -80°C until the RNA extraction was performed.

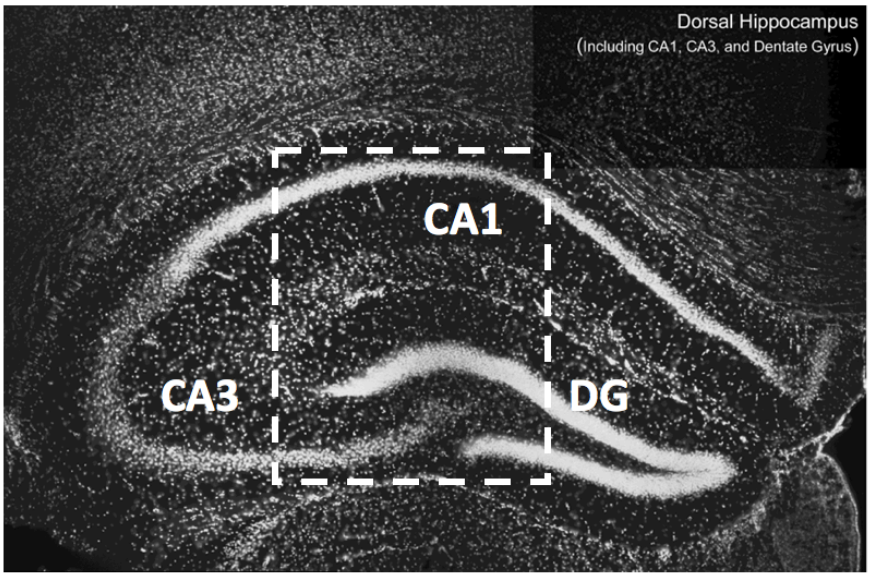


Figure 19: Brain section of a WT animal showing the hippocampus. The dashed line indicates where samples were taken. The section was stained with DAPI. Slice preparation and image performed by Dr Eric Tam. DG = Dentate Gyrus.

G. RNA extractions, cDNA synthesis and RTqPCR

Those steps were performed exactly as in the qRT-PCR described in Chapter 2. cDNA synthesis, however, was performed with Superscript IV VILO (ThermoFisher Scientific) instead of qScript (QuantaBio, USA). Normalisation of the results was done against 3 housekeeping genes (*Arbp, Gapdh, Psmb2*).

The primers used had the following sequences:

- ARC-forward: 5' GCT GAG CTC TGC TCT TCT TCA 3'
- ARC-reverse: 5' GGT GAG CTG AAG CCA CAA AT 3'
- cFOS-forward: 5' ATC GGC AGA AGG GGA AAG TAG 3'
- cFOS-reverse: 5' GCA ACG CAG ACT TCT CAT CTT CAA G 3'

The results were analysed as in Chapter 2 (calculation of 2^{-Ct} values, divided by the geometric mean of the 2^{-Ct} values of the housekeeping genes) on Microsoft Excel and Matlab (The MathWorks Inc., USA), and statistical tests were performed using SPSS Statistics (IBM Corp, Version 23, Release 23.0.0.2).

3. RESULTS

A. Pilot cohort

i. Novel object recognition task

To investigate the learning and memory ability of the *Sleepy6* mice, simple object and spatial recognition tasks were carried out. The recognition ratios obtained (see the Methods section for a description of the calculation) following novel object recognition (NOR) testing in the pilot cohort revealed that mice homozygous for the *Sleepy6* mutation showed overall no preference for the new objects (score ≈ 0, see Figure 20), or even tended to explore the familiar object more than the novel object (score < 0, in females, 24-h delay). However, a mixed-design ANOVA revealed no significant main effect of delay ($F(1,13)=0.970$, $p=0.343$), and no significant main effect of sex ($F(1,13)=1.141$, $p=0.305$) nor of genotype ($F(1,13)=1.767$, $p=0.207$). The trends appearing on Figure 20 may not reach significance because of the low number of animals in each group.

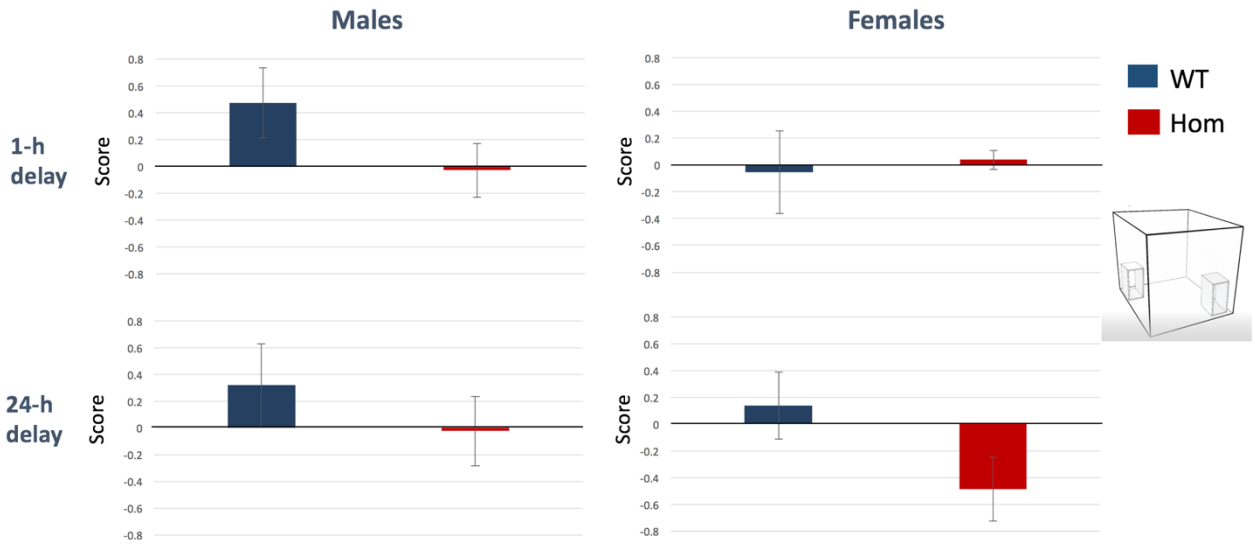


Figure 20: Performance for the novel object recognition task, expressed as a score (see Methods) in WT and Homozygous male and female mice. Mean ± SEM. n(♂, WT)=3, n(♂, Hom)=5, n(♀, WT)=6, n(♀, Hom)=3. A mixed-design ANOVA revealed no significant main effects of delay, sex or genotype (see text).

ii. Object-in-place recognition task

The object-in-place (OIP) recognition test allows to study the ability of the mice to make an association between an object and its surroundings (Barker and Warburton, 2015). Similarly to the novel object recognition task, the OIP test showed that *Sleepy6* mice, both males and females, seemed to manifest no preference for a familiar object placed in a novel location (Figure 21). In WT mice, however, results appeared more nuanced, with only males showing a possible preference for the object placed in the novel location after a relatively short delay (1 h) but not 24 h. Importantly, none of these observable trends reached significance: a mixed-design ANOVA revealed no significant main effect of genotype ($F(1,12)=1.298$, $p=0.277$) nor gender ($F(1,12)=0.111$, $p=0.744$), and no main effect of delay ($F(1,12)=0.057$, $p=0.815$). Finally, a mixed design ANOVA combining the data from both the NOR and OIP tasks showed no significant difference depending on the type of test performed ($F(1,12)=0.002$, $p=0.962$).

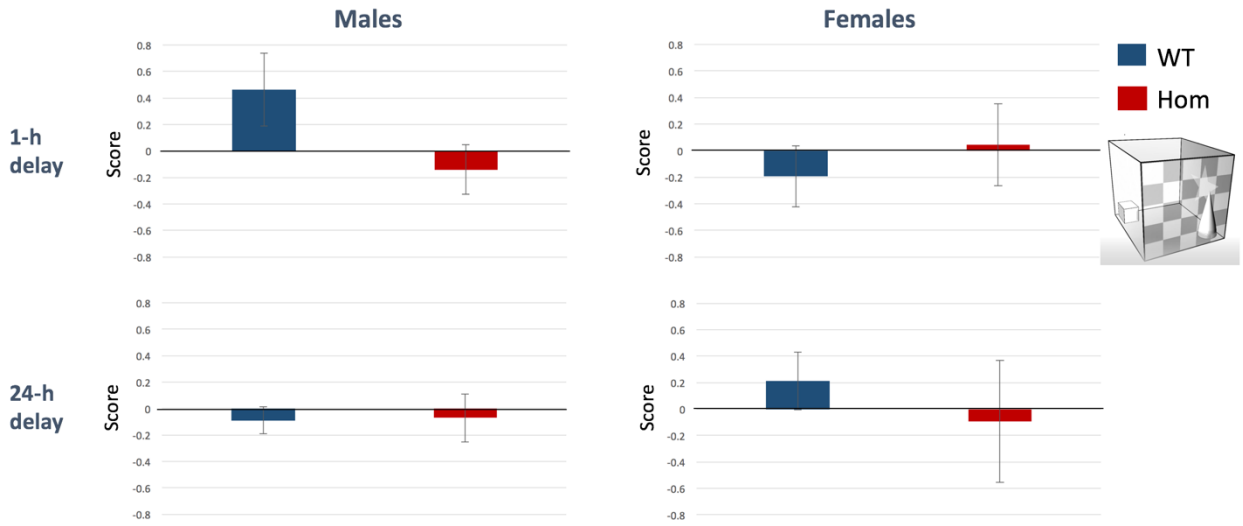


Figure 21: Performance for the object-in-place recognition task, expressed as a score (see Methods) in WT and Homozygous male and female mice. Mean ± SEM. n(♂, WT)=3, n(♂, Hom)=4, n(♀, WT)=6, n(♀, Hom)=3. A mixed-design ANOVA revealed no significant main effects of delay, sex or genotype (see text).

As the number of animals used in this pilot study was small, experiments were therefore replicated with a larger cohort of mice. The number of animals per group (≈10) was based on previous experience and feasibility. Additionally, as it seemed that the difference may lie primarily in the ability of the *Sleepy6* mice to perform well – in comparison to wild-types – for shorter delays, a 5-min delay testing was added. Indeed, the object-in-place task reveals that just as *Sleepy6* mice, WT mice may not perform well when a day separates the sample and test phases (24-h delay, Figure 21). The question was therefore to see whether a stronger difference could be observed between genotypes for delays shorter than 1 h.

B. Main experiment

i. Novel-object recognition task

When replicating the tasks with a larger cohort of animals, results still revealed nuanced differences (Figure 22). The trends, however, appeared in line with the ones observed in the pilot cohort:

- *Sleepy6* mice seem to show little preference for the novel object, especially in comparison to their wild-type littermates.
- both WT and *Sleepy6* mice seem to perform poorly at the task when the delay between the sample and test phases reaches 24 h.

No significant effects were observed with a mixed design ANOVA (Genotype: $F(1,44)=1.765$, $p=0.191$; Sex: $F(1,44)=0.107$, $p=0.745$;Delay: $F(2,88)=2.356$, $p=0.101$).

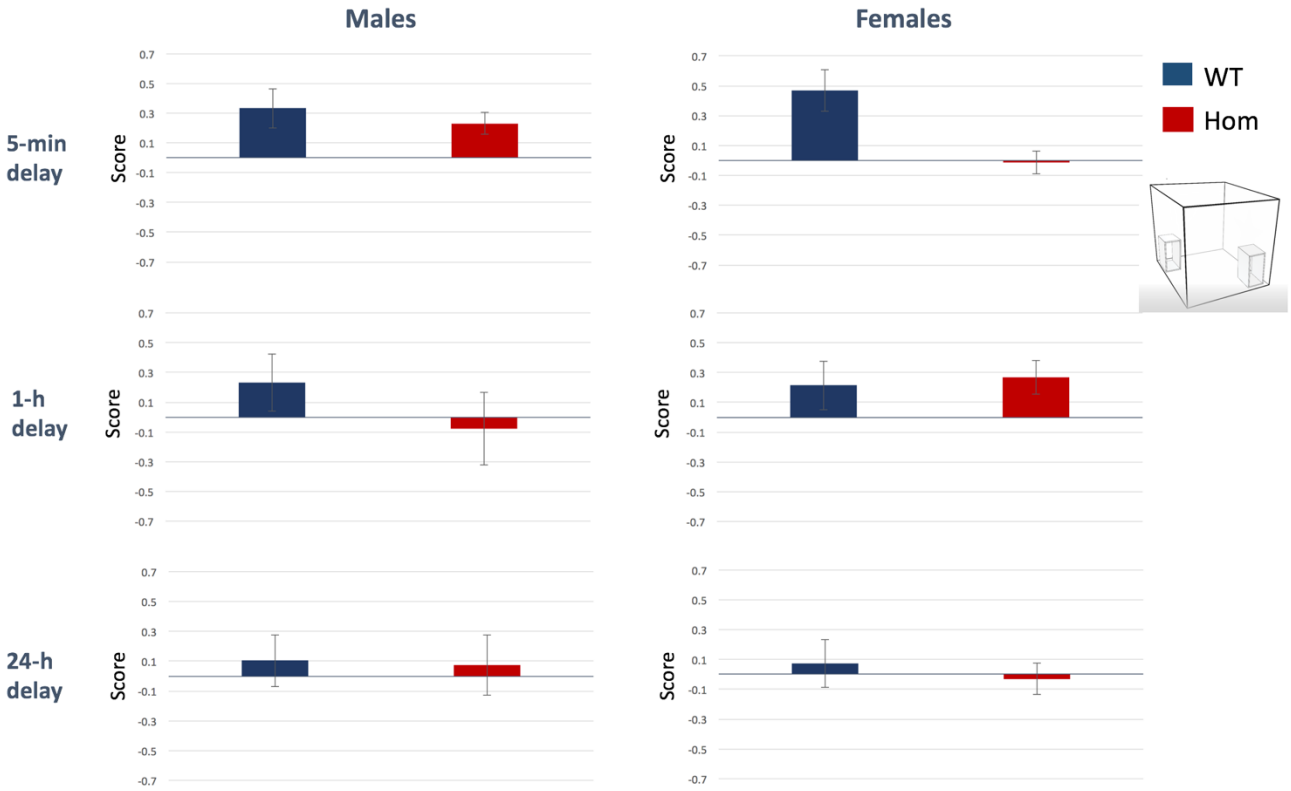


Figure 22: Performance for the novel object recognition task (larger cohort), expressed as a score (see Methods) in WT and Homozygous male and female mice. Mean ± SEM. n(♂, WT)=14, n(♂, Hom)=9, n(♀, WT)=14, n(♀, Hom)=12. A mixed-design ANOVA revealed no significant main effects of delay, sex or genotype (see text).

ii. Object-in-place recognition task

When confronted with a familiar object placed in a familiar or novel place, it appears that *Sleepy6* mice not only show no preference for the object placed in a novel location (score close

to 0), but that they seem to prefer the object situated in the familiar location (score < 0), as shown in Figure 23. A mixed-design ANOVA showed a significant main effect of genotype ($F(1,45)=8.926$, $p=0.005$), with the *Sleepy6* mice performing overall more poorly than their WT littermates. There was also a significant main effect of delay ($F(2,90)=3.982$, $p=0.022$), but not of gender ($F(1,45)=0.544$, $p=0.465$).

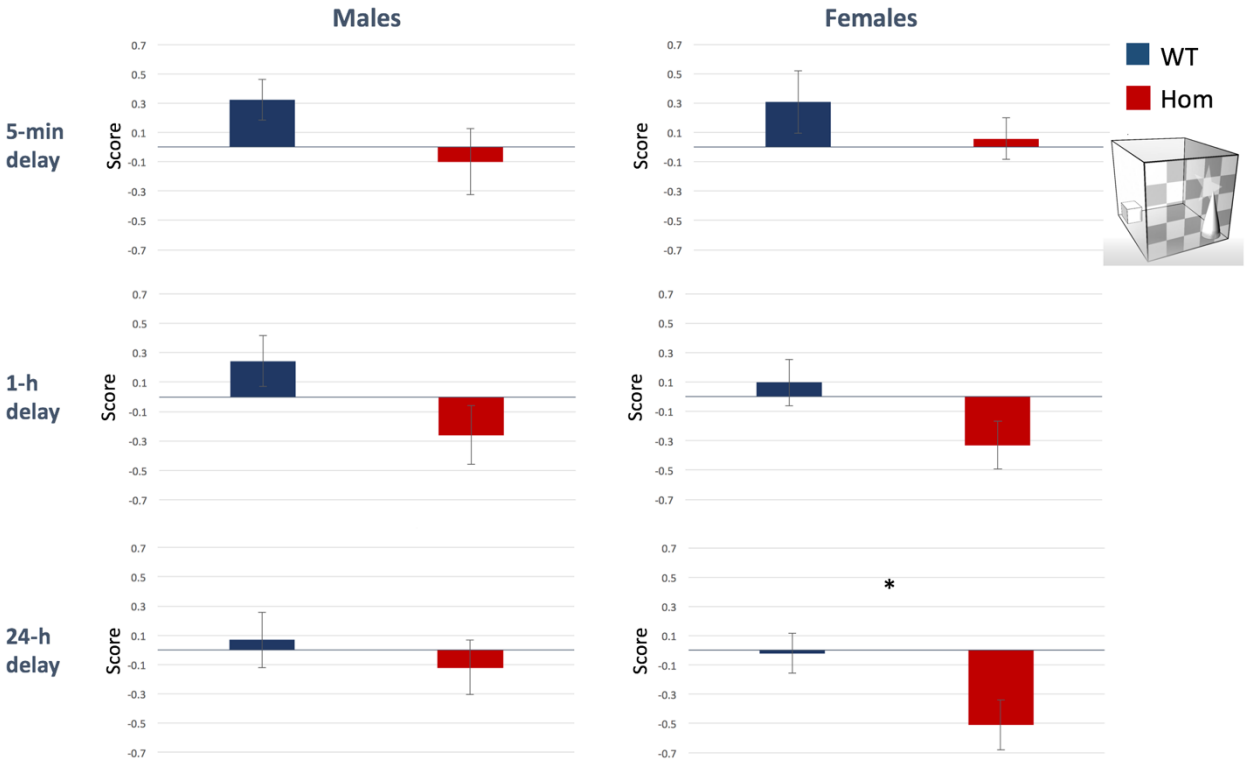


*Figure 23: Performance for the object-in-place recognition task (larger cohort), expressed as a score (see Methods) in WT and Homozygous male and female mice. Mean ± SEM. n(♂, WT)=14, n(♂, Hom)=9, n(♀, WT)=14, n(♀, Hom)=12. A mixed-design ANOVA revealed a significant main effect of genotype ($F(1,45)=8.926$, $p=0.005$), and of delay ($F(2,90)=3.982$, $p=0.022$), but not of sex ($F(1,45)=0.544$, $p=0.465$). Independent samples t-tests revealed an effect in females only for the 24-h delay ($t(24)=2.284$, $p=0.032$). If corrected for multiple comparisons, this is no longer significant. * indicates $p<0.05$.*

Interestingly, if running a mixed-design ANOVA combining the results from both tests (NOR and OIP), it appears that WT mice indeed perform better than their *Sleepy6* counterparts ($F(1,44)=6.856$, $p=0.012$), that mice overall perform better at the NOR task than the OIP task ($F(1,44)=7.026$, $p=0.011$) and that – quite intuitively – the longer the delay, the worse their

performance (F(2,88)=5.902, p=0.004). There is no significant differences between males and females however (F(1,44)=7.026, p=0.011).

The differences in performance observed between the two genotypes may reveal a possible learning or memory deficit in the *Sleepy6* homozygotes. However, these results should be interpreted with caution, as they may stem from a lack of attention in Homozygotes, or from differences in total time spent with the objects overall.

C. Total time of interaction with objects

We therefore evaluated whether there were significant differences in the time *Sleepy6* mice spend interacting with the objects, as this would impact their recognition ratios. Interestingly, when comparing the total time spent interacting with either of the two objects during the test phase of the NOR task (larger cohort), it seems that overall, *Sleepy6* Homozygotes spent more time exploring the objects (Figure 24).

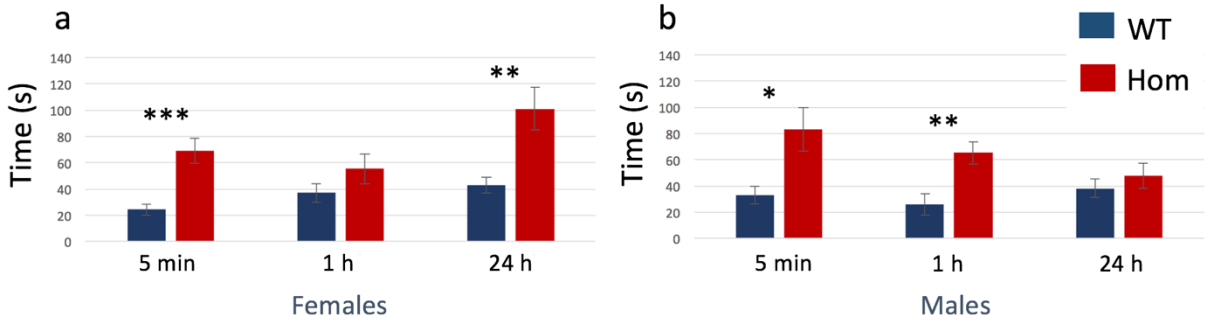


*Figure 24: Total time spent interacting with any of the objects during the 3 min of test following the 3 delays, in female (a) and male (b) WT and Homozygous (Hom) mice from the larger cohort. Data taken from the NOR task. Mean ± SEM. n(♂, WT)=14, n(♂, Hom)=9, n(♀, WT)=14, n(♀, Hom)=12. See main text for details of ANOVA. Post-hoc testing was performed using independent sample t-tests. *, **, *** indicate p< 0.05, 0.01 and 0.001, respectively.*

A mixed-design (repeated-measures) ANOVA highlighted a significant main effect of genotype (F(1,45)=37.283, p<0.001), a significant main effect of delay (F(2,90)=1.687, p=0.191), but no main effect of gender (F(1,45)=1.011, p=0.320). There were also significant interactions

Delay*Gender ($F(2,90)=5.283$, $p=0.007$), and male and female data was therefore not pooled. We found a significant interaction Delay*Gender*Genotype ($F(2,90)=4.073$, $p=0.020$), likely due to the fact that homozygous males tend to spend less time interacting with objects when the delay lengthens, whereas WT males interact for a similar amount of time with the objects, regardless of the delay (Figure 24b).

It is also possible however, that homozygous mice spend more time in the vicinity of the objects (i.e. are within the object zone, as delimited on the tracking software ANY-maze, see Methods), but that they do not explore the objects as such. Experimental observations indeed revealed that *Sleepy6* are hyperactive in comparison with WT littermate controls (see below), and run around the arena, going from one object to the next, passing each object rather than exploring it. These observations do not exclude the possibility of an actual learning or memory impairment in those mice, but highlight the importance of interpreting the differences observed in the light of the animal's locomotor behaviour.

D. Locomotor activity

i. Distance travelled

We therefore investigated the distance travelled during the 3-min test phase of the NOR task in the larger cohort. This revealed striking differences in locomotor behaviour between *Sleepy6* mice and their wild-type littermates (Figure 25). Homozygous mice – both male and female – travel a significantly longer distance than WT animals ($F(1,45)=53.177$, $p<0.001$). There is also a significant effect of delay length ($F(2,90)=16.680$, $p<0.001$): in homozygous mice, the shorter the delay, the longer the distance travelled. Additionally, a mixed-design ANOVA confirmed the significance of a striking interaction Delay*Genotype ($F(2,90)=14.111$, $p<0.001$): while WT mice travel a stable distance across tests following varying delays, the distance travelled by

Homozygotes is strongly negatively correlated to the duration between the sample and test phases (Figure 25, red bars). It is probable that this observation in homozygous *Sleepy6* mice stems from a cumulative effect of the repeated handling at short time intervals in a 5-min delay setting: each mouse is handled 3 times in the 15 minutes preceding the test phase (beginning and end of the sample phase, then 5 min later to start the test phase). In the 24-h delay setting, on the other hand, the mouse is handled once to start the test phase, the sampling phase handling dating back to the previous day. Although this holds true for all mice (WT and Homs), the hyperactive behaviour of *Sleepy6* mice may exacerbate the effects of handling, such as increased arousal or stress (Balcombe et al., 2004; Hurst and West, 2010). It is important to note however that the mice had been habituated to regular and gentle handling prior to testing. These observations are also in line with previous findings showing that following a change of environment, such as a cage change, *Sleepy6* Homozygotes displayed an hyperactive behaviour for around 30 min, when their WT littermates settled down more quickly (Heise, 2015). Finally, no difference between sexes was observed ($F(1,45)=0.101$, $p=0.752$).

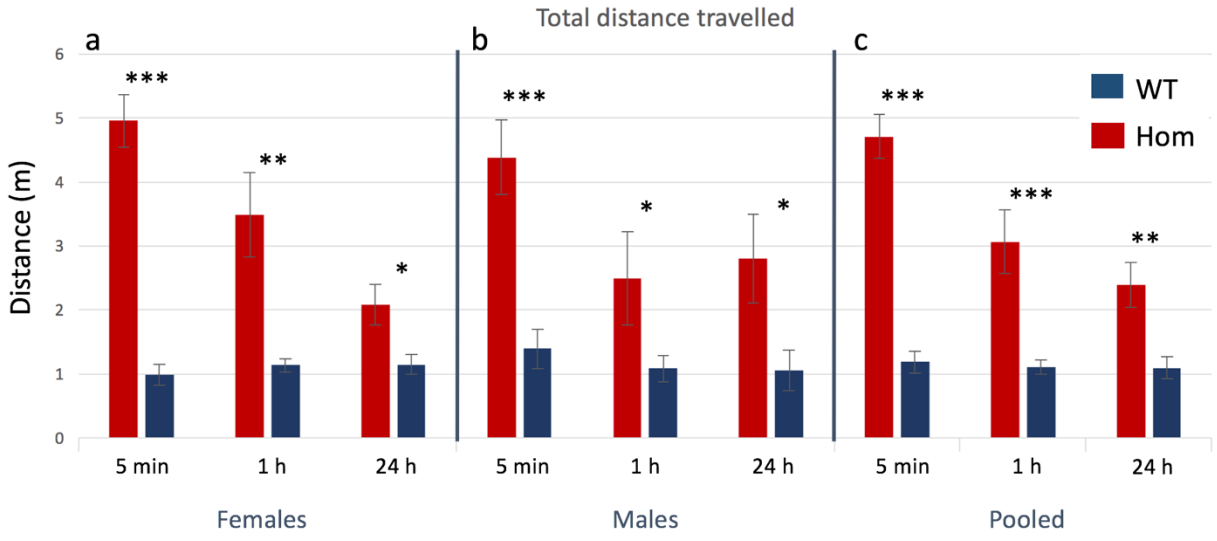


*Figure 25: Total distance travelled by the mice during the 3 min of the test phase after the 3 delays in the larger cohort, in females (a), males (b) and all animals (c). Data taken from the NOR task. Mean ± SEM. n(♂, WT)=14, n(♂, Hom)=9, n(♀, WT)=14, n(♀, Hom)=12. See main text for details of ANOVA. Post-hoc testing was performed using independent sample t-tests. *, **, *** indicate p< 0.05, 0.01 and 0.001, respectively.*

ii. Total time of mobility

We were also interested to see whether, out of the 3 min (180 s) of the test phase, *Sleepy6* homozygotes spent more time running around the arena than their WT counterparts. This is indeed the case, as shown in Figure 26 and by a mixed-design ANOVA, which revealed a significant main effect of genotype ($F(1,45)=36.183$, $p=0.496$) and of delay ($F(2,90)=13.085$, $p<0.001$), but not of gender ($F(1,45)=0.470$, $p=0.496$), with no significant interactions.

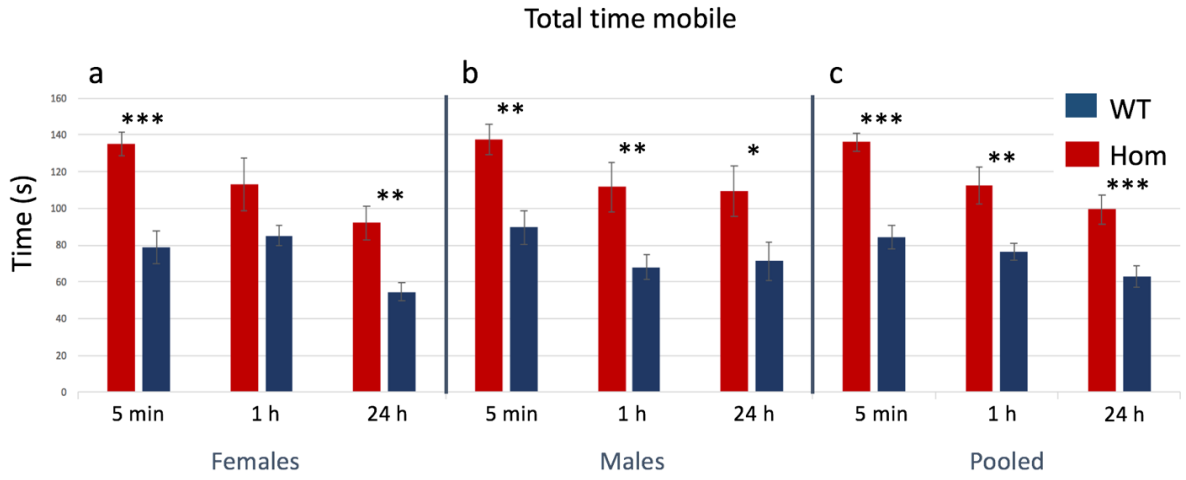


*Figure 26: Total time of mobility of the mice during the 3 min of the test phase after the 3 delays in the larger cohort. Data taken from the NOR task. Mean ± SEM. n(♂, WT)=14, n(♂, Hom)=9, n(♀, WT)=14, n(♀, Hom)=12. See main text for details of ANOVA. Post-hoc testing was performed using independent sample t-tests. *, **, *** indicate p< 0.05, 0.01 and 0.001, respectively.*

iii. Average speed while mobile

Not only do *Sleepy6* mice travel longer distances than WTs and spend more time moving within the arena, but their average speed is also higher than in WTs ($F(1,45)=41.036$, $p<0.001$, Figure 27). This may partly explain how Homozygotes are able to travel longer distances than WT mice (Figure 25), while also spending more time interacting with objects (Figure 24). No significant differences between sexes could be observed in terms of speed ($F(1,45)=1.624$, $p=0.209$). Note

that the average speed was calculated by dividing the total distance travelled by the total time mobile (and therefore does not corresponds to the default "average speed" than can be calculated by ANY-maze, whereby the total distance travelled is merely divided by the total duration of the test i.e. 30s in all animals).

In a similar manner to the distance travelled, the average speed results show significant differences depending on the duration of the delay ($F(2,90)=8.697$, $p<0.001$), with a significant interaction Delay*Genotype ($F(2,90)=18.380$, $p<0.001$). As mentioned above (see 3.D), the effects of repeated handling at short time intervals may be exacerbated in *Sleepy6* homozygotes, accounting for the pattern observed: higher speeds with shorter delay duration (Figure 27).

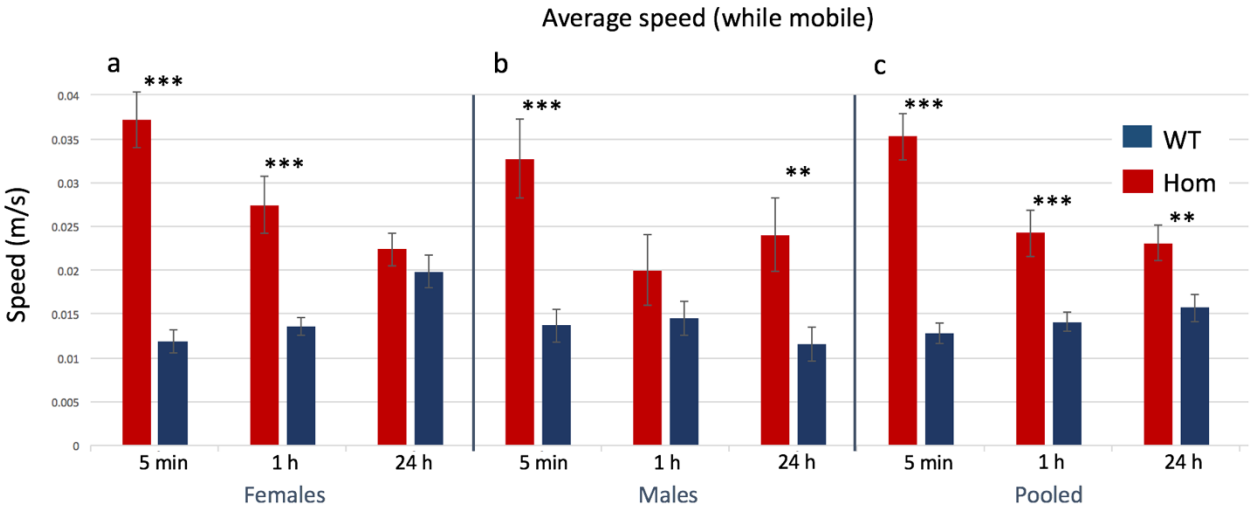


*Figure 27: Average speed of the mice (while mobile) during the 3 min of the test phase following the 3 delays in the larger cohort. Data taken from the NOR task. Mean ± SEM. n(♂, WT)=14, n(♂, Hom)=9, n(♀, WT)=14, n(♀, Hom)=12. See main text for details of ANOVA. Post-hoc testing was performed using independent sample t-tests. **, *** indicate p< 0.01 and 0.001, respectively.*

E. qPCR

It has been shown that neuronal activity induced by learning and memory rapidly, but transiently, upregulates the transcription of immediate early genes (IEG) in some subsets of

neurons of specific brain areas (Minatohara et al., 2016). Therefore, to investigate neuronal activity in the hippocampus following exposition to new objects, the levels of expression of two IEGs – namely *c-Fos* and the activity-regulated cytoskeleton-associated protein *Arc* – were evaluated by reverse-transcription quantitative PCR (RT-qPCR). The expression of *Arc* in the hippocampus has been linked to the consolidation of spatial and contextual memories (Heroux et al., 2018), while *c-Fos* has generally been linked to memory encoding (Minatohara et al., 2016).

i. Pilot cohort

Results from the pilot cohort showed only a trend for a higher expression of *c-Fos* in WT mice than in Homs ($F(1,8)=4.43$, $p=0.069$), and revealed that its expression is significantly higher in females than in males ($F(1,8)=5.93$, $p=0.041$) – see Figure 28 a & b. No significant differences in the expression of *Arc* were found however, neither between genotypes ($F(1,8)=0.926$, $p=0.364$) nor between males and females ($F(1,8)=0.427$, $p=0.532$) – see Figure 28 c & d. It seemed plausible that those differences may become more significant with a larger cohort of animals.

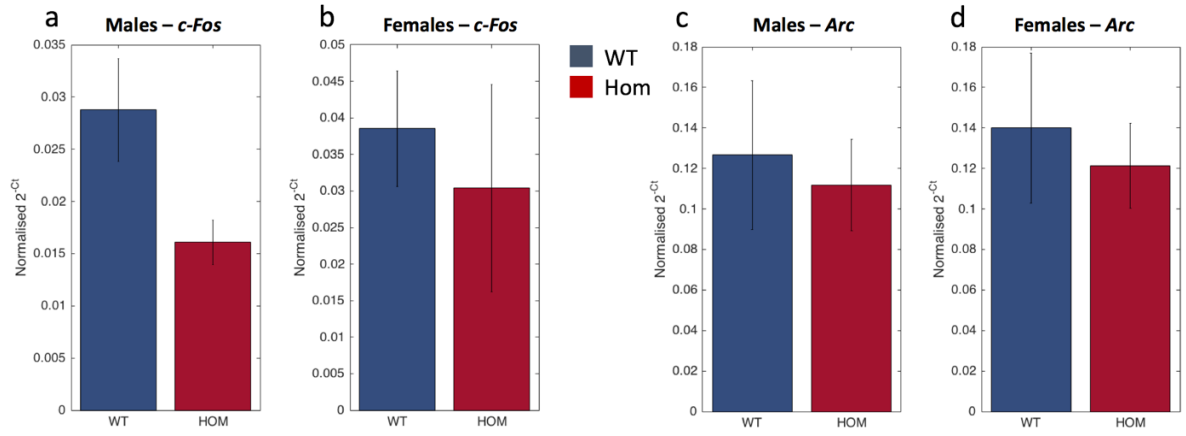


Figure 28: Expression (transcript levels) of the immediate early genes c-Fos (a, b) and Arc (c, d) in WT and homozygous male (a, c) and female (b, d) mice. Mean ± SEM. n(♂, WT)=3, n(♂, Hom)=3, n(♀, WT)=3, n(♀, Hom)=3. Details of statistical analyses are presented in the main text.

ii. Main experiment

In the pilot experiments, all animals were exposed to objects. As such, to determine the effects of object exposure, a control (unexposed) group was also included when replicating experiments with the larger cohort of mice (i.e. some mice were not exposed to new objects prior to the collection of hippocampal samples (see Methods)).

When plotting the results in a similar manner to the pilot cohort (i.e. without considering the control group), no differences were apparent (Figure 29). A univariate analysis of variance (Dependent variable: *c-Fos*; Fixed factors: Genotype, Sex and Treatment – control or exposed to objects) revealed no differences between WT and homozygous mice in the expression of *c-Fos* ($F(1,33)=3.37$, $p=0.076$), nor between males and females ($F(1,33)=1.82$, $p=0.187$) – see Figure 29 a & b.

As may be seen in Figure 30 a,b,e & f, there was however a significant main effect of treatment, with the control group expressing significantly less the gene *c-Fos* compared to the animals which had been provided new objects to explore 45 minutes before sacrifice ($F(1,33)=9.08$, $p=0.005$).

The impact of genotype, sex and treatment on the levels of expression of *Arc* were similar to those observed for *c-Fos*, with no significant main effect of the genotype ($F(1,33)=0.137$, $p=0.714$) or sex ($F(1,33)=0.021$, $p=0.886$) of the animals (Figure 29 c & d). There is however a significant effect of the exposure to objects prior to the collection of hippocampus samples, as control animals showed significantly lower levels of *Arc* expression in comparison to the exposed animals ($F(1,33)=9.059$, $p=0.005$) – see Figure 30 c,d,g & h.

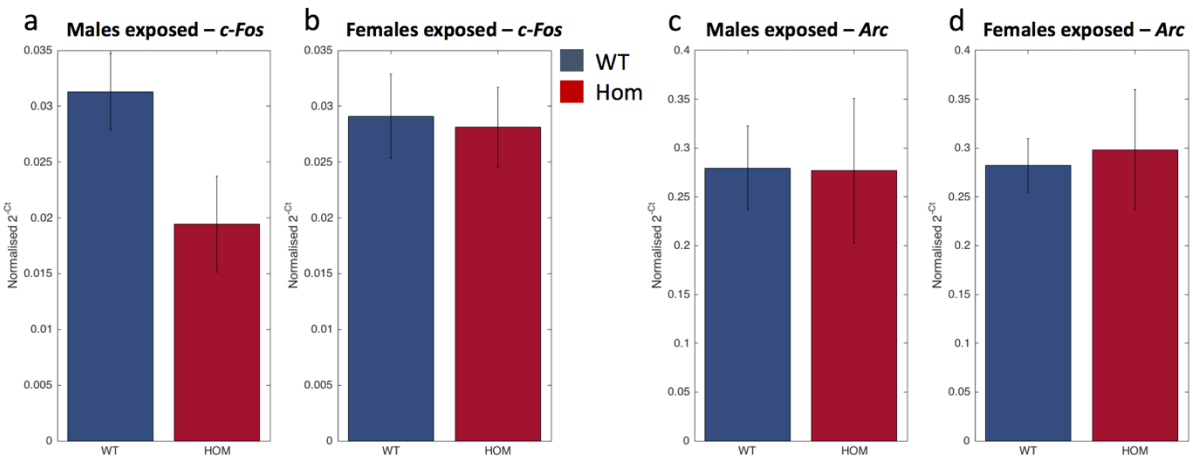


Figure 29: Expression of c-Fos (a, b) and Arc (c, d) in the larger cohort in WT and homozygous male (a, c) and female (b, d) mice exposed to new objects. Mean ± SEM. n(♂, WT)=14, n(♂, Hom)=9, n(♀, WT)=14, n(♀, Hom)=12. Details of statistical analyses are presented in the main text.

Overall, those results suggest that the expression of IEG induced by learning, memory and other behavioural and sensory experiences is conserved in *Sleepy6* mice and therefore cannot account for the performance impairments discussed above. Effectively, these results show that basic molecular processes that have been associated with learning and memory in the hippocampus occur normally in the *Sleepy6* homozygotes.

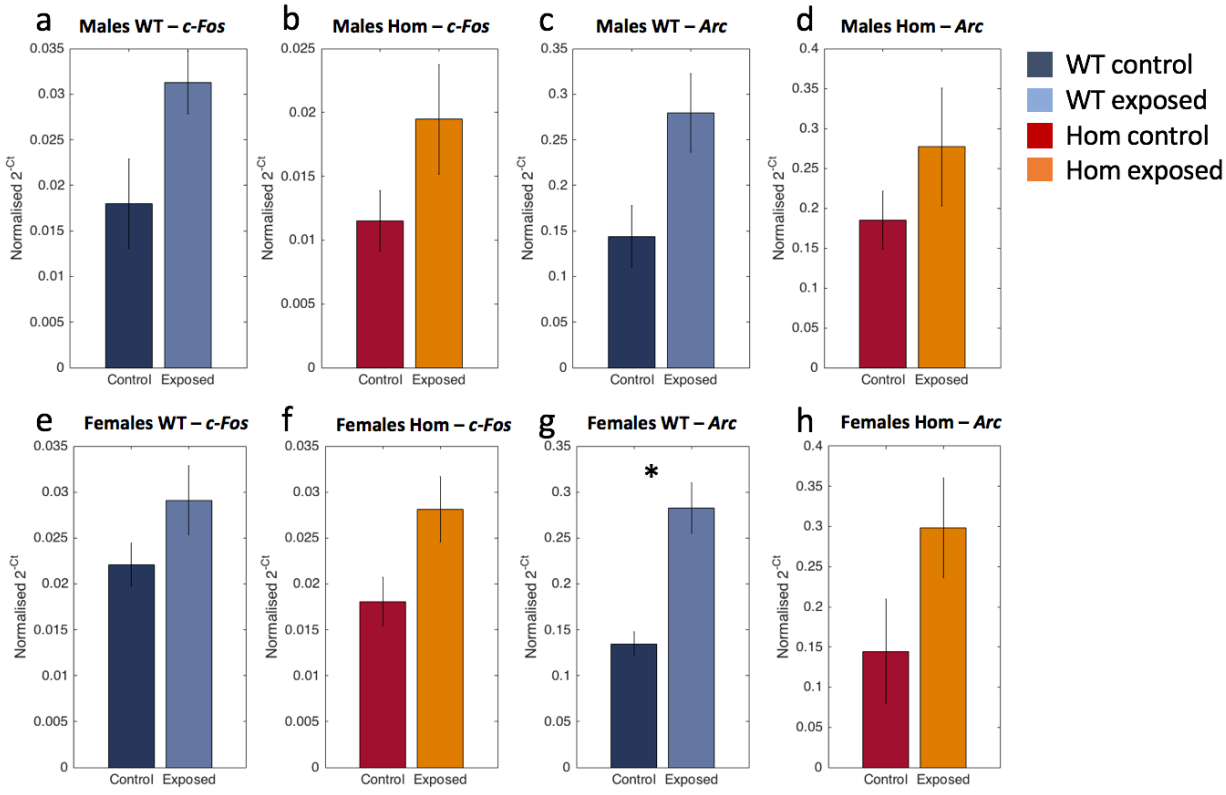


*Figure 30: Normalised expression of c-Fos (a,b,e,f) and Arc (c,d,g,h) in males (a-d) and females (e-f). RNA extractions were performed from hippocampus samples, collected 45 min after animals had been exposed to new objects ('Exposed') or not ('Control'). See 'Methods' section for additional details. Mean ± SEM. n(♂, WT)=14, n(♂, Hom)=9, n(♀, WT)=14, n(♀, Hom)=12. See main text for details of ANOVA. Post-hoc testing was performed using independent sample t-tests. * indicates p< 0.05.*

4. DISCUSSION

A. Summary of findings

Our findings show that the *Sleepy6* mice present a mild impairment in performing the NOR and OIP tasks (Figure 23). Whether these results indicate a memory and learning deficit or an attention deficit is difficult to disentangle with the data available. Homozygous mice show increased locomotor activity, both in terms of distance and time, and run at a higher speed (3.D). These observations could suggest a possible hyperactivity, an attention deficit, or stress (Zimprich et al., 2014). Anxiety, unlike stress, is usually associated with decreased locomotor

activity in rodents, particularly exploratory activity in novel environments (Liebsch et al., 1998; Sestakova et al., 2013). And yet, *Sleepy6* mice spend more time interacting with the objects, which would contradict the idea that they show a deficit in attention. This increased time spent interacting with the objects also goes against previous findings where *Sleepy6* homozygotes were found to spend less time exploring the objects (Heise, 2015). Contrary to our current findings presented here, these previous data showed no differences in performance between WT and *Sleepy6* mice (Heise, 2015). Whilst these studies used a similar number of animals, they used a different experimental design based upon exposure to novel objects in the home-cage. A learning and memory impairment can therefore not be excluded, but it is also possible that the differences in performance obtained stem from a hyperactive behaviour and a deficit in attention. In particular, the time interacting with objects may be biased as the video tracking does not allow to differentiate – when an animal's head is close to an object – whether it is exploring or not.

B. SNARE proteins, attention and ADHD

There is extensive evidence of a link between attention deficit hyperactivity disorder (ADHD) and certain variants or mutations in genes coding for SNARE proteins in human subjects (Bonvicini et al., 2016; Cupertino et al., 2017; Gao et al., 2015). Animal studies have also shown such a link, for instance, the "coloboma" mice, which present a deletion affecting the SNAP-25 sequence (although possibly, other genes too) show hyperactivity (Hess et al., 1992). Another study highlighted that genes commonly duplicated in patients with ADHD were on the one hand associated with learning and memory impairments in mouse models where those genes were altered or lost, and on the other hand were co-expressed with genes whose mouse orthologues lead to hyperactive mice (Taylor et al., 2015).

There is evidence that impairment in neurotransmitter systems – from synthesis to breakdown, or uptake – likely plays a role in the pathophysiology of ADHD (Curatolo et al., 2010; Oades, 2008). Since the mutation of the *Sleepy6* line occurs in the *Vamp2* gene, and VAMP2 is involved in the SNARE complex and thus in membrane fusion and vesicular release (Chen and Scheller, 2001; Schoch et al., 2001; Südhof, 2013), it likely affects the release of various neurotransmitters throughout the brain (Raptis et al., 2005). It is therefore plausible that *Sleepy6* mice may display features of ADHD, especially as the *Sleepy6* mutation occurs in the transmembrane domain of VAMP2, and research has shown that the transmembrane domain of the protein is crucial for membrane fusion and exocytosis (Hastoy et al., 2017). Additionally, it has been argued that the susceptibility for ADHD induced by mutations in SNARE proteins may also be linked to their critical role in brain development, beyond their role in vesicular fusion and neurotransmitter release (Cupertino et al., 2016).

One possibility would therefore be to evaluate the attentional capacity of the *Sleepy6* mutant mice. Pre-attentive processes and attention can be evaluated using behavioural tests such as pre-pulse inhibition (PPI) which assesses sensorimotor gating (Rodriguiz and Wetsel, 2006). This test was performed in *Sleepy6* mice and showed that homozygous *Sleepy6* females have a sensorimotor gating deficit, as revealed by a significant reduction in PPI; no such observation could be made in *Sleepy6* males however (Heise, 2015). This is particularly striking as most data presented in this chapter revealed very few differences between male and female mice, both in terms of cognitive performance and locomotor behaviour. This previous PPI results would however suggest that *Sleepy6* homozygous females are not able to filter out irrelevant environmental stimuli as efficiently as their WT littermates, while *Sleepy6* homozygous males wouldn't be affected. These observations then raise the question of how both male and female *Sleepy6* mice perform similarly in tasks involving attention and learning. Fully evaluating

attention – and possible attention deficits – is however complex as it involves many cognitive processes and therefore requires multiple tests (Bushnell, 1998), beyond the PPI test.

C. Limitations

Although the NOR and OIP provided us with some additional insights regarding the behaviour and learning capacity of the *Sleepy6* mice, the information they provide is nonetheless limited and do not allow to fully characterize the *Sleepy6* homozygous phenotype. Additional tests would be needed to understand, for instance, whether *Sleepy6* homozygotes have intact memory but impaired attention, or whether their levels of stress following stressful stimuli are significantly higher than WT littermates. Attention could be investigated using tests such as the go/no-go task, the five-choice serial reaction time task, or the latent inhibition task, which can help evaluate impulsivity, visual attentional processes and/or the ability to associate meaning to an already familiar stimulus (which requires further attention than association to a novel stimulus) (Bari et al., 2008; Lubow, 1989; Rodriguiz and Wetsel, 2006). Note that visual acuity was tested in *Sleepy6* mice, revealing no impairment, and if anything, a higher visual acuity for *Sleepy6* homozygotes compared to WT littermates (Heise, 2015).

Additionally, as the impairments in performance observed seemed stronger in the OIP task, which involves spatial memory, than in the NOR – which does not – tests evaluating contextual memory further would be needed, such as the Morris water maze or Barnes maze (Lipp and Wolfer, 1998; Sunyer et al., 2007). Non-spatial contextual memory tasks could also be relevant and provide us with insights regarding the ability of *Sleepy6* homozygotes to learn and/or focus their attention on different types of cues and stimuli. Test involving odour or auditory detection and discrimination could be used, such as a go/no-go operant conditioning procedure using odour cues (Bodyak and Slotnick, 1999) or a shuttle-box auditory stimulus discrimination task (Kurt and Ehret, 2010), where the complexity of the tasks can also be modulated.

Finally, the sleep phenotype observed in *Sleepy6* mice may provide additional insights on which cognitive processes may be affected depending on which sleep states (NREMS or REMS) are mainly affected. Indeed, as discussed in the introduction, REMS and NREMS have differential but complementary roles in memory and learning. Therefore, significantly different amounts of REMS or NREMS in *Sleepy6* homozygotes compared to their WT littermates may impact their cognition in various ways.

CHAPTER 4: Electrophysiology recordings in *Sleepy6* mice

1. INTRODUCTION

The *Sleepy6* line was originally screened and identified for its sleep phenotype from an ENU mutagenesis screen at MRC Harwell. Homozygous mice tended to sleep less than littermate controls, particularly in the dark (active) phase (Heise, 2015). However, this data had been acquired using video tracking, a non-invasive technique allowing for a range of other tests to be performed in the phenotyping pipeline. EEG recordings were thus necessary to characterise the sleep of *Sleepy6* homozygous mice further, to be able to investigate the amount of time spent in rapid eye movement sleep (REMS) and non-REMS (NREMS), as well as other features (e.g. changes in power spectra) that can be derived from continuous EEG recordings across vigilance states.

Pilot EEG results obtained using telemetry indicated a reduction in REMS time in both the dark and light phases, and in NREMS time in the dark phase only (Heise, 2015). These pilot experiments, performed in 3 *Sleepy6* homozygotes and 3 WT littermates, also showed abnormalities in power density spectra and in the response to sleep deprivation. EEG recordings enable slow-wave activity (SWA) to be measured, which corresponds to the EEG power in the slow-wave frequency range (0.5-4 Hz) in NREMS. Indeed, slow-waves tend to dominate the EEG during NREMS and can be recorded across the entire cortical surface (Massimini et al., 2004; Steriade et al., 1993a). Both animal and human studies have shown that SWA levels are closely linked to sleep-wake history, where SWA levels at the onset of NREMS positively correlate with

preceding time spent awake, and levels subsequently decrease during NREMS (Achermann and Borbély, 2003; Borbély and Neuhaus, 1979a). SWA has therefore been traditionally used as a marker of sleep pressure (Borbély et al., 1981; Dijk et al., 1987).

We were interested to see how the levels of SWA would compare between *Sleepy6* homozygotes and WT littermate controls. The pilot results mentioned above indicated that following sleep deprivation *Sleepy6* homozygotes displayed a lower rebound in SWA levels than WT mice. These observations could be explained in different ways, and are of particular interest given the results obtained in Chapter 3. If one assumes, for instance, a chronic state of sleep deprivation in *Sleepy6* animals, where their decreased sleep duration does not result from an inherently decreased need for sleep but via mechanisms that prevent them from getting their required amount of sleep, then the decrease in learning and memory performance observed in *Sleepy6* homozygotes may be expected (Alhola and Polo-Kantola, 2007; Patti et al., 2010; Prince and Abel, 2013). By contrast, if *Sleepy6* animals naturally need less sleep, then the impaired learning performance could originate from their hyperactive behaviour and lack of attention, for instance, rather than a constant need for sleep (see Chapter 3).

However, a reduced rebound in SWA levels following sleep deprivation in the *Sleepy6* animals is not sufficient to draw any conclusions in this regard. It is possible that sleep pressure does not accumulate as fast in *Sleepy6* Homozygotes (which will be further analysed and discussed in Chapter 5), and it cannot be excluded that a 6-h sleep deprivation does not represent a particular challenge to *Sleepy6* mice which tend to spend more time awake throughout the day. An alternative possibility is that levels of SWA in *Sleepy6* Homozygotes are generally more stable across 24h due to mechanisms that remain to be elucidated. For example, if *Sleepy6* homozygotes are chronically sleep deprived, their sleep pressure – as measured by SWA – may be constantly close to the upper saturating threshold (SWA and sleep pressure are generally described with saturating exponential functions, see Chapter 5 and (Borbély and Achermann,

1999)) and few variations could thus be observed, even following sleep deprivation. Additional EEG recordings in a larger cohort of animals and an in-depth analysis should therefore provide us with new insights into those processes.

To gain a better understanding of the topology of such processes, we also aimed to use a second EEG derivation to be able to investigate EEG dynamics in distinct cortical regions. It has been shown that SWA presents with pronounced topographical variations, such as a frontal predominance of SWA during NREMS, which may reflect differences in SWA dynamics and regulation across the brain (Huber et al., 2000b; Rusterholz and Achermann, 2011; Schwierin et al., 1999; Werth et al., 1996a, 1997; Zavada et al., 2009). It seemed important, therefore, to investigate whether the differences observed between *Sleepy6* Homozygotes and WTs are conserved across brain areas, or whether they would show predominantly in one area. If this were to be the case, this could be put in perspective with the role of the cortical regions recorded (motor and visual cortex): various studies have shown a local build-up of sleep pressure, related to the recruitment of brain areas during preceding wake (Huber et al., 2004; Kattler et al., 1994; Vyazovskiy et al., 2002). For instance, if SWA dynamics are different between genotypes in the frontal cortex, but not as much in the occipital region, this could indicate that the recruitment of the motor cortex (frontal area) is affected in *Sleepy6* mice, which may then be further linked to their increased locomotor activity, for example, as shown in Chapter 3.

Regardless of the differences found in the EEG data, one is limited by the fact that EEG records global signals across the cortical surface. If marked EEG differences are observed, then local field potentials and multi-unit activity may be valuable in understanding the neuronal mechanisms underlying these changes. For example, as slow-waves correspond to periods of neuronal silence (Calvet et al., 1973; Contreras and Steriade, 1995; Mukovski et al., 2007; Steriade et al., 1993b, 2001; Vyazovskiy et al., 2009), which also depend on the levels of network synchrony (Vyazovskiy et al., 2009), multi-unit activity would allow us to investigate the patterns of

neuronal silence and activity in *Sleepy6* animals. For instance, do *Sleepy6* homozygotes show longer or shorter periods of neuronal silence during NREMS?

We therefore chose to implant animals with laminar probes, the design of which was chosen to permit recordings of multi-unit activity from multiple channels aligned vertically, allowing to study differential dynamics across the cortical layers. We also chose to study the response of *Sleepy6* homozygotes to auditory stimulation, to gain a better understanding of their sleep depth. Auditory stimuli are commonly used to investigate sleep depth, sensory dissociation during sleep and arousal thresholds from NREMS and REMS (Neckelmann and Ursin, 1993; Nir et al., 2015; Rechtschaffen et al., 1966).

Using EEG and laminar probe recordings, we were able to confirm the sleep phenotype of *Sleepy6* homozygotes in terms of sleep architecture, as well as to investigate their phenotype at a neuronal level. In addition to exploring the effect of sleep deprivation, the response of *Sleepy6* homozygotes to auditory stimulation was also evaluated.

2. MATERIALS AND METHODS

A. Animals and housing conditions.

All work was carried out under a UK Home Office PPL (P828B64BC) and a personal license (PIL I8D8D5669), in accordance with Animal [Scientific Procedures] Act 1986 and the University of Oxford's Policy on the Use of Animals in Scientific Research.

Two series of surgeries were performed:

- A first batch of n=4 *Sleepy6* homozygotes and n=4 WT littermates were implanted. The average age and weight of the animals at the time of surgery was 19.0 ± 2.1 weeks & 24.9 ± 2.0 g for the homozygotes and 13.2 ± 0.6 weeks & 31.0 ± 1.7 g for the WTs.

3 homozygous animals could not be used for the recordings (one due to illness, one to poor surgical recovery and one due to poor signal quality). We associated the poorer recovery of the *Sleepy6* Homozygotes following surgery to their smaller initial body weight, as the only homozygote which could be recorded was also the only one which presented with an initial weight >30 g (30.7 g) at surgery, while the 3 other homozygous mice had initial weights between 21.6 g and 24.8 g. The following changes were thus implemented for the second batch of surgeries: during the two months preceding surgeries, to promote weight gain, *Sleepy6* homozygote mice were fed a high-nutrient diet (RM3 diet, ground, Special Diets Services, U.-K.) in the form of mash, on a daily basis and in addition to the regular pellets. Mice were implanted once they had reached a weight nearing or above 30g, which meant that mice were overall 5 weeks older at surgery (see below).

- A second batch of n=4 *Sleepy6* homozygotes and n=1 WT littermate was therefore implanted to obtain n=5 in each group. Power calculations were not performed here, but an n-value of 5 was chosen based on previous studies and rodent literature where n=6-7 is common (Nir et al., 2015; Tobler and Borbély, 1986; Vyazovskiy et al., 2009), on technical & cost considerations, as well as on the effects seen in the first batch. The average age and weight of the animals at the time of surgery was 24.3 ± 1.4 weeks & 32.2 ± 1.0 g for the homozygotes and 20.6 weeks & 34.5 g for the WT mouse.

B. EEG and laminar probe implantation surgeries

The week preceding surgery, all mice were habituated to jelly (via which post-operative analgesia was to be administered). On the day preceding surgery, mice were injected with Dexamethasone (0.2 mg/kg, subcutaneous route).

On the day of surgery, mice were weighed, then placed in an anaesthetic chamber for induction of anaesthesia with an isoflurane level of 5% and an oxygen flow around 1.0 L/min. Once induced, the mouse was transferred to a preparation area with a heating pad, and the isoflurane dose was decreased to 2.5%. The head of the mouse was shaved using clippers, then cleaned with 70% isopropyl alcohol. Metacam (meloxicam, 5 mg/kg s.c.), Vetergesic (buprenorphine, 0.1 mg/kg) and Dexamethasone (0.2 mg/kg) were administered subcutaneously.

The mouse was then transferred to a heat mat monitoring body temperature via a rectal probe, and the head fixed to a stereotaxic frame (David Kopf Instruments, USA). The shaved area was cleaned with Providone-iodine and artificial tears were applied on the eyes. The dose of anaesthesia was adjusted regularly (≈1.5 – 2 %), as required depending on loss of pedal reflex and breathing rate (>60 breaths/min in WT, >40 breaths/min in Homozygotes). From this point, after checking once more the loss of all reflexes, surgery was performed under sterile conditions.

An incision was made across the scalp using a size-15 scalpel blade to expose an area expanding from around 3 mm in front of bregma to 5 mm behind lambda, paying attention not to damage the neck muscle. Skin edges were retracted using 4 clamps attached to the hair or membrane (not outer skin). Using the scalpel blade, the surface of the skull was scratched thoroughly and scored, and any remaining tissue was cleaned using cotton tips with saline followed by 70% isopropyl alcohol. Etching gel was then applied on the skull for 2 min, staying away from the skin edges and muscle, before being carefully removed and the skull further cleaned with saline, then dried with cotton tips.

Using the stereotaxic frame, the horizontality of the brain was checked – aiming to have similar dorso-ventral coordinates for bregma and lambda (± 0.2 mm). Coordinates of the screws and

electrodes were calculated (starting from bregma) and marked with a surgical pen. Holes for the EEG screws were drilled (drill tip size: 0.6mm):

- Frontal (motor cortical area): AP +2 mm, ML +2 mm.
- Occipital (visual cortical area): AP -3.5 mm, ML + 2.5 mm.
- Cerebellum: 2 mm behind lambda.
- Anchor screw: AP -3.5 mm, ML -2.5 mm.

All screws (except the anchor screw) were connected to the headstage (Figure 31).

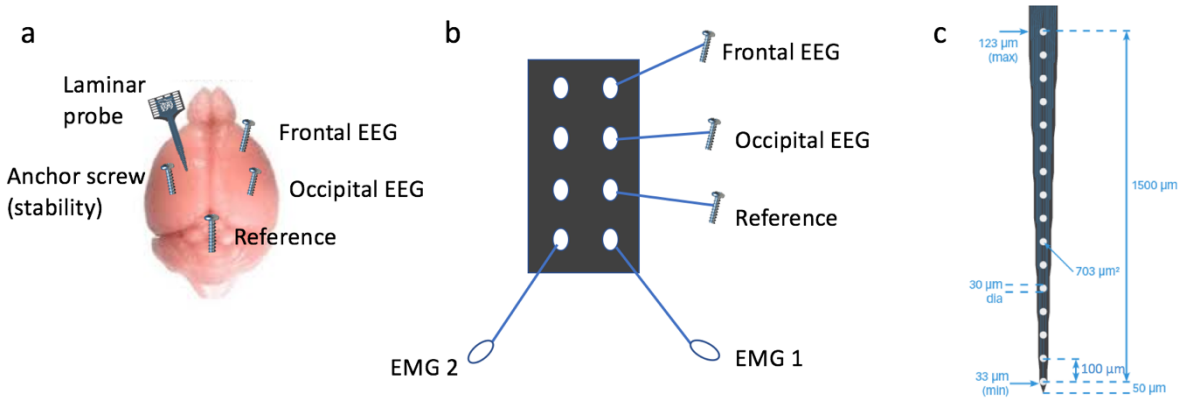


Figure 31: EEG and laminar probe designs. ***a)*** *Positions of the EEG screws and laminar probe (Laminar probe: AP +1.1mm, ML -1.75mm; Frontal EEG: AP +2 mm, ML +2 mm; Occipital EEG: AP -3.5 mm, ML +2.5 mm; Cerebellar reference screw: lambda-2 mm).* ***b)*** *Design of the EEG headstage.* ***c)*** *Design of the laminar probe (figure adapted from https://neuronexus.com).*

Frontal and occipital screws (self-tapping bone screws, stainless steel, length: 4 mm, shaft diameter: 0.85 mm, Fine Science Tools Inc.) were placed one by one, applying dental cement for fixation. The cerebellar and anchor screws were then placed, but not cemented until a further stage, to be used as grounding and reference sites for the laminar probe.

Using the dental drill, and under the microscope, a small craniotomy was performed around the laminar probe insertion point (≈0.8mm x 0.8 mm, primary motor cortex, AP +1.1, ML -1.75, DV

1.8, tilt of 14°), any remaining bone being removed with fine tweezers. The craniotomy was then washed with saline to remove any bone dust and kept moisturised by applying more saline regularly with a syringe. After the dura had been removed using a needle tip, the laminar probe was placed on the stereotaxic frame (type A1x16-3mm-100-703-Z16, i.e. 1-shank of 3-mm length, with 16 sites of 703 μm^2, 100 µm between each site, NeuroNexus Technologies, Ann Arbor, USA). Electrodes were dyed prior to the surgery with 1,1'-Dioctadecyl-3,3,3',3'-Tetramethylindocarbocyanine Perchlorate dye ('DiI', ThermoFisher Scientific). The grounding wire was wrapped around the anchor screw and the reference wire wrapped around the cerebellar screw. The laminar probe was then carefully lowered into the cortex (1.8 mm from the point at which the tip touches the surface of the brain). Silicon gel (Kwik-Sil, World Precision Instruments, USA) was then applied on the craniotomy, being careful not to cover a wider surface, which would prevent the cement from attaching to the skull.

Cement was applied around the laminar probe, anchor and cerebellar screws to create a strong head cap fixed to the skull. Two electromyography (EMG) electrodes (stainless steel wires ending with a loop to avoid damage of the tissue) were then inserted in the neck muscle and fixed at the back of the head cap with dental cement.

Saline was injected subcutaneously (0.1 mL/20 g) to compensate for fluid loss during the duration of the surgery, before placing the mouse in a recovery chamber at 28°C. Once the animals had recovered from anaesthesia (able to sit or maintain sternal recumbency), they were returned to their home cage and provided with thermal support (heat mat).

Animals were monitored for a minimum of 7 days post-operatively and administered with Dexamethasone (0.2 mg/kg, s.c.) and with Metacam (meloxicam, 5 mg/kg, s.c. post-op day 1, oral post-op days 2&3) for 1 and 3 days following surgery, respectively. At all times following surgery mice were singly housed.

C. Recordings

Animals were allowed to recover for at least 2 weeks before being moved to custom-made clear plexiglas cages (20.3 x 32 x 35 cm^3) placed in ventilated, sound-attenuated Faraday chambers (Campden Instruments, UK). Mice were kept in a 12h:12h light-dark cycle (lights on at 9am), with water and food available *ad libitum*. Temperature within the room was kept at 22±2 °C, with a humidity level of 55±10 %, and light levels of ~ 120-180 lux.

Mice were left to habituate to their new environment for 3 days before being tethered. The custom-made EEG cable was connected first, followed 24 h later by the laminar probe cable (16-Channel ZIF-Clip Headstage, Tucker-Davis Technologies Inc. (TDT), Alachua, USA). Recordings were started at least 3 days after tethering, to let the mice habituate to the cables. Signals were recorded using the Multichannel Neurophysiology Recording System (TDT, USA) and the Synapse software (TDT, USA). Multi-Unit activity (MUA), EEG and EMG were continuously recorded using pre-amplifier sampling-rate settings of ~ 25 kHz (MUA) and ~ 750 Hz (EEG and EMG), were filtered between 0.5-150 Hz, amplified (PZ5 NeuroDigitizer pre-amplifier, TDT) and stored on a local computer at a sampling rate of ~ 305 Hz (305.1758 Hz), before being resampled offline at 256 Hz. Using custom-written Matlab (The MathWorks Inc., USA) scripts, signals were converted to .txt format. Txt files were then transformed to European Data Format (EDF) using the open-source Neurotraces software.

D. Data analysis

Vigilance states were scored manually, by visual inspection of consecutive 4-s epochs, using the SleepSign software (Kissei Comtec Co, Nagano, Japan). In order to facilitate scoring, one local-field potential (LFP) channel, two EEG channels (frontal and occipital) and EMG were displayed

(Figure 32). Vigilance states were defined as waking (W, low-amplitude high-frequency EEG with a high level of EMG activity - Figure 32 c), non-rapid eye movement sleep (NREMS, presence of slow-waves, high amplitude and low-frequency EEG with a low level of EMG activity - Figure 32 a), rapid eye movement sleep (REMS, low-amplitude high-frequency EEG with a low level of EMG activity - Figure 32 b), or brief awakenings (M, periods of no more than 4 consecutive 4-s epochs occurring during NREMS or immediately following REMS episodes, and characterised by the presence of EMG activity). If the visualised LFP channel or EEG channels were contaminated by artifacts, the epoch was scored as artifactual (i.e. the vigilance state was defined, but signal values were ignored in subsequent analyses). Once scored, EEG power-density spectra were computed for each 4-s epoch by a fast Fourier transform (Hanning window, 0.25Hz resolution, frequency range 0 to 20 Hz) and exported for further analyses.

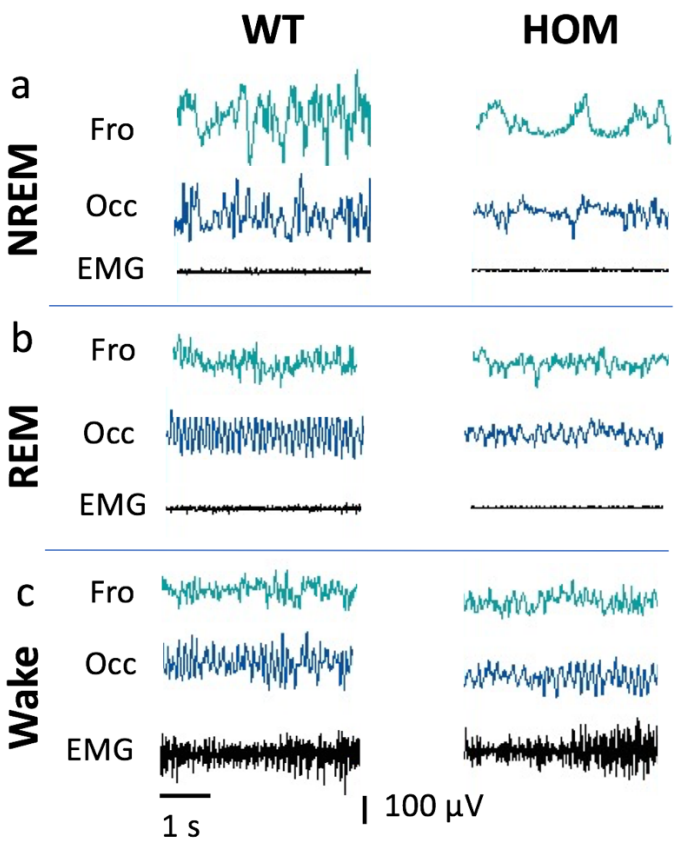


Figure 32: Characteristic frontal and occipital EEG and EMG traces in different vigilance states. ***a)*** *NREM sleep,* ***b)*** *REM sleep and* ***c)*** *wake, in representative WT and Sleepy6 homozygous (HOM) mice. Scale bars indicated at the bottom of the figure.*

E. Sleep deprivation

Sleep deprivation (SD) was performed for 6 consecutive hours starting from light onset. Animals were kept awake by providing them with new objects to explore. If the mice were getting drowsy, nesting material was taken away from the cage temporarily and the mouse gently handled. SD was successful as only 7.8 ± 1.7 minutes (mean ± SEM) of sleep were detected during the 6h of SD. Following sleep deprivation, mice were left undisturbed for at least 18h until the next morning.

F. Auditory stimulation

While electrophysiology signals were being recorded, sounds of 8kHz, 75dB were played for 8 s every minute during 1h30 (90 repetitions of an 8-s sound, 52-s silence). This 1h30 session was performed 4 times across 24 h (Figure 33): ZT 0.5 – 2; ZT 7.5 – 9; ZT 12.5 – 14; ZT 20 – 21.5 (ZT = zeitgeber time, ZT 0 = light onset). Speakers were placed 70 cm above each animal, within the Faraday sound-attenuated chambers.

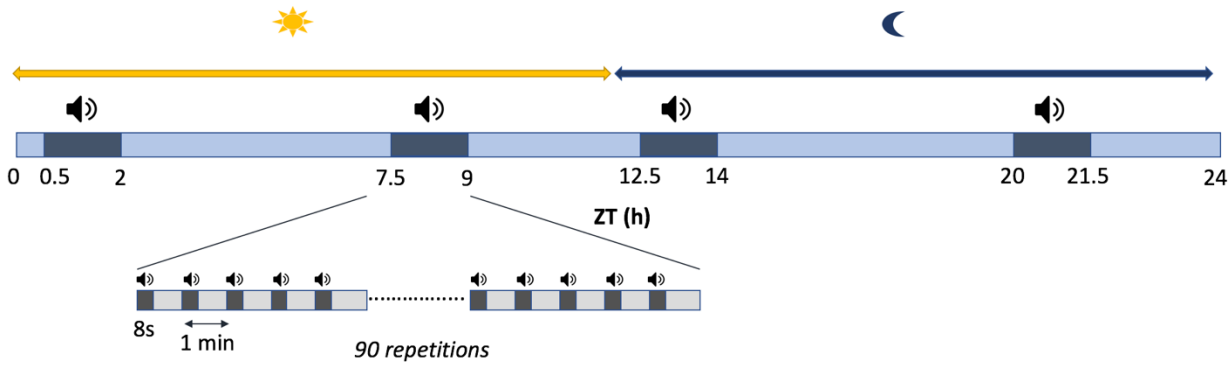


Figure 33: Auditory experiment design: an 8-s sound (8 kHz, 75 dB) was repeated every minute for 1h30; such a session was then repeated 4 times throughout the 24-h period. ZT=zeitgeber time (by convention light onset = ZT 0).

G. Perfusions and micro-lesions

Mice were injected with Euthatal (Pentobarbital 200mg in 1 mL, i.p. injection of 0.01mL/g body weight), and once all reflexes (pedal, tail, and corneal) lost, the laminar probe was connected to a NanoZ device (White Matter LLC, Seattle, U.-S.). Impedances of each channel were measured before performing micro-lesions on 3 channels along the probe with a current of 10 µA applied for 25s.

The mice were then transcardially perfused with a PBS solution, followed by paraformaldehyde (PFA, 4%; in PBS). The brains were removed and placed in PFA (4%; in PBS) for 24 – 48 h, after which they were transferred to a 30% sucrose solution (in PBS) for cryoprotection. Once sunk to the bottom of the vial, brains were briefly rinsed in PBS and embedded in O.C.T. compound and frozen at -80°C until cutting.

H. Histology

Slices were prepared using a cryostat (Cryotome FSE, ThermoScientific; -22°C, 50m-thick sections) and mounted on glass slides. Slides were subsequently mounted under cover glasses with ProLong Glass Antifade mountant with NucBlue® stain (ThermoFisher Scientific). Sections were digitized using an LSM 710 laser scanning confocal microscope and ZEN image acquisition software (Zeiss).

I. Statistical analysis

All statistical analyses were performed using SPSS (IBM Corp., Release 23.0.0.2). The nature of the tests used and corresponding results are reported within figure legends or within the main text of the Results section.

3. RESULTS

A. Position of laminar probes

The position of the laminar probes within the primary motor cortex (left hemisphere) was confirmed using histology and microscopy methods. Micro-lesions and DiI dye allowed the positioning to be performed more accurately (Figure 34).

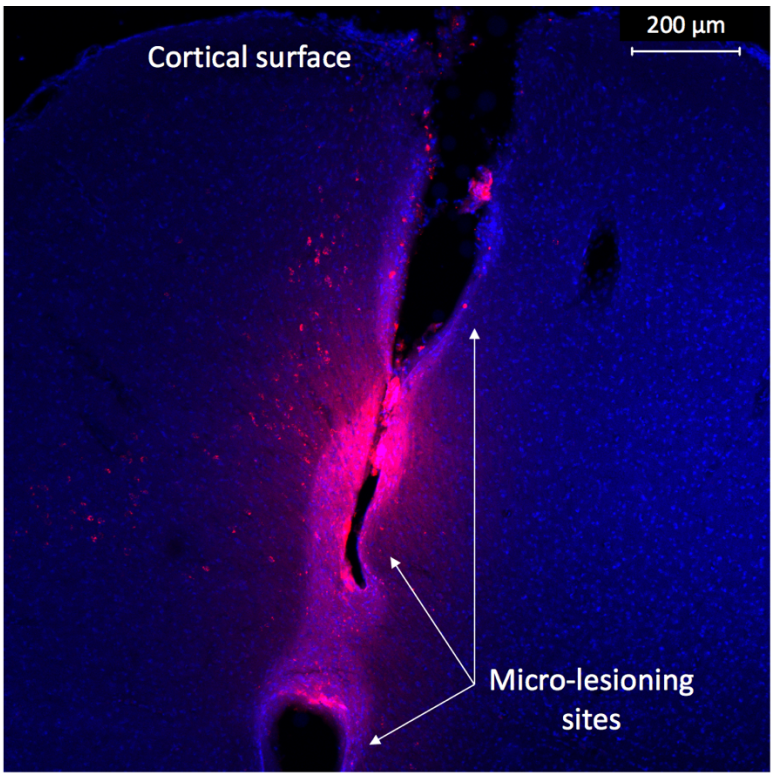


Figure 34: Image of a silicon probe implantation site within the cortex (left hemisphere) in one mouse. 3 micro-lesioning sites can be observed, alongside DiI staining. Nuclei were stained with NucBlue from the ProLongGlass mounting medium (ThermoFisher Scientific).

B. Sleep architecture in *Sleepy6* homozygotes and WT littermate controls

Raw signals, such as the LFP and EMG variance as plotted in Figure 35 in two representative animals, revealed no striking difference between the WTs and *Sleepy6* Homozygotes, although it appeared that Homozygotes may have more consolidated periods of sleep and wakefulness (see below).

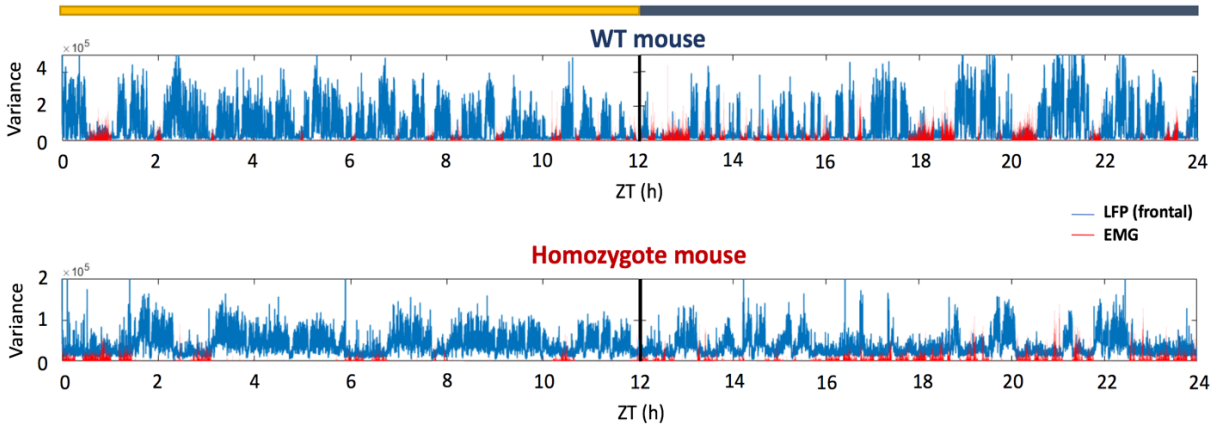


Figure 35: LFP and EMG variances from a baseline day in a representative WT (top panel) and Sleepy6 homozygous mouse (bottom panel) across 24 h of baseline recordings. LFP variance is shown in blue, EMG in red. Periods of low EMG activity and high LFP variance usually correspond to NREM sleep. Light and dark phases are represented with a yellow and dark blue bar – respectively – above the plots. ZT = zeitgeber time.

Further analysis of the recordings revealed that, as expected, *Sleepy6* homozygous mice spent overall less time asleep, both in NREMS and REMS compared to their WT littermates (Figure 36 a&b). Consequently, they also spend a higher amount of time awake (Figure 36 c). Interestingly, when looking at light and dark phases separately (Figure 37), it appears that *Sleepy6* mutants tend to spend more time in NREMS during the light phase, but much less during the dark phase, which accounts for the overall smaller amount over 24h. The most striking difference is seen in REMS, as *Sleepy6* Homozygotes spend less than 1 h during a baseline day in this state, compared to an average surrounding 2 h for their WT littermates.

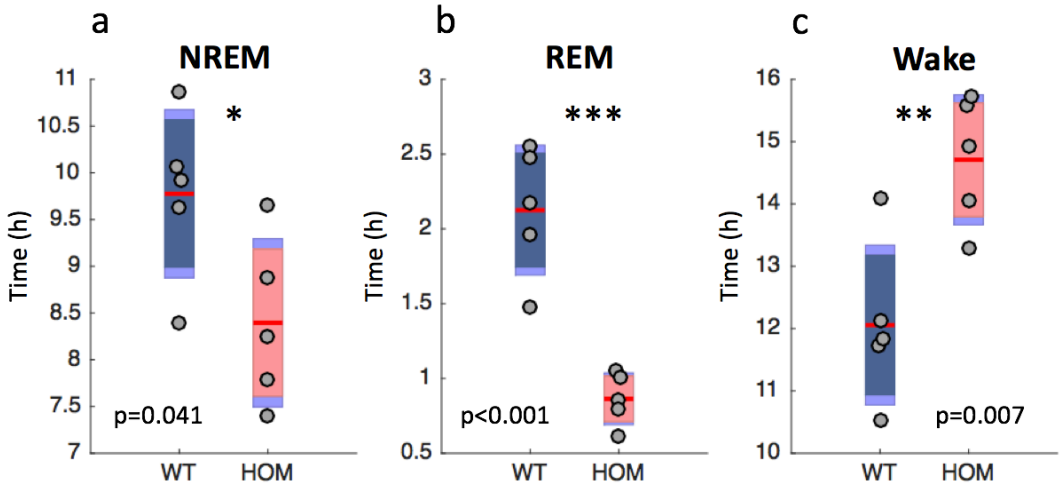


Figure 36: Total time in each vigilance state across 24h in Sleepy6 homozygous (HOM) and WT animals. n(WT)=5, n(HOM)=5. Red line: group mean, dark blue(WT)/red(HOM) area: 95-% CI, purple area=1 STD, grey circles represent individual animals. A two-way mixed design ANOVA revealed no main effect of genotype (F(1,8)=0.429, p=0.531), but a main effect of vigilance state (F(2,16)=315, p<0.001) and a significant interaction (F(2,16)=10, p=0.001). Interactions were analysed by post-hoc testing (independent samples t-tests) for each vigilance state separately, which revealed a significant effect of genotype in all cases (NREM: t(8)=2.431, p=0.041; REM: t(8)=6.022, p<0.001; Wake: t(8)=-3.589, p=0.007).

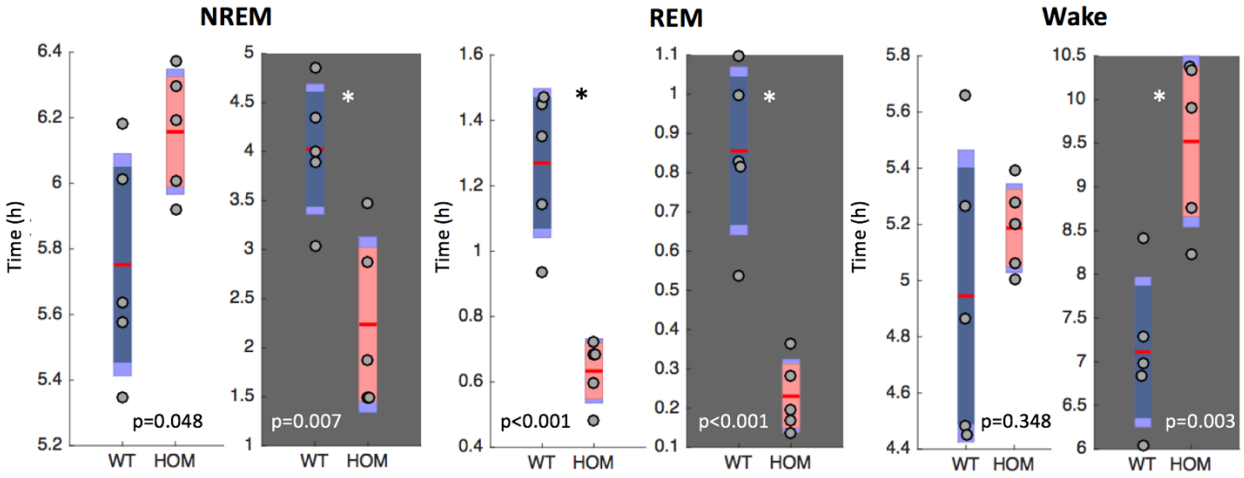


*Figure 37: Amount of time spent in each vigilance state during the light and dark phases of a baseline day in wild-type (WT) and Sleepy6 homozygotes (HOM). Mean ± SEM. n(WT)=5, n(HOM)=5. Red line: group mean, dark blue(WT)/red(HOM) area: 95-% CI, purple area=1 STD, grey circles represent individual animals. A two-way mixed-design ANOVA run independently for each vigilance state revealed significant main effects of genotype and light phase in each vigilance state (Wake: Genotype: F(1,8)=12.878, p=0.007, Light phase: F(1,8)=169.111, p<0.001, interaction: F(1,8)= 18.798, p=0.002; NREM: Genotype: F(1,8)=5.910, p=0.041, Light phase: F(1,8)=136.381, p<0.001, interaction: F(1,8)=20.566, p=0.0.002; REM: Genotype: F(1,8)=36.264, p<0.001, Light phase: F(1,8)=280.866, p<0.001, interaction: F(1,8)=0.048, p=0.832). Interactions were investigated further using post-hoc independent samples t-tests with a Bonferroni correction (new α = 0.05/6= 0.008). Cases where p-value< new α are reported with an * on the graphs, and the corresponding p-value is indicated at the bottom of each graph.*

We asked whether those differences between genotypes in the time spent in each state resulted from a decrease in the overall number of sleep episodes in *Sleepy6* Homozygotes compared to WT littermates, or whether the number of such episodes was conserved, but their length was abbreviated, or possibly a combination of both a reduction in episodes' number and duration. As expected, the number of NREMS and REMS episodes was significantly decreased in both the light and dark phases of a baseline day (Figure 38). Strikingly, however, the number of wake episodes was also decreased significantly in the dark phase, when animals are mostly awake, and show a decreasing trend in the light phase too (Figure 38 c). As *Sleepy6* Homozygotes spend more time awake (Figure 36) but have less wake episodes than the WT mice, this means that wake bouts are overall longer. Regarding NREMS and REMS bouts, the conclusion is not as straightforward as the animals have less bouts (Figure 38 a&b), but spend also overall less total time in each of this sleep states (Figure 36).

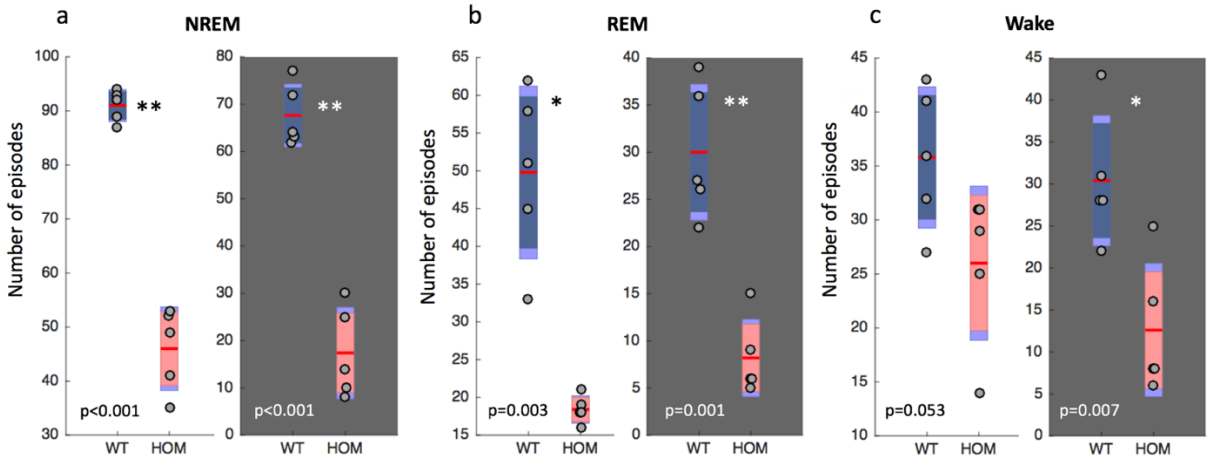


*Figure 38: Number of episodes in each vigilance state during the light and dark phases of a baseline day. Mean ± SEM. n(WT)=5, n(Hom)=5. Red line: group mean, dark blue(WT)/red(HOM) area: 95-% CI, purple area=1 STD, grey circles represent individual animals. A two-way mixed-design ANOVA run independently for each vigilance state revealed significant main effects of genotype and light phase (Wake: Genotype: F(1,8)=13.820, p=0.006, Light phase: F(1,8)=11.380, p=0.010, interaction: F(1,8)= 2.212, p=0.175; NREM: Genotype: F(1,8)=156.563, p<0.001, Light phase: F(1,8)=100.390, p<0.001, interaction: F(1,8)=0.768, p=0.406; REM: Genotype: F(1,8)=33.490, p<0.001, Light phase: F(1,8)=95.911, p<0.001, interaction: F(1,8)=11.770, p=0.009). Interactions were investigated further using post-hoc independent samples t-tests with a Bonferroni correction (new α = 0.05/6= 0.008). Cases where p-value< new α are reported with an * on the graphs, and the corresponding p-value is indicated at the bottom of each graph.*

We therefore asked whether the distribution of bout length would differ between genotypes. As shown in Figure 39, *Sleepy6* homozygous mice have significantly less NREMS and REMS bouts of short durations in both the light and dark phases, than WT littermate controls. *Sleepy6* Homozygotes also tend to have a higher number of long NREMS bouts in the light phase (Figure 39 a, left panel), although this is not significant if applying a Bonferroni correction for the multiple comparisons made.

These results therefore point towards two separate conclusions:

- *Sleepy6* Homozygotes spend more time awake than their littermate controls.
- Once *Sleepy6* Homozygotes enter a state – regardless of whether this is a wake or sleep state – they tend to remain in such a state for longer periods of time and do not show as many short bouts of any vigilance state as their WT littermates.

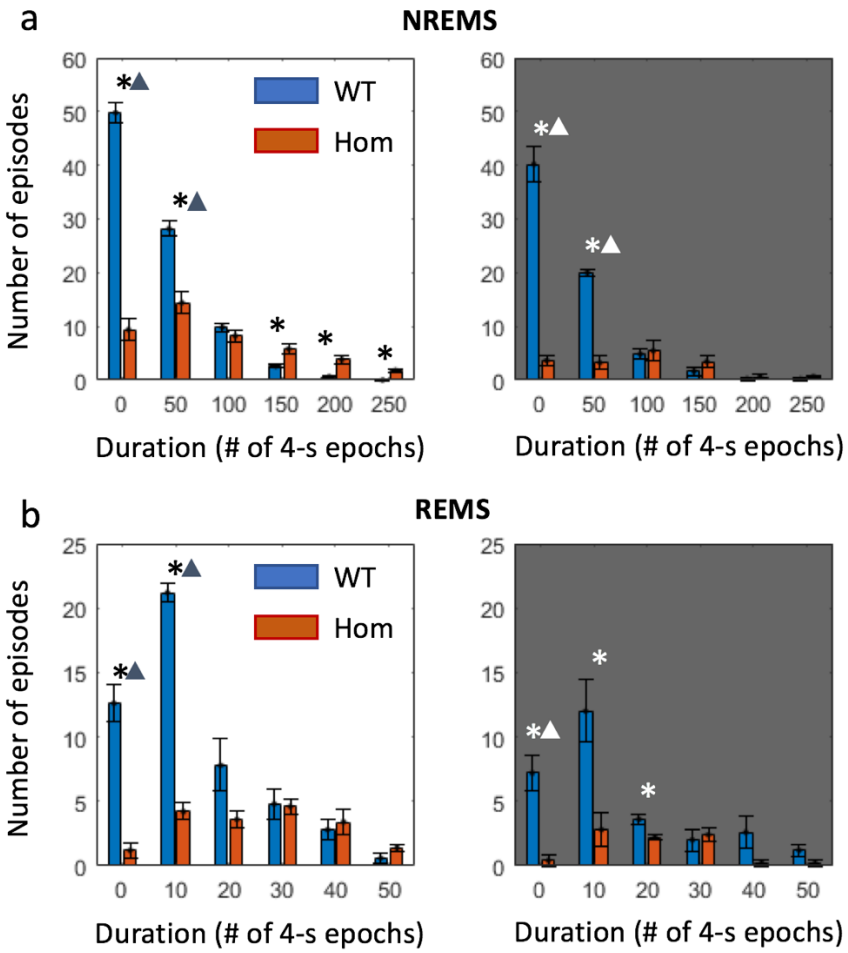


*Figure 39: Distribution of NREMS episodes (a) and REMS episodes (b) according to their duration, in the light and dark phases. Mean ± SEM. n(WT)=5, n(Hom)=5. Mixed-design ANOVAs (factors Genotype, Duration, Light Phase) were run independently for NREMS and REMS and revealed a significant main effect of genotype, light phase and duration in both cases (**NREMS**: genotype: F(1,8)=136.174, p<0.001, light phase: F(1,40)=84.333, p<0.001, duration: F(5,40)=275.391, p<0.001; **REMS**: genotype: F(1,8)=33.490, p<0.001, light phase: F(1,40)= 95.911, p<0.001, duration: F(5,40)=50.496, p<0.001). Post-hoc testing was performed with independent sample t-tests, with a Bonferroni correction (new α=0.05/6=0.008). Instances where p-values were <0.05 are reported with a * on the graphs, and those which were also <0.008 are reported with triangles.*

C. Spectral analysis across vigilance states and derivations

We next investigated the power density across frequencies in different vigilance states, in the two EEG derivations recorded and LFP channels. The differences observed were striking, with *Sleepy6* homozygotes showing a decrease in power density for most frequency bins, except in the delta band (0.5-4 Hz), and more precisely in the very slow frequencies (<2 Hz), where they show an increase in spectral power – Figure 40. The theta peak (theta range: 5-10 Hz) is still

observable in REMS in *Sleepy6* mice, except in the LFP channel plotted here (Figure 40, lower panels). This is not too surprising as the laminar probe was implanted in the frontal cortex, where the theta peak is generally not as predominant (Buzsaki, 2011; Vyazovskiy and Tobler, 2008). The fact that differences in higher frequency power do not always reach significance in the LFP data, when they do in both the frontal and occipital EEG derivations, likely stems from the reduced number of WT animals that could be included in the LFP analysis (two WT animals showed noisy laminar probe recordings and were therefore not included here).

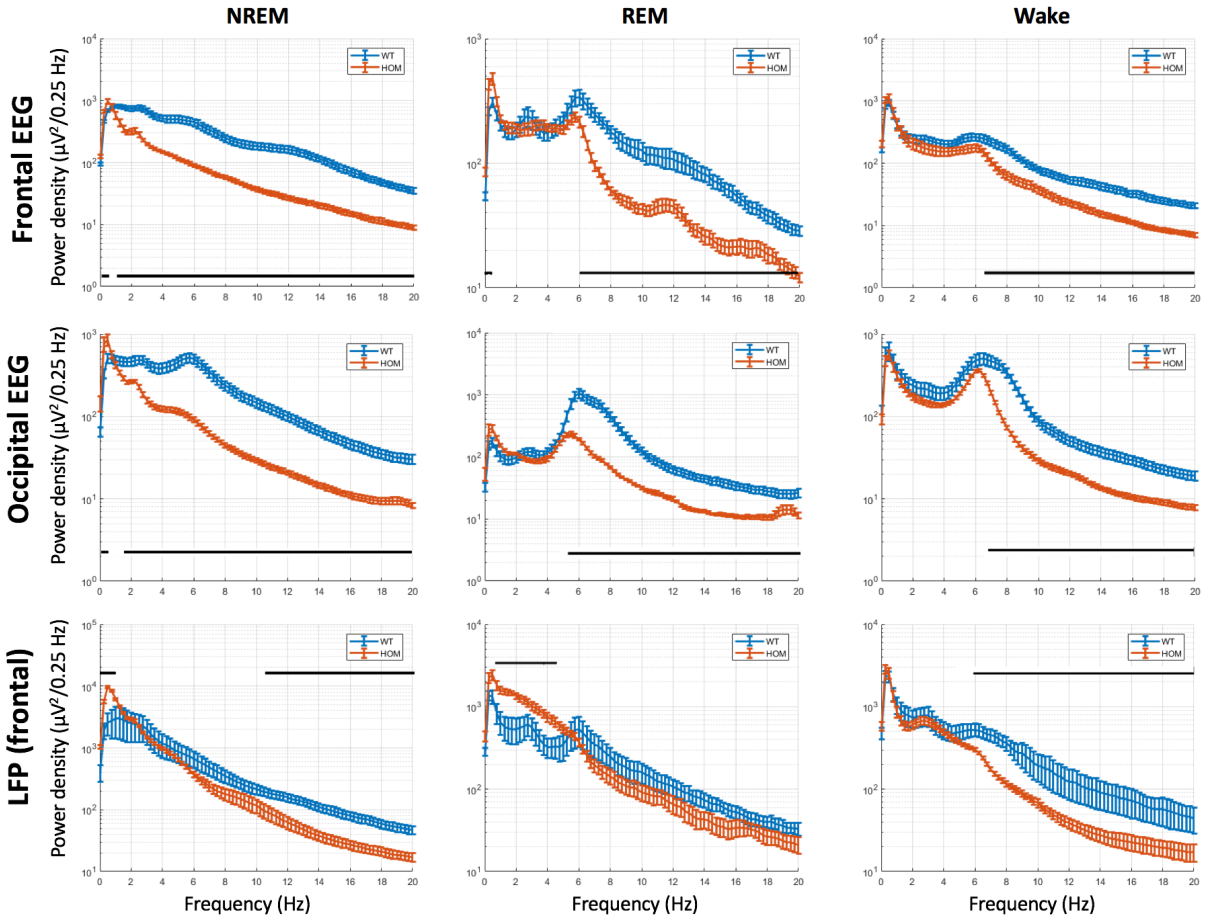


Figure 40: Absolute EEG and LFP spectra in NREM, REM and Wake in Sleepy6 homozygotes (HOM) and WT littermates. Spectra are shown for Frontal EEG (top panels), Occipital EEG (middle panels), and LFP channel (bottom panels). Mean ± SEM. EEG derivations: n(WT)=5, n(Hom)=5, LFP: n(WT)=3, n(Hom)=5. Independent t-tests were performed across frequencies from the log-transformed power density values; p-values ≤ 0.05 are indicated with black bars above or below the curves.

Such striking differences in the EEG and LFP spectra (Figure 40) could be anticipated given the differences observed in the recordings themselves: long period of neuronal silence could be observed in *Sleepy6* homozygous mice during NREMS, corresponding to unusually long-lasting slow-waves (Figure 41 b). This could not be observed in any of the WT littermates (Figure 41 a). This suggested a possible increase in the power density in the slower frequencies during NREMS in *Sleepy6* homozygotes, which is indeed the case, as shown in Figure 40. Interestingly, this increase in slow-wave activity is also significant in REMS, in the frontal EEG derivation and in the LFP.

These results suggest that the phenotypic differences observed do not only occur at a global level (i.e. differences in the total time spent in each state and in the duration of wake or sleep episodes), but also at a local – possibly cellular – level. Indeed, the long periods of neuronal silence recorded concomitantly by several channels of the laminar probe suggest that neurons cease firing together at least at a local network level, as can also be observed in WT littermates (and more generally as has been reported in the literature – see Introduction), but most importantly, that they also cease firing for extended periods of time of up to 4 s (Figure 41 b).

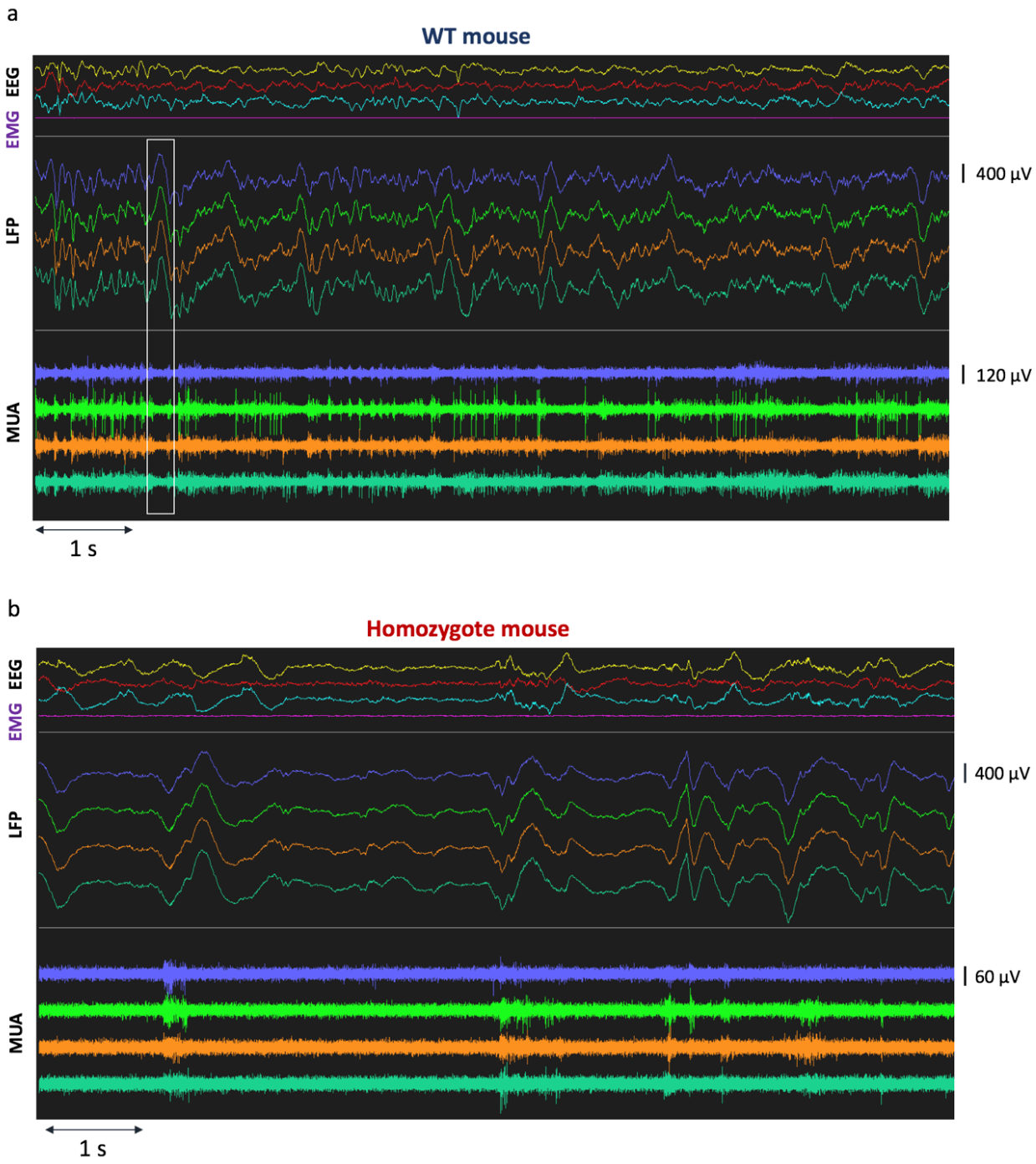


Figure 41: Sample EEG, LFP and multi-unit activity (MUA) recordings in NREMS from a WT mouse (a) and a Sleepy6 Homozygous mouse (b). Traces represent (in order, from top to bottom): frontal EEG, occipital EEG, fronto-occipital EEG, EMG, 4 consecutive LFP channels, 4 MUA traces from the same channels as those shown for LFP. A slow-wave with the corresponding period of neuronal silence ('OFF period') is highlighted in the top panel (white box). Note the increased length of such periods of neuronal silence in the Sleepy6 homozygote.

D. Reponses to sleep deprivation in *Sleepy6* homozygous mice

Given the striking differences observed in the total amount of time spent in NREMS, as well as given the increase in power density in slower frequencies, we next investigated the effects of sleep deprivation on *Sleepy6* mice. It is well known that an extended period of enforced wakefulness during an animal's natural rest phase results in an increase in slow-wave activity (SWA). SWA is defined as the EEG power density in the slow-wave frequency range (0.5-4Hz) during NREMS, and is a common measure of sleep need (see Introduction). On the one hand, it may be hypothesised that sleep deprivation would affect *Sleepy6* Homozygotes more strongly given their natural decreased sleep duration. On the other hand, an increase in power density in slower frequencies would suggest an ability for *Sleepy6* homozygous mice to dissipate sleep pressure more efficiently, or possibly for sleep pressure to build-up at a slower rate.

The distribution of the time spent in each vigilance state across baseline and sleep deprivation days revealed no striking differences between genotypes in the amount of time spent in each state following SD (Figure 42). If *Sleepy6* homozygotes appear to spend an increased amount of time in NREMS and REMS shortly after the 6 h of sleep deprivation, this should be put into perspective, as these significant differences are observable at similar zeitgeber times (i.e. indexed on the light-dark cycle, ZT 0 = lights on) during a baseline day. Similarly, although *Sleepy6* mice may seem to recover more quickly from sleep deprivation, sleeping more immediately after the deprivation period and spending an increased amount of time awake at the end of the recovery period, this is also the case at a similar time of day during the baseline recordings. It therefore seems that the baseline patterns in the distribution of vigilance states across 24 h are largely conserved in both WT and homozygous mice following SD.

Interestingly, Figure 42 also reveals that even during a baseline day, when *Sleepy6* mice spend generally more time awake than WTs (see above), this is not consistent throughout the 24h. *Sleepy6* homozygotes spend significantly more time in NREMS at the end of the light phase than their WT littermates. If they overall sleep less, this is because they then spend most of their time awake during the remaining of the 24 h (Figure 42, upper panels).

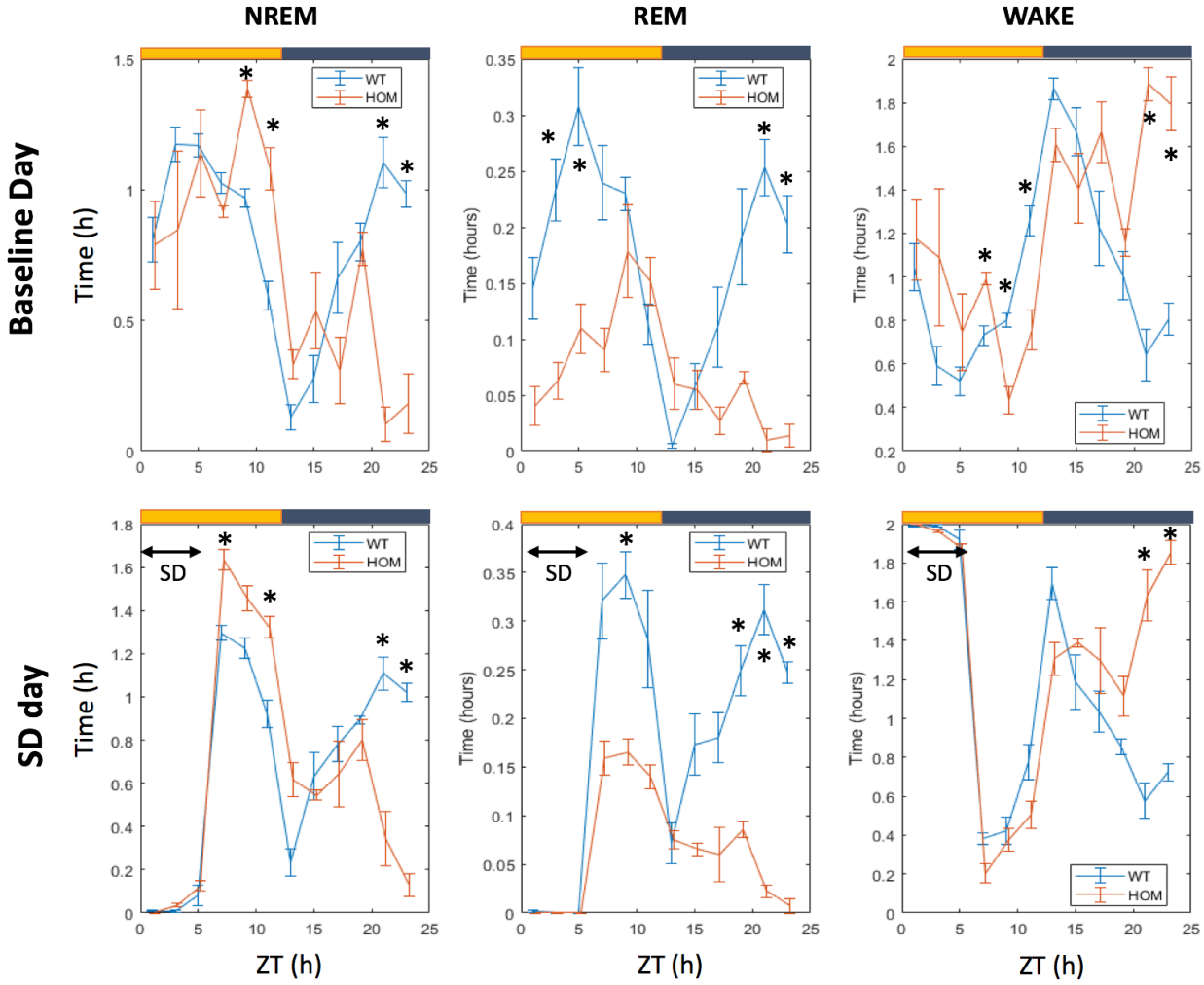


*Figure 42: Distribution of vigilance states across 24h of a baseline day (top panels) and sleep deprivation day (bottom panels). Data plotted in 2-h bins. n(WT)=5, n(HOM)=5. Mean ± SEM. Baseline day: Main effects analysed with a two-way mixed-design ANOVA revealed significant main effects of Time Point and Genotype, and a significant interaction Time Point*Genotype in all 3 vigilance states (**NREM**: Genotype: F(1,8)=5.355, p=0.049, Time point: F(11,88)=15.483, p<0.001, interaction: F(11,88)=8.909, p<0.001; **REM**: Genotype: F(1,8)=31.109, p=0.001, Time Point: F(11,88)=13.425, p<0.001, interaction: F(11,88)=10.255, p<0.001; **Wake**: Genotype: F(1,8)=11.605, p=0.009, Time point: F(11,88)=17.520, p<0.001, interaction: F(11,88)=9.959, p<0.001). Interactions were investigated further using post-hoc independent samples t-tests with a Bonferroni correction (new α = 0.05/12= 0.004). Cases where p-value< new α are reported with a **

*on the graphs. Sleep-deprivation (SD) day: Statistical tests run as in baseline day; we found significant main effects of Genotype and Time Point, as well as a significant interaction, in all 3 states except in NREM, where the effect of genotype was not significant (**NREM**: Genotype: F(1,8)=3.138, p=0.114, Time point: F(11,88)=104.375, p<0.001, interaction: F(11,88)=18.849, p<0.001; **REM**: Genotype: F(1,8)=165.493, p<0.001, Time Point: F(11,88)=41.023, p<0.001, interaction: F(11,88)=12.312, p<0.001; **Wake**: Genotype: F(1,8)=26.507, p=0.001, Time point: F(11,88)=110.965, p<0.001, interaction: F(11,88)=19.015, p<0.001). Post-hoc testing performed and reported as described in a). ZT = zeitgeber time.*

Given this conserved pattern of vigilance state distribution between a baseline and a sleep deprivation day, we then asked whether the response to SD in terms of SWA may appear different between *Sleepy6* homozygotes and WTs. When plotting SWA levels across 24 h of baseline recordings, followed by 6 h of SD (starting at the beginning of the light phase) and 18 h of recovery, it appears that the SWA rebound following SD (which expresses an increase in sleep pressure) is visible in WT mice (Figure 43 a – from ZT 30). This is not as discernible in *Sleepy6* homozygotes (Figure 43 b – from ZT 30), despite the fact that Figure 43 shows SWA in an LFP channel, where slow-waves appeared larger than in the EEG.

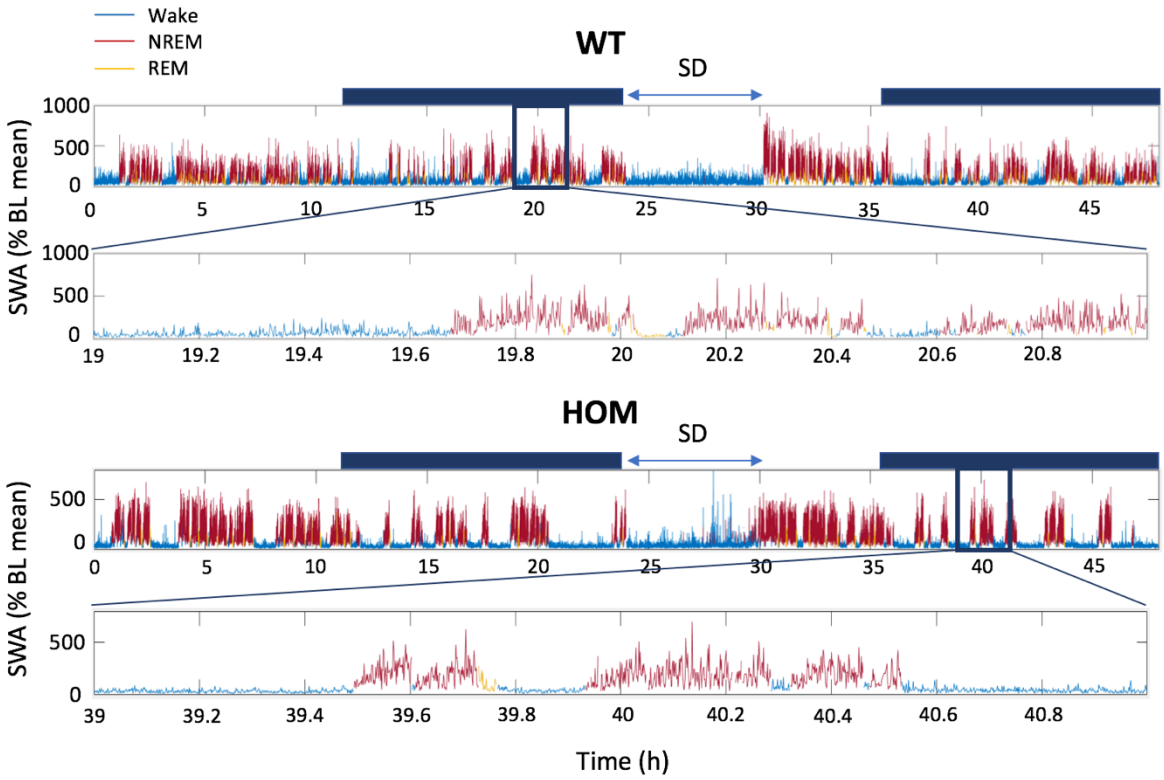


Figure 43: Slow-wave activity (SWA) levels across 48h and 2h in one individual WT mouse (top panels, frontal EEG) and one Sleepy6 homozygous (HOM) mouse (bottom panels, LFP). SWA levels are expressed as a percentage of baseline (BL) mean. Colour-coding indicates different vigilance states (blue for waking, red for NREM sleep and yellow for REMS). Light and dark phases are represented at the top of the 48-h plots (dark blue bars = dark phase). The 6 h of sleep deprivation (SD) are indicated with a blue arrow above the graphs. Note that signals can occasionally become noisy during waking.

We then quantified the amount of SWA in NREMS across those 48 h (24 h baseline + 6 h SD + 18 h recovery) in all mice (Figure 44). This revealed that the rebound in SWA following SD was significantly smaller in *Sleepy6* mice compared to WT. The difference between genotypes at the first time point following SD did not reach significance however (see Figure 44). It is important to note that values are normalised against mean SWA in NREMS during the 24-h baseline, and given that *Sleepy6* Homozygotes present with higher delta power in NREMS and REMS during baseline recordings (Figure 40), the rebound following SD might therefore not appear as pronounced for this reason.

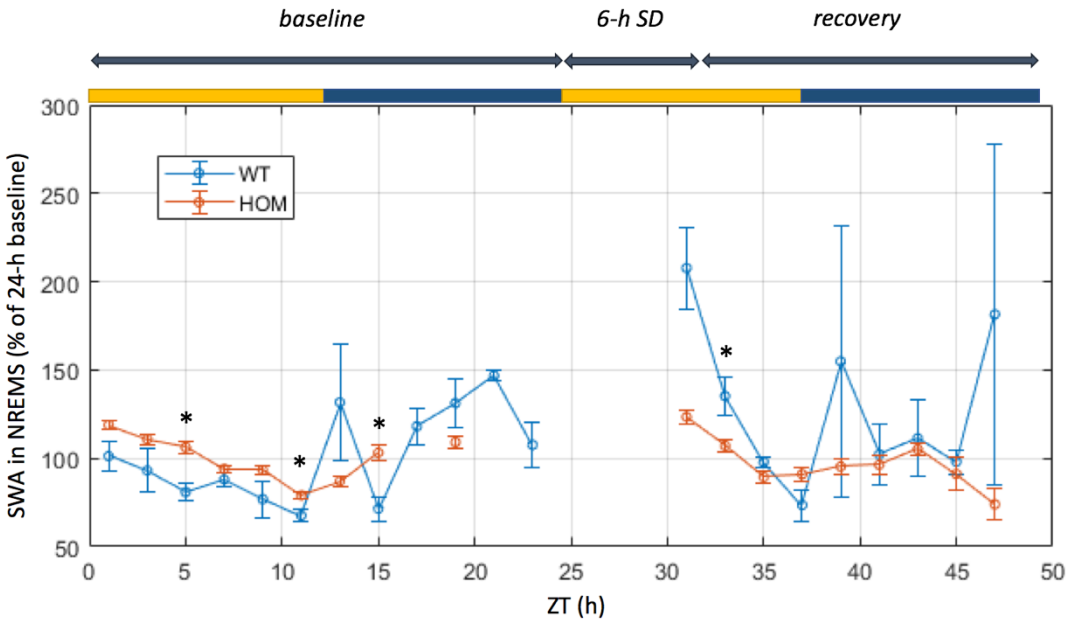


*Figure 44: SWA levels during baseline and following sleep deprivation. Values calculated from an LFP channel. Mean ± SEM; n(WT)=3, n(Hom)=5. Due to missing values, running an ANOVA was not practical. Independent t-tests were therefore performed, and as values are not independent, a Bonferroni correction was applied with a new α=0.05/number of tests=0.05/18=0.003; as this is a stringent criterion, p-values<0.05 are reported on the graph with * for reference; none of those values was <0.003. The first value following sleep deprivation (ZT=31 h) is not reported as significant as the Levene's test for equality of variances revealed that variances could not be assumed equal, and the adequate p-value was therefore p=0.063 (p=0.003 with equal variances incorrectly assumed).*

Additionally, Figure 44 reveals that during a baseline day, SWA is more evenly distributed in *Sleepy6* animals, compared to WT littermates which show an increase in SWA throughout the dark (active) phase. Both genotypes show a decreasing trend throughout the light (resting) phase, showing that as time spent asleep accumulates, sleep pressure (as measured by SWA) slowly decreases, both in Homozygotes and WTs.

Given the striking difference found in baseline spectra (Figure 40), to investigate the effect of sleep deprivation further, we plotted spectra in NREMS following sleep deprivation – normalised against the mean spectra across all NREMS occurring during the baseline day (Figure 45). While WTs show an increase in power density in the delta band (0.5-4Hz) immediately following SD (ZT6-8) (Figure 45, left panels), this increase is not as remarkable in

homozygous mice, in both Frontal EEG and LFP (Figure 45, right panels). Statistical analyses revealed that normalised spectra was significantly different between genotypes in the 4 hours following SD (ZT6-8 and ZT8-10), after which the recovery – in terms of changes in spectra relative to baseline – is comparable between *Sleepy6* Homozygotes and WTs (see Figure 45, legend). Evaluating the response to SD in terms of REMS may however be less relevant, and we therefore aimed to investigate REMS dynamics further, using alternative approaches.

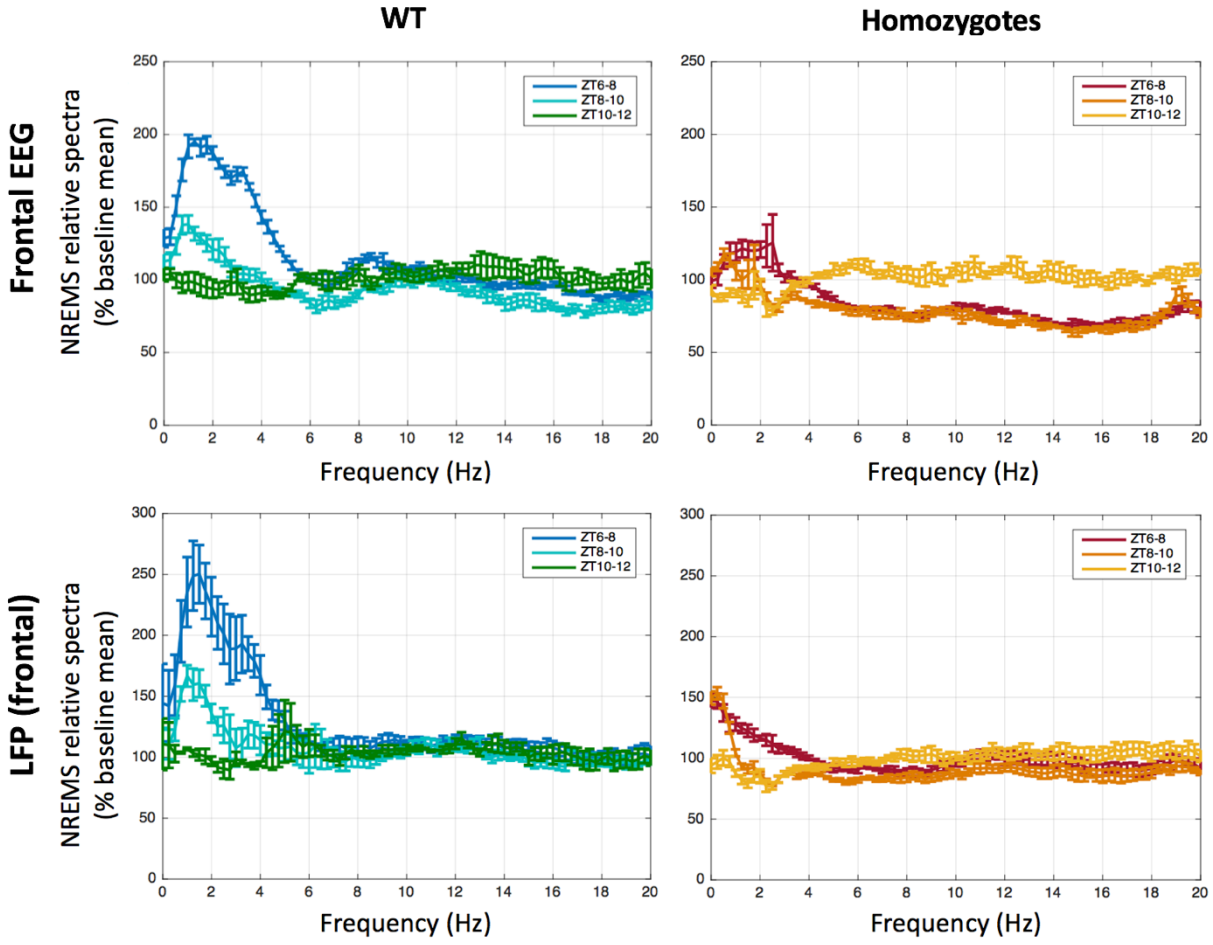


*Figure 45: NREM spectra over the 6h following sleep deprivation (SD) in the frontal EEG (top panels) and LFP (bottom panels). Each curve represents the average spectra across NREMS episodes pooled in 2-h bins from ZT 6 (end of SD) to ZT12. Mean ± SEM; EEG: n(WT)=n(Hom)=5, LFP: n(WT)=3, n(Hom)=5. Two-way mixed-design ANOVAs (factors: genotype and frequency bin) were run separately for the EEG and LFP and for each 2-h bin. This revealed a significant main effect of frequency bin in all cases, and of genotype for ZT6-8 & ZT8-10, but not for the subsequent time bin (**EEG**: ZT6-8: genotype: F(1,8)=259.063, p<0.001; ZT8-10: genotype: F(1,8)=40.233, p<0.001; ZT10-12: genotype: F(1,8)=0.004, p=0.948; ZT12-14: genotype: F(1,8)=3.093, p=0.117; **LFP**: ZT6-8: genotype: F(1,6)=22.341, p=0.003; ZT8-10: genotype: F(1,6)=23.432, p=0.003; ZT10-12: genotype: F(1,6)=1.390, p=0.283; ZT12-14: genotype: F(1,6)=1.323, p=0.294).*

E. Changes in signals across REM sleep episodes

The decreased amount of time spent in REMS by *Sleepy6* homozygotes could stem from a scoring bias whereby REMS would not be as easily distinguishable in Homozygotes than in WTs. As can be seen in Figure 46, REMS however presented with a characteristic trace in the occipital EEG – with low-amplitude theta waves – in both *Sleepy6* homozygotes and WT mice. It is therefore unlikely that the difference in the amount of REMS observed is merely due to scoring errors.

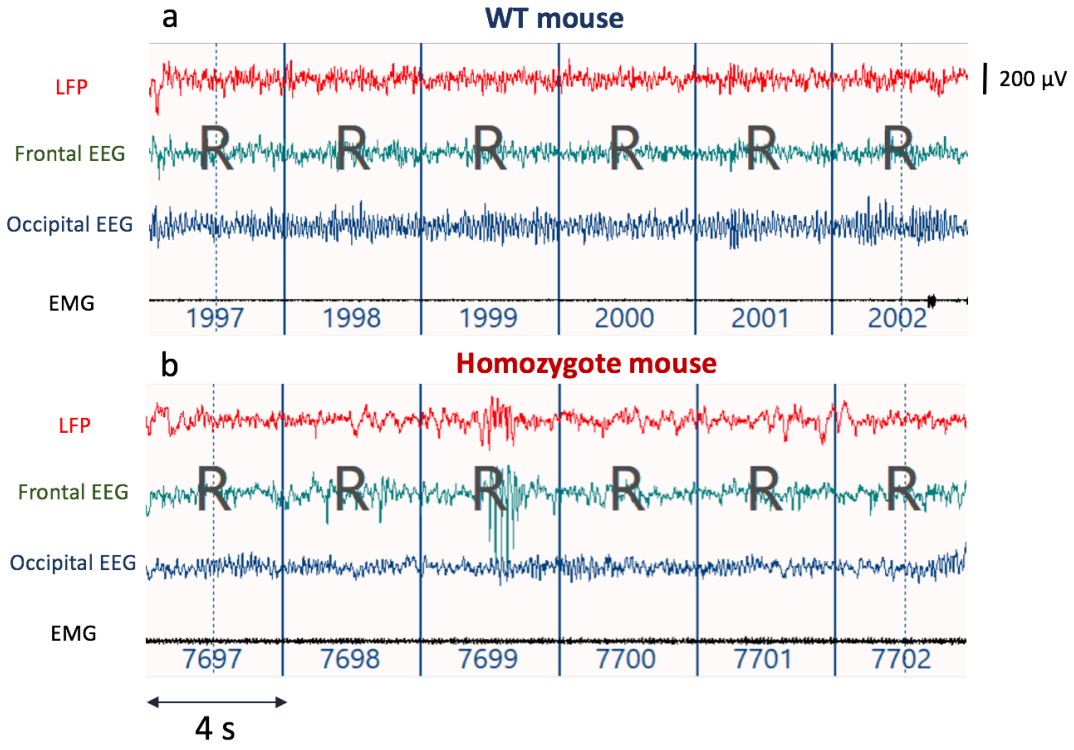


Figure 46: REMS LFP, frontal EEG, occipital EEG and EMG traces in a WT littermate (a) and Sleepy6 homozygote (b) across six 4-s epochs (=24 s). Data presented as it looks when scoring is being performed on the SleepSign software (see Methods). R=REMS.

Given that *Sleepy6* homozygous mice do not show many short REMS episodes, but show longer REMS episodes than WT mice (Figure 38 b), and that they display an increase in power density in slower frequencies in the LFP channel (Figure 47 a), we next investigated the evolution of signal frequency within individual REMS episodes. For this purpose, raw EEG or LFP signals

were filtered (Figure 47 b); each REMS episode was then arbitrarily divided into 6 sections (Figure 47 c), and the number of peaks within each section was calculated (using the *findpeaks* function of Matlab) before being normalised to the absolute length of a section (Figure 47 d).

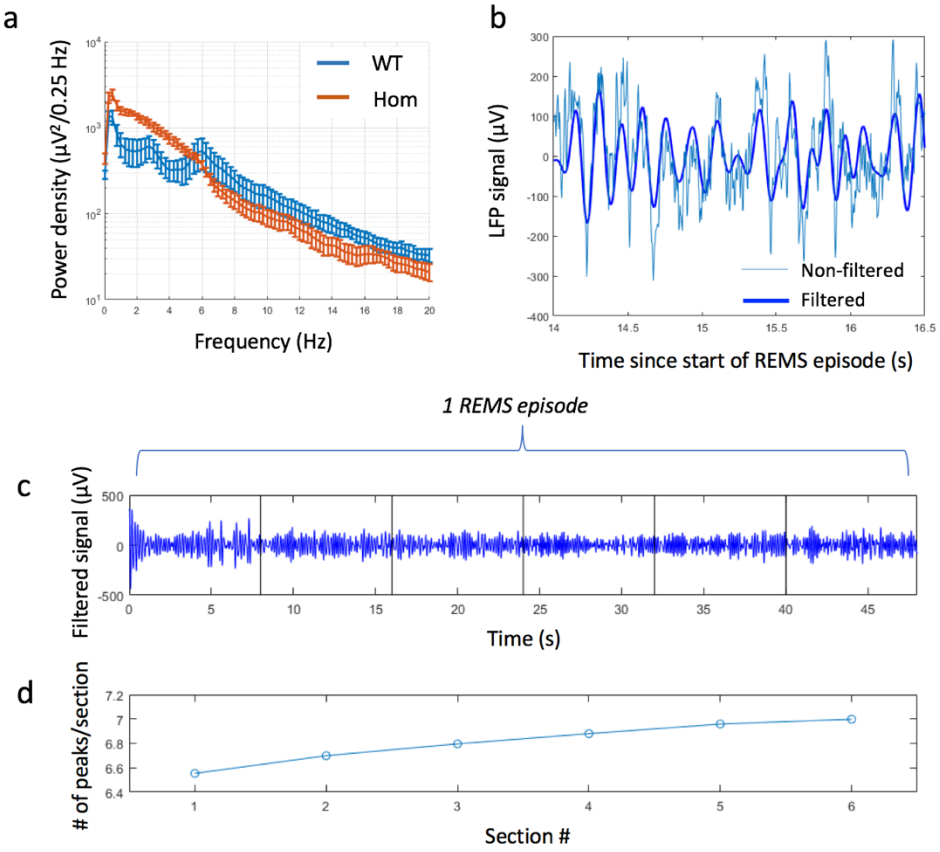


Figure 47: Evaluation of the evolution of peak frequency across REMS episodes. ***a)*** *Spectra in REMS in an LFP channel, replicated from Figure 40.* ***b)*** *Example of LFP raw and filtered signals (filtering between 5 and 9 Hz, using the* cheb2ord *function of Matlab).* ***c)*** *Filtered signal in one entire sample REMS episode. Episodes were arbitrarily divided into 6 sections.* ***d)*** *Number of peaks in the filtered trace within each section, calculated using the* findpeaks *function of Matlab, and normalised against the duration (in s) of a section. Only REMS episodes longer than 40 s were selected.*

Strikingly, we found that within REMS episodes, while the number of peaks within the first section was similar across genotypes, WTs subsequently showed an increase in the number of peaks (increasing frequency) while the mutant mice showed a slow but consistent decreasing trend (Figure 48). This resulted in significant differences in the number of peaks between

Sleepy6 homozygotes and WTs in both frontal and occipital EEG derivations, as well as in the LFP signal (Figure 48). This would suggest that when WTs enter REMS, it requires some time for theta power (5-10 Hz, the dominating rhythm during REM sleep) to fully build-up, while in *Sleepy6* homozygotes, theta power stays consistently similar within episodes, and slowly decreases until the animals wakes up or reverts to NREMS.

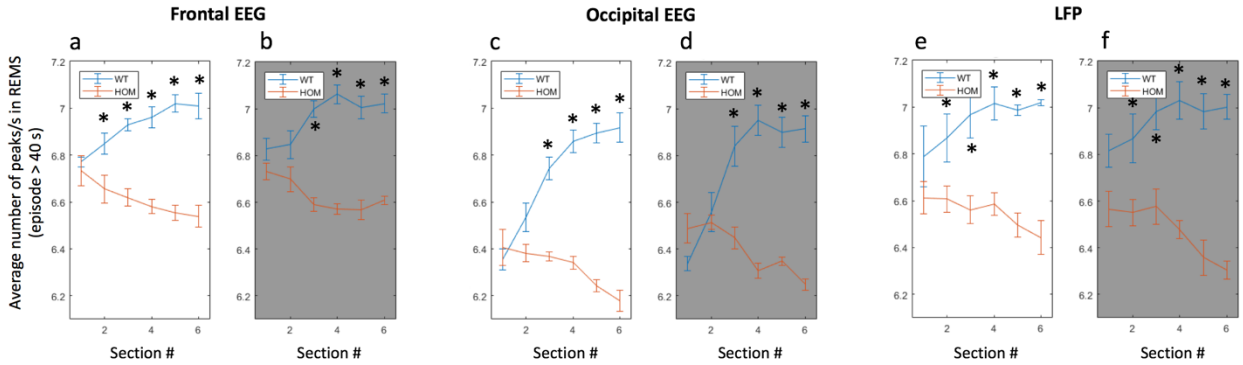


*Figure 48: Evolution of peak frequency across REMS episodes in the frontal and occipital EEG derivations and in an LFP channel See Figure 47 for an explanation of how values were calculated. Mean ± SEM; EEG: n(WT)=5, n(Hom)=5; LFP: n(WT)=3, n(Hom)=5. Mixed-design ANOVAs run independently for each derivation revealed a significant main effect of genotype in all cases, and of time point in some cases, but not of light phase (**Frontal EEG**: genotype: F(1,8)=81.430, p<0.001; **Occipital EEG**: genotype: F(1,8)=64.990, p<0.001, time point: F(5,40)= 14.197, p<0.001; **LFP**: genotype: F(1,6)=26.225, p=0.002, time point: F(5,30)=3.101, p=0.023). Post-hoc analysis was performed using independent sample t-tests, with a Bonferroni correction (new α=0.05/6= 0.008). p-values < 0.008 are reported with * on the graphs.*

Given these results, we then analysed the transitions from NREMS to REMS more closely. In particular, the changes in spectra were investigated when animals transition from a consolidated NREMS state (preceding NREMS episode lasting at least 1 min), to a consolidated REMS state (episodes of at least 40 s) (Figure 49). This revealed that while WT animals show a characteristic drop in the delta-band power when transitioning from NREMS to REMS (Figure 49 b&c), this is not observed in *Sleepy6* mice, where the spectra stays similar across states (Figure 49 a&c).

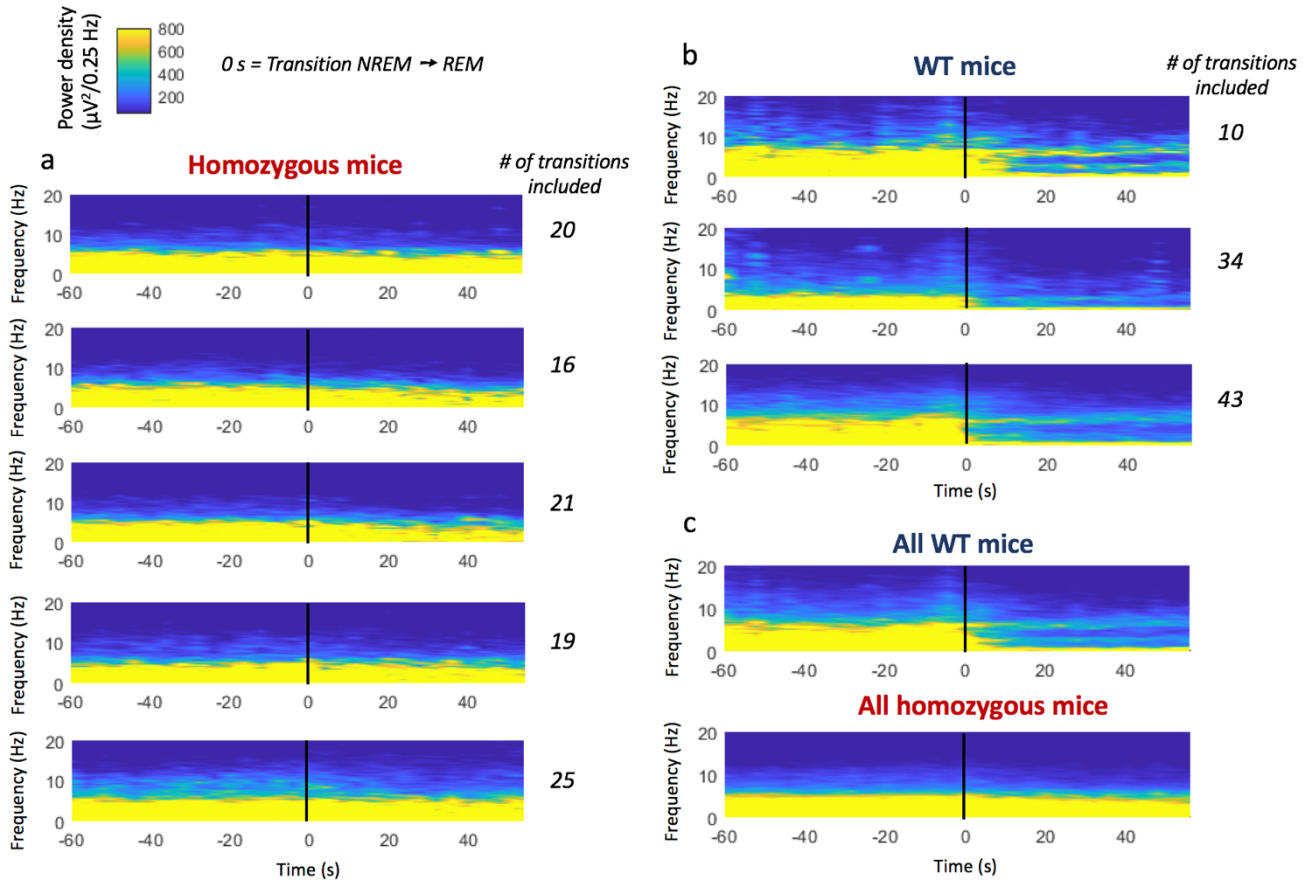


Figure 49: Average spectrum at the transition from NREM to REM sleep, in the local field potential, showing 1 min before and after each transition. ***a)*** *Spectra in 5 individual Sleepy6 homozygous mice. Colour map in top left-hand corner.* ***b)*** *Spectra in 3 individual WT littermates.* ***c)*** *Average spectra in WT littermates (n=3) and homozygotes (n=5). The number of transitions contributing to each figure is indicating on the right-hand side. Only transitions with at least 1 min of NREM sleep preceding the transition, and at least 40 s of REM sleep following the transition were included. For transitions where REM sleep did not last for up to 1 min following the transition, the spectrum values of the following state were not included in the analysis.*

F. Responses to auditory stimulation

To evaluate the arousal threshold of *Sleepy6* homozygotes in comparison to their WT littermates, 8-s sounds were played each minute for 1h30 (such a session was then repeated 4 times in the auditory experiment day – see Methods). This showed that the sounds elicited "twitches" in the EEG and EMG signals (Figure 50b) in a similar manner in WT and mutant mice (Figure 50a – right panel). A similar proportion of sounds occurring during NREM sleep led to a

sustained arousal (i.e. beyond the 8 s the sound lasted for) in WT and homozygote mice (Figure 50a – left panel). However, there were overall more arousals in WT mice, suggesting that brief arousals were less frequent in *Sleepy6* mutants.

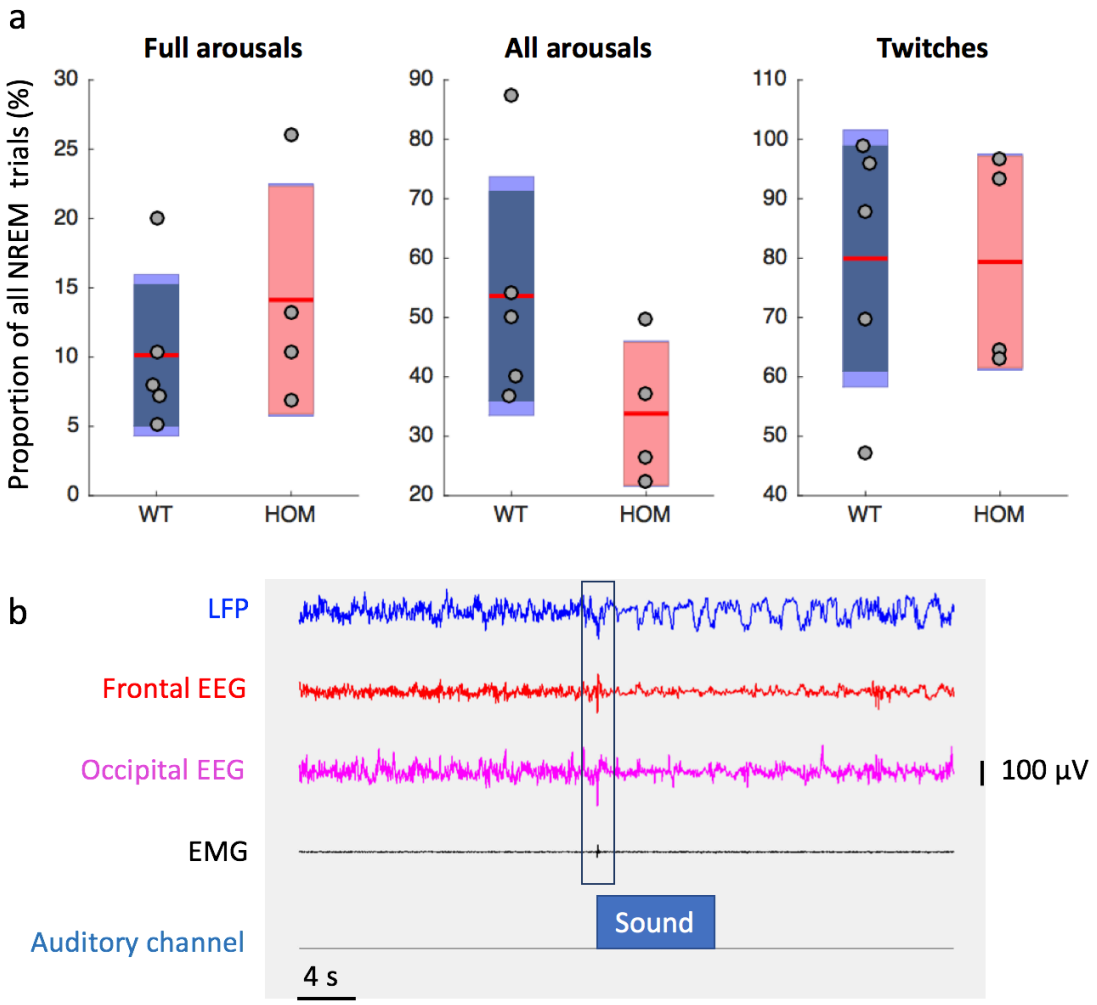


Figure 50: Effect of auditory stimulation on vigilance states in WT and Sleepy6 homozygous (HOM) mice. ***a)*** *Proportion of all trials happening during NREM which led to a full arousal (i.e. the mouse wakes up during the sound and stays awake for at least 16 s after the sound), to an arousal (the mouse shows signs of movement at least during the sound, note that this includes full arousals) and to twitches (as illustrated in panel b.) Red line: group mean, dark blue(WT)/red(HOM) area: 95-% CI, purple area=1 STD, grey circles represent individual animals.* ***b)*** *Illustration of a "twitch" in a Sleepy6 homozygous mouse occurring at the beginning of an 8-s sound. Note the subsequent increase in slow-waves in the local field potential (LFP). n(WT)=5, n(HOM)=4. Independent samples t-tests showed no significant effect of genotype in the numbers of full arousals (t(7)=-0.845, p=0.426), brief arousals (t(7)=1.720, p=0.129) or twitches (t(7)=0.043, p=0.967). Calculation of Pearson's correlation coefficient showed a large effect size in the case of all arousals (r=0.545), showing that the genotype accounts for more than 25% of the variance in the number of all arousals.*

The evolution of the power density spectra before, during and after a sound – depending on whether an animal was in NREM or REM sleep before the occurrence of the sound – showed that during the sound, power seems to decrease for most frequency bins, and subsequently increases again after the sound terminates (Figure 51). This occurs in both genotypes. However, the significant interaction Genotype*Time Point (see Figure 51 legend) when animals were initially in NREM sleep suggests that *Sleepy6* mutants respond differently to the sound than their WT littermates.

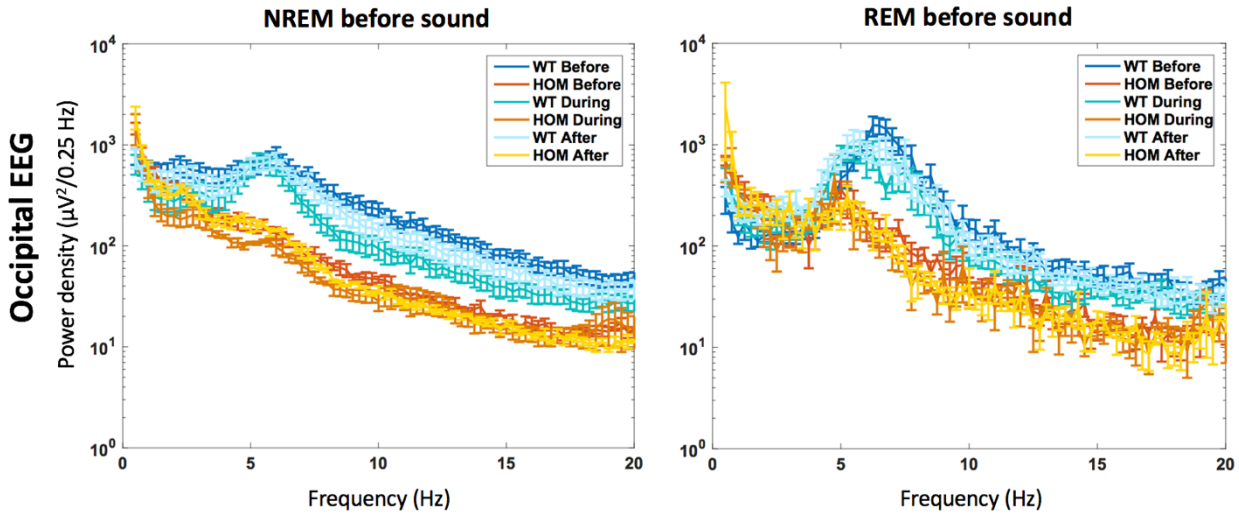


*Figure 51: Power density spectra in WT and Sleepy6 homozygous (HOM) mice in the occipital EEG derivation before, during and after an 8-s sound when the animal was initially in NREM sleep (left panel) or in REM sleep (right panel) prior to the start of the sound. Values are calculated over 8 seconds (before, during or after the sounds). Plots show mean±SEM for each frequency bin. n(WT)=5, n(HOM)=4. Mixed-design ANOVAs for repeated measures run on the log-transformed values of power densities – factors Genotype, Time Point (before, during or after the sound) and frequency bin – revealed that when animals were in NREM sleep before the sound, there was a significant main effect of Genotype (F1,7)=19.309, p=0.003), of Time Point (F(2,14)=43.219, p<0.001) and of frequency bin (F(78,546)=587.649, p<0.001) and a significant interaction TimePoint*Genotype (F(2,14)=5.431, p=0.018). If animals were in REM sleep before the sound, there was a significant main effect of Genotype (F1,7)=12.359, p=0.010), of Time Point (F(2,14)=10.337, p=0.002) and of frequency bin (F(78,546)=84.193, p<0.001) but no significant interaction TimePoint*Genotype (F(2,14)=1.395, p=0.280).*

4. DISCUSSION

The EEG and laminar probe recordings described and analysed in this chapter have confirmed that *Sleepy6* homozygous mice display a characteristic sleep architecture, where total waking time is increased, while both REMS and NREMS times are decreased, and where episodes of each vigilance state are longer and more consolidated than in WT mice. Spectral analysis of the EEG and LFP signals revealed striking differences, with an increase in delta (0.5-4 Hz) power in *Sleepy6* Homozygotes in both NREMS and REMS, and a decrease in EEG power for most frequency bins > 6 Hz in all vigilance states (Figure 40). Despite this increase in delta power in NREMS during baseline recordings, the SWA rebound following a period of 6 h of sleep deprivation was not as pronounced in *Sleepy6* mice compared to their WT littermates. This may partially stem from higher baseline delta-power values.

A. Increased sleep efficiency or chronic sleep deprivation?

This increase in lower-frequency power is open to two opposing interpretations. On the one hand, it could reveal more efficient sleep and thus would explain why *Sleepy6* mice tend to sleep less: they need less time asleep to dissipate their sleep pressure thanks to a higher sleep intensity – which is indeed often evaluated using NREMS SWA (Achermann and Borbély, 2003; Borbély et al., 1989). On the other hand, this constant increase in the EEG and LFP power in the slow-wave frequency range could reflect a state of constant sleep need, which would explain why every time the animals eventually enter NREMS, their SWA levels are higher; this would also be consistent with the attenuated increase in SWA following SD. Indeed, as discussed in the introduction, assuming that sleep pressure increases in a saturating exponential manner, if the *Sleepy6* mice are consistently closer to the upper threshold of sleep need, then the absolute

amplitude of the variations in SWA will be diminished (Borbély, 1982; Daan et al., 1984). This second interpretation would be in agreement with other experimental observations: *Sleepy6* homozygotes were much more difficult to keep awake towards the end of the sleep deprivation period, and if they entered NREMS during that time, it proved harder to wake them up. The auditory stimulation experiment however showed no significant difference in the arousal threshold of *Sleepy6* homozygotes compared to their WT littermates, although once woken up, they tend to stay awake (fewer number of brief arousals).

This observation would also be relevant with clinical literature showing that children with ADHD may hide an increased need for sleep behind their hyperactivity: ADHD is indeed associated with sleep disturbances, which include increased daytime sleepiness, increased sleep onset latency, decreased sleep time and difficult awakening in the morning (Cassoff et al., 2012; Hvolby, 2015; Owens, 2009). This is in line with the results obtained in the *Sleepy6* mice, which take longer to fall sleep at light onset and show a peak of activity late after dark onset (see Figure 35 & Figure 42). Given the links that can be drawn between the *Sleepy6* line and ADHD with regards to the specific mutation affecting the Sleepy 6 mice (see Chapter 3), this is of particular interest.

B. An impairment in the "sleep switch"?

The difficulty to wake *Sleepy6* mice is also in line with the finding that they go through a decreased number of episodes of each vigilance state during a 24-h period, and that episodes are overall longer (Figure 38 & Figure 39). This leads to a lower frequency of transitions between vigilance states in *Sleepy6* mice. This is consistent with previous findings showing that *Sleepy6* homozygotes have a dramatically prolonged period of sleep following a light pulse compared to their WT littermates (Heise, 2015). This result also suggests that when *Sleepy6*

mice enter a new state, it takes them longer to switch to another vigilance state, and may reveal an impairment in switching between states. This is further suggested by the auditory experiment which showed that very brief arousals are less frequent in *Sleepy6* mutants, although full arousals are as frequent as in WT littermates. This may indicate that if a mutant mice wakes up, it is less likely that it will go back to sleep immediately after. As mentioned in Chapter 1, recent studies have suggested a mechanism for a sleep/wake switch in both flies and rodents (Pimentel et al., 2016; Saper et al., 2010). A "flip-flop" switch has been proposed, to allow for a rapid transition between NREM sleep and wake states and prevent animals from lingering between two vigilance states – half awake and half asleep (Saper et al., 2001, 2010). *Sleepy6* mice do not show any notable mixed states (it is actually their WT littermates which show striking NREM/REM and REM/wake mixed states); therefore such a putative flip-flop switch would not take longer to move from one state to the next in *Sleepy6* Homozygotes, but would instead require a stronger "force" to be moved. Saper et al. (2001) propose that if neuronal firing is weakened on either side of this bistable switch, then the stability of the switch is compromised; on the other hand, they also propose that the time it takes to transition from one state to the next may depend on the ability for a population of neuron that promote a given state to overcome the "resistance" of the population of neurons promoting the current state (Saper et al., 2010). In *Sleepy6* mice, we observe an increased stability of each state, suggesting that the neuronal populations responsible for stabilising each state have a stronger firing pattern and their inhibitory pathways may be impaired. However, how plausible is this scenario, given the consequences at a cellular level of the *Vamp2* mutation present in the *Sleepy6* line?

C. Neuronal silence and vesicular release.

MUA recordings shed light on a striking neuronal firing pattern in *Sleepy6* mice during NREMS. Slow-waves are associated with prolonged periods of neuronal silence, where all neighbouring neurons seem to stop firing altogether for up to 4 s, resulting in an almost flat EEG signal (Figure

41). Such patterns of neuronal activity are seldom seen during natural sleep and are a more common feature of general anaesthesia (Antkowiak, 2002; Buzsaki, 2011; Lukatch and MacIver, 1996).

Data obtained at MRC Harwell indicate an impairment in vesicular release due to the mutation in *Vamp2*, which plays a key role in vesicular and cellular membrane fusion (se Chapter 1). It appears that vesicles dock to the membrane but do not fuse as efficiently, preventing the adequate release of the neurotransmitter(s) they contain in the synaptic cleft. This is particularly consistent with previous findings from *Vamp2* knock-out studies, which obtained similar findings (Schoch et al., 2001). An impairment in vesicular release could be related to an anesthetised state: it has been shown that general anaesthetics – such as isoflurane, propofol or etomidate – induce a decrease in synaptic neurotransmitter release machinery by interacting with multiple SNARE proteins (Herring et al., 2009, 2011; Xie et al., 2013b). This could account for the long periods of neuronal silence observed in *Sleepy6* homozygotes while they are (naturally) asleep: given their mutation in VAMP2, which is a SNARE protein, *Sleepy6* mice may present features of an "inherently anesthetised" state.

Additionally, results obtained from collaborators at University College London from the *Sleepy6* mice are complementary with the data presented in this thesis. *Sleepy6* homozygotes showed a 10-fold decrease in vesicular-release probability following single action potentials, while such an effect was not observed in response to a train of spikes. Although it is not yet clear how this may relate to the results obtained from the *in vivo* electrophysiology recordings presented in this chapter, it confirms that the behavioural phenotype seen in *Sleepy6* homozygotes is incontestably linked to changes at the cellular level. It is possible that the impaired vesicular release in response to a single action potential, but not to a train of spikes, reflects an inherent "inertia" in the neuronal circuitry of the mutant *Sleepy6* mice.

D. REMS and body temperature

Our results also showed differences in REMS dynamics, with not only a decreased total time spent in REMS, but also differences between *Sleepy6* Homozygotes and WTs regarding the frequency of the trace during REMS episodes (Figure 48) and at the transition from NREMS to REMS (Figure 49).

Interestingly, it has been shown that brain temperature can affect the EEG signals during REMS: for instance, the drop in temperature during torpor has been shown to create a shift of the theta peak towards slower frequencies (Deboer, 1998, 2002), consistent with our findings. *Sleepy6* mice have been shown to have a reduced core body temperature compared to WT controls, except during the last 4 h of the dark phase when they tend to have a higher temperature than the WTs (possibly due to their level of activity peaking at this time when WTs tend to be more quiet before the start of the light/resting phase) (Heise, 2015). Therefore, it cannot be excluded that the differences relating to REMS observed in *Sleepy6* mice may originate – at least in part – to independent features of the *Sleepy6* phenotype, such as body temperature. These observations all stem from the original mutation however, as indeed VAMP2 also plays a role in endocrine and fat cells (Baumert et al., 1990; Olson et al., 1997), which likely accounts for the reduced fat mass and reduced body temperature observed by Heise and colleagues (2015) in *Sleepy6* mice.

Finally, it has been shown that theta rhythms during REMS play a role for spatial and memory consolidation (Boyce et al., 2016). Given the reduced amount of time *Sleepy6* mice spend in REMS, and given the changes in theta rhythm itself during REMS episodes (Figure 48 & Figure 49), this could provide a partial explanation for the learning and memory impairments in the object-in-place task described in Chapter 3.

E. Limitations

This therefore brings a necessary question: given the variety of abnormalities shown by the *Sleepy6* homozygotes, how relevant is this line as a model to study sleep homeostasis? This will be discussed further in Chapter 6. As it is acknowledged that sleep serves several functions spanning from cognitive processes to immune function (Krueger et al., 2016) – see Chapter 1, it is possible that no *in vivo* model can exist with solely an impairment in sleep homeostasis that does not affect other bodily systems. The different abnormalities observed in *Sleepy6* mice may therefore be direct consequences of the mutation in the *Vamp2* gene, but part of those abnormalities may well stem directly from the sleep phenotype itself. For this reason, the *Sleepy6* line may still be relevant and useful as a sleep homeostasis model of research.

F. Further investigation of sleep homeostasis in *Sleepy6* mice.

A possible way to investigate further how sleep homeostasis may be affected in *Sleepy6* homozygotes is to apply a mathematical model of sleep regulation to the data recorded in those mice. The two-process model, for instance, would prove valuable to determine whether the sleep pressure builds up at a slower rate in *Sleepy6* mice than in WT controls, or whether it decreases at a different rate (Borbély, 1982; Franken et al., 2001; Guillaumin et al., 2018; Huber et al., 2000a). It could also tell us whether *Sleepy6* homozygotes err near their upper threshold of sleep pressure – as discussed above – or on the contrary benefit from a deep and efficient sleep that allows them to come back to low levels of sleep pressure more quickly than their WT counterparts. Sleep modelling would provide us with important additional insights to try and understand the SWA dynamics observed in *Sleepy6* mice.

We have shown here for the first time that the sleep phenotype observed in *Sleepy6* mutant mice goes beyond mere changes in sleep duration. Alternations between vigilance states are impaired, and neuronal activity during NREM sleep shows striking periods of silence. This provides a cellular basis for the changes in sleep homeostasis observed following sleep deprivation. The next chapter will give us insights into changes at a more global level in the dynamics of sleep homeostasis in *Sleepy6* mice.

CHAPTER 5: Computational modelling of sleep-wake regulation in C57BL/6J and *Sleepy6* mice

Part of the data presented in this chapter was published in the journal Sleep *in April 2018 under the title: "Cortical region-specific sleep homeostasis in mice: effects of time of day and waking experience." All texts and figures presented here are entirely my own work, and most have been modified for inclusion in this chapter. Additional unpublished data from the Sleepy6 mice has also been included. The electrophysiology recordings from C57BL/6J mice on which the 'initial' modelling study is based were performed by Laura McKillop, Nanyi Cui and Simon Fisher. All recordings from Sleepy6 wild-type and homozygous mice are my own work (see Chapter 4).*

1. INTRODUCTION

Throughout 24 hours all animals spend time awake and sleeping, and the propensity for sleep and waking are determined by the time of day, preceding sleep-wake history and homeostatically regulated needs such as hunger (Brown et al., 2012; Fuller et al., 2006; Huber et al., 2007; Szentirmai et al., 2010). As introduced in Chapter 4, slow-waves (0.5-4 Hz) during non-rapid eye movement sleep (NREMS) have been shown to be correlated with sleep intensity, and EEG slow-wave activity (SWA, EEG power density in the slow-wave frequency range) is commonly used as a biomarker of sleep need. SWA indeed displays a global declining trend

during sleep and its levels at the onset of the first NREMS episode depend on prior waking (Achermann and Borbély, 2003; Borbély et al., 1981; Dijk et al., 1990).

A. Processes underlying the regulation of sleep/wake architecture

The mechanisms responsible for the architecture of waking and sleep, and the dynamics of SWA remain unclear. It has been proposed that sleep pressure reflects processes implicated in energy homeostasis, synaptic plasticity or prophylactic cellular maintenance (Benington and Heller, 1995; Cantor, 2015; Krueger et al., 2008, 2016; Scharf et al., 2008; Siegel, 2005). For example, as discussed in Chapter 2, adenosine levels increase with time spent awake in some brain areas (Basheer et al., 2004; Benington and Heller, 1995; Porkka-Heiskanen et al., 1997). This increase may then have an impact on subcortical circuits responsible for sleep control (Krueger et al., 2008), or may inhibit specific neuronal populations in the cortex (Benington and Heller, 1995; Krueger et al., 2008). The role of adenosine in sleep homeostasis is still a matter of discussion however (Basheer et al., 2004; Blanco-Centurion et al., 2006; Scharf et al., 2008).

At the same time, several electrophysiological and molecular markers of synaptic strength change across waking and sleep (Liu et al., 2016; Vyazovskiy et al., 2011b). During prolonged waking, EEG becomes progressively slower as the animal spends more time in quiet waking, and slow waves intrude into the wake EEG (Borbély and Neuhaus, 1979b; Tobler and Borbély, 1986; Vyazovskiy and Tobler, 2005a). Waking activities recruiting specific local cortical areas may therefore lead to a local accumulation of sleep need differentially across brain areas (Huber et al., 2004; Krueger et al., 2008; Tononi and Cirelli, 2003). During subsequent sleep, SWA declines progressively, although this happens at a different rate between lower and faster frequencies within the SWA band (Achermann and Borbély, 1997; Huber et al., 2000b; Vyazovskiy et al., 2007). This may result from a redistribution of EEG power towards slower frequencies, which

is in turn accounted for by changes in the underlying network dynamics, such as neuronal excitability, and the number and duration of neuronal population ON and OFF periods (Vyazovskiy and Tobler, 2005b). Our understanding of the cellular and network mechanisms underlying sleep homeostasis have recently developed further (Donlea et al., 2014; Pimentel et al., 2016; Pirone et al., 2016; Saper et al., 2001, 2010). Yet, the temporal dynamics of this process remains to be fully elucidated, and computer modelling approaches may offer complementary insights in that respect.

B. History of the two-process model of sleep

Mathematical modelling is an essential tool to investigate sleep regulation. The "two-process" model, which posits that sleep is regulated via the interaction between a homeostatic, sleep-dependent component (Process S) and a circadian component (Process C) , has been extensively used since it was first published in 1982 (Borbély, 1982; Daan et al., 1984). In humans, Process C reflects the daily variations of sleep propensity controlled by the internal circadian clock, generated in the suprachiasmatic nuclei of the hypothalamus (Klein et al., 1991), and therefore keeps track of environmental time. Process S, on the other hand, reflects instantaneous sleep need; since SWA during NREMS, as mentioned above, is commonly used as a biomarker of sleep need, it has also been traditionally used to calculate parameters necessary to simulate Process S.

The first qualitative version of the two-process model was described in 1982 by Alexander Borbély (1982), and two years later, an implementation of a quantitative version of the model was published (Daan et al., 1984). In both versions, Process S levels were allowed to oscillate between thresholds subject to circadian variations, and both assumed the presence of a single

circadian pacemaker; indeed, the presence of several pacemakers was still debated at the time (Daan et al., 1984; Moore-Ede et al., 1982).

While the original model accounted for a wide range of experimental observations, it did not include intra-episodic dynamics of SWA – an omission that has been redressed in 1993, when a new elaborated version of the model was developed (Achermann et al., 1993). The three aforementioned versions of the model were based on human EEG recordings. The model, however, was also applied to recordings performed in rodents, both rats (Franken et al., 1991), and mice – showing that sleep/wake architecture differs greatly between mouse strains (Huber et al., 2000a).

C. Contribution of the model to our understanding of sleep/wake regulation.

Although the model originally tackled the build-up of sleep pressure as a global process throughout the brain, evidence soon showed that SWA varies in a topographical manner, suggesting differential dynamics between cortical regions (Rusterholz and Achermann, 2011; Werth and Borbély, 1995; Werth et al., 1996a, 1997; Zavada et al., 2009). For example, a frontal predominance of SWA during NREMS has been shown in rodents (Huber et al., 2000b; Schwierin et al., 1999; Vyazovskiy et al., 2002).

Although the underlying mechanisms still remain to be fully elucidated, it is hypothesised that activities engaged in during the preceding wake period or anatomical discrepancies may play a role in the differential dynamics of sleep need across cortical areas (Huber et al., 2004; Murphy et al., 2011; Tononi and Cirelli, 2006; Vyazovskiy et al., 2006). As early as 1997, showing that levels of SWA were higher in the anterior derivation, Werth and colleagues (1997) predicted that Process S, as formalised in the two-process model, would decline at a steeper rate in the anterior regions of the brain, as compared to more posterior regions, resulting in regional

differences in sleep-homeostasis processes. Since then, further studies have focused on investigating whether the dynamics of Process S indeed show regional specificity. A first study showed local differences in the decay rate of Process S (Zavada et al., 2009). Another study then analysed topographical differences in the rise and decay rates of Process S and found that those dynamics were slower in the fronto-central areas than in the parieto-occipital and frontal areas (Rusterholz and Achermann, 2011).

Additionally, SWA is affected by lighting conditions and it cannot be excluded that the dynamics of Process S may be continuously influenced by circadian processes (Borbély et al., 2016). While some aspects of sleep homeostasis – such as EEG power densities in the delta and theta frequencies – have been shown to be independent of circadian time (Dijk et al., 1987), other aspects of sleep homeostasis may depend on time of day. For example, it was found that the time constant of decline of SWA was lower after a sleep deprivation happening in the dark, as compared to deprivation happening in the light period (Vyazovskiy et al., 2007). Another study showed that the fit between data and simulation (using the two-process model) depended on the time of day (Franken et al., 2001); one proposed explanation was that delta power would be modulated by the drive for wakefulness, which itself varies with circadian time.

While the dynamics of Process S show fundamental similarities between humans and animals, the latter provide an additional opportunity to investigate underlying cellular and network mechanisms. Several animal studies used a simplified version of the model, which overall describes well the time course of Process S on a time scale of hours (Franken et al., 1991, 2001; Huber et al., 2000a; Vyazovskiy et al., 2007). However, SWA levels vary on a much finer time scale (seconds to minutes), and these oscillations depend both on the immediate preceding state and on the longer times-scale sleep/wake history (Cui et al., 2014).

D. Initial aims of the study

The present work aimed to adapt, for the first time, an elaborated version of the two-process model to mouse data. We started from the 1993 model published by P. Achermann and colleagues (1993), and adapted the parameters and equations to fit recordings performed in mice. Data was acquired from both occipital and frontal regions, allowing to examine whether some key parameters of the model differed between brain regions.

We also chose to investigate how the model would perform in predicting SWA levels if experimental conditions were changed. Our hypothesis was that if sleep need builds up at different rates depending on the activities animals have engaged in during waking, then the model's predictions would not be as accurate with conditions deviating from baseline recordings against which it has been optimised. Such "novel" conditions included learning a novel motor skill on an irregular wheel, or enforcing wakefulness at the beginning of the light phase by providing the mice with novel objects.

However, we found that the model performed well across conditions, with neither waking experience nor time of day appearing to have a profound influence on the fit between simulated and empirical SWA levels.

E. Adapting sleep modelling to *Sleepy6* mice

Given the ability of the model to predict SWA levels in wild-type C57BL/6J mice across various conditions, we then asked whether applying it to recordings obtained from the *Sleepy6* line could provide insights into the dynamics of sleep regulation in those mice.

As presented in Chapter 4, *Sleepy6* homozygotes present with decreased amounts of sleep, which raises the question of whether they naturally need less sleep. The modelling approach

can give us indications on the rates of increase and decrease of sleep pressure. Assuming a faster decay of sleep need, for instance, this could explain why *Sleepy6* mice sleep less, as they dissipate their sleep pressure faster when asleep. Alternatively, Process S may increase at a slower rate, allowing them to stay awake for longer until their sleep pressure is high enough for them to eventually fall asleep. Applying the model to our data will therefore give us clues on whether any of these assumptions hold true.

2. MATERIALS AND METHODS

A. Animals.

i. Initial study cohort

The initial modelling study used recordings from adult male C57BL/6J mice (Harlan UK Ltd, Bicester, United-Kingdom), with data obtained under 3 experimental conditions:

- ***Regular-wheel (RW)*:** In this first group (n=7, age=13±2 weeks, mean ± STD), mice were given access to a standard running wheel (to which they had been habituated for at least a week) and left undisturbed for 48 h (12:12 h light/dark cycle); such conditions are referred to as "baseline".
- ***Complex-wheel (CW)*:** In the second group (n=7, age=15±1 weeks, mean ± STD), after 24 h of undisturbed recordings with access to a regular wheel, mice were provided with complex wheels (i.e. wheels missing rungs with an irregular pattern, Figure 52), and the recordings continued for at least 24 h. The aim of this wheel exchange was to investigate the influence of waking behaviour, such as learning a novel motor skill, on the performance of the model. Following the introduction of the complex wheel, one mouse hardly run at all and has therefore been excluded from some of the analyses

where appropriate (in which case it is indicated). Apart from this mouse, no significant difference in time spent running was observed between RW and CW nights (ANOVA test, factor 'day'; entire dark phase: $F(1,6)=1.006$, $p=0.355$; long wake bout only: $F(1,6)=0.199$, $p=0.671$).

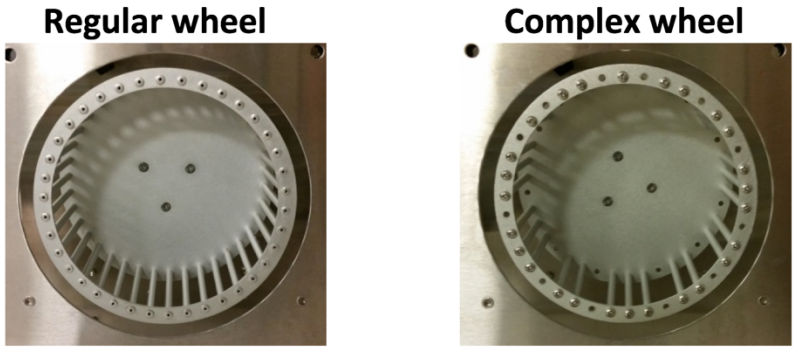


Figure 52: Examples of a regular wheel (RW) and a complex wheel (CW).

- ***Exploratory wakefulness (EW):*** In the third group of animals (n=7, age=17±5 weeks, mean ± STD), undisturbed 24-h recordings were followed by 6-h sleep deprivation (from light onset) and 18-h recovery recordings. The purpose of this group was to investigate how accurate would the model predictions be when an extended period of waking happened at a different time of day with different sensory stimuli (exploration of new objects).

The number of animals used in this study was determined based on previous studies using the two-process model in rodents (Franken et al., 1991, 2001; Huber et al., 2000a, 2000b; Vyazovskiy et al., 2006, 2007). We did not perform initial power calculations, given that the elaborated version of the model had only been used with human data in the past, and the effect sizes were therefore uncertain, given the differences between human and rodent sleep/wake architecture.

Ages were compared across groups and a one-way ANOVA revealed no significant differences ($F(2,18)=2.57$, $p=0.104$). Other general experimental conditions were as described in Chapter 4. All work was carried out under a UK Home Office PPL in accordance with Animal [Scientific Procedures] Act 1986 and the University of Oxford's guidelines.

ii. *Sleepy6* cohort

The recordings were obtained from the experiments presented in Chapter 4. Only two days for each mouse were used (with no access to a running wheel): 24 h of undisturbed baseline recordings, followed by 24 h starting with a 6 h sleep deprivation (first 6 h of the light phase) followed by 18 h of undisturbed recovery.

B. Surgical Procedure

Methods for the surgical procedure were as described in Chapter 4. Note that in the initial modelling cohort, some of the animals were implanted with a microwire array in the frontal cortex (instead of a silicon probe) to record neuronal activity, which was not analysed here.

All mice from the *Sleepy6* cohort were implanted with 16-channel laminar probes as in Chapter 4, and local field potentials will therefore be used for the modelling analysis alongside EEG recordings.

C. Data acquisition and Signal processing.

i. Initial cohort

Data for this cohort were acquired before introduction of the new recording software "Synapse" (Tucker-Davis Technologies Inc. (TDT), USA) and thus filtering is not identical to the settings given in Chapter 4. Recordings were also performed using the Multichannel Neurophysiology

Recording System (TDT), and EEG and EMG were filtered between 0.1-100 Hz, amplified (PZ5 NeuroDigitizer pre-amplifier, TDT) and stored on a local computer at a sampling rate of 256.9 Hz, before being resampled offline at 256 Hz.

Further file format conversion and data analyses are as described in Chapter 4.

ii. *Sleepy6* cohort

All data used for the modelling work were acquired during the experiment presented in Chapter 4.

D. Scoring of vigilance states.

Scoring was performed as described in Chapter 4.

In the RW and CW groups of the initial cohort, only 2.8±0.6 % (mean ± SEM) of all epochs were scored as artefactual, with the percentages of artefactual epochs being highest during wake, but remaining below 6% in all cases (Wake: 4.4±1.2 %; NREMS: 1.5±1.2 %; REMS: 1.3±1.0 %, mean ± SEM).

E. Calculation of EEG slow-wave activity

SWA was defined as EEG power in the slow-wave range (0.5-4 Hz). In the initial study cohort, and unless otherwise stated, SWA values were normalised to the mean over all NREMS epochs belonging to the baseline recording (i.e. baseline 48 h for the RW and CW conditions, first 24 h only for the EW condition, as described below). In the *Sleepy6* cohort, SWA values were normalised against all NREMS epochs belonging to the 48 h used for the modelling.

RW recordings. As mentioned in paragraph 2.A.i, this group of animals was left undisturbed for 48 h with access to a standard running wheel; 'baseline' recordings in this group will therefore correspond to the full 48 h that will also be used for the modelling work.

CW recordings. In the 7 animals forming this group, at least 24-h baseline recordings with access to a standard wheel were followed by 24 h with access to a "complex wheel". As recordings in baseline conditions had been performed for at least 48 h before the replacement of the standard wheel with a CW, optimisation of the model parameters (see below) was done using the 2 days preceding the wheel exchange. Note that for all other subsequent analyses, the 48-h dataset which will be referred to for this CW group consists of the last day of access to a regular wheel and of the first day the animals had access to a CW.

EW recordings. In this third group of animals, after at least 24 h of baseline recordings, a 6-h sleep deprivation was performed starting at light onset, followed by 18 h of undisturbed recovery. The choice to start sleep deprivation at the beginning of the light phase was orientated by our aim to test whether the model would accurately predict the increase in SWA following a long period of wake happening at the mice's usual rest phase. Indeed, mice naturally stay awake for extended periods of time during the dark phase. Thus, if we wanted to test the model against a condition significantly deviating from baseline – against which the parameters have been optimised – performing the sleep deprivation during the light phase was a more appropriate choice. Sleep deprivation was otherwise performed as described in Chapter 4.

In the initial study cohort, sleep deprivation proved successful as mice only spent 1.6±0.2 % (mean ± SEM) of the time asleep (NREMS and REMS episodes included) during the 6 h of deprivation. Although mice became gradually drowsy, especially towards the end of the

procedure, they kept exploring if provided with new objects on a more regular basis. It is important to note, however, that the aim of this experimental group was not solely to sleep deprive the mice, but also to investigate the impact of an exploratory activity on the performance of the model, as compared to the RW and CW conditions.

The 48-h EW dataset used for all analyses consists of 24 h of baseline followed by 6 h of sleep deprivation/exploratory wakefulness and 18 h of recovery. However, for optimisation purposes, and in that case only, the initial 24 h were duplicated to allow the model parameters to be optimised against 48 h of baseline conditions. The choice to duplicate the 24 h of baseline to artificially create a 48-h baseline file in those EW mice, rather than simply optimising parameters against a 24 h file, was motivated by two reasons:

- keeping an approach as similar to the RW and CW groups as possible.
- previous work (Achermann et al., 1993; Rusterholz et al., 2010) and our initial simulations showed that a better and more stable fit is obtained if optimising parameters against longer recordings.

F. Selection of NREMS episodes.

In most cases, we defined 'NREMS episodes' (Trachsel et al., 1991) as periods of NREMS of at least 1-min duration, allowing for short interruptions of no more than 4 ts (=16 s) at a time. The choice of 1min as a minimum duration for NREMS episodes was based on previous findings (McShane et al., 2010; Vyazovskiy and Tobler, 2012), but also on the observation from our data that when NREMS episodes are too short (< 1min), the full build-up of SWA does not have time to occur, and thus does not reflect the actual level of sleep pressure.

Additionally, 1-min duration was not always long enough to analyse the intra-episodic dynamics of SWA during NREMS episodes. In such cases, episodes lasting at least 3 minutes were chosen,

and are referred to as *long* NREMS episodes.

Note that 'sleep bouts', on the other hand, are periods of sustained sleep, which include both NREMS and REMS (and some brief awakenings).

G. Description of the model.

The model was based on the following equations, adapted from Achermann et al.(1993):

(1) Slow-wave activity (SWA(t)): Empirical and simulated SWA are always expressed – unless otherwise stated – as a percentage of mean SWA across NREMS in the baseline period used for optimisations (RW & CW: 48 h, EW: 2x24 h – as described above).

$$\frac{\mathrm{dSWA}}{\mathrm{dt}} = rc\,.SWA\,.\frac{\mathrm{S}}{\mathrm{S_U}}\,.\left(1-\frac{\mathrm{SWA}}{\mathrm{S}}\right).\big(1-WT(t)\big).\big(1-REMT(t)\big)$$

$$-\,fc_R\,.(SWA-SWA_L).REMT(t)$$

$$-\,fc_W\,.(SWA-SWA_L).WT(t)$$

(2) REMS (REMT(t)):

$$REMT(t)=\begin{cases}1\ during\ REMS\ 'trigger'\ (see\ below)\\ 0\ otherwise\end{cases}$$

(3) Waking (WT(t)):

$$WT(t)=\begin{cases}1\ during\ wake\ 'trigger'(see\ below)\\ 0\ otherwise\end{cases}$$

(4) Process S (S(t)):

$$\frac{\mathrm{dS}}{\mathrm{dt}} = -\,gc\,.SWA\;+\;(S_U-S).rs$$

Table 6: Parameters and functions used in the model.

Parameters	***Definition***	***Description***	***Value used for the simulations****
rc	rise constant	Determines the rise of SWA within NREMS episodes	0.5
fc_R	fall constant REMT	Determines the fall of SWA triggered by REMT	(0.1; 0.2; 0.3)
fc_W	fall constant WT	Determines the fall of SWA triggered by WT	0.2
SWA_L	lower asymptote of SWA		20
SWA_0	initial level of SWA at the beginning of the simulation		Adjusted for each animal & derivation
REMT(t)	REMS trigger	Activates the fall of SWA	1 or 0 (see equations)
t_a	advance of REMT	Advance of REMT with respect to the onset of empirical REMS	8
t_p	prolongation of REMT	Prolongation of REMT with respect to the duration of empirical REMS	6
WT(t)	wake trigger	Activates the fall of SWA	1 or 0 (see equations)
t_{aw}	advance of WT	Advance of WT with respect to the onset of empirical waking	8
t_{pw}	prolongation of WT	Prolongation of WT with respect to the duration of empirical waking	4
gc	gain constant	Determines the decay of Process S	Optimised for each animal & derivation.
rs	rise rate of S	Determines the increase of Process S	Optimised for each animal & derivation.
S_0	initial level of S at the beginning of the simulation		Adjusted for each animal & derivation.
S_U	upper asymptote of S		Optimised for each animal & derivation.

*** The time unit used in the simulations was the time step ts=4 s. rc, fc_R, fc_W, g_c, r_s are expressed in ts^{-1}; t_a, t_p, t_{aw}, t_{pw} are expressed in ts; SWA_L, SWA_0, S_0, S_U are expressed as a percentage of mean SWA over NREMS in baseline (regular wheel & complex wheel groups: 48 h of baseline, enforced/exploratory wakefulness group: 24 h of baseline). SWA= slow-wave activity, NREMS= non-rapid eye movement sleep, REMS= rapid-eye movement sleep.**

All parameters and their definition can be found in Table 6. Although the original (human-data based) elaborated model (Achermann et al., 1993) used time steps of 1 min, we based our analyses on 4-s time steps, as this is more adequate to describe mouse data, where alternation between vigilance states occur within seconds.

Differential **equation (1)** governs the time course of SWA; it contains a sigmoid-like build-up component and two fall components, which depend on the REMS trigger (REMT) and wake trigger (WT) functions. These two 'trigger' functions, which are directly derived from the empirical data, are defined as follows:

- a REMT episode starts t_a epochs before a REMS episode and last t_p epochs longer (Figure 53).
- a WT episode starts t_{aw} epochs before a wake episode and lasts t_{pw} epochs longer.

These functions were introduced in the 1993 version of the model (Achermann et al., 1993), and allow a better fit between data and simulation thanks to the anticipation of the occurrence of REMS and wake.

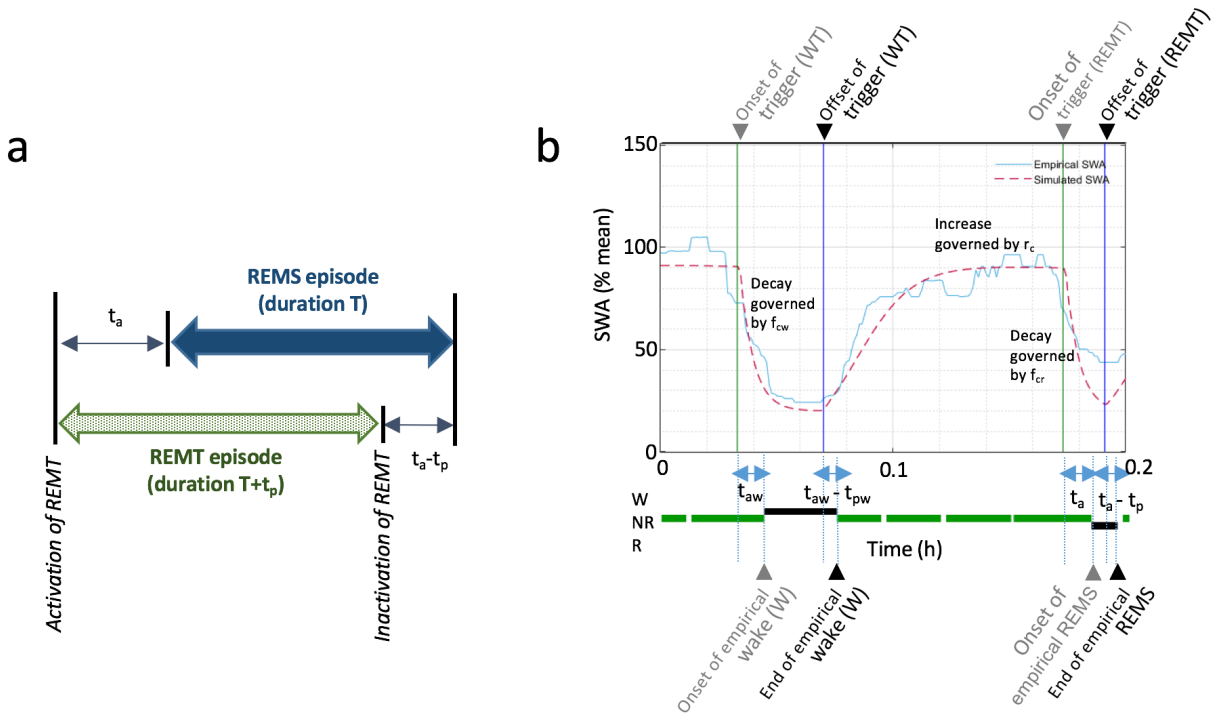


Figure 53: Definition of rapid-eye movement sleep (REMS) and wake trigger functions. ***a)*** *In comparison to a REMS episode, a rapid-eye movement trigger (REMT) episode starts t_a epochs earlier and lasts t_p epochs longer (with $t_p < t_a$); the offset of REMT therefore occurs t_a-t_p epochs before the REMS episode ends. This works identically for the wake trigger function (WT) in relation to wake episodes (with t_{aw} and t_{pw} replacing t_a and t_p).* ***b)*** *Onsets (green vertical lines) and offsets (blue vertical lines) of WT and REMT in relation to empirical wake and REMS episodes are shown (empirical states are indicated in the hypnogram below the graph). The decay and decrease rates governing the variations of simulated slow-wave activity are indicated on the plot. NR= non-rapid eye movement sleep; R= REMS= rapid-eye movement sleep; REMT= rapid-eye movement sleep trigger; SWA= slow-wave activity; W= wake; WT= wake trigger.*

Equation (4) governs the time course of Process S. Its decline component is proportional to the level of SWA. Importantly, its rise component is permanently activated, as S_U – S is always positive (S cannot go higher than its upper asymptote); this means that unless the decline component is strong enough, S will increase regardless of the vigilance state. As SWA is usually high during NREMS, the decline component is then sufficiently large (in absolute value) to overcome the rise term of the equation, and the derivative becoming negative, S eventually falls during NREMS.

The terms in blue shade in equation **(1)** are additions to the original equations (Achermann et al., 1993). Their introduction was motivated by the fact that in mice, the fall in SWA levels at the transition from NREMS to REMS or wake is steeper than in humans – and introducing those two terms allowed for a steeper fall of simulated SWA at those transitions. Indeed, without those added terms, SWA would fall steeply for a few seconds at the end of a NREMS episode, before falling in a much more attenuated manner as SWA levels became lower, which does not reflect the variations we observe in the empirical data. Therefore, "switching off" the build-up component of equation **(1)** as soon as an animal enters REMS or wake – as those blue-tone multiplication factors allow – helped to obtain a better fit between empirical and simulated SWA levels. Additionally, these terms served as a correction against a deviation in the saturating increase of Process S during wake.

H. Implementation of the equations and defining parameter values

The differential equations were implemented in Matlab (The MathWorks Inc., USA), using the 'ode15s' solver, given that the system of equations was stiff (mainly due to state transitions). Given that our time step was 4 s, it is important to note that:

- the solver was constrained to take steps of a maximum size of 4 s, to obtain at least one data point for each 4-s epoch.
- the solver was left free to take smaller steps if necessary (this is crucial, as it lets the algorithm take smaller steps in areas where levels of SWA or S undergo substantial variations, such as at state transitions). This means, however, that the final 48-h solution obtained from ode15s could contain more than one data point per 4-s epoch. Therefore, data points belonging to the same 4-s epoch were averaged together to get one value per 4-s epoch.

REMS trigger (REMT) and wake trigger (WT) were calculated using annex functions. Of all the parameters present in the equations (Table 6), only 3 were formally optimised, to reduce computational time. Such an approach had also been used in the original 1993 model, and led to satisfactory results. Hence, given that most of the parameters are inter-dependent, those that could be evaluated visually and of which the influence on the fit was limited were fixed first. For instance, the fall constants fc_R and fc_W were estimated by calculating the slope of the decrease of SWA at the transition from NREMS to REMS or to wake, respectively.

Sensitivity analysis is usually a more rigorous approach than visual inspection. However, given how the error is calculated (see below) – based on one mean value per NREMS episode – it is not suited to evaluate parameters which play a role in the fine-scale variations of SWA levels, such as fc_R, fc_W and rc; in those cases, sensitivity analysis usually led to a poorer fit than visual inspection. Here, "visual inspection" refers to 3 different observers visualising a zoomed-in version of a 48-h simulation (such as in Figure 53b) to check how empirical and simulated SWA curves overlapped. Such a 'visual inspection' approach was chosen for the parameters fc_W, SWA_L, t_a/t_{aw}, t_p/t_{pw}.

- **fc_R & fc_W:** In the first elaborated version of the two-process model (Achermann et al., 1993), which used human EEG recordings, fc_W was approximately equal to $5*fc_R$. In the present version, using mouse EEG data, better results were obtained when fc_R and fc_W were taken in a similar order of magnitude (approximately 0.2 ts^{-1}). Additionally, the impact of variations in fc_W was small (and a value of 0.2 was applied for all animals and all derivations), whereas fc_R played a more determinant role on the fit between empirical and simulated SWA at the transitions from NREMS to REMS. Therefore, the value of fc_R was allowed to vary between 0.1, 0.2 or 0.3 for each animal and derivation.
- **SWA_L:** its value was fixed to 20 % of mean SWA. Given that it does not contribute significantly to the error (it is an arbitrary value at which SWA levels fall during wake

and REMS), we wanted to keep the same values across animals and derivations. Several values were explored; 20% was a good average of SWA levels during wake across animals.

- **rs, gc, S_U and S_0:** Given that those four parameters refer to the dynamics of Process S and not SWA, their values could be inferred from previous studies using the original (non-elaborated) two-process model. Therefore, we started with values derived from a previous study using this model in 6 mouse strains (Franken et al., 2001). We subsequently chose to formally optimise rs, gc and S_U, (see 2.J). S_0, on the other hand, was chosen equal to the mean value of SWA calculated over the first NREMS episode (longer than 3 minutes) of the 48-h file to be used for the simulation.
- **SWA_0** was chosen as equal to the starting value of empirical SWA (i.e. at the beginning of the 48-h recording to be simulated).
- **t_a, t_p, t_{aw} and t_{pw}:** these values were calculated by estimating the number of time steps necessary for the increase (respectively decrease) of SWA before (resp. after) a NREMS episode preceded (resp. followed) by a REMS (for t_a and t_p) or wake (for t_{aw} and t_{pw}) episode (Table 6).
- **rc:** given that it represents the rate of increase of SWA, its value was initially taken equal to the average increase rate of SWA at the beginning of NREMS calculated over all NREMS episodes which immediately followed wake. We also attempted to formally optimise rc alongside gc, S_U and rs, but did not pursue this approach as the impact of rc on the fit was small and optimising 4 parameters instead of 3 already slowed the optimisation process significantly. Therefore, multiple arbitrary values ranging from 0.2 to 1.5 were tested; a value of 0.5 was eventually chosen by visual inspection, as it provided the best fit in most animals.

I. Optimisation/estimation process of the parameters.

Our optimisation approach was similar to the one used in the original elaborated version of the two-process model (Achermann et al., 1993), except for an additional step which we introduced to test the stability of the solution at the end of the optimisation (see 2.J, and Figure 54a).

Custom-made scripts were written to optimise the parameters gc, rs and S_U based on a 'least-squares' algorithm: we minimised the squared error between simulated and empirical SWA (using SWA values from NREMS episodes longer than 1 min) using Matlab's *fminsearch* function.

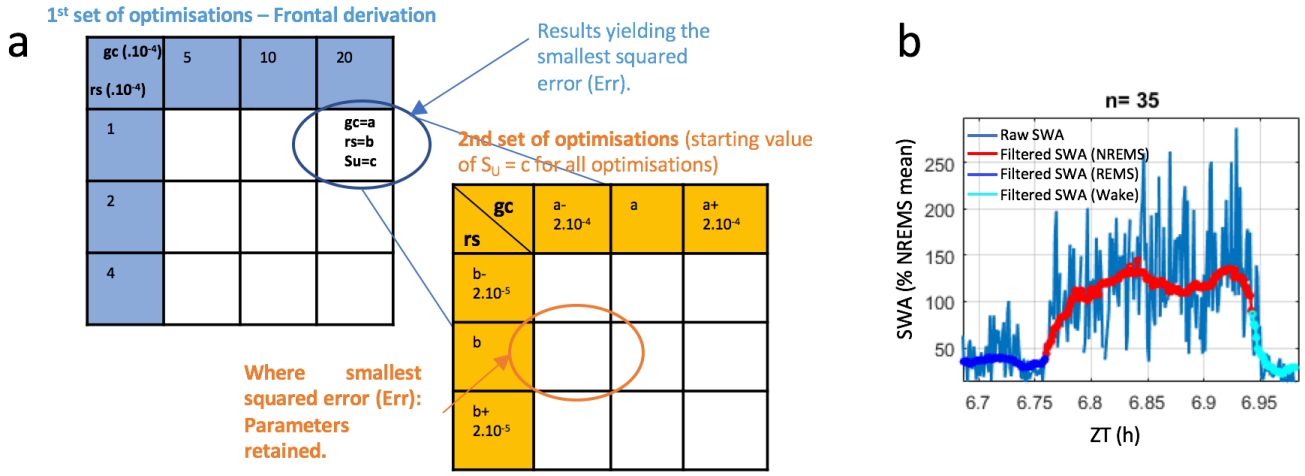


Figure 54: Illustration of the optimisation process. ***a)*** *Diagram illustrating the optimisation process of the 3 parameters gc (gain constant of Process S), rs (rise rate of S) and S_U (upper asymptote of S). To initialise the optimisation, 3 starting values for gc and rs were evaluated, where the orders of magnitude of these parameters were realistically chosen based on existing literature. Similarly, a good initial estimate of S_U was obtained from literature, and this starting value was chosen for further optimisation with all 9 possible combinations of gc and rs (blue table – derivations treated separately). Starting from the values a, b and c of gc, rs and S_U, which yielded the smallest squared error after optimisations of the first round, a second optimisation round was performed (orange table). See main text for more details on the optimisation procedure.* ***b)*** *Example of smoothing empirical slow-wave activity (SWA, plotted on a 4-s epoch basis) with a moving median filter (n=35, i.e. 35 ts = 35 x 4 s, per moving window). Smoothing was performed continuously regardless of vigilance states (which are shown in different colours here for clarity). The mean value of the red segment would represent the mean empirical SWA levels for this given non-rapid eye movement sleep (NREMS) episode. ZT= zeitgeber time.*

Firstly, to minimise the impact of noise and less relevant variations in the signal, the empirical

SWA was smoothed using a moving median filter with a moving window of n=35 ts (Figure 54b).

Then, for a given i^{th} NREMS episode occurring in the light period, a mean SWA value was calculated from both the empirical data ($m_{empirical}(i)$) and the simulated data ($m_{simulation}(i)$). The difference d(i) between those two means was calculated: $d(i)= m_{empirical}(i)-m_{simulation}(i)$.

Those differences were squared and added over all NREMS episodes occurring in the light phase to give:

$$M(\text{light}) = \sum_{i=1}^{n} \frac{d(i)^2}{n}$$

The same calculation was done in the dark phase to obtain M(dark).

The overall squared error Err was simply:

$$\text{Err} = \frac{M(light)+M(dark)}{2}$$

As mentioned above, the optimisation process then aimed to minimise Err. It is important to note that at no point in this procedure are the variations of SWA within NREMS episodes fitted; indeed, the error is calculated only from mean SWA values per episode.

Errors were first calculated separately in the light and dark periods (before being averaged together to obtain Err) to avoid a bias of the optimisation process towards the light phase. Indeed, as mice naturally spend more time asleep during the light phase, there are more NREMS episodes in the light than in the dark phase (number of NREMS episodes over 2 light periods (2x 12 h) in RW group of the initial study cohort: 155±20 (mean ± SD); over 2 dark periods: 49±22).

On the other hand, this approach means that a greater confidence is granted to each NREMS episode occurring during the dark phase: there are 3 times less NREMS episodes in the dark phase, but both phases have an equal contribution to the overall error. Given that the largest changes in SWA levels occur in the dark period, this was a reasonable concession to make.

J. Step-by-step optimisation approach.

As mentioned in 2.H, values for the 3 parameters gc, rs and S_U were initially derived from Franken et al. (2001), thanks to which, after a few trials, a reasonable range of starting values for the optimisation process was obtained. The following method was then observed for each animal (Figure 54a):

1- **A first step** of 9 optimisations, which combined 3 different starting values of gc with 3 different values of rs was performed individually for each animal and derivation. The starting value for S_U was kept the same for these 9 optimisations. Starting values were:

- in the frontal derivation: gc(0)= 0.0005, 0.0010, 0.0020 ts^{-1}; rs(0)= 0.0001, 0.0002, 0.0004 ts^{-1}; $S_U(0)$=400 %.

- in the occipital derivation: gc(0)= 0.0002, 0.0004, 0.0008 ts^{-1}; rs(0)= 0.0001, 0.0002, 0.0004 ts^{-1}; $S_U(0)$=450 %.

2- In **a second step**, the parameters yielding the smallest squared error in the first round of optimisations were chosen as the starting values of a new run of 9 optimisations, with the following rules (Figure 54a):

- gc(0)=gc value yielding best result - 0.0002 ts^{-1};

  gc value yielding best result ts^{-1};

  gc value yielding best result + 0.0002 ts^{-1};

- rs(0)= rs value yielding best result - 0.00002 ts^{-1};

  rs value yielding best result ts^{-1};

  rs value yielding best result + 0.00002 ts^{-1};

- $S_U(0)$= S_U value yielding best result, for all 9 [gc(0); rs(0)] combinations.

Each animal and derivation therefore had a unique set of starting values for the second set of optimisations (except in the rare occurrence of two animals showing the smallest squared error for the same set of values at the end of the first step).

Following this second set of optimisations, the variation in the 9 squared errors obtained was mostly <10%, i.e. $\frac{\text{highest squared error} - \text{smallest squared error}}{\text{smallest squared error}} < 0.10$

This showed a relative stability of the solutions obtained, and no further step was performed. This means that for each animal and derivation, the set of gc, rs and S_U values kept for subsequent simulations was the one which yielded the smallest squared error in this second step.

3- Finally, *simulations* (as opposed to *optimisations*) were run using those optimised values of gc, rs and S_U, based on the same set of equations (1) – (4) as shown in 2.G and the trigger functions REMT and WT. The values used for the other parameters are indicated in Table 6. It is important to emphasise that in the initial study cohort, parameters were optimised against baseline recordings (see 2.E) and these baseline-derived values were kept to predict SWA and Process S levels in EW and CW recordings. Indeed, the aim of this study was also to look at whether the model's predictions could remain accurate across various waking experiences.

K. Calculation of the error to evaluate how well the model predicts the data.

To compare empirical and simulated SWA, two types of errors were used: an 'absolute error' and an 'error'.

- The absolute error consists in taking the mean of the absolute values of the differences d(i) (see description above) over a period of interest.

- The error is the mean of the differences d(i) (without taking their absolute value). This leads to an important bias, as the individual differences may cancel each other (if some are positive and others negative). However, it remains of interest as it gives an indication on the directionality of the overall misfit, i.e. does the model over- or under-estimates the empirical data?

L. Statistical analysis.

All statistical analyses were performed using SPSS Statistics (IBM Corp., Release 23.0.0.2). Tests used and their results are reported within figure legends or within the main text.

3. RESULTS

A. Results from the initial study cohort (wild-type C57BL/6J mice)

i. Sleep-wake architecture in the regular-wheel (RW) group.

Recordings were stable over the two-day period included in the analyses. The daily sleep and activity pattern of mice from the RW group was typical of animals kept under a 12:12 h light/dark cycle, with mice being predominantly asleep during the light period, and mostly awake during the dark period (Table 7, Figure 55a). Mice were awake 25±1 % (mean ± SEM, n=7) of the time during the light period, and 79±3 % of the time during the dark period. No difference in the amount of time spent in each vigilance state could be observed between the two days (Table 7).

Table 7: Percentage of time spent in different vigilance states in the regular wheel (RW) condition across 12-h light & dark periods.

	Non-rapid eye movement sleep	Rapid eye movement sleep	Wake	Brief awakenings
Day1- Light	60±1 %	11±1 %	25±1 %	4±1%
Day1- Dark	17±2 %	2±1 %	79±3 %	1±1 %
Day2-Light	60±1 %	11±1 %	25±2 %	4±1 %
Day2-Dark	19±3 %	2±1 %	78±4 %	1±1 %

Values expressed as mean ± SEM. Brief awakenings are characterised by short bouts of movement (EMG activity) occurring during sleep episodes, and lasting no more than 20 s.

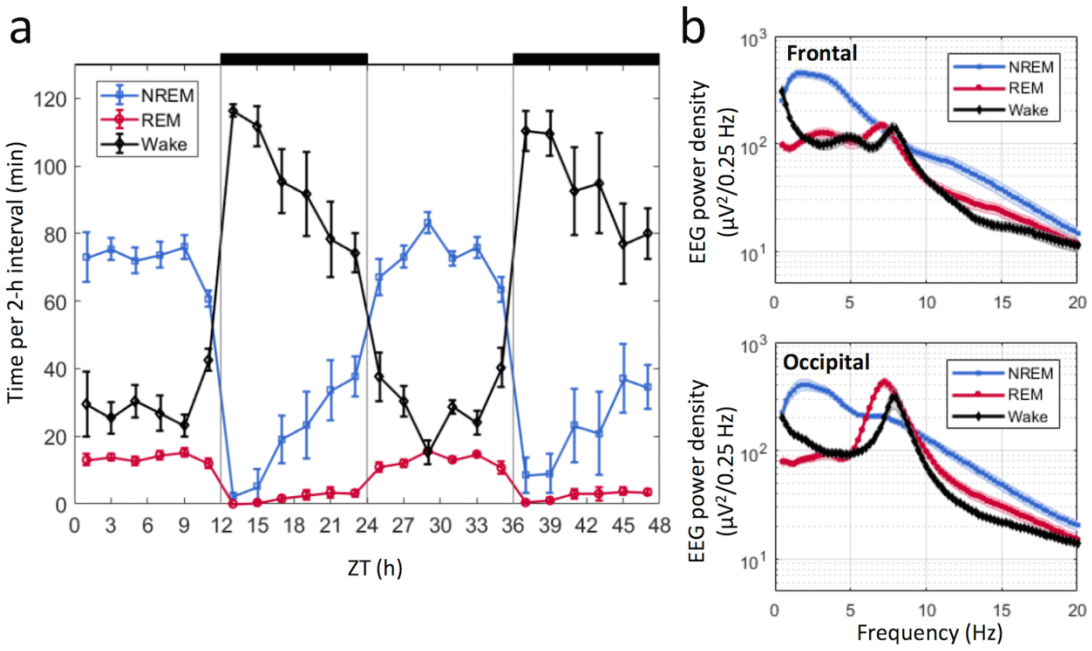


Figure 55: Distribution of vigilance states and power density spectra. ***a)*** *Time spent in each vigilance state (wake, rapid eye movement sleep (REM), non-rapid eye movement sleep (NREM)) per 2-h interval. n=7 (RW condition); mean ± SEM.* ***b)*** *Mean EEG power density spectra during wake, NREM and REM sleep in the frontal (top) and occipital (bottom) derivations. n=7 (RW condition); mean ± SEM. ZT= zeitgeber time.*

Interestingly, extended bouts of wakefulness could be observed in all animals from the RW group during the dark period (Figure 56). In 6 animals out of 7, this long waking period started shortly after the light-to-dark transition (less than 6 min after dark onset, except in the 7th animal for which a consolidated waking bout started only 5 h after the light-dark transition). Long wake bouts lasted on average 6.2±1.0 h and were both preceded and followed by consolidated periods of sleep. It is likely that the access to a running wheel encouraged the mice to stay awake for sustained periods of time (Edgar et al., 1991; Vyazovskiy and Tobler, 2012). Note that mice used their wheels voluntarily (i.e. at no point was wheel-running enforced) and ran on average 33±7 % (mean±SEM) of their waking time.

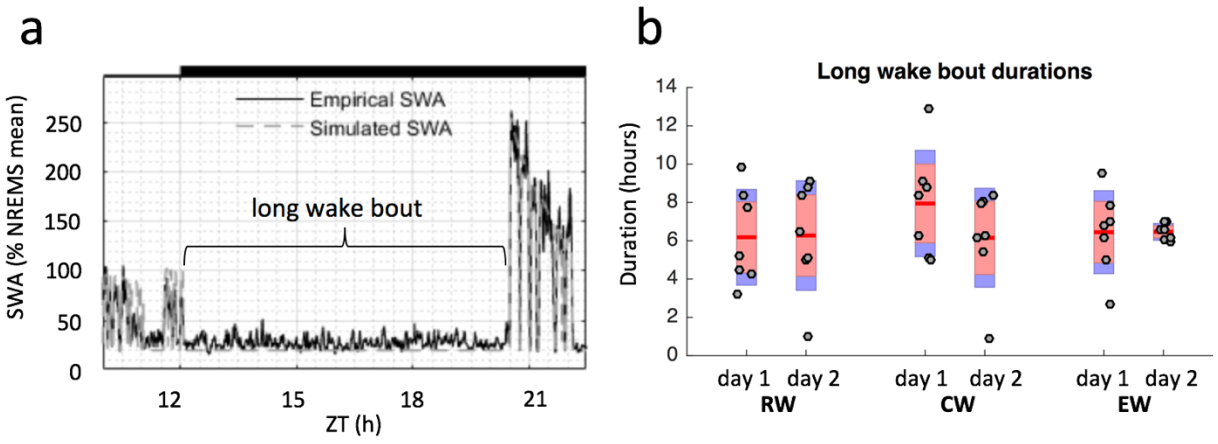


Figure 56: Evaluation of long wake bouts (LWB) durations. ***a)*** *Representation of a LWB in one animal from the RW group (plotted with one value per 4-s epoch).* ***b)*** *Average LWB durations across the 3 conditions (RW, CW, EW) in the first and second days of each dataset. In each condition, n=7; red area: 95-% CI, blue area: 1 SD; grey circles represent individual animals. A mixed-design ANOVA (factors 'condition' and 'day') revealed no significant main effects or interaction.*

As extended periods of wakefulness could also be observed in the CW and EW groups, "long wake bouts" were subsequently defined as the longest waking period for each animal on a given day. In the EW group, the longest waking bout occurring during the second day corresponds to the 6-h sleep deprivation and therefore is the only case for which the long waking period occurs

in the light phase and as can be expected, the variability in duration across the animals was the smallest. Remarkably, the spontaneous long wake bouts in the RW and CW groups and during the first day of the EW group also lasted around 6 h, which led to no significant difference in long wake bout durations between groups and across days (Figure 56b); this came as a welcome coincidence.

Finally, the average EEG power spectra during NREMS, REMS and waking in the RW group showed characteristic differences, with an increase in delta power (0.5-4 Hz) during NREMS and a peak in the theta-frequency band (5-10 Hz) during wake and REMS, especially prominent in the occipital derivation (Figure 55b).

ii. Accuracy of the elaborated model in predicting intra-episodic dynamics of SWA.

Given that EEG SWA is a common biomarker of sleep pressure, as expected, we found that its time course showed a declining trend across the light period (when the animals are mainly asleep) and increased following prolonged consolidated wake periods (Figure 57). As has been described in previous studies (Huber et al., 2000b; Vyazovskiy and Tobler, 2005b; Werth et al., 1996a), we found that SWA levels were overall higher in the frontal derivation than in the occipital derivation.

The aim of this work was initially to test the ability of an elaborated version of the two-process model to predict the dynamics of SWA across 48 h of recordings when mice naturally alternate between wake and sleep periods. The main difference between the 1993 'elaborated' version of the model (Achermann et al., 1993) and the original model was that not only did it account for the declining trend of SWA during sleep, but also for the variations of SWA within successive NREMS episodes. Figure 57 shows empirical SWA alongside simulated SWA and Process S for an individual representative mouse. A good fit was obtained between empirical and simulated

SWA levels in both derivations, and the model accurately predicted low SWA levels, as well as higher levels during early sleep following prolonged waking bouts.

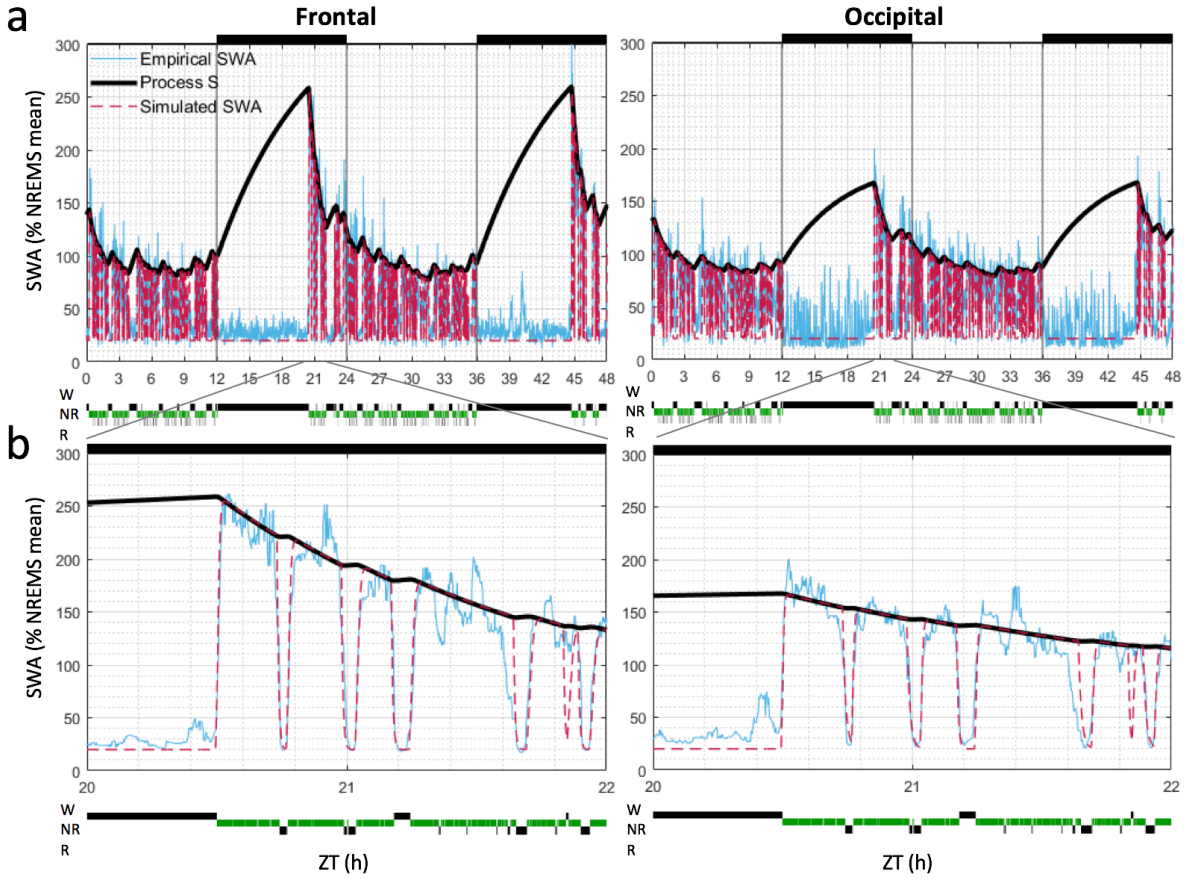


Figure 57: EEG SWA levels are shown across 48h (a) and 2h (b) (from 20 to 22 h) in one representative mouse, in the frontal (left panels) and occipital (right panels) derivations. Curves are plotted with one value per 4-s epoch, although the simulation solver was allowed to take steps of any size < 4 s (see Methods). SWA levels were normalised (expressed as percentage) against mean SWA over 48 h in non-rapid eye movement sleep (NREMS) only. Light and dark phases are represented at the top of the figures (black bars = dark phase). Hypnograms of vigilance states are shown at the bottom of each panel. NR= non-rapid eye movement sleep, R= rapid eye movement sleep, W= wake, ZT= zeitgeber time.

Additionally, the fit between empirical and simulated SWA levels during individual NREMS episodes was satisfactory, highlighting how SWA levels in NREMS are higher in the dark phase than in the light phase (Figure 58a, only NREMS episodes longer than 3 min were included and averaged; lengths of NREMS episodes included = 7.9±3.9 min, mean ± STD). There was also a

good fit during the overall light periods, although the gradual decrease in SWA levels throughout the light period (Figure 58b) correlated with a weak increasing trend in the error between data and simulation, mostly observable in the frontal derivation (Figure 58c).

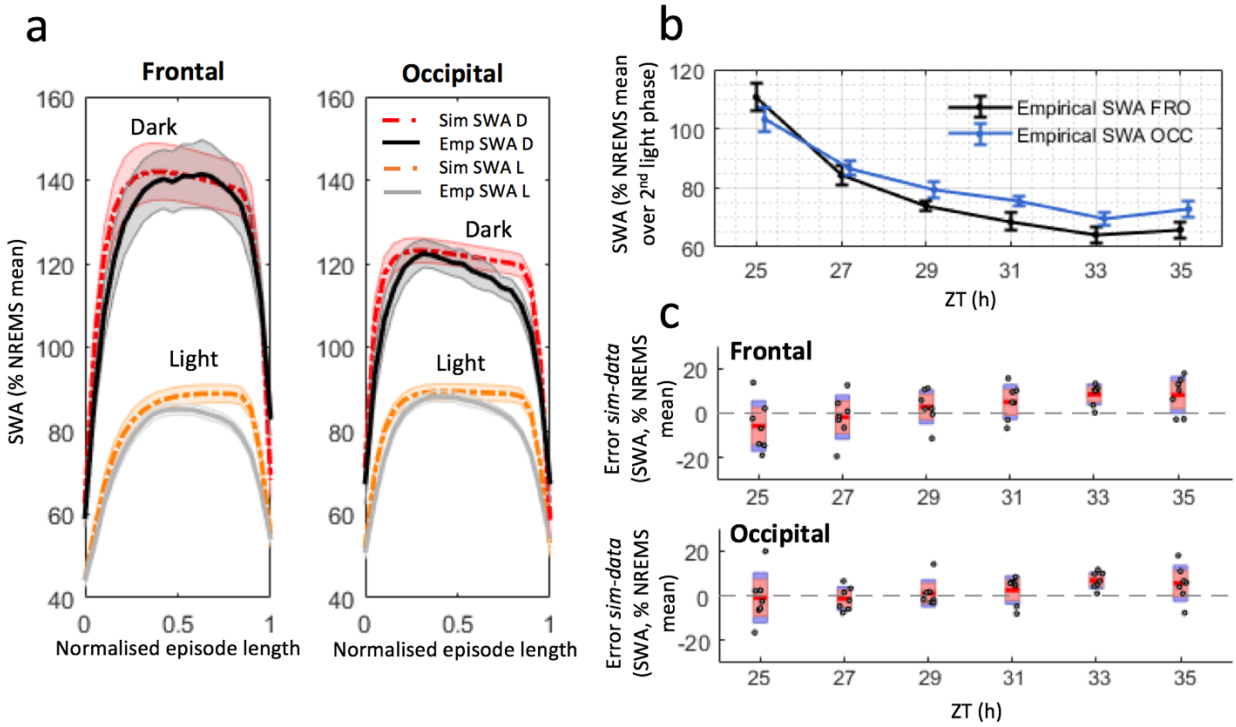


Figure 58: Evaluation of the fit between data and simulations. ***a)*** *Average empirical and simulated SWA levels during NREMS episodes, in light (L) and dark (D) periods. Only NREMS episodes lasting > 3 min were included (average length = 7.9 ± 3.9 min, mean ± STD). Individual episodes' lengths were normalised to an arbitrary length of 1, to allow averaging between episodes. n=7, mean ± SEM (shaded areas).* ***b)*** *Time course of empirical SWA levels during NREMS in the light phase of the second day of regular wheel (RW) condition in the frontal (FRO) and occipital (OCC) derivations. n=7; mean ± SEM. 2-h values of SWA were normalised against the mean over the 2nd light phase only (see Methods).* ***c)*** *2-h values of the difference between simulated and empirical SWA in the light phase of the second day of regular wheel (RW) condition. Only SWA values in NREMS episodes lasting > 1 min were included in this analysis. Red area: 95-% CI, blue area: 1 STD. Dots represent individual mice. An ANOVA for repeated measures (factors 'derivation' and 'time point') revealed a significant main effect of time point (F(5,30)=5.518, p≤0.001) and a significant interaction derivation*time point (F(5,30)=5.49, p≤0.001). ZT= zeitgeber time.*

Figure 58a shows the dynamics of individual NREMS episodes, with the build-up of SWA at the beginning of an episode, and its decrease at the end. The two essential constants that govern the rate of decrease at the transitions from NREMS to wake or REMS, are fc_W and fc_R respectively

(Table 6). A higher value of fc_W and fc_R, means that SWA will show a steeper fall at NREMS -> wake/REMS transitions. We found that SWA increases and decreases sharply in both derivations at the transitions between NREMS and wake/REMS (Figure 58a), as was previously reported (Achermann and Borbély, 1990; Rozov et al., 2016; Vyazovskiy et al., 2004). Interestingly, in the 1993 version of the model which used human data, the fall constants differed significantly between REMS and wake (Achermann et al., 1993), while in the present model using recordings from mice, those two constants can be taken equal and still lead to very good predictions.

Overall, the simulation followed the intra-episodic variations closely, although occasional mismatches with SWA levels could be observed (Figure 58a), especially towards the end of NREMS episodes, as can be seen at 21.6 h preceding REMS in Figure 57b. This could be caused by the intrusion of spindle activity and an instatement of mixed states, which has been shown to increase during the light period in mice (Astori et al., 2011; Gottesmann, 1996; Poe et al., 2010; Vyazovskiy et al., 2004).

iii. Regional differences in parameter values

Given that absolute EEG power levels, spectral composition and dynamics of SWA are known to differ between cortical regions (Huber et al., 2000b; Leemburg et al., 2010; Vyazovskiy and Tobler, 2005b; Werth et al., 1996a), we asked whether the parameters describing the dynamics of Process S within the present version of the model would also differ between the frontal and occipital derivations.

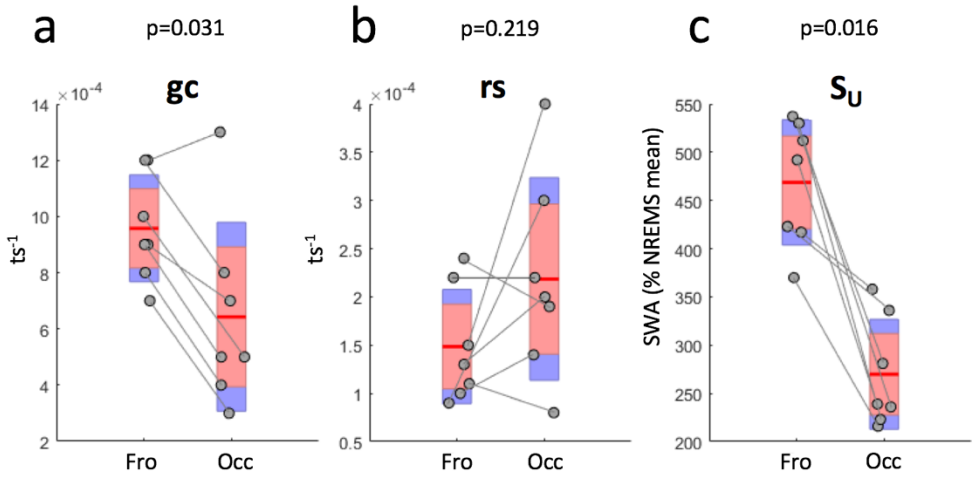


Figure 59: Parameters values in the occipital and frontal EEG derivation in WT C57BL/6J mice with access to a regular wheel. ***a-c)*** *Mean (red line) and individual animal values (grey circles) of the parameters gc, rs, S_U in the frontal (Fro) and occipital (Occ) derivations in the regular-wheel group. ts = 4 s; n=7; red area: 95-% CI, blue area=1 STD. The significance of the difference in parameter values between derivations was assessed with a non-parametric Wilcoxon signed-rank test; p-values are indicated above each plot.*

As described in the Methods section, three essential parameters of Process S (its gain constant gc , rise rate rs and upper asymptote S_U) were optimised separately for each animal and each derivation and revealed that:

- gc, which governs the rate of decrease of Process S depending on SWA levels, was significantly higher in the frontal derivation than in the occipital derivation (Figure 59a).
- rs, which determines the build-up of Process S, was similar in the two derivations (Figure 59b).
- S_U, the upper asymptote of S, was significantly higher in the frontal derivation (Figure 59c).

These results remained unchanged when pooling data from the RW and EW groups (Figure 60).

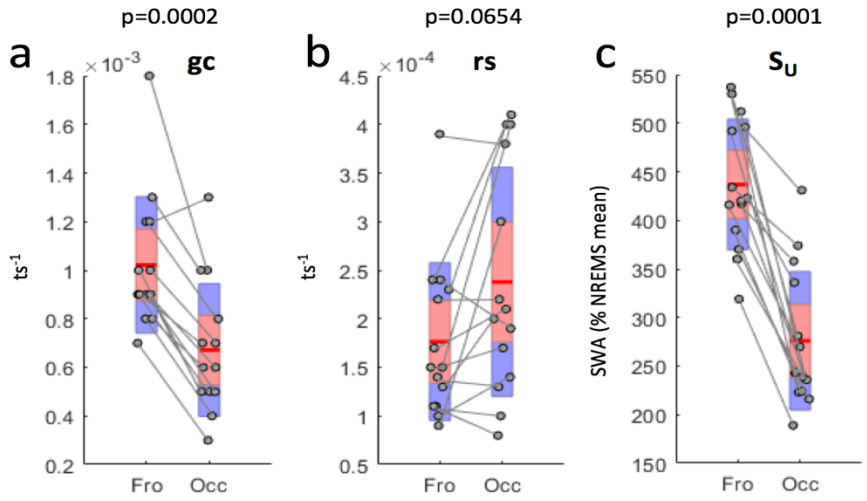


Figure 60: Parameter values in the regular- and complex-wheel groups. ***a-c)*** *Mean (red line) and individual animal values (grey circles) of the parameters gc, rs, S_U in the frontal (Fro) and occipital (Occ) derivations in the regular-wheel and complex-wheel groups (pooled together). ts = 4 s; n=14; red area: 95-% CI, blue area=1 STD. The significance of the difference in parameter values between derivations was assessed with a non-parametric Wilcoxon signed-rank test; p-values are indicated above each plot.*

These results suggest that not only sleep-wake history, but also cortical regions are major determinants of the dynamics of Process S.

iv. Influence of the light phase on the performance of the model.

Lighting conditions strongly influence sleep-wake architecture across 24 h. We therefore asked whether the model's performance would be significantly different in the light and dark periods, especially as the current version of the model does not include a circadian modulation in the equations themselves. Additionally, as mentioned in the Methods section 2.J, given that mice spend less time asleep during the dark period, the optimisation process may be biased by the fact that the light period contributes more to the squared error term on which the optimisation algorithm is based. To prevent this, two mean squared errors were first calculated separately

over NREMS episodes occurring in the light or in the dark periods, before being averaged together (see Methods 2.J).

As a result, the fit between data and simulation – quantified by the error term – was found similar between the light and dark phases, and across derivations (Figure 61).

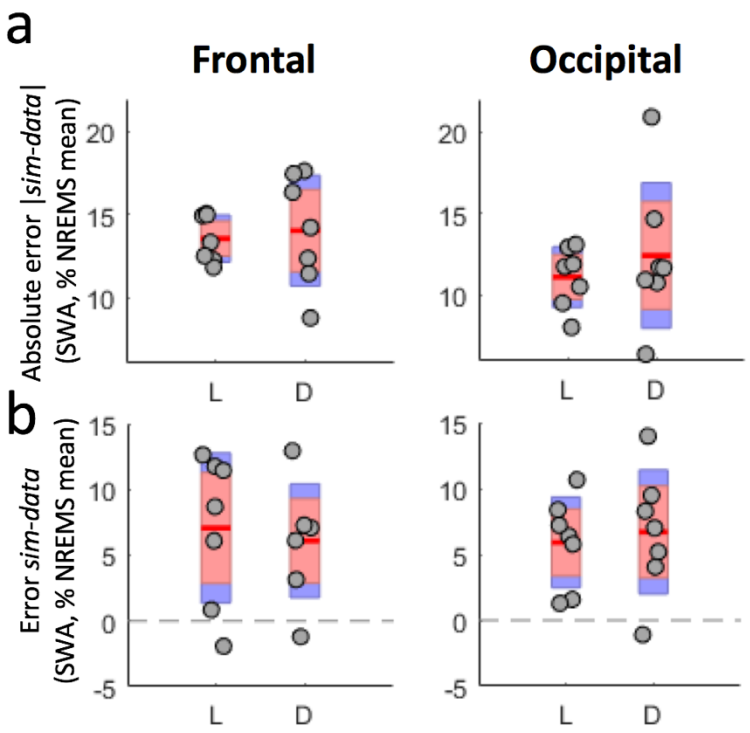


Figure 61: Evaluation of the absolute and real values of the error between data and simulations. ***a)*** *Mean (red line) and individual (grey circles) absolute differences between simulated and empirical SWA levels in the regular wheel (RW) group.Values calculated over NREMS episodes lasting > 1 min; n=7. Red area: 95-% CI, blue area: 1 STD. Significance was assessed with a two-way ANOVA for repeated-measures, factors 'derivation' and 'light phase'. No significant main effect or interaction were found (derivation, p=0.056; light phase, p=0.529; interaction, p=0.488).* ***b)*** *As in a), but the error (and not absolute error) value of the difference d=$SWA_{simulation}$ – $SWA_{empirical}$ is kept, allowing to see whether the model over- (positive difference) or under-estimated the empirical data. No significant main effect or interaction were found (derivation, p=0.873; light phase, p=0.956; interaction, p=0.136). NREMS = non-rapid eye movement sleep, sim= simulation, L=light, D=dark, ZT= zeitgeber time.*

Figure 61b reveals that overall, the model slightly overestimates empirical average SWA levels, as the error errs in the positive values in both light and dark and in both derivations. When combining the errors over the light and dark periods, simulated SWA is indeed significantly higher than empirical SWA (one-way ANOVA run separately for each derivation; Fro:

F(1,6)=13.071, p=0.011; Occ: F(1,6)=26.667, p=0.002); no significant difference between the light and dark periods was observed.

Additionally, as shown in Figure 58a, although SWA levels are higher during the dark period, the performance of the model within individual episodes was similar across both light phases. We noted however that the absolute error was more variable across animals in the dark phase (Figure 61a). The homogeneity of variances of the absolute error and error between the light and dark phases was therefore tested by running paired-sample t-tests on the (absolute) differences between error-values and their group mean. This is a similar approach to that used in a Levene's test (Levene, 1960), the main difference being that here, the samples compared were not independent (the errors in the light and dark phases were measured in the same group of animals). Results from this statistical analysis revealed that the variance of the absolute error, but not error, was slightly higher in the dark than in the light in both derivations; however this did not reach significance (Fro: t(6)=-1.957, p=0.098; Occ: t(6)=-1.586, p=0.164).

v. Impact of waking behaviour on the performance of the model.

Our next aim was to investigate the impact of varying waking experiences on SWA levels and on the ability of the model to fit empirical data following a prolonged bout of wakefulness. To that end, we compared three experimental conditions: a regular-wheel group (RW), a complex-wheel group (CW) and an exploratory wakefulness group (EW) – see Methods 2.A.i. and Figure 62a.

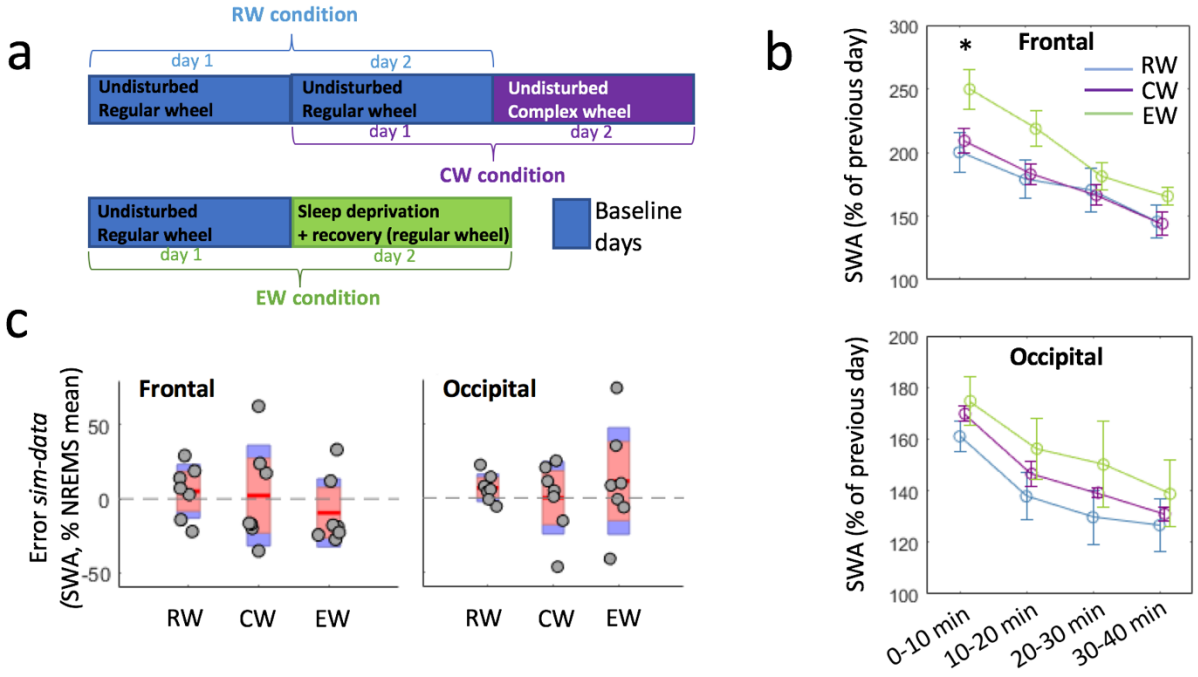


Figure 62: Accuracy of the model's predictions following long wake bouts. ***a)*** *Definition of the 48-h recordings used for each group: regular wheel (RW), complex wheel (CW) and enforced wakefulness (EW). Blue rectangles: days used for optimisation of the parameters; purple & green rectangles: days for which predictions were made.* ***b)*** *Time course of EEG SWA in NREMS during the 40 min following long wake bouts (10-min intervals) in the 3 conditions. Mean ± SEM, n=7 in each condition. SWA levels were normalised against mean SWA levels in NREMS during the previous 24 h of baseline. An ANOVA followed by independent t-tests revealed a significantly higher value in the EW group in the frontal derivation in the first 10 min only (t(12)=-2.272, p=0.042).* ***c)*** *Average error between empirical data and simulations in the 3 conditions in the 40 min following long wake bouts (day 2). Only NREMS epochs were considered. For each condition, n=7; red area: 95-% CI, blue area: 1 STD; grey circles represent individual animals. A mixed design two-way ANOVA (factors 'derivation' and 'condition') revealed no significant main effect of group or derivation, and no significant interaction group*derivation. sim= simulation, ZT= zeitgeber time.*

The presence of an extended bout of wakefulness in all animals from all 3 groups facilitated the comparison of model performance across conditions, especially as the bout length was of similar duration across groups and days (RW: 6.23±2.58 h, CW: 7.05±2.74 h, EW: 6.46±1.50 h, mean ± SD) – see paragraph 3.A.i and Figure 56 for further details.

In all three conditions, the long wake bouts were followed by an increase in SWA (Figure 62b). In the frontal derivation and immediately following wake, this increase was significantly higher in the EW than in the RW and CW cohorts (p=0.042).

Given that waking behaviour is different between RW, CW and EW conditions, if wake experience has a strong impact on SWA dynamics, then performance of the model should be impaired in the CW and EW groups (as all model parameters are optimised over baseline conditions – similar to RW – before being applied to the 48h containing a new waking condition – see Methods). Yet, the model appeared robust to preceding waking experience, with no statistically significant difference in the error or absolute error being observed between the groups (Figure 62c).

The results obtained in CW and EW cohorts seemed more variable across animals than in the RW cohort, however. A Levene's test (Levene, 1960) was run to investigate differences in the homogeneity of variances, which confirmed that variance of the absolute difference d=|*simulation-data*| differed across conditions; this reached significance in the occipital derivation only (Fro: $F(2,18)=2.442$, $p=0.115$; Occ: $F(2,18)=4.46$, $p=0.027$). Variance of the absolute difference (in the occipital derivation) was highest in the EW group ($F(1,12)=7.69$, $p=0.017$).

Note that the absolute difference provides an indication on the *magnitude* of the discrepancy between data and simulation, as opposed to the error, which provides an indication on the *directionality* of the difference. The above results therefore suggest that the model does not predict SWA levels equally well in all the animals of the EW group directly following the 6 h of sleep deprivation.

To examine this aspect further, we performed within-subject comparisons in the EW group only, to investigate how the error evolved over the 40 min following long wake bouts, either during

the first day (baseline) or during the second day (when the sleep deprivation/EW occurred). We found a small difference in the error between days in the frontal derivation (Day1: 8.9±2.3, Day2: -9.2±8.7 % mean SWA in NREMS, mean±SEM, $F(1,6)=5.336$, $p=0.060$), but not in the occipital derivation (Day1: 9.1±2.7, Day2: 11.5±13.6 % mean SWA in NREMS, mean±SEM, $F(1,6)=0.034$, $p=0.861$).

Although we found no significant difference in long wake bout durations across groups and days (Figure 56), it is still possible that the difference in the error between days 1 and 2 in the frontal derivation of the EW group stemmed from systematic differences in wake bout duration between both days. Therefore, to explore whether the length of a wake bout could indeed impact the fit between data and simulation in the few minutes following such a bout, we evaluated the correlation between 'long wake bout duration' and error in the fit in the subsequent 40 min. This revealed no statistically significant correlation (Figure 63a). This absence of correlation between wake bout duration and the error suggests that the model is able to accurately predict the SWA increase following a wake bout of substantial length, regardless of the activity animals engaged in while awake or of the exact duration of the wake bout.

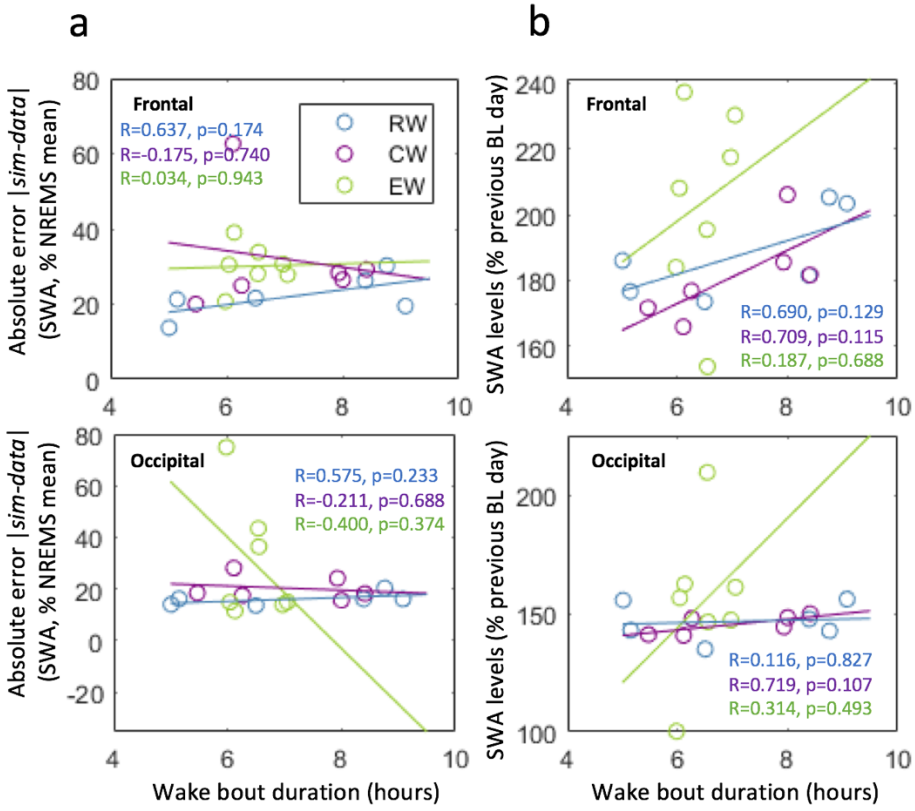


Figure 63: Correlations between wake bout durations and predicted & empirical SWA. ***a)*** *Correlation between long wake bout durations (day 2 only) and the absolute difference between simulated and empirical SWA levels in NREMS epochs in the 40 min following long wake bouts, in the frontal (top) and occipital (bottom) derivations. Regular wheel (RW) & complex wheel (CW): n=6, enforced wakefulness (EW): n=7.* ***b)*** *Correlation between long wake bout durations (day 2 only) and the mean SWA levels in NREMS epochs in the 40 min following long wake bouts. RW & CW: n=6, EW: n=7. In a) and b) the lines were fitted with a least-square algorithm. To prevent bias in the correlation, 1 RW individual and 1 CW individual with very short wake bout durations (≤ 1 h) were excluded from this analysis. BL= baseline, sim= simulation.*

vi. Impact of waking experience on the EEG

It has previously been shown that enforced wakefulness is associated with characteristic changes in the wake EEG spectra (Leemburg et al., 2010; Vyazovskiy and Tobler, 2005a). It is also known that wake quality can have an impact on the dynamics of Process S (Vassalli and Franken, 2017). To investigate those two aspects further, spectral analysis of the EEG during prolonged waking bouts was performed. As expected, waking was associated with high levels of theta-frequency activity (5-10 Hz); this held true across the 3 experimental groups (Figure 64a).

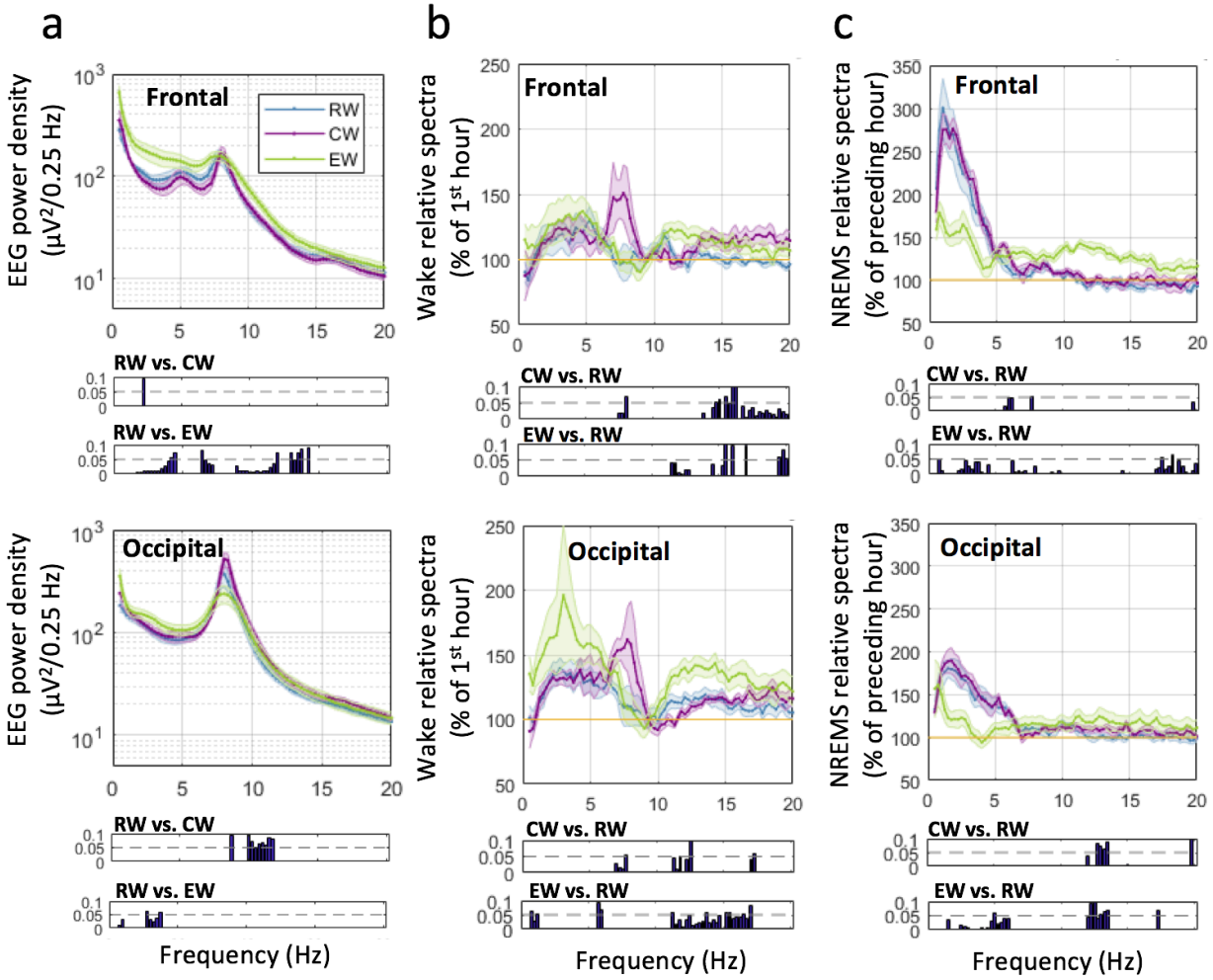


Figure 64: Impact of long wake bouts on EEG spectra. ***a)*** *Wake EEG spectra during long wake bouts in the frontal and occipital derivations across the 3 conditions. In each condition, n=7; mean ± SEM. An ANOVA revealed a significant main effect of frequency in both derivations (Frontal (Fro) & Occipital (Occ): p<0.001), but a main effect of condition was only significant in the frontal derivation (Fro: p=0.014, Occ: p=0.542). There was a significant interaction in both derivations however (Fro & Occ: p<0.001). In the frontal derivation, post-hoc testing with a Bonferroni correction revealed that the enforced wakefulness (EW) group was significantly different from the complex wheel (CW) group (p=0.019; EW vs RW: p=0.055). Independent t-tests were performed across frequencies; p-values<0.1 are reported below the graphs.* ***b)*** *EEG power spectra in the last hour of the long wake bout (day 2 only) expressed as a % of the first hour of the corresponding bout. Regular wheel (RW) and CW: n=6, EW: n=7; mean ± SEM. ANOVA revealed, in both derivations, a significant main effect of frequency (p<0.001), but no main effect of condition (Fro: p=0.334, Occ: p=0.086) and a significant interaction frequency*condition (p<0.001). Post-hoc testing was performed with independent sample t-tests for RW vs. CW on the one hand and RW vs. EW on the other hand. p-values < 0.1 are reported below the figures. ANOVA tests to compare the first and last hours of waking revealed that those hours were significantly different in all 3 conditions and in both derivations, except for the RW frontal EEG (Fro: RW: p=0.199, CW: p=0.005, EW: p=0.092; Occ: RW: p=0.007, CW: p=0.001, EW: p=0.008).* ***c)*** *EEG spectra in NREMS during the hour following long wake bouts as a % of the hour preceding wake (day 2 only). RW and EW: n=7, CW: n=6; mean ± SEM. ANOVA tests revealed, in both derivations, a significant main effect of frequency (p<0.001), but no main effect of condition (Fro: p=0.805, Occ: p=0.876) and a significant interaction frequency*condition (p<0.001). Post-hoc testing was performed with independent sample t-tests for RW vs. CW on the one hand and RW vs. EW on the other hand. p-values < 0.1 are reported below figures.*

ANOVA tests to compare the hours preceding and following long wake bouts revealed that those hours were significantly different in all 3 conditions and in both derivations, except for the EW occipital (Fro: RW: p=0.001, CW: p=0.001, EW: p<0.001; Occ: RW: p=0.003, CW: p=0.001, EW: p=0.154). Note that for clarity and conciseness, no direct comparison between the EW and CW cohorts was performed here, especially as this would not have provided information for the question addressed.

Notably, access to a complex wheel led in both derivations to an increase in theta power in the last hour of a prolonged wake bout when normalising against the first hour of that same bout (Figure 64b). This result suggests that transitioning from a regular wheel to a complex wheel, which likely implies transitioning from stereotypic running to learning a new running pattern, has an impact on the EEG. We therefore checked whether the wheel transition affected running pattern and speed (Figure 65). This analysis showed that the introduction of a complex wheel resulted in a shift of the running speed distribution towards lower paces (Figure 65f). This shift suggests that the mice experience the introduction of the complex wheel as a challenge and therefore likely implies learning a new motor skill. However, there was otherwise no significant difference in running speed, time spent running, number of running bouts or mean running bout length between the baseline and complex-wheel days (Figure 65b-e).

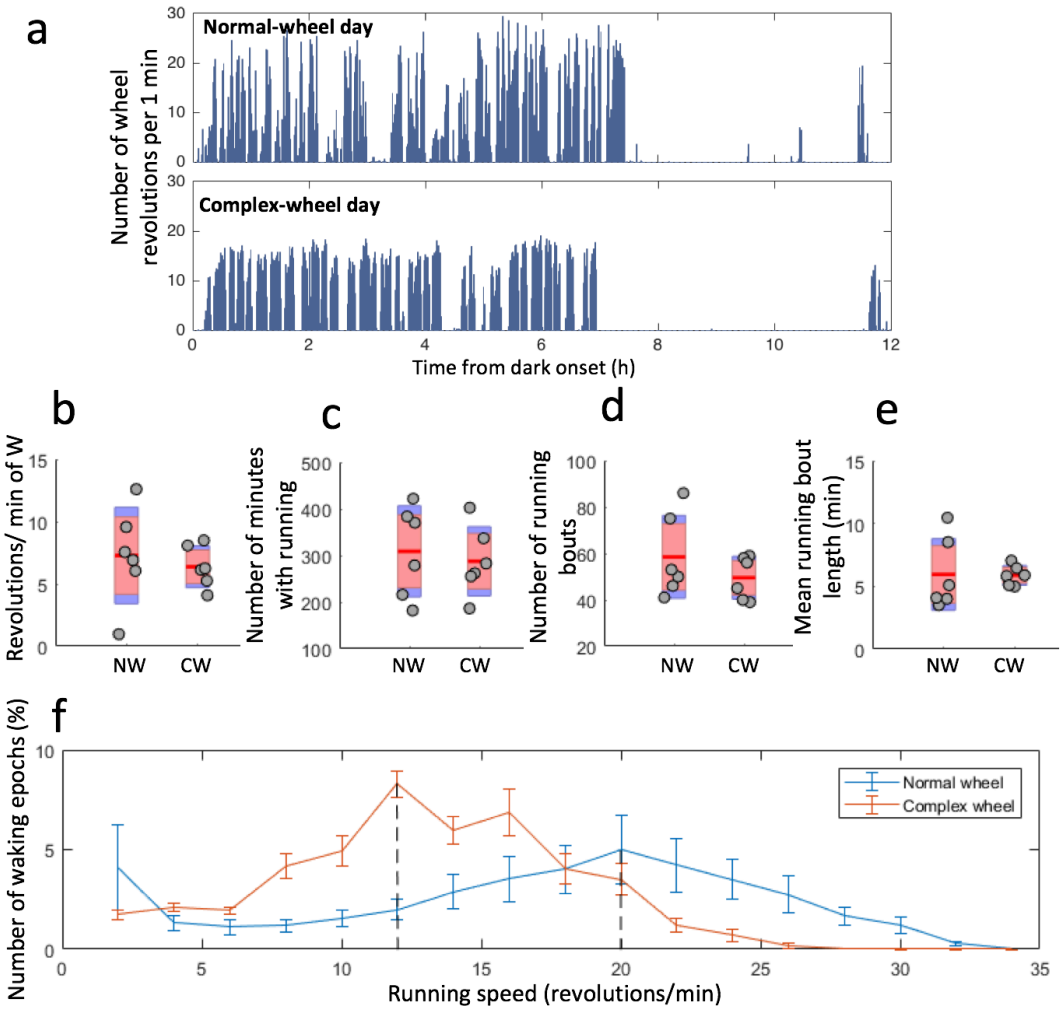


Figure 65: Wheel-running activity in the normal- and complex-wheel groups. ***a)*** *Bar plots of running speed (wheel revolutions/min) in each 4-s epoch across the dark period in the first day (access to a normal wheel – NW) and second day (complex wheel) of one animal from the CW cohort.* ***b)*** *Average running-wheel revolutions per minute of waking in the dark period of the NW and CW days of the CW group.* ***c)*** *Total number of minutes with running activity recorded in the NW and CW days (dark periods only) of the CW group.* ***d)*** *Number of running bouts in the dark period of the NW and CW day of the CW group. Bouts were defined with a minimum duration of 16 s (4 x 4-s epochs); short interruptions of up to 16 s within a bout were permitted.* ***e)*** *Average running-bout lengths (expressed in minutes) in the dark period of the NW and CW day of the CW cohort. Running bouts were defined as in d).* ***b-e)*** *Red line: group mean, red area: 95-% CI, blue area=1 STD, grey circles represent individual animals. ANOVAs for repeated-measures revealed no significant differences between the NW and CW days in average speed of running (b), amount of running (c), running bout numbers (d) and running bout lengths (e).* ***f)*** *Distribution of running speed (expressed in revolutions/min) across waking epochs. Only epochs with an average running speed of at least 2 revolutions/min were plotted. Data was subdivided in 2 revolutions/min bins. The number of epochs within a given bin is expressed as a percentage of the total number of waking epochs. Error bars: mean ± SEM. Dotted lines highlight the running speed at the peak of each distribution curve.* ***b-f)*** *Only 6 animals of the CW cohort were used as one mouse did not run and was therefore excluded from analyses reported in panels b-f.*

Finally, SWA showed an increase in the last hour of the wake bout compared to the first hour (note that we are referring to SWA within the wake spectra, and not NREMS) in all three groups. As expected following sleep deprivation during the light phase, the EW group showed the highest increase, although this was mainly noticeable in the occipital derivation only (Figure 64b– lower panel). These observations are consistent with previous studies showing that wake EEG undergoes changes across prolonged waking (Aeschbach et al., 1997; Cajochen et al., 1998, 2002; Finelli et al., 2000; Vyazovskiy and Tobler, 2005a).

We then asked whether there was a correlation between the duration of the long wake bouts and subsequent SWA levels, as sleep pressure is known to build-up with time spent awake, and SWA in NREMS is a measure of sleep pressure (see Introduction). However, we found no such correlation in any of the 3 conditions (Figure 63b). This does not mean that SWA is not a good measure of sleep need; instead, it shows that if wake bouts are already substantially long, and of similar lengths (as shown in Figure 56b), SWA is not sensitive enough to reflect fine variations in wake bout lengths.

Furthermore, the value of the absolute error |simulation-data| in the 40-min interval immediately following long wake bouts did not show any correlation with the levels of empirical SWA in any of the experimental groups (Figure 66). This implies that the performance of the model is not affected by the magnitude of SWA increase following long wake periods and that it matches such increases well.

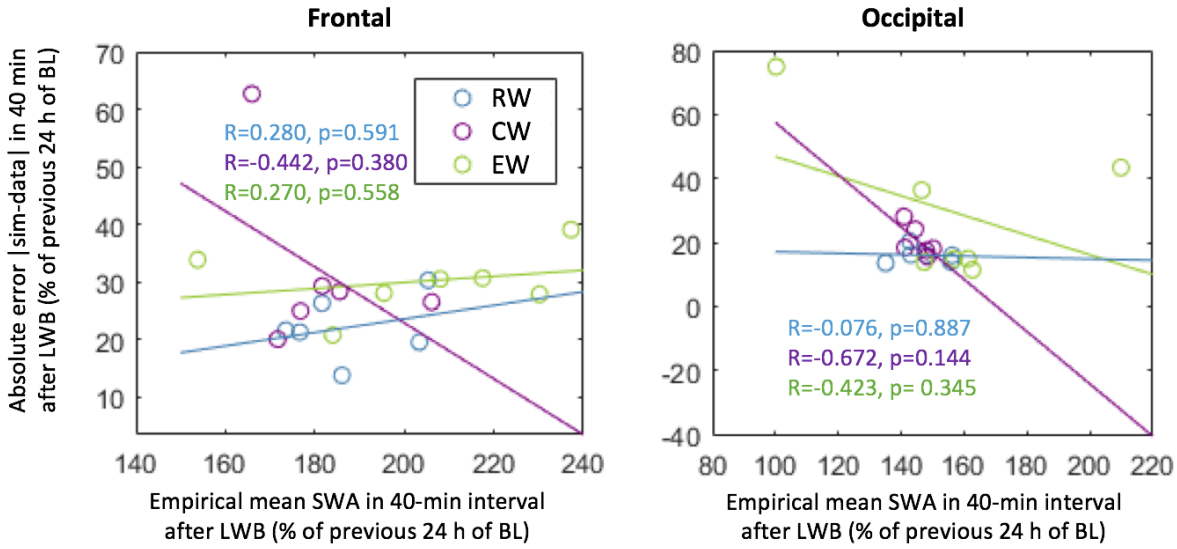


Figure 66: Effect of empirical SWA on the model's predictions. Correlation between empirical SWA after long wake bouts in day 2 (mean SWA over the 40 min following long wake bouts – expressed as a % of day 1) and the absolute error in the same 40 min in the 3 experimental groups; RW: n=6, CW: n=6, EW: n=7. Lines were fitted with a least-square algorithm. To prevent bias in the correlation, 1 RW individual and 1 CW individual with very short wake bout durations (≤ 1 h) were excluded from this analysis. sim= simulation.

Finally, we asked whether the time spent running on a wheel during a long wake bout could affect the performance of the model in matching SWA levels following the wake bout. For instance, it was shown that stereotypic wheel-running is associated with a reduction in firing rates in a population of cortical neurons (Fisher et al., 2016b). Therefore one could hypothesise that if a mouse runs a lot during a wake bout, the time spent engaging in a stereotypic activity could lead to a smaller increase in SWA than predicted by the model and thus to a higher error. Indeed, although the model parameters are optimised against baseline conditions when mice have access to a regular wheel, the 48-h recordings include episodes during which mice run and sometimes not; therefore, if the running activity was particularly strong during the long wake bout, it could still lead to a smaller SWA increase than predicted. There was however no correlation between the percentage of time spent running on a wheel during long wake bouts and subsequent SWA levels (Figure 67a), nor between the percentage of time spent running on a wheel and the performance of the model (as measured by the absolute error) - Figure 67b.

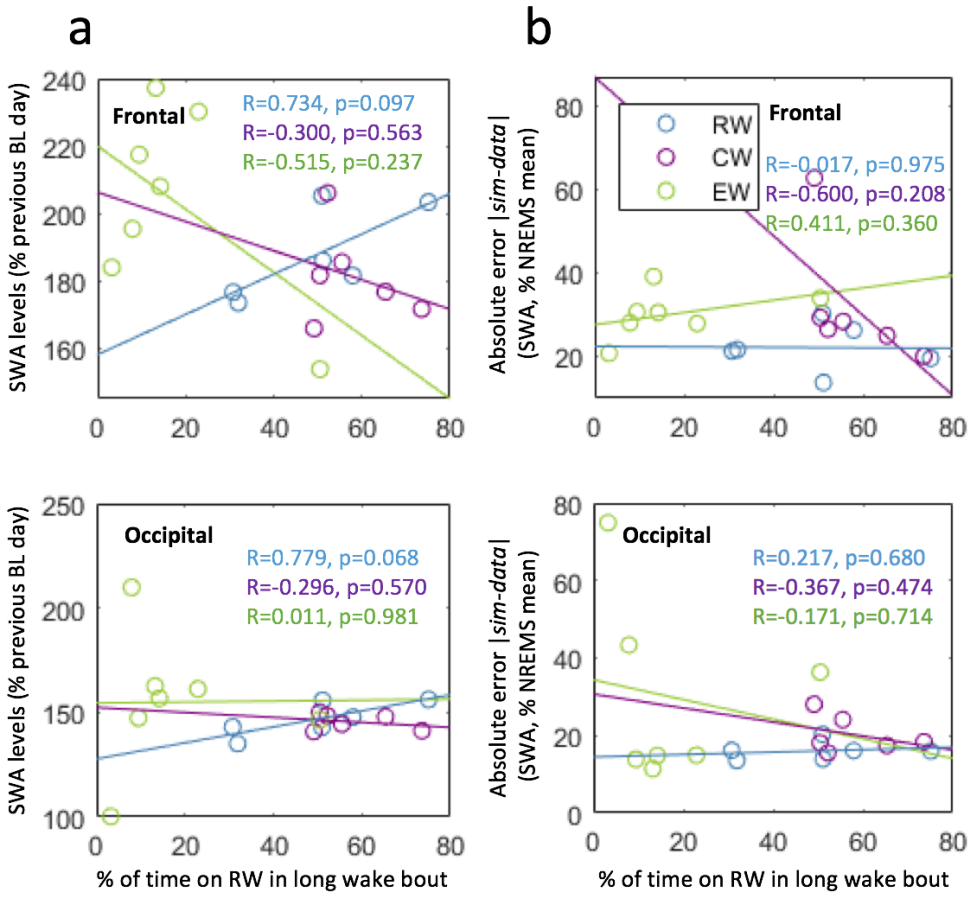


Figure 67: Correlations between time spent running, SWA and model predictions. ***a)*** *Correlation between % of time spent running on a wheel during the long wake bout (day 2 only) and the mean SWA levels in NREMS epochs in the 40 min following wake bouts, in the frontal (top) and occipital (bottom) derivations. RW & CW: n=6, EW: n=7.* ***b)*** *Correlation between % of time spent running during long wake bouts (day 2 only) and the absolute difference between simulated and empirical SWA levels in NREMS epochs in the 40 min following long wake bouts, in the frontal (top) and occipital (bottom) derivations. RW & CW: n=6, EW: n=7. In a) and b) the lines were fitted with a least-square algorithm. To prevent bias in the correlation, 1 RW individual and 1 CW individual with very short wake bout durations (≤ 1 h) were excluded from this analysis. BL= baseline, sim=simulation.*

B. Results from *Sleepy6* mice

To investigate the dynamics of SWA and sleep homeostasis in the *Sleepy6* mice, we applied the elaborated model to recordings obtained in *Sleepy6* homozygotes and wild-type littermates. We initially chose an approach similar to that observed in the EW group of the initial study described above and optimised the parameters of the model against a baseline day duplicated to obtain a 48-h baseline. Additionally, as we had both EEG (frontal and occipital) and LFP recordings, we tested the ability of the model to predict SWA levels from recordings obtained with the laminar probe (LFP).

The model's predictions were overall satisfactory but variable across mice; two examples are presented in Figure 68. In particular, the fit was particularly poor in some WT mice. This possibly stems from a more fragmented sleep wake/architecture in those animals, as opposed to the homozygotes, which have more consolidated bouts of sleep and wakefulness.

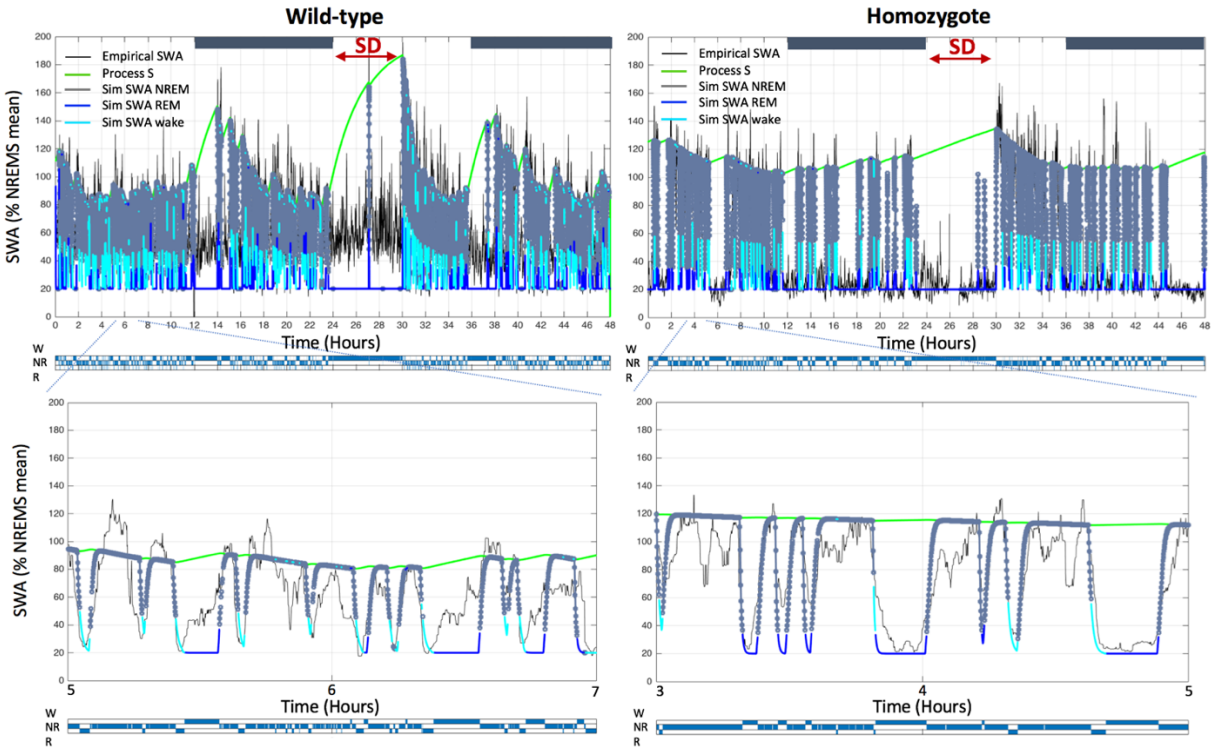


Figure 68: Empirical and simulated EEG SWA levels in WT and Sleepy6 homozygous mice. SWA levels are shown across 48 h (upper panels) and 2 h (lower panels) in a wild-type (left) and homozygote mouse (right). The recordings from the wild-type mouse are from the occipital EEG derivation, while those from the homozygous mouse are from the LFP derivation. Curves are plotted with one value per 4-s epoch, although the simulation solver was allowed to take steps of any size < 4 s (see Methods). SWA levels were normalised (expressed as percentage) against mean SWA over 48 h in non-rapid eye movement sleep (NREMS) only. The plots also showed Process S (sleep pressure), obtained from the mathematical model. Light and dark phases are represented at the top of the figures (black bars = dark phase). The 6h of sleep deprivation (SD) are indicated at the top of the graphs in red. Hypnograms of vigilance states are shown at the bottom of each panel. NR= non-rapid eye movement sleep, R= rapid eye movement sleep, W= wake. Sim=simulation.

As the model performs better when faced with longer wake bouts (which present a "challenge" to the model because they eventually lead to a higher SWA build-up), we next performed optimisations again, using 24 h of baseline followed by a sleep deprivation day (6 h sleep deprivation and 18 h recovery). This ensured that in all mice, at least one wake bout of 6 h would be present in the 48 h against which parameters are optimised, so as to promote a better final fit. It is important to note that here, we were aiming to compare dynamics (i.e. parameters) between wild-type and homozygous *Sleepy6* mice, as opposed to the initial study where we were

comparing the performance of the model across waking experiences. Therefore, optimising parameters against a dataset containing a sleep deprivation protocol is not an issue as long as the same approach is followed for all mice to be compared. Additionally, comparing dynamics between wild-type and homozygotes can only be reliable if the fit obtained in both genotype is satisfactory – a sign that the results obtained are reliable.

The model was however expected to perform satisfactorily regardless of the optimisation approach chosen ('double baseline' or 'baseline + sleep deprivation') and we therefore compared the results obtained with both approaches, as shown in Figure 69 and Figure 70. This revealed that the parameter values obtained with either approach are overall similar, except when optimisations are run against LFP data. This suggests that the equations are better designed to fit EEG recordings than LFP for reasons that remain to be elucidated. This was particularly surprising as slow-waves were better defined in the LFP channels than EEGs, and we were therefore expecting a better fit with the LFP data – whereas we find here that the model's performance was more robust with EEG recordings.

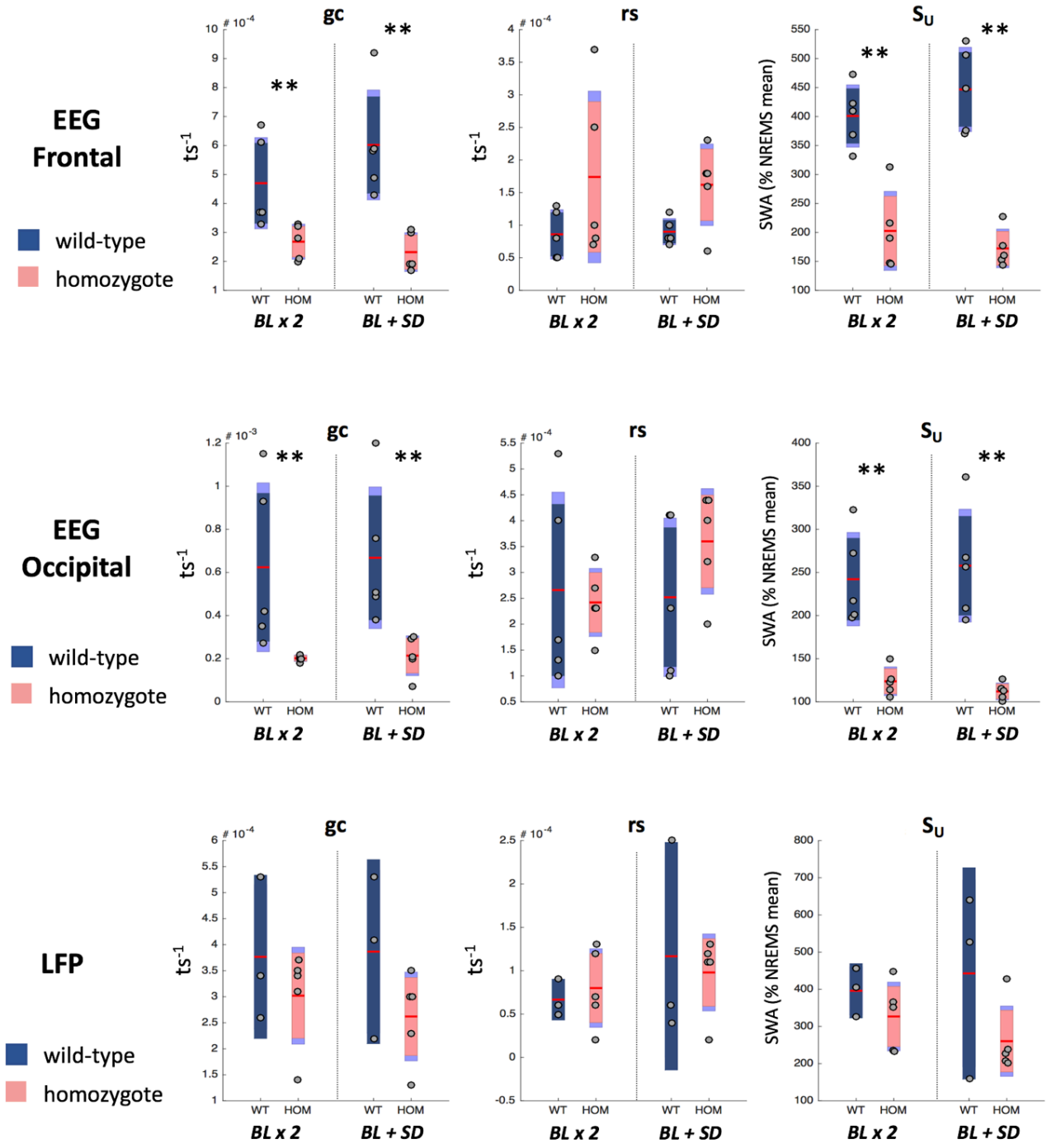


*Figure 69: Evaluating model parameters in WT and Sleepy6 mutant mice. Mean (red line) and individual animal values (grey circles) of the parameters gc, rs, S_U in the frontal EEG, occipital EEG and LFP in Sleepy6 wild-types (WT) and homozygotes (HOM). In each plot, the left part shows the results obtained when running optimisations in a baseline day duplicated ('BL x 2'), while the right part shows the parameters obtained when using a 24h baseline day directly followed by a sleep deprivation day (6 h sleep deprivation and 18 h recovery) – ' BL + SD'. ts = 4 s; EEGs: n=5 in both groups; LFP: n=3 in WT and n=5 in HOM. Dark blue/Pink area: 95-% CI, light blue area=1 STD. The significance of the difference in parameter values between derivations was assessed with a non-parametric Mann Whitney test; ** indicates p-value < 0.01.*

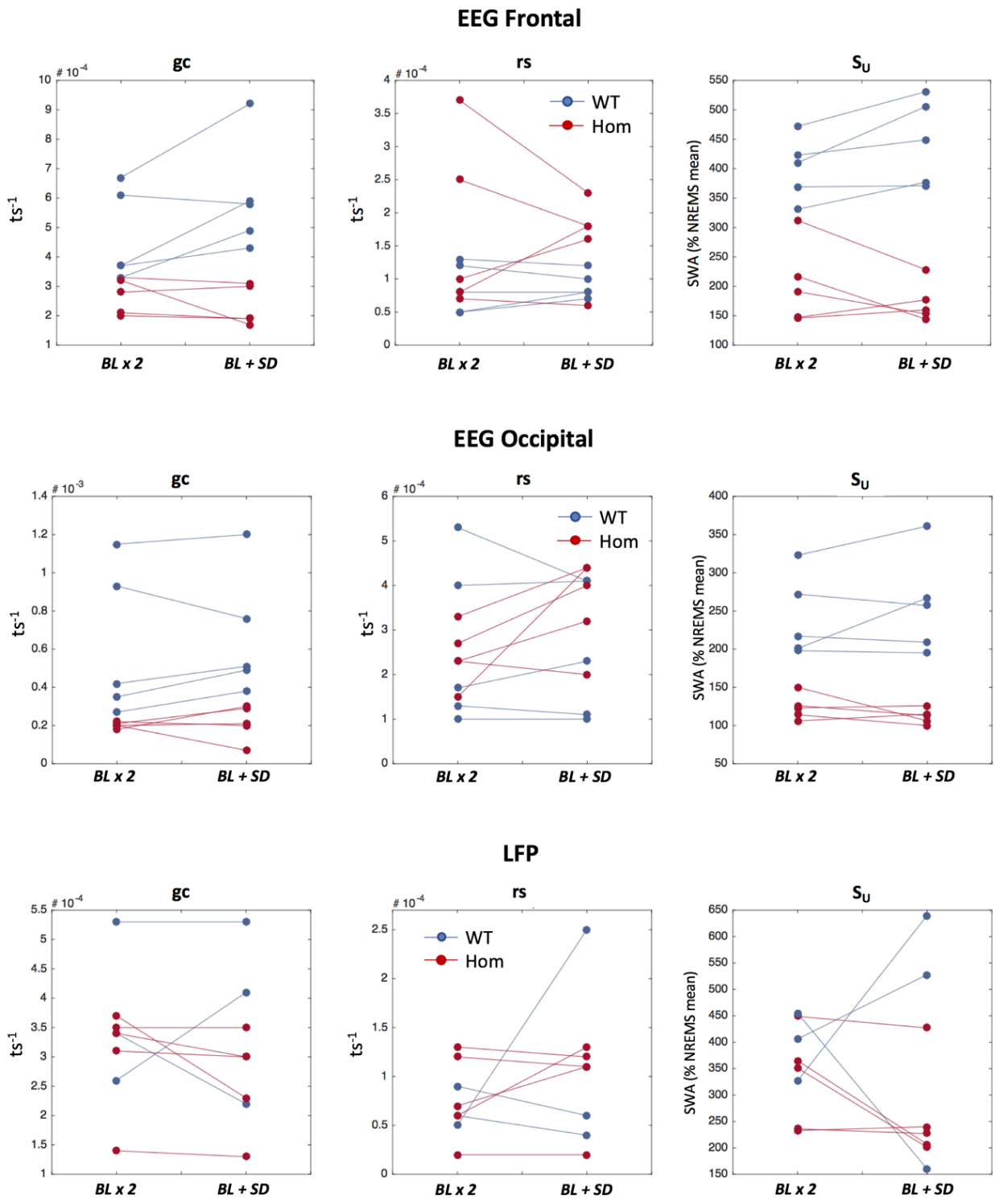


Figure 70: Comparison of the values obtained for the parameters gc, rs, S_U in the frontal EEG, occipital EEG and LFP in Sleepy6 wild-types (WT) and homozygotes (HOM) using a duplicated 24 h baseline optimisation approach ('BL x 2') or an optimisation based on 24 h baseline + 24 h sleep deprivation day ('BL + SD' – 6 h sleep deprivation at the beginning of the second day). ts = 4 s; EEGs: n=5 in both groups; LFP: n=3 in WT and n=5 in HOM. Dark blue lines: WT, Dark red lines: Homozygotes (Hom).

Overall, the results obtained reveal that *Sleepy6* homozygotes have significantly reduced values of gc and S_U in both EEG derivations, but not LFP (Figure 69). This means that the rate at which Process S decreases in those mice (gc) is slower, but that the upper threshold to which sleep pressure can build-up (S_U) is also lower. This would indicate that sleep need does not reach as high levels in homozygotes as in wild-types, and although the decay is slower, this may not prevent the mice from having shorter sleep as the levels of sleep pressure that need dissipating are initially lower following wake bouts.

4. DISCUSSION

A. Evaluation of the performance of the model in C57BL/6J mice.

We applied for the first time an elaborated version of the two-process model to sleep recordings obtained in mice. Our aim was to assess whether this version of the model could describe the dynamics of sleep homeostasis in wild-type C57BL/6J mice and if so, how it would be affected by recordings performed while mice experienced varying waking conditions. In addition, as we had access to recordings which had been performed in both the frontal and occipital cortex, two anatomically and functionally distinct cortical regions, we were able to address whether the dynamics of sleep homeostasis are conserved globally across the brain, or whether they have a local regulatory component.

We found that the elaborated model can successfully simulate variations of SWA in mice on time scales spanning from minutes to hours, and that some essential parameters of the model differed between cortical areas. Conversely, the model appeared robust to varying waking conditions.

B. Differences between cortical regions in the dynamics of Process S.

Our finding that important parameters of the model which govern the variations of Process S showed differences between the frontal and occipital derivations was expected, as the levels and dynamics of SWA have previously been shown to vary across brain regions (Huber et al., 2000b; Leemburg et al., 2010; Vyazovskiy and Tobler, 2005b; Werth et al., 1996a), and topographic differences in Process S dynamics were highlighted for the first time in mice in 2000 (Huber et al., 2000b). In particular, we found that gc, the decay rate of Process S, was higher in the frontal derivation, which was in line with previous findings from human studies (Werth et al., 1997; Zavada et al., 2009). Our study also agrees with previous suggestions that sleep recovery processes may occur at specific locations in the brain and that SWA variations are controlled in a topographical way (Beersma, 1998).

Various explanations for the topographical differences observed in the dynamics of Process S have been proposed, such as:

- The role of prior waking activity cannot be excluded as it has been shown that sleep pressure (measured by SWA) builds up at different rates across brain regions depending on which areas were mainly active during previous waking (Borbély and Achermann, 1999; Cajochen et al., 1998; Schwierin et al., 1999; Werth et al., 1998). A larger SWA increase following sleep deprivation has also been shown in the anterior prefrontal regions (Finelli et al., 2000; Massimini et al., 2004; Vyazovskiy et al., 2002), supporting the idea of a local build-up of sleep need which varies across brain regions.
- The dynamics of Process S may vary between cortical areas because of anatomical differences (Kilduff et al., 2011).

C. Effect of lighting conditions.

The effect of light on the model performance was analysed in two complementary ways. First, we asked whether the error between empirical data and simulations would differ between the light and the dark phases in baseline undisturbed conditions. Second, the performance of the model was assessed following a prolonged waking bout which either terminated in the middle of the dark or the light period. Overall, the simulation fitted the data equally well in both light and dark phases, which therefore suggests that good predictions can be obtained while keeping parameter values equal across the light-dark cycle. It is worth noting, however, that a previous study in rats obtained a better fit between data and simulation if using different time constants for the decrease of Process S in the light and in the dark periods (Franken et al., 1991). This suggests a possible circadian influence – that our version of the model does not currently tackle – which would lead to different rates of increase and decrease of Process S depending on the time of day. Another study showed that if rats were kept in constant darkness, the rate of increase of SWA underwent circadian modulation, which could therefore not be caused by the direct influence of light (Deboer, 2009). Both subject-based and simulation studies also reported a circadian influence on slow-wave characteristics in humans (Lazar et al., 2015; Werth et al., 1996b). In mice, however, the fit between simulations and empirical data is usually satisfactory when keeping the model parameters unchanged across 24 h, just as was done in the present work (Franken et al., 2001; Huber et al., 2000a). The fact that a circadian influence on SWA dynamics has been shown in both human and rat studies but not so far – to our knowledge – in mice, suggests that circadian variations affecting SWA may be stronger in some species than in others. And yet, although we found that the model predicted SWA in NREMS well following a long wake bout occurring in the dark phase (spontaneous wake) or in the light phase (sleep deprivation), it cannot be excluded that the type of behaviour is different between spontaneous and enforced wakefulness.

D. Impact of wake experiences on model predictions.

We next asked whether specific waking experiences would play a major role in the dynamics of Process S. Indeed, although wake has long been considered a homogeneous state, it has also been proposed that waking dominated by automatic behaviours (such as regular wheel-running) led to reductions in firing rates in some neuronal populations of the cortex, and could therefore lead to a slower accumulation of sleep need (Fisher et al., 2016b; Vyazovskiy et al., 2017). In modelling terms, this would mean that the predicted levels of 'sleep need' if prior waking was mainly 'quiet' or dominated by stereotypic behaviours would overestimate empirical levels, or conversely, would underestimate sleep pressure if an animal has engaged in 'demanding' activities, such as learning a novel motor skill or exploratory behaviour.

To test this, we used data recorded in animals which were given access to complex wheels following days of habituation to a regular wheel, on which they already ran extensively. The use of a complex wheel is associated with sensorimotor learning as it requires a different pattern of running. The presence of a complex wheel triggered an increase in EEG power density in the *theta* range over the course of waking. Given that the model is based on slow-wave activity – which is the EEG power in the *delta* range – the introduction of a complex wheel did not have a significant impact on the goodness of fit between data and simulations, as indeed, the levels of SWA themselves were not significantly different from corresponding values after regular wheel running.

Additionally, the increase in the theta range mentioned above suggests that in some respect, running on a complex wheel is a qualitatively different experience to running on a regular wheel, and could either reflect a higher arousal level or a learning process, both of which have been associated with higher EEG theta-activity (Aeschbach et al., 1997; Fisher et al., 2016b; Strijkstra

et al., 2003; Vyazovskiy and Tobler, 2005a). These results suggest that wake duration – rather than specific wake experience – may be the main factor accounting for the dynamics of Process S.

Interestingly, a recent study proposed a reformulation of the sleep homeostasis model, whereby Process S would increase during wakefulness dominated by high theta (5-10 Hz) activity (Vassalli and Franken, 2017). This is an interesting – although debatable – hypothesis, which would support the idea that sleep pressure builds up at different rates depending on the type of waking activity.

E. Limitations of the present modelling work.

All initial analyses were performed using data recorded in a single mouse strain (C57BL/6J) and only in males. Given the variations observed between strains in other modelling studies (Huber et al., 2000a), it could be expected that the model performs differently in other mouse lines. However, the present version of the model was subsequently adapted to *Sleepy6* mice, which have a predominant C3H-Pde6B+ background, and the results obtained were satisfactory. Therefore, although the fit may not be as optimal – especially depending on whether a strain naturally shows consolidated or fragmented sleep/wake architecture – it seems likely that the model can be used across a wider variety of backgrounds than the C57BL/6J line on which we developed it initially.

Similarly, as we did not test the model against recordings performed in female mice, it cannot be excluded that performance may vary across sexes, or that extrinsic factors such as waking behaviour may impact sleep homeostasis in females in a different manner than in males.

Additionally, one aim of this study was to investigate topographical differences in the dynamics of Process S; however, only two cortical areas were used (motor and visual cortex) and

evaluating SWA dynamics in additional areas could provide further insights into the topographical variations of sleep homeostasis. Another limitation of this initial modelling study is that our findings regarding an absence of effect of waking behaviour on the model performance may not hold should the number of animals be increased. Although this is a possibility, it should be noted that the numbers included here (7 animals per group) are in line with previous studies (Franken et al., 1991, 2001; Huber et al., 2000a, 2000b; Vyazovskiy et al., 2006, 2007). A more likely alternative is that sleep pressure builds up or dissipates at different rates with or without access to a regular or complex wheel, but that our modelling approach was not sensitive enough. Similarly, other waking experiences may have had a stronger influence on the dynamics of Process S, such as stressful activities, which have been shown to enhance sleep intensity in the following sleep episode (Tobler and Borbély, 1990).

F. Conclusions of the modelling work using C57BL/6J mice.

Our modelling approach provided us with strikingly robust predictions across several experimental conditions. This could reflect a fundamental – although yet to be fully defined – aspect of sleep homeostasis, whereby as long as a mouse remains awake, Process S builds up (and conversely decreases when the mouse is asleep), regardless of circadian time, light or waking behaviour. The only difference we consistently observe is not across mice and experimental conditions but across cortical regions within mice. These results would therefore support the hypothesis that the daily sleep/wake architecture is under the control of two separate systems:

- one system could be responsible for initiating, maintaining and terminating sleep/wake bouts, mainly based on extrinsic factors (e.g. lighting conditions, vital needs such as hunger) and with preceding sleep-wake history having little influence.

- a second system would keep track of sleep/wake history, but not contribute actively to sleep-wake initiation.

Of course, such an hypothesis would need to be further tested and certainly does not exclude that the interaction between intrinsic and extrinsic factors remains essential for most efficient sleep – 'efficient' being interpreted from both a physiology and an ecology perspective (Borbély et al., 1989).

G. Conclusions regarding the *Sleepy6* results

The application of the elaborated version of the two-process model to *Sleepy6* recordings proved overall successful, and confirmed the ability of this version of the model to predict SWA variations in mouse strains other than C57BL/6J on which we developed it.

More importantly, this modelling work applied to *Sleepy6* mice provided us with additional insights into the dynamics of sleep homeostasis in those animals, although the results may appear counter-intuitive at first sight. *Sleepy6* homozygotes have a reduced total sleep time, which could suggest either a more efficient sleep (that would be reflected in a higher decay rate gc) or a slower build-up of sleep pressure during wake (that would appear in a smaller rise constant rs of Process S). And yet, we observed a significantly decreased decay rate in *Sleepy6* homozygotes as opposed to their wild-type littermates, and no significant difference in the rise constant. These results held true in both EEG derivations, but not in the LFP recordings.

Importantly however, *Sleepy6* homozygotes also displayed a significantly reduced upper asymptote of Process S. This, interestingly, could account for several of the observations made in the previous chapters:

- With a lowered upper threshold of Process S, *Sleepy6* mutants may be able to come back to a low sleep pressure level more quickly (simply because they are starting from an

already low level of sleep pressure at the onset of NREMS); this would explain the decreased total sleep time. Such a hypothesis is possible even though their decay rate is slower, as it depends on the fine interaction between gc (the decay rate) and S_U (the upper asymptote). It is true that if gc is below a critical value (to be determined individually for each mouse), then this hypothesis may not hold anymore.

- A decreased upper threshold could mean that mice reach a state where their sleep pressure is at its highest (from an individual perspective) more quickly – in particular as the rise constant of S is similar to wild-types who have a higher upper threshold to reach. This may account for the poorer score that *Sleepy6* mutants show at the behaviour tasks, or for their hyperactive and decreased attention traits (see Chapters 1&3). Additionally, a lower decay rate could reflect an impaired ability to fully and efficiently dissipate sleep pressure and thus could also account for the impaired performance that *Sleepy6* homozygotes showed during memory tasks. This hypothesis would also be in line with literature showing that ADHD symptoms are often linked with excessive daytime sleepiness (Golan et al., 2004; Ito et al., 2017).

Taken together, these results do not fully allow us to answer the question of whether the reduced sleep time observed in *Sleepy6* mice reflects a decreased need for sleep or not. However, it provided insights into the sleep homeostasis dynamics in those mice, that would need to be put in perspective with the results from Chapter 4. For instance, how can the more consolidated bouts of sleep and wake be linked to the differences we observed in parameter values? This will be discussed further in the next and final chapter.

CHAPTER 6: General discussion

1. SUMMARY OF THE RESULTS OBTAINED

The aim of this work was to characterise the *Sleepy6* line further, and investigate the molecular and cellular mechanisms underlying the observed phenotypes, to gain a new understanding of sleep disturbances in those mice, and more generally, in sleep/wake regulation.

Previous data showed that the *Sleepy6* homozygotes displayed decreased sleep time, as well as an array of other phenotypic differences with their wild-type littermates, in their behaviour (e.g. absence of nest building, absence of marble burying, social dominance of WT males over homozygous males, etc.), in their response to stimuli (e.g. absence of freezing behaviour following a foot shock), and in their physiology (e.g. reduced body weight and peripheral temperature). Pilot EEG studies also pointed towards a potential difference in REM sleep.

A. Molecular findings

We therefore wanted to define the *Sleepy6* sleep phenotype in more detail, as well as confirm the memory testing, while also starting to investigate possible changes in neurotransmitter pathways.

HPLC methods revealed no striking difference in the levels of serotonin or its metabolite 5-HIAA in any of the brain regions tested (cerebellum, cortex, hippocampus, hypothalamus), thus refuting our initial hypothesis. No differences were observed either in those same brain regions of the other neurotransmitter (dopamine) and metabolites tested (DOPAC, HVA), except for a decreased level of DOPAC in the cortex in homozygous mice. Interestingly, decreased levels of

DOPAC have been reported in the anterior cingulate cortex of schizophrenia patients (Wyatt et al., 1995). Another study also found decreased DOPAC levels in the prefrontal cortex (and increased levels in the nucleus accumbens and striatum) in rats with higher locomotor activity when exposed to novelty, which are used as a model of increased addiction susceptibility (Piazza et al., 1991). Given that SNARE variants have been associated with schizophrenia (see Chapter 1) and that *Sleepy6* mice show increased running and locomotion when exposed to novel objects and a novel environment, our findings are in agreement with the two aforementioned studies.

We therefore went on to test, using RT-qPCR methods, the expression of genes involved in the serotonergic and dopaminergic pathways, such as the serotonin and dopamine transporters. Again, we found no relevant differences. Levels of expression of *Vamp2* and the two genes coding for the SNARE-complex proteins SNAP25 and STX1A were also tested and revealed no differences either.

B. Differences occurring at a cellular level

Additionally, the EEG and laminar probe recordings (Chapter 4) confirmed that *Sleepy6* mice spend less time in both REMS and NREMS compared to their WT littermates, and that the EEG power spectra in all vigilance states is shifted towards lower powers for frequencies above 6 Hz, and higher power for very slow frequencies (<2 Hz).

Even more strikingly, these experiments highlighted major differences in neuronal activity patterns, with periods of silence at a population level that can last for a few seconds, and overall last much longer than in WT mice. These periods of silence were reflected in almost flat EEG traces, reminiscent of deeply anesthetised states (see Chapter 4 - Discussion).

C. Learning and memory in *Sleepy6* mice

To evaluate whether the decreased sleep time observed in *Sleepy6* mice leads to cognitive impairments, we ran novel-object and object-in-place recognition tests to assess the learning and memory capacities of *Sleepy6* homozygotes. This did not reveal major impairments, but the *Sleepy6* mutants did perform more poorly than the WT controls, which, as discussed in Chapter 3, could either reflect a learning & memory impairment, or a possible deficit in attention, coupled with hyperactivity. Indeed, given that the differences observed were mild, they could very well stem from a lack of attention, or a combination of poorer memory and attention capacity, for instance. This is plausible given the known associations between ADHD and variants in VAMP2 and other SNARE proteins (see discussions of Chapters 3 & 4).

D. Findings obtained from mathematical modelling

Finally, the EEG and laminar probe recordings obtained in the *Sleepy6* homozygous and WT mice were further analysed using a computational model of sleep-wake regulation which was developed during the course of this DPhil (originally using recordings from WT C57BL/6J mice – see Chapter 5). These analyses revealed that both the rate of decrease of Process S (sleep need) and its upper threshold were smaller in *Sleepy6* Homozygotes compared to WT littermates, while the rate of increase was similar. Given the reduced sleep time observed in *Sleepy6* mice, different findings may have been expected – namely that sleep pressure builds up more slowly (i.e. the rise constant would appear significantly smaller), or that sleep pressure would decrease faster (i.e. the decay rate would be higher and not smaller). As discussed in Chapter 5, the findings obtained are nonetheless consistent with data from other chapters. Namely, the lower asymptote could partly explain why the animals sleep less (they need to dissipate an initially lower level of sleep pressure) or why they may perform worse at learning tasks (they reach their

individual sleep pressure threshold more quickly). With a decreased upper asymptote, a sleep need increasing at the same rate as WT mice and dissipating more slowly, *Sleepy6* mice would indeed reach their upper threshold of sleep pressure more easily.

Process S, however, is an "artificial" process that was introduced for modelling purposes, and which should ultimately reflect underlying physiological mechanisms. One may wonder, therefore, how the differences observed in parameter values between WT and mutant *Sleepy6* mice may relate to the cellular and molecular discrepancies that have also been noted.

2. MODEL PARAMETERS AND SLEEP/WAKE ARCHITECTURE OF THE *SLEEPY6* MICE

Despite an increase in power for the slower frequencies (<2 Hz), *Sleepy6* mutants may still be able to display an overall lower asymptote of Process S (which is inferred from SWA levels, i.e. EEG power in the 0.5-4 Hz range) as they then display similar-to-lower power for all frequencies above 2-3 Hz. It is therefore highly plausible that had the modelling approach been based on EEG power in the 0.5-2 Hz only, different parameter values would have been obtained. One could hypothesise that *Sleepy6* mutants would have displayed a higher upper asymptote for instance, although it is more difficult to predict how such an alternative approach would have impacted the rates of increase and decay.

Additionally, our findings show that *Sleepy6* mice have more consolidated bouts in all vigilance states. Interestingly, the two-process model has been reported to perform better when faced with a "challenge", for instance an extended bout of wakefulness, and the model can fail to predict sleep pressure dynamics in mouse lines that have a naturally fragmented sleep/wake architecture, leaving little time for SWA to build-up and resulting in little variations in SWA levels across 24 h (Huber et al., 2000a). In the present study, the model therefore performed

better in *Sleepy6* mutants compared to their WT littermates, possibly explained by the fact that *Sleepy6* homozygotes have long bouts of both wake and sleep, while the WT alternate between states much more often (see Chapter 4). It is therefore worth highlighting that the comparisons are based on the significance of the difference in parameters between the two genotypes – but this comparison may be partly biased by the better fit obtained in *Sleepy6* mice.

It is also interesting to note that the time constant of increase T_i of Process S has been reported to be variable between mouse genotypes and strains and across species while the time constant of decrease T_d has been reported to be fairly stable across species, strains and (mouse) genotypes (Franken et al., 2001; Huber et al., 2000a). When comparing the *Sleepy6* homozygotes to their WT littermates, the difference was however found in the rate of decrease rather than the rate of increase (note that the rate of increase rs is inversely proportional to the time constant of increase T_i used in other papers, i.e. rs $\propto 1/T_i$; similarly the rate of decrease gc $\propto 1/T_d$). Additionally, it has been proposed that the longer T_i values (i.e. smaller increase rate) observed in humans and rats, could reflect the increase in the duration of sleep/wake cycles (Huber et al., 2000a). Since no difference was observed between *Sleepy6* homozygous and WT mice, this could reflect the fact that although homozygotes have more consolidated bouts of sleep and wakefulness, the overall length of a sleep/wake cycle is comparable between genotypes.

3. EEG POWER, SLEEP PRESSURE IN *SLEEPY6* AND OTHER MOUSE LINES: WHAT CAN IT TELL US?

A mouse model expressing solely in astrocytes a dominant negative SNARE (dnSNARE) transgene – coding for the cytosolic SNARE domain of VAMP2 – was developed; this mutation leads to inhibition of gliotransmission selectively in astrocytes (Pascual et al., 2005).

Gliotransmission, which consists in the release of various neurotransmitters and molecules by astrocytic cells, modulates both neuronal excitability and synaptic transmission (Fellin et al., 2009). It was found that the dnSNARE mice display no obvious changes in sleep/wake architecture and sleep duration, however, an attenuation in sleep pressure build-up was noticed following sleep deprivation (Halassa et al., 2009). The authors proposed that the modulation in the accumulation of sleep need in those mice is mediated via adenosine pathways involving the A1 receptor.

The selective expression of the dnSNARE transgene in astrocytes is currently debated, with a study reporting expression of the transgene in cortical neurons, which could account for many aspects of the dnSNARE mice phenotype (Fujita et al., 2014). However, assuming that the dnSNARE mice indeed express the dominant-negative truncated variant of VAMP2 in astrocytes only, these results – put in perspective with our own – would suggest that the differences we observe in the spectra cannot be solely linked to changes in gliotransmission. Indeed, Halassa et al (2009) found no significant differences in any frequencies of the spectra during baseline recordings, and found only a decrease in the sleep-deprivation induced increase of SWA, especially in the slower band (0.5 – 1.5 Hz). These data therefore go in the opposite direction to our findings. However, the fact that the discrepancies observed, regardless of their direction (increase or decrease), vary depending on the frequency band (slow delta band, upper delta band, frequencies above the delta band) suggest that the mechanisms underlying EEG dynamics may be distinct across frequencies.

The authors went on to show, in another publication, that inhibition of astrocytic gliotransmission directly affected cortical slow-oscillations (Fellin et al., 2009). Strikingly, they found that their mouse model presented with shorter periods of neuronal depolarisation and prolonged hyperpolarisations – just as we see in *Sleepy6* mice. This is even more surprising given that, as mentioned above, the consequences on the EEG spectra of such similar neuronal

firing and slow-wave dynamics are opposite in dnSNARE and *Sleepy6* homozygous mice. The authors propose that such effects are modulated by NMDA receptors on the postsynaptic membranes and by reduced levels of extracellular adenosine which in turn affect A1 receptor-mediated mechanisms. Importantly, this study shows that brain oscillations can be modulated by a combination of neuronal and non-neuronal processes.

4. THE *SLEEPY6* MUTATION, SLEEP AND MEMORY.

A. Exocytosis and cognition

Impairments in vesicular release will probably affect many neurotransmitters and therefore numerous cognitive processes (Ramakrishnan et al., 2012). Additionally, as the dnSNARE mouse model discussed above suggests, the array of phenotypes observed in *Sleepy6* homozygous mice is likely to stem from altered exocytosis not only at the synapse, but also in astrocytic cells, or endocrine cells.

For example, as briefly discussed in Chapter 2, VAMP2 is involved in the release of insulin (Thurmond, 2013), which beyond impairing sleep could also impair memory and learning (Zhao et al., 2004). It was shown that insulin may promote synaptic plasticity and memory function via its action on glutamatergic receptors (NMDA receptors) in the hippocampus; this effect would be mediated by insulin, acting via its receptor to regulate the delivery of new NMDA receptors through SNAP-25 dependent exocytosis (Skeberdis et al., 2001). The role of the SNARE partners of SNAP-25 is not discussed in this study, but it is possible that a mutation in VAMP2 could affect such mechanisms as it commonly binds with SNAP-25. Thus a mutation in *Vamp2* could have an effect on learning and memory via two different routes: its impact on insulin secretion (which has a role in learning via various mechanisms (Zhao et al., 2004)) and

a more direct impact on specific insulin-mediated memory-potentiating mechanisms. This is only one example showing how the change in the amino-acid sequence of VAMP2 may affect sleep and cognitive processes via a multitude of pathways, even those that may seem more remotely related to sleep and memory such as insulin. It also illustrates how disentangling processes affecting cognitive function and sleep is difficult: not only are the basic neuronal mechanisms underlying learning and regulating sleep (such as neuronal excitability and neurotransmitter release) bound to overlap, but the effects of NREMS and REMS on cognition are also extensive. Indeed, sleep stages are characterised by specific neurotransmitter milieus, which in turn play a role in memory processes (Rasch and Born, 2013).

B. The roles of NREMS and REMS in learning and memory and their relevance to the *Sleepy6* line.

As introduced in Chapter 3, it is currently recognised that sleep represents an optimal brain state for memory consolidation, following periods of waking during which neuronal processes are optimal for retrieval of memories and the encoding of new ones (Rasch and Born, 2013). Our understanding of how sleep-mediating memory consolidation occurs is still progressing, but differential roles for NREMS and REMS have been proposed (Ackermann and Rasch, 2014). REMS, in particular, has long been associated with memory consolidation – possibly due to its characteristic EEG trace, reminiscent of that of wake (Rasch and Born, 2013). However, the strong reduction of REMS (for instance following administration of antidepressants such as selective serotonin reuptake inhibitors) does not seem to strongly affect memory formation – and has even been reported to improve skill memory in some instances (Rasch et al., 2009). It would therefore be difficult to predict whether the reduced amount of REMS observed in *Sleepy6* animals leads to any memory impairment. Indeed, the mild learning deficiency observed in

Sleepy6 homozygotes could also be linked to reduced NREMS, or as previously discussed, to an attention deficit – or possibly other mechanisms not suggested here.

A transgenic mouse line with a mutated human tau transgene has strikingly similar sleep abnormalities than the *Sleepy6* mice (Holth et al., 2017). These mice develop a tauopathy with age and display increased wake time, decreased NREMS and REMS time from 11 months of age (decreased REMS time is visible from 9 months of age). They also have a reduced number of both sleep and wake episodes, and an overall decreased EEG power for frequencies spanning from around 0 to 8 Hz. This decreased EEG power has been associated to a decreased cortical volume (Holth et al., 2017). Cortical volume in *Sleepy6* mice has not yet been evaluated; skull size has been shown to be similar to WT littermates (Heise, 2015), but to assess whether there are changes in the volume of some brain areas, a future structural MRI approach has been proposed.

Tauopathies include Alzheimer's disease and patients often display sleep disturbances (Guarnieri et al., 2012), which shows, once more, that sleep phenotypes and learning and memory impairments are often co-occurring. Although it is not always possible to define which of the two is the consequence and which is the cause, it has been proposed that sleep disturbances associated with Alzheimer's disease, for instance, accelerate disease progression by facilitating other disease mechanisms, such as amyloid pathology (Holth et al., 2017).

C. SWA and memory

Evidence suggests that slow waves are one of the mechanisms via which NREMS exerts its beneficial effects on memory consolidation, and in particular declarative memory, and that SWA also allows to 'refresh' brain capacities to be able to encode new information during the following wake episodes possibly by allowing synaptic downscaling (Rasch and Born, 2013) –

see chapter 1 - 1.D. Here again, it is difficult to predict how this could affect memory processes in *Sleepy6* mice: on the one hand, they have less NREMS and show overall decreased SWA levels (as shown, for instance, by the upper asymptote from the modelling work), but on the other hand, they display increased EEG power in very slow frequencies (< 2 Hz) and much longer periods of neuronal silence leading to longer slow waves (see Chapter 4). It may also be worth noting that the overall decrease in EEG power density observed in *Sleepy6* mice may also affect other events, for instance spindles (~10-15 Hz EEG oscillatory activity), and thus the memory and synaptic plasticity mechanisms that have been associated with spindle-activity (Astori et al., 2013).

5. AN IMPAIRMENT OF THE SLEEP SWITCH?

As discussed in Chapter 4, given the more consolidated bouts of wake and sleep (including REMS) that are observed in *Sleepy6* mice, an impairment in the ability of those mice to switch from one vigilance state to the next could be hypothesised.

A. Switching between naturally-occurring vigilance states

As outlined in Chapter 1, several mechanisms for a sleep switch have been proposed, both for a NREMS/wake switch and a REMS switch, where populations of neurons would mutually inhibit each other.

Interestingly, a mouse model obtained with a forward genetic approach displayed decreased REMS time, with REMS sleep episodes lasting for shorter durations. The authors thus named those mice *Dreamless* (*Drl*) and proposed that the mutation present in this new line (a gain-of-function mutation in the sodium leak channel NALCN) led to an increased excitability of REMS-inhibiting neurons. This would be in line with the REMS switch mechanisms discussed above,

whereby an increase in excitability of REMS-inhibiting neurons would destabilise this switch, leading to more frequent REMS => wake/NREMS transitions, and to shorter REMS duration due to the instability of the REMS state, just as is observed in those mice (Figure 71).

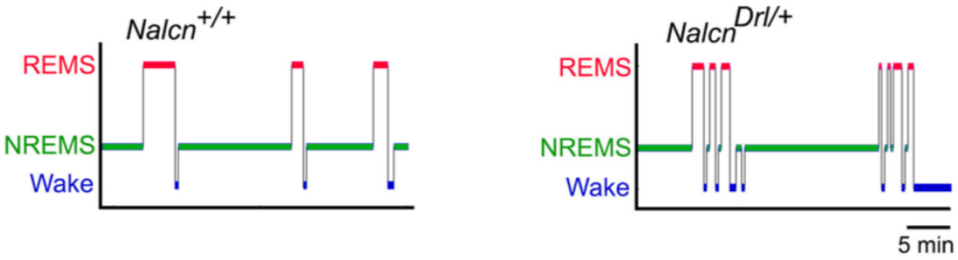


Figure 71: Enlarged hypnogram from a WT (left panel) and a sodium-leak-channel mutant mouse $Nalcn^{Drl/+}$ (right panel) at zeitgeber time 7. This illustrates the frequent transitions between NREMS and REMS occurring in $Nalcn^{Drl/+}$ mice, possibly reflecting an impairment in the REMS/NREMS switch with a decreased stability of the REMS state. Figure adapted from the supplementary materials of Funato et al. (2016).

Another *Sleepy* (*Slp*) mouse line was also developed using a forward genetics approach which exhibited increased NREMS time; the gain-of-function mutation present in these mice affected the *Sik3* gene, and led to a shorter SIK3 protein kinase (Funato et al., 2016). The hypersomnia observed in those mice is more noticeable in the dark phase, and is allele-dosage dependent (i.e. homozygotes for the mutation slept even more than the heterozygotes). The NREMS delta power was increased in those mice, with an exaggerated response to sleep deprivation, suggesting an increased inherent sleep need. However, their response to wake-promoting stimuli (cage change, caffeine, modafinil) was conserved compared to their WT littermates, suggesting no major impairment in arousal mechanisms.

It is interesting to note that these mice have both common and opposite phenotypes as those observed in *Sleepy6* mice: they sleep more when *Sleepy6* mice sleep less, and have an increased response to sleep deprivation, as can be partially observed in *Sleepy6* mice (which are more difficult to keep awake towards the end of the 6-h sleep deprivation period, but which display a

lower SWA rebound). This suggests that if both lines are inherently sleepier than their WT littermates, this does not necessarily lead to increased sleep time, as other mechanisms are involved in regulating sleep/wake architecture. For instance, assuming that sleep is a default state to which animals naturally return to (Hinard et al., 2012; Horne, 2000; Sanchez-Vives and Mattia, 2014; Vyazovskiy, 2015), then the following distinctions between the *Slp* and *Sleepy6* lines could be made:

- in the ***Slp*** mice, as shown by the authors, the ability of the mice to stay awake when exposed to arousal-promoting stimuli is conserved, showing that their ability to be awake should the need arise is not impaired (Funato et al., 2016). But their accumulation of sleep pressure is enhanced leading to longer sleep time when left in undisturbed conditions.
- in the ***Sleepy6*** mice, it seems that as soon as an animal transitions from NREMS to any other state (wake or REMS), then it remains 'locked' in such a state for longer. This could explain why they have such a small number of brief awakening (such 'brief' episodes cannot occur often as anything brief tends to become long in these mice) and why they may be more sleepy despite their seemingly increased drive for wakefulness: they may indeed be unable to switch back to the 'default' sleep state as easily as the WT mice do, and may thus be forced by an impaired sleep switch to remain awake for longer than physiologically relevant. Starting from the sleep switch proposed by Saper et al. (2010) (whereby the ventrolateral and median preoptic nuclei (VLPO & MnPO) send inhibitory projections to wake-promoting regions in the brain, while themselves receiving inhibitory projections from many of these regions), one could hypothesise that the change in amino acid in the VAMP2 protein observed in *Sleepy6* mice affect neurotransmitter release in such a way that either the inhibitory projections from the VLPO and MnPO are weakened, or that the inhibitory projections from wake-promoting

regions to the VLPO/MnPO are strengthened – or both at the same time (Figure 72). Although these neuronal populations resort to various neurotransmitters to communicate (GABA, serotonin, norepinephrine, acetylcholine, glutamate, dopamine, histamine) (Saper et al., 2010), given the widespread role of VAMP2 in synaptic neurotransmitter release, it is possible that it impacts the release of any of those molecules, although it may preferentially inhibit the release of some of them.

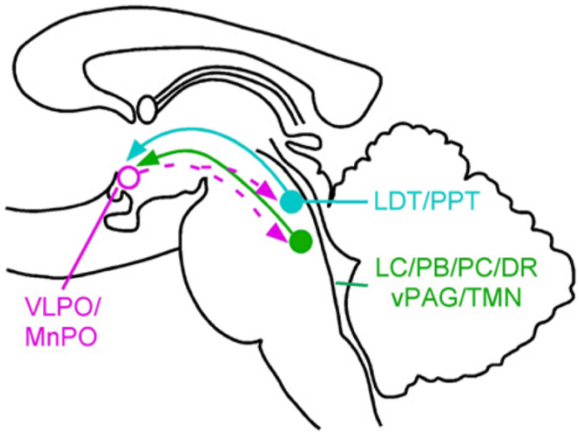


Figure 72: Illustration of a hypothetical impairment in the sleep switch as it could occur in the Sleepy6 mice. Wake-promoting neurons are shown in cyan & green and have inhibitory projections to the sleep-promoting VLPO and MnPO nuclei, which in turn send inhibitory projections to the former. It could be proposed that the wake-promoting projections (full cyan and green lines) are strengthened in Sleepy6 mice and/or that the wake-inhibiting projections (dashed magenta lines) are weakened. DR: dorsal raphe nucleus, LC: locus coeruleus, LDT: laterodorsal tegmental nucleus, MnPO: median preoptic nucleus, PB: parabrachial nucleus, PC: precoeruleus area, PPT: pedunculopontine tegmental nucleus, TMN: tuberomammillary nucleus, VLPO: ventrolateral preoptic nucleus, vPAG: ventral periaqueductal grey. Figure adapted from Saper et al. (2010).

Data from the *Sleepy6* line obtained at University College London by K. Volynski's laboratory showed that vesicular release happens normally when evoked by a train of spikes, while the fusion process is dramatically impaired (10-fold decrease) following a single spike (see Chapter 4). It is therefore possible that as sleep need increases, the probability of action potentials inducing vesicular release at the wake-inhibitory synapses also increases. This would soon allow WT mice to switch back to sleep while in *Sleepy6* mice, falling asleep may require a series

of spikes (rather than a few isolated action potentials) to occur, thus delaying sleep onset. Such a hypothesis would also account for the reduced numbers of NREMS => brief awakenings, REMS => NREMS and NREMS => REMS transitions. The fact that overall the amount of wake is higher than the amount of sleep remains to be fully elucidated but could stem from the fact that – as discussed above and in Chapter 5 – if sleep comes as a default state, the necessity to be awake which arises from external and environmental cues is sufficient for *Sleepy6* Homozygotes to be woken up, while the "necessity" to be asleep can only arise from internal needs, which in the case of the *Sleepy6* mice, may not be regulated optimally.

B. Switching between anaesthesia and wake

The decreased ability of *Sleepy6* homozygotes to switch between different vigilance states does not only apply to naturally occurring states. Indeed, following isoflurane anaesthesia, these mice took over an 1 h to emerge from anaesthesia (as opposed to around 15 minutes in WT mice) and took 4 to 6 h to start behaving normally (bearing in mind post-surgical effects) as opposed to under one hour for the WT mice. Although these are only observations made during post-operative care, and have not yet been fully quantified, differences were systematic (i.e. affected all homozygous mice and none of the WT mice), and striking enough to be significant, had durations been precisely measured.

Studies in *Drosophila* have shown that some 'narrow abdomen' mutants with altered bi-stability between wakefulness and sleep, also displayed increased sensitivity to anaesthesia (Joiner et al., 2013; Krishnan and Nash, 1990). Those mutants present with an altered response to halothane (Krishnan and Nash, 1990) and isoflurane (Joiner et al., 2013): the flies lost consciousness in less time than the WT flies, but were more resistant to the anaesthetic's effects on motor control (Krishnan and Nash, 1990). This is of interest as the *Sleepy6* homozygotes did

not seem to require longer to lose consciousness in the induction chamber, but it was necessary to wait longer and to reach a lower breathing rate (as reported in Chapter 4 – 2.B) for them to lose all traces of pedal or tail-pinch reflexes. It was shown that those narrow abdomen mutant flies have, just as *Sleepy6* mice, altered transitions between wake and anaesthesia, and the authors support the view that the narrow-abdomen gene is one of 4 genes necessary for 'neural inertia'. 'Neural inertia' is the term proposed to describe a 'barrier' that allows the separation and stabilization of vigilance states and prevents rapid and detrimental transitions between states (Joiner et al., 2013). The narrow-abdomen gene would also be needed to allow mutual inhibition between arousal-promoting and arousal-suppressing loci, forming a bistable switch between waking and anesthetized states, similar to the sleep switch (Joiner et al., 2013). And indeed, the mutation in those flies affects the orthologous gene to the one affected in the *Dreamless* mice (NALCN), who show decreased REMS-state stability. A later study went on to show that the mutation affecting the narrow-abdomen flies impacts neuronal excitability and firing rates under the control of the circadian clock, and participated in a 'bicycle model' of membrane excitability (Flourakis et al., 2015). By 'bicycle', the author refers to a mechanism whereby membrane oscillations would be driven by two cycles running with opposite temporal phases. This seems to further support the idea discussed above that switching between states requires tightly-regulated excitatory and inhibitory actions between populations of neurons, that such circadian and sleep homeostatic processes are inter-dependent and that such mechanisms are conserved from flies to mammals. Also, as mutations with similar effects on neural inertia but opposite effects on anaesthesia induction were observed in flies, it was proposed that the genes (and also possibly brain regions) responsible for anaesthesia induction and state stability are distinct (Joiner et al., 2013) – such a hypothesis is in agreement with our findings in the *Sleepy6* mice. Additionally, the same authors proposed that the molecular and anatomical pathways involved in sleep homeostasis also contribute to neural inertia (Joiner et

al., 2013), which could explain how impairments in state switching in *Sleepy6* mice co-exist with altered Process S dynamics and lower SWA levels. Finally, evidence suggests that the reversible loss of consciousness caused by anaesthetics occurs via the arousal and sleep pathways, involving both the thalamus and hypothalamus (Franks, 2008), and that the mechanisms underlying sleep homeostasis and anaesthesia overlap (Pal et al., 2011; Tung et al., 2002). Further characterisation of the *Sleepy6* mice may therefore shed light on the processes that underlie vigilances state stability and transitions.

6. *SLEEPY6* MICE: A GOOD MODEL TO STUDY THE SLEEP HOMEOSTAT?

The overlap between pathways underlying sleep homeostasis and anaesthesia leads back to a more general question: can sleep homeostasis be studied in isolation? Could a mutation in a gene affect sleep homeostasis dynamics and (almost) no other process? The inter-dependence of the circadian and homeostatic processes are not yet fully elucidated (Deboer, 2018), let alone the interdependence of sleep homeostasis and other cognitive or body processes. Therefore, how good a model are *Sleepy6* mice to investigate the genetic basis of the sleep homeostat? Indeed, changes in the dynamics of Process S co-exist in those mice with various behavioural and physiological abnormalities (lower body weight, hyperactivity, absence of some innate behaviours such as nest building, etc.).

Genetic factors influencing sleep – without focusing on the sleep homeostat – have also been investigated. For instance, a study using a quantitative trait loci (QTL) approach found that only a few candidate genomic regions – and only a few genes – may influence the duration and timing of REMS, while no significant association was found for NREMS (Tafti et al., 1997). Strikingly, the findings also reveal that REMS may be regulated by different genetic factors in the light and dark periods (Tafti et al., 1997). The absence of significant associations between genomic

variants and NREMS is surprising, and possibly illustrates the fact that a very large number of genes have an impact on NREMS/wake architecture, and thus sleep homeostasis, making it hard to pin down a few genomic regions only (Winrow et al., 2009).

Surprisingly, only two other forward genetics studies (in addition to the one this thesis is based on) aiming at unravelling the genetic underpinnings of the sleep homeostat have been reported to date: the one discussed earlier from which the *Sleepy* and *Dreamless* mice stem from (Funato et al., 2016), and an earlier study which found a QTL on the mouse chromosome 13 to be associated with the homeostatic regulation of SWA (Franken et al., 2001). The candidate gene proposed was *Homer1a*, a gene known to be involved in synaptic scaling and neuroprotection (Mackiewicz et al., 2008; Mongrain and Franken, 2013). Interestingly, this same QTL study identified another gene (the retinoic-acid receptor beta) determining the contribution of delta oscillations to NREMS EEG and regulating cortical synchrony (Maret et al., 2005). The authors thus concluded that different genes can impact the same variable (here EEG SWA) and that differences in SWA dynamics do not necessarily imply differences in the sleep homeostat itself (Mongrain and Franken, 2013). This makes it all the more difficult to identify genes underlying sleep homeostasis as SWA is the common marker used to assess Process S and thus the sleep homeostat.

It may still be argued that a forward genetics approach can be useful to investigate the genes underlying the sleep homeostat via the detection of new mouse mutants with altered NREMS/wake architecture and/or SWA dynamics. However, it was generally considered that a forward genetics approach using solely non-invasive sleep screens would not allow the identification of REMS phenodeviants. The *Sleepy6* mutant has shown that this is not necessarily true. This line has provided insights into the regulation of REMS, and in possible genes having an impact on the REMS/NREMS switch – if such a switch indeed exists. It is exact, however, that the *Sleepy6* line is not only a model of REMS disturbances, but more generally of vigilance state

switching disturbances, thus leading to alterations in all naturally occurring and drug-induced vigilance states.

7. LIMITATIONS

Beyond the question of whether the *Sleepy6* mouse line is an adequate model to study sleep homeostasis, several additional technical limitations should be highlighted. Firstly, as discussed in Chapter 2, the molecular analysis looking at neurotransmitter levels and pathways would need to be extended to additional neurotransmitters (beyond serotonin and dopamine) and to other genes, using higher throughput methods (such as RNAseq). The behavioural characterisation of the *Sleepy6* line would also benefit from additional tests; although extensive testing had been undertaken prior to this PhD at MRC Harwell (Heise, 2015), those tests mostly characterised general features and behaviours of the mice, and more work could be done to evaluate learning, attention and memory (see Chapter 3 - Discussion). Also, while the behaviour work was performed in both males and females, all EEG and MUA recordings were limited to male mice. Given that differences between males and females were observed in some behaviour tests (Heise, 2015), it may be informative to record EEG and neuronal activity in females too.

Although the circadian phenotype of *Sleepy6* mice was shown to be similar to WT littermates, confirming that no subtle differences exist may be useful. For instance, *Sleepy6* mice tend to fall asleep later after light onset: does that reflect a change in the circadian process or only stems from their reduced sleep time? The modelling approach we used focused on sleep homeostasis dynamics and did not allow us to evaluate changes in Process C (the circadian process). Applying an earlier (and simpler) version of the two-process model (such as the one used by Huber et al. (2000)) to *Sleepy6* data may therefore provide additional insights regarding Process C.

Finally, the striking differences observed in EEG and LFP traces may also stem from changes in brain size (whole brain, or limited to some regions). This would also need to be assessed as if important changes in size occur, interpretation of the data would need to be nuanced. For instance, as mentioned above (4.B), a decrease in EEG amplitude could reflect changes in cortical thickness rather than changes in sleep need.

8. CONCLUSION

To try to understand the genetic basis of sleep homeostasis, we chose a forward genetics approach and characterised the sleep and behavioural phenotype of the *Sleepy6* mouse line. Mice homozygous for the *Sleepy6* mutation affecting the VAMP2 protein, which plays a key role in exocytosis in the brain and throughout the body, showed decreased NREMS and REMS durations as well as impairments in some innate and evoked behaviours, while no major circadian phenotype could be observed. This mouse line therefore appeared as a relevant model to study sleep/wake regulation from a homeostatic perspective.

We started with the hypothesis that those mice may present with changes in the serotonergic pathway, based on previous findings (Müller et al., 2014), as this could explain several of the deviations in phenotype observed in *Sleepy6* homozygotes compared to WT mice. This was tested using molecular techniques and the results obtained did not confirm such a hypothesis, and seemed to reveal that if changes in neurotransmitter levels occurred in those mice, these were either small or affected other neurotransmitters that we did not test.

We then asked whether the decreased sleep time led to cognitive impairments, which we investigated with memory tests. Here again, memory performance was not strikingly dissimilar between genotypes, however, locomotor activity was significantly increased in homozygotes.

This supports the idea that the *Sleepy6* line has a behavioural and neurophysiological phenotype that may be potentially relevant to investigate ADHD.

More importantly, continuous recordings of EEG and neuronal activity – combined with a mathematical modelling approach – revealed striking differences not only in sleep-wake architecture, but also in the neuronal firing patterns and sleep pressure variations. Our findings suggest an impairment in the mice's ability to alternate between vigilance states, as well as in the cellular mechanisms that contribute to the EEG trace, in particular slow-waves. It seems reasonable to consider the sleep homeostat to be tightly linked to the way an animal shifts between vigilance states at the relevant time, and it is widely acknowledged that slow-wave activity is a biomarker of sleep need. We can therefore conclude that our findings contributed to our understanding of how the sleep homeostat can be affected by genetic factors. Future work in these mice is promising in its potential to extend our knowledge of the molecular and cellular mechanisms of the putative sleep-wake switch, and of the function of EEG slow-waves. It may also prove useful to further our understanding of the mode of action of anaesthetics, in particular regarding the overlapping neural pathways between sleep and anesthetised states, both of which lead to a loss of consciousness.

ANNEXES

1. ANNEX 1 – BIOSYNTHESIS AND CATABOLISM PATHWAYS OF SEROTONIN.

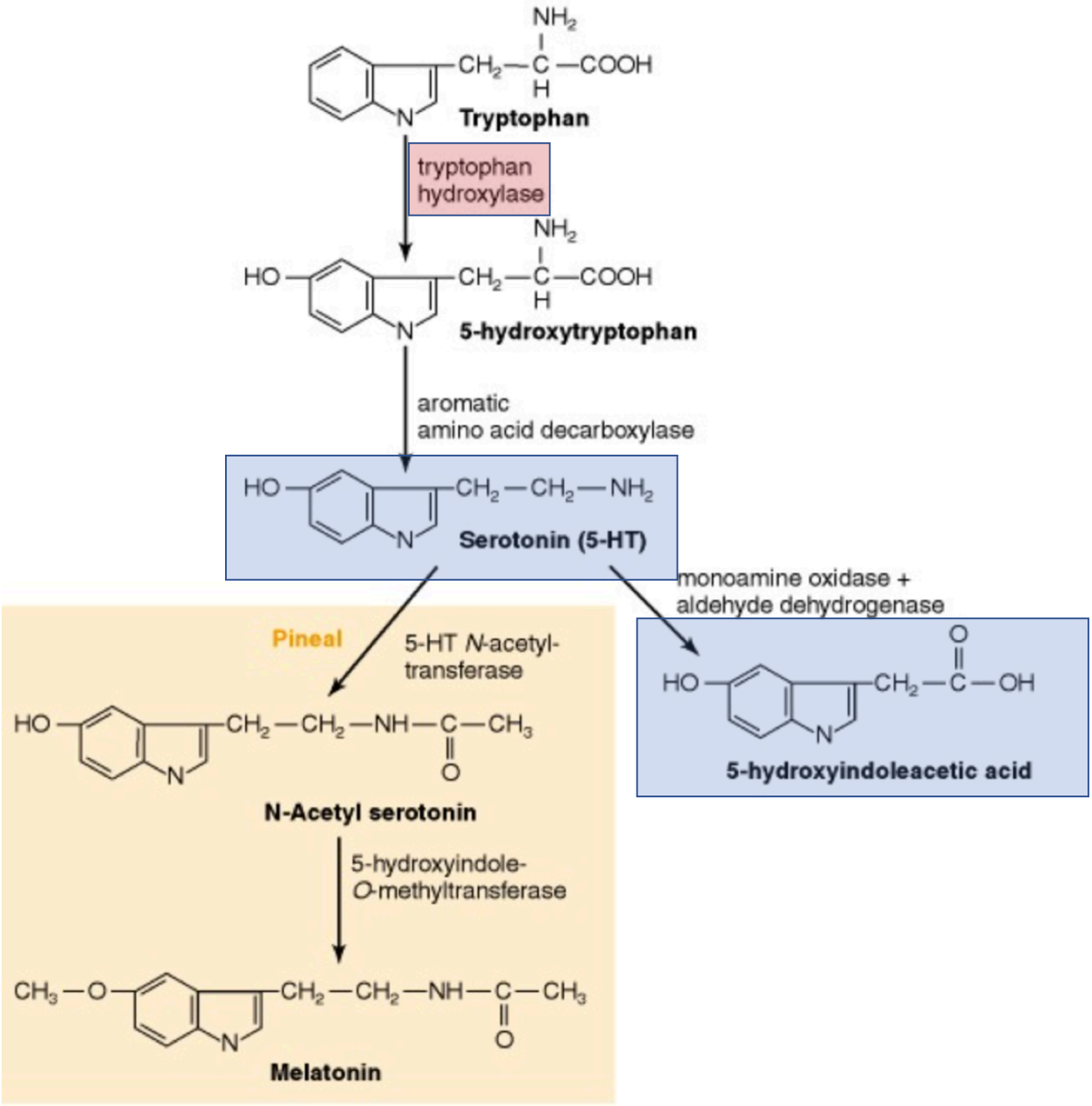


Figure adapted from (Frazer and Hensler, 1999). Serotonin (5-HT) and 5-hydroxyindolacetic acid (5-HIAA) are highlighted in blue. Tryptophan hydroxylase is highlighted in red.

2. ANNEX 2 – BIOSYNTHESIS AND CATABOLISM PATHWAYS OF DOPAMINE

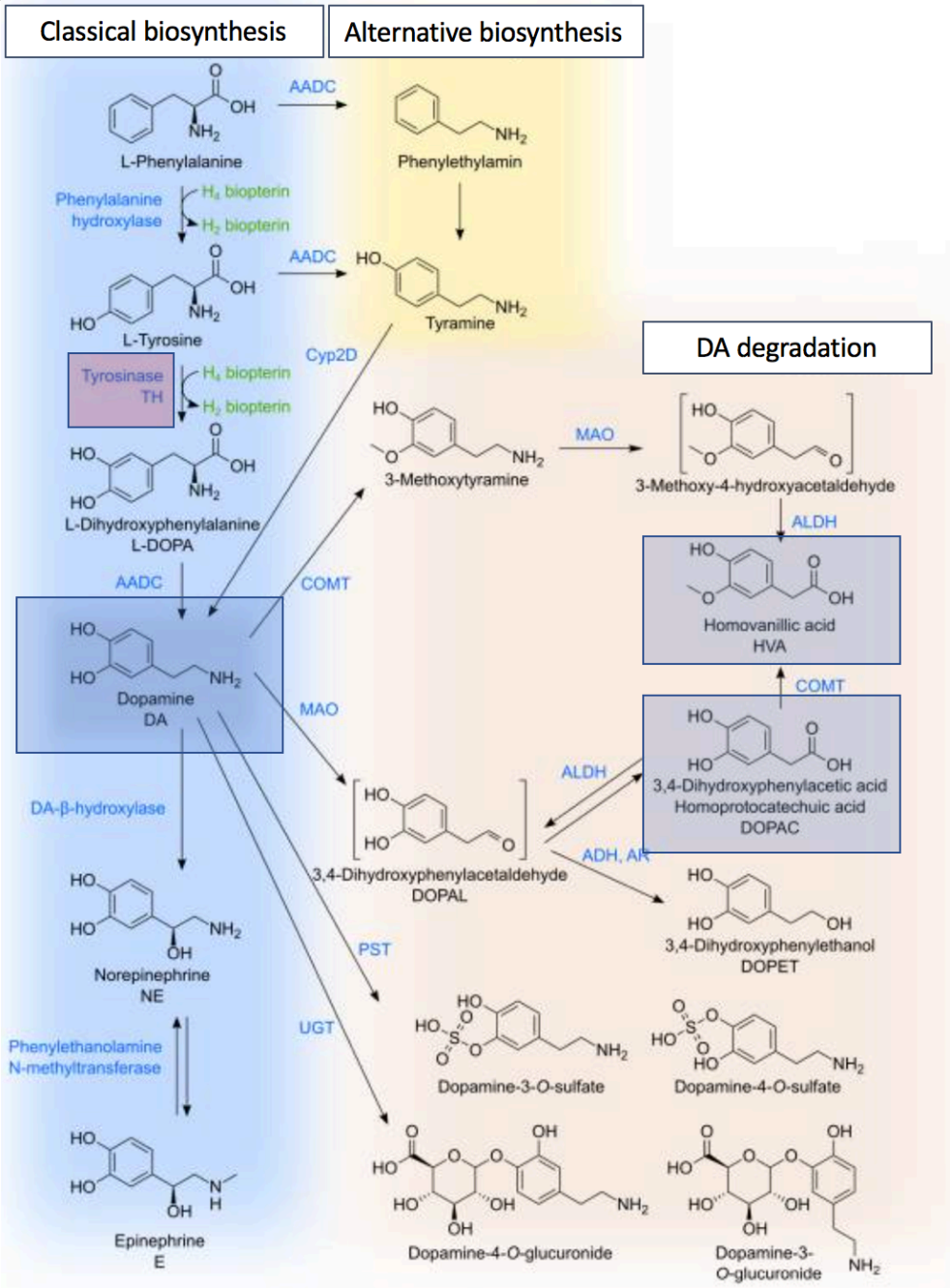


Figure adapted from (Meiser et al., 2013). Dopamine (DA), homovanillic acid (HVA) and 5,4-dihydroxyphenylacetic acid (DOPAC) are highlighted in blue boxes. Tyrosine hydroxylase (TH) is highlighted in red.

REFERENCES

Abbott, N.J., Pizzo, M.E., Preston, J.E., Janigro, D., and Thorne, R.G. (2018). The role of brain barriers in fluid movement in the CNS: is there a "glymphatic" system? Acta Neuropathol. (Berl.) *135*, 387–407.

Abou Jamra, R., Gobina, C.M., Becker, T., Georgi, A., Schulze, T.G., Schmael, C., Cichon, S., Propping, P., Rietschel, M., Nöthen, M.M., et al. (2008). Association study between genetic variants at the VAMP2 and VAMP3 loci and bipolar affective disorder. Psychiatr. Genet. *18*, 199–203.

Acevedo-Arozena, A., Wells, S., Potter, P., Kelly, M., Cox, R.D., and Brown, S.D.M. (2008). ENU mutagenesis, a way forward to understand gene function. Annu. Rev. Genomics Hum. Genet. *9*, 49–69.

Achermann, null, and Borbély, null (1992). Combining different models of sleep regulation. J. Sleep Res. *1*, 144–147.

Achermann, P., and Borbély, A.A. (1990). Simulation of human sleep: ultradian dynamics of electroencephalographic slow-wave activity. J. Biol. Rhythms *5*, 141–157.

Achermann, P., and Borbély, A.A. (1997). Low-frequency (< 1 Hz) oscillations in the human sleep electroencephalogram. Neuroscience *81*, 213–222.

Achermann, P., and Borbély, A.A. (2003). Mathematical models of sleep regulation. Front. Biosci. J. Virtual Libr. *8*, s683-693.

Achermann, P., Dijk, D.J., Brunner, D.P., and Borbély, A.A. (1993). A model of human sleep homeostasis based on EEG slow-wave activity: quantitative comparison of data and simulations. Brain Res. Bull. *31*, 97–113.

Ackermann, S., and Rasch, B. (2014). Differential effects of non-REM and REM sleep on memory consolidation? Curr. Neurol. Neurosci. Rep. *14*, 430.

Adamantidis, A.R., Zhang, F., Aravanis, A.M., Deisseroth, K., and de Lecea, L. (2007). Neural substrates of awakening probed with optogenetic control of hypocretin neurons. Nature *450*, 420–424.

Aeschbach, D., Matthews, J.R., Postolache, T.T., Jackson, M.A., Giesen, H.A., and Wehr, T.A. (1997). Dynamics of the human EEG during prolonged wakefulness: evidence for frequency-specific circadian and homeostatic influences. Neurosci. Lett. *239*, 121–124.

Alhola, P., and Polo-Kantola, P. (2007). Sleep deprivation: Impact on cognitive performance. Neuropsychiatr. Dis. Treat. *3*, 553–567.

Allada, R., and Siegel, J.M. (2008). Unearthing the phylogenetic roots of sleep. Curr. Biol. CB *18*, R670–R679.

Andersen, M.L., Margis, R., Frey, B.N., Giglio, L.M.F., Kapczinski, F., and Tufik, S. (2009). Electrophysiological correlates of sleep disturbance induced by acute and chronic administration of D-amphetamine. Brain Res. *1249*, 162–172.

Antkowiak, B. (2002). In vitro networks: cortical mechanisms of anaesthetic action. BJA Br. J. Anaesth. *89*, 102–111.

Astori, S., Wimmer, R.D., Prosser, H.M., Corti, C., Corsi, M., Liaudet, N., Volterra, A., Franken, P., Adelman, J.P., and Lüthi, A. (2011). The CaV3.3 calcium channel is the major sleep spindle pacemaker in thalamus. Proc. Natl. Acad. Sci. *108*, 13823–13828.

Astori, S., Wimmer, R.D., and Lüthi, A. (2013). Manipulating sleep spindles--expanding views on sleep, memory, and disease. Trends Neurosci. *36*, 738–748.

Ayala-Guerrero, F., and Huitrón-Reséndiz, S. (1991). Sleep patterns in the lizard Ctenosaura pectinata. Physiol. Behav. *49*, 1305–1307.

Bacaj, T., Wu, D., Burré, J., Malenka, R.C., Liu, X., and Südhof, T.C. (2015). Synaptotagmin-1 and -7 Are Redundantly Essential for Maintaining the Capacity of the Readily-Releasable Pool of Synaptic Vesicles. PLOS Biol. *13*, e1002267.

Bacyinski, A., Xu, M., Wang, W., and Hu, J. (2017). The Paravascular Pathway for Brain Waste Clearance: Current Understanding, Significance and Controversy. Front. Neuroanat. *11*, 101.

Baker, R., Gent, T.C., Yang, Q., Parker, S., Vyssotski, A.L., Wisden, W., Brickley, S.G., and Franks, N.P. (2014). Altered activity in the central medial thalamus precedes changes in the neocortex during transitions into both sleep and propofol anesthesia. J. Neurosci. Off. J. Soc. Neurosci. *34*, 13326–13335.

Balcombe, J.P., Barnard, N.D., and Sandusky, C. (2004). Laboratory routines cause animal stress. Contemp. Top. Lab. Anim. Sci. *43*, 42–51.

Bari, A., Dalley, J.W., and Robbins, T.W. (2008). The application of the 5-choice serial reaction time task for the assessment of visual attentional processes and impulse control in rats. Nat. Protoc. *3*, 759–767.

Barker, G.R.I., and Warburton, E.C. (2015). Object-in-Place Associative Recognition Memory Depends on Glutamate Receptor Neurotransmission Within Two Defined Hippocampal-Cortical Circuits: A Critical Role for AMPA and NMDA Receptors in the Hippocampus, Perirhinal, and Prefrontal Cortices. Cereb. Cortex *25*, 472–481.

Basheer, R., Strecker, R.E., Thakkar, M.M., and McCarley, R.W. (2004). Adenosine and sleep-wake regulation. Prog. Neurobiol. *73*, 379–396.

Bathgate, R.A.D., Samuel, C.S., Burazin, T.C.D., Layfield, S., Claasz, A.A., Reytomas, I.G.T., Dawson, N.F., Zhao, C., Bond, C., Summers, R.J., et al. (2002). Human relaxin gene 3 (H3) and the equivalent mouse relaxin (M3) gene. Novel members of the relaxin peptide family. J. Biol. Chem. *277*, 1148–1157.

Baumert, M., Takei, K., Hartinger, J., Burger, P.M., Mollard, G.F. von, Maycox, P.R., Camilli, P.D., and Jahn, R. (1990). P29: a novel tyrosine-phosphorylated membrane protein present in small clear vesicles of neurons and endocrine cells. J. Cell Biol. *110*, 1285–1294.

Beaulieu, I., and Godbout, R. (2000). Spatial learning on the Morris Water Maze Test after a short-term paradoxical sleep deprivation in the rat. Brain Cogn. *43*, 27–31.

Bedont, J.L., and Blackshaw, S. (2015). Constructing the suprachiasmatic nucleus: a watchmaker's perspective on the central clockworks. Front. Syst. Neurosci. *9*, 74.

Beersma, D.G. (1998). Models of human sleep regulation. Sleep Med. Rev. *2*, 31–43.

Benagiano, V., Lorusso, L., Flace, P., Girolamo, F., Rizzi, A., Bosco, L., Cagiano, R., Nico, B., Ribatti, D., and Ambrosi, G. (2011). VAMP-2, SNAP-25A/B and syntaxin-1 in glutamatergic and GABAergic synapses of the rat cerebellar cortex. BMC Neurosci. *12*, 118.

Bengel, D., Jöhren, O., Andrews, A.M., Heils, A., Mössner, R., Sanvitto, G.L., Saavedra, J.M., Lesch, K.P., and Murphy, D.L. (1997). Cellular localization and expression of the serotonin transporter in mouse brain. Brain Res. *778*, 338–345.

Benington, J.H., and Heller, H.C. (1995). Restoration of brain energy metabolism as the function of sleep. Prog. Neurobiol. *45*, 347–360.

Berridge, C.W., and Waterhouse, B.D. (2003). The locus coeruleus-noradrenergic system: modulation of behavioral state and state-dependent cognitive processes. Brain Res. Brain Res. Rev. *42*, 33–84.

Berridge, C.W., Schmeichel, B.E., and España, R.A. (2012). Noradrenergic Modulation of Wakefulness/Arousal. Sleep Med. Rev. *16*, 187–197.

Bjorness, T.E., and Greene, R.W. (2009). Adenosine and Sleep. Curr. Neuropharmacol. *7*, 238–245.

Blanco-Centurion, C., Xu, M., Murillo-Rodriguez, E., Gerashchenko, D., Shiromani, A.M., Salin-Pascual, R.J., Hof, P.R., and Shiromani, P.J. (2006). Adenosine and sleep homeostasis in the Basal forebrain. J. Neurosci. Off. J. Soc. Neurosci. *26*, 8092–8100.

Bodyak, N., and Slotnick, B. (1999). Performance of Mice in an Automated Olfactometer: Odor Detection, Discrimination and Odor Memory. Chem. Senses *24*, 637–645.

Bonvicini, C., Faraone, S.V., and Scassellati, C. (2016). Attention-deficit hyperactivity disorder in adults: A systematic review and meta-analysis of genetic, pharmacogenetic and biochemical studies. Mol. Psychiatry *21*, 872–884.

Borbély, A.A. (1982). A two process model of sleep regulation. Hum. Neurobiol. *1*, 195–204.

Borbély, A.A., and Achermann, P. (1999). Sleep homeostasis and models of sleep regulation. J. Biol. Rhythms *14*, 557–568.

Borbély, A.A., and Neuhaus, H.U. (1979a). Sleep-deprivation: Effects on sleep and EEG in the rat. J. Comp. Physiol. *133*, 71–87.

Borbély, A.A., and Neuhaus, H.U. (1979b). Sleep-deprivation: Effect on sleep and EEG in the rat. J. Comp. Physiol. 71–87.

Borbély, A.A., Baumann, F., Brandeis, D., Strauch, I., and Lehmann, D. (1981). Sleep deprivation: effect on sleep stages and EEG power density in man. Electroencephalogr. Clin. Neurophysiol. *51*, 483–495.

Borbély, A.A., Achermann, P., Trachsel, L., and Tobler, I. (1989). Sleep initiation and initial sleep intensity: interactions of homeostatic and circadian mechanisms. J. Biol. Rhythms *4*, 149–160.

Borbély, A.A., Daan, S., Wirz-Justice, A., and Deboer, T. (2016). The two-process model of sleep regulation: a reappraisal. J. Sleep Res. *25*, 131–143.

Boutrel, B., and Koob, G.F. (2004). What keeps us awake: the neuropharmacology of stimulants and wakefulness-promoting medications. Sleep *27*, 1181–1194.

Boyce, R., Glasgow, S.D., Williams, S., and Adamantidis, A. (2016). Causal evidence for the role of REM sleep theta rhythm in contextual memory consolidation. Science *352*, 812–816.

Brown, R.E. (2016). Dopaminergic Transmission and Wake-Promoting Effects of Central Nervous System Stimulants. In Dopamine and Sleep, (Springer, Cham), pp. 19–37.

Brown, T.M., and Piggins, H.D. (2007). Electrophysiology of the suprachiasmatic circadian clock. Prog. Neurobiol. *82*, 229–255.

Brown, R.E., Basheer, R., McKenna, J.T., Strecker, R.E., and McCarley, R.W. (2012). CONTROL OF SLEEP AND WAKEFULNESS. Physiol. Rev. *92*, 1087–1187.

Bryant, P.A., Trinder, J., and Curtis, N. (2004). Sick and tired: Does sleep have a vital role in the immune system? Nat. Rev. Immunol. *4*, 457–467.

Buchsbaum, M.S., Gillin, J.C., Wu, J., Hazlett, E., Sicotte, N., Dupont, R.M., and Bunney, W.E. (1989). Regional cerebral glucose metabolic rate in human sleep assessed by positron emission tomography. Life Sci. *45*, 1349–1356.

Buhr, E.D., and Takahashi, J.S. (2013). Molecular components of the Mammalian circadian clock. Handb. Exp. Pharmacol. 3–27.

Buhr, E.D., Yoo, S.-H., and Takahashi, J.S. (2010). Temperature as a universal resetting cue for mammalian circadian oscillators. Science *330*, 379–385.

Buitelaar, J.K., Kan, C.C., and Asherson, P. (2011). ADHD in Adults: Characterization, Diagnosis, and Treatment (Cambridge University Press).

Bushnell, P.J. (1998). Behavioral approaches to the assessment of attention in animals. Psychopharmacology (Berl.) *138*, 231–259.

Buzsáki, G. (2002). Theta oscillations in the hippocampus. Neuron *33*, 325–340.

Buzsaki, G. (2011). Rhythms of the Brain (Oxford, New York: Oxford University Press).

Buzsáki, G., and Draguhn, A. (2004). Neuronal oscillations in cortical networks. Science *304*, 1926–1929.

Cairney, S.A., Durrant, S.J., Power, R., and Lewis, P.A. (2015). Complementary Roles of Slow-Wave Sleep and Rapid Eye Movement Sleep in Emotional Memory Consolidation. Cereb. Cortex *25*, 1565–1575.

Cajochen, C., Khala, S.B.S., Czeisler, C.A., and Dijk, D.J. (1998). Course of EEG power density during wakefulness and subjective sleepiness during a 24-h constant routine. *21(Suppl)*, 243.

Cajochen, C., Wyatt, J.K., Czeisler, C.A., and Dijk, D.J. (2002). Separation of circadian and wake duration-dependent modulation of EEG activation during wakefulness. Neuroscience *114*, 1047–1060.

Calais, J.B., Ojopi, E.B., Morya, E., Sameshima, K., and Ribeiro, S. (2015). Experience-dependent upregulation of multiple plasticity factors in the hippocampus during early REM sleep. Neurobiol. Learn. Mem. *122*, 19–27.

Calvet, J., Fourment, A., and Thiefry, M. (1973). Electrical activity in neocortical projection and association areas during slow wave sleep. Brain Res. *52*, 173–187.

Camacho-Arroyo, I., Alvarado, R., Manjarrez, J., and Tapia, R. (1991). Microinjections of muscimol and bicuculline into the pontine reticular formation modify the sleep-waking cycle in the rat. Neurosci. Lett. *129*, 95–97.

Cantor, R.S. (2015). The evolutionary origin of the need to sleep: an inevitable consequence of synaptic neurotransmission? Front. Synaptic Neurosci. *7*, 15.

Carter, M.E., Adamantidis, A., Ohtsu, H., Deisseroth, K., and de Lecea, L. (2009). Sleep homeostasis modulates hypocretin-mediated sleep-to-wake transitions. J. Neurosci. Off. J. Soc. Neurosci. *29*, 10939–10949.

Cassoff, J., Wiebe, S.T., and Gruber, R. (2012). Sleep patterns and the risk for ADHD: a review. Nat. Sci. Sleep *4*, 73–80.

Cedernaes, J., Rångtell, F.H., Axelsson, E.K., Yeganeh, A., Vogel, H., Broman, J.-E., Dickson, S.L., Schiöth, H.B., and Benedict, C. (2015). Short Sleep Makes Declarative Memories Vulnerable to Stress in Humans. Sleep *38*, 1861–1868.

Chefer, V.I., Thompson, A.C., Zapata, A., and Shippenberg, T.S. (2009). Overview of Brain Microdialysis. Curr. Protoc. Neurosci. Editor. Board Jacqueline N Crawley Al *CHAPTER*, Unit7.1.

Chemelli, R.M., Willie, J.T., Sinton, C.M., Elmquist, J.K., Scammell, T., Lee, C., Richardson, J.A., Williams, S.C., Xiong, Y., Kisanuki, Y., et al. (1999). Narcolepsy in orexin knockout mice: molecular genetics of sleep regulation. Cell *98*, 437–451.

Chen, G.-L., and Miller, G.M. (2012). Advances in tryptophan hydroxylase-2 gene expression regulation: new insights into serotonin-stress interaction and clinical implications. Am. J. Med. Genet. Part B Neuropsychiatr. Genet. Off. Publ. Int. Soc. Psychiatr. Genet. *159B*, 152–171.

Chen, Y.A., and Scheller, R.H. (2001). SNARE-mediated membrane fusion. Nat. Rev. Mol. Cell Biol. *2*, 98–106.

Chen, Y., Palm, F., Lesch, K.-P., Gerlach, M., Moessner, R., and Sommer, C. (2011). 5-hydroxyindolacetic acid (5-HIAA), a main metabolite of serotonin, is responsible for complete Freund's adjuvant-induced thermal hyperalgesia in mice. Mol. Pain *7*, 21.

Chou, T.C., Scammell, T.E., Gooley, J.J., Gaus, S.E., Saper, C.B., and Lu, J. (2003). Critical role of dorsomedial hypothalamic nucleus in a wide range of behavioral circadian rhythms. J. Neurosci. Off. J. Soc. Neurosci. *23*, 10691–10702.

Cirelli, C. (2017). Sleep, synaptic homeostasis and neuronal firing rates. Curr. Opin. Neurobiol. *44*, 72–79.

Colwell, C.S. (2011). Linking neural activity and molecular oscillations in the SCN. Nat. Rev. Neurosci. *12*, 553–569.

Colwell, C.S., and Michel, S. (2003). Sleep and circadian rhythms: do sleep centers talk back to the clock? Nat. Neurosci. *6*, 1005–1006.

Contreras, D., and Steriade, M. (1995). Cellular basis of EEG slow rhythms: a study of dynamic corticothalamic relationships. J. Neurosci. Off. J. Soc. Neurosci. *15*, 604–622.

Cooper, J.R., Bloom, F.E., and Roth, R.H. (1996). The Biochemical Basis of Neuropharmacology (Oxford University Press).

Cui, N., Mckillop, L.E., Fisher, S.P., Oliver, P.L., and Vyazovskiy, V.V. (2014). Long-term history and immediate preceding state affect EEG slow wave characteristics at NREM sleep onset in C57BL/6 mice. Arch. Ital. Biol. *152*, 156–168.

Cupertino, R.B., Kappel, D.B., Bandeira, C.E., Schuch, J.B., da Silva, B.S., Müller, D., Bau, C.H.D., and Mota, N.R. (2016). SNARE complex in developmental psychiatry: neurotransmitter exocytosis and beyond. J. Neural Transm. Vienna Austria 1996 *123*, 867–883.

Cupertino, R.B., Schuch, J.B., Bandeira, C.E., da Silva, B.S., Rovaris, D.L., Kappel, D.B., Contini, V., Salatino-Oliveira, A., Vitola, E.S., Karam, R.G., et al. (2017). Replicated association of Synaptotagmin (SYT1) with ADHD and its broader influence in externalizing behaviors. Eur. Neuropsychopharmacol. J. Eur. Coll. Neuropsychopharmacol. *27*, 239–247.

Curatolo, P., D'Agati, E., and Moavero, R. (2010). The neurobiological basis of ADHD. Ital. J. Pediatr. *36*, 79.

Curtis, A.M., Bellet, M.M., Sassone-Corsi, P., and O'Neill, L.A.J. (2014). Circadian clock proteins and immunity. Immunity *40*, 178–186.

Czerniawski, J., Ree, F., Chia, C., Ramamoorthi, K., Kumata, Y., and Otto, T.A. (2011). The importance of having Arc: expression of the immediate-early gene Arc is required for hippocampus-dependent fear conditioning and blocked by NMDA receptor antagonism. J. Neurosci. Off. J. Soc. Neurosci. *31*, 11200–11207.

Daan, S., Beersma, D.G., and Borbély, A.A. (1984). Timing of human sleep: recovery process gated by a circadian pacemaker. Am. J. Physiol. *246*, R161-183.

Daubner, S.C., Le, T., and Wang, S. (2011). Tyrosine Hydroxylase and Regulation of Dopamine Synthesis. Arch. Biochem. Biophys. *508*, 1–12.

Deboer, T. (1998). Brain temperature dependent changes in the electroencephalogram power spectrum of humans and animals. J. Sleep Res. *7*, 254–262.

Deboer, T. (2002). Electroencephalogram theta frequency changes in parallel with euthermic brain temperature. Brain Res. *930*, 212–215.

Deboer, T. (2009). Sleep and sleep homeostasis in constant darkness in the rat. J. Sleep Res. *18*, 357–364.

Deboer, T. (2018). Sleep homeostasis and the circadian clock: Do the circadian pacemaker and the sleep homeostat influence each other's functioning? Neurobiol. Sleep Circadian Rhythms *5*, 68–77.

Dhara, M., Yarzagaray, A., Makke, M., Schindeldecker, B., Schwarz, Y., Shaaban, A., Sharma, S., Böckmann, R.A., Lindau, M., Mohrmann, R., et al. (2016). v-SNARE transmembrane domains function as catalysts for vesicle fusion. ELife *5*.

Diekelmann, S., and Born, J. (2010). The memory function of sleep. Nat. Rev. Neurosci. *11*, 114.

Dijk, D.J., and Czeisler, C.A. (1995). Contribution of the circadian pacemaker and the sleep homeostat to sleep propensity, sleep structure, electroencephalographic slow waves, and sleep spindle activity in humans. J. Neurosci. Off. J. Soc. Neurosci. *15*, 3526–3538.

Dijk, D.J., Beersma, D.G., and Daan, S. (1987). EEG power density during nap sleep: reflection of an hourglass measuring the duration of prior wakefulness. J. Biol. Rhythms *2*, 207–219.

Dijk, D.J., Brunner, D.P., Beersma, D.G., and Borbély, A.A. (1990). Electroencephalogram power density and slow wave sleep as a function of prior waking and circadian phase. Sleep *13*, 430–440.

Do, O.H., Low, J.T., Gaisano, H.Y., and Thorn, P. (2014). The secretory deficit in islets from db/db mice is mainly due to a loss of responding beta cells. Diabetologia *57*, 1400–1409.

Donlea, J.M., Pimentel, D., and Miesenböck, G. (2014). Neuronal machinery of sleep homeostasis in Drosophila. Neuron *81*, 860–872.

Dworak, M., McCarley, R.W., Kim, T., Kalinchuk, A.V., and Basheer, R. (2010). Sleep and Brain Energy Levels: ATP changes during sleep. J. Neurosci. Off. J. Soc. Neurosci. *30*, 9007–9016.

Edgar, D.M., Kilduff, T.S., Martin, C.E., and Dement, W.C. (1991). Influence of running wheel activity on free-running sleep/wake and drinking circadian rhythms in mice. Physiol. Behav. *50*, 373–378.

Endo, T., Schwierin, B., Borbély, A.A., and Tobler, I. (1997). Selective and total sleep deprivation: effect on the sleep EEG in the rat. Psychiatry Res. *66*, 97–110.

Engert, V., and Pruessner, J.C. (2008). Dopaminergic and Noradrenergic Contributions to Functionality in ADHD: The Role of Methylphenidate. Curr. Neuropharmacol. *6*, 322–328.

Ennaceur, A., and Delacour, J. (1988). A new one-trial test for neurobiological studies of memory in rats. 1: Behavioral data. Behav. Brain Res. *31*, 47–59.

Favor, J. (1998). The mutagenic activity of ethylnitrosourea at low doses in spermatogonia of the mouse as assessed by the specific-locus test. Mutat. Res. Mol. Mech. Mutagen. *405*, 221–226.

Fellin, T., Halassa, M.M., Terunuma, M., Succol, F., Takano, H., Frank, M., Moss, S.J., and Haydon, P.G. (2009). Endogenous nonneuronal modulators of synaptic transmission control cortical slow oscillations in vivo. Proc. Natl. Acad. Sci. U. S. A. *106*, 15037–15042.

Finelli, L.A., Baumann, H., Borbély, A.A., and Achermann, P. (2000). Dual electroencephalogram markers of human sleep homeostasis: correlation between theta activity in waking and slow-wave activity in sleep. Neuroscience *101*, 523–529.

Fisher, H., and Braun, J.E. (2000). Modulation of the SNARE core complex by dopamine. Can. J. Physiol. Pharmacol. *78*, 856–859.

Fisher, S.P., Foster, R.G., and Peirson, S.N. (2013). The circadian control of sleep. Handb. Exp. Pharmacol. 157–183.

Fisher, S.P., Guillaumin, M.C.C., and Vyazovskiy, V.V. (2016a). Unravelling the complexity of sleep. PHENOTYPE Neurosci. *Supplement to issue 23*, 5–7.

Fisher, S.P., Cui, N., McKillop, L.E., Gemignani, J., Bannerman, D.M., Oliver, P.L., Peirson, S.N., and Vyazovskiy, V.V. (2016b). Stereotypic wheel running decreases cortical activity in mice. Nat. Commun. *7*, 13138.

Flanigan, W.F. (1973). Sleep and wakefulness in iguanid lizards, Ctenosaura pectinata and Iguana iguana. Brain. Behav. Evol. *8*, 401–436.

Flint, R.R., Chang, T., Lydic, R., and Baghdoyan, H.A. (2010). GABAA receptors in the pontine reticular formation of C57BL/6J mouse modulate neurochemical, electrographic, and behavioral phenotypes of wakefulness. J. Neurosci. Off. J. Soc. Neurosci. *30*, 12301–12309.

Flourakis, M., Kula-Eversole, E., Hutchison, A.L., Han, T.H., Aranda, K., Moose, D.L., White, K.P., Dinner, A.R., Lear, B.C., Ren, D., et al. (2015). A Conserved Bicycle Model for Circadian Clock Control of Membrane Excitability. Cell *162*, 836–848.

Folkard, S., and Åkerstedt, T. (1991). A three process model of the regulation of alertness and sleepiness Sleep arousal and performance. Probl. Promises 11–26.

Fon, E.A., and Edwards, R.H. (2001). Molecular mechanisms of neurotransmitter release. Muscle Nerve *24*, 581–601.

Forssberg, H., Fernell, E., Waters, S., Waters, N., and Tedroff, J. (2006). Altered pattern of brain dopamine synthesis in male adolescents with attention deficit hyperactivity disorder. Behav. Brain Funct. *2*, 40.

Foster, R.G. (1998). Shedding light on the biological clock. Neuron *20*, 829–832.

Foster, R.G., and Wulff, K. (2005). The rhythm of rest and excess. Nat. Rev. Neurosci. *6*, 407–414.

Franken, P., and Dijk, D.-J. (2009). Circadian clock genes and sleep homeostasis. Eur. J. Neurosci. *29*, 1820–1829.

Franken, P., Tobler, I., and Borbély, A.A. (1991). Sleep homeostasis in the rat: simulation of the time course of EEG slow-wave activity. Neurosci. Lett. *130*, 141–144.

Franken, P., Chollet, D., and Tafti, M. (2001). The homeostatic regulation of sleep need is under genetic control. J. Neurosci. Off. J. Soc. Neurosci. *21*, 2610–2621.

Franks, N.P. (2008). General anaesthesia: from molecular targets to neuronal pathways of sleep and arousal. Nat. Rev. Neurosci. *9*, 370–386.

Frazer, A., and Hensler, J.G. (1999). Serotonin. Basic Neurochem. Mol. Cell. Med. Asp. 6th Ed.

Fuentealba, P., and Steriade, M. (2005). The reticular nucleus revisited: intrinsic and network properties of a thalamic pacemaker. Prog. Neurobiol. *75*, 125–141.

Fujita, T., Chen, M.J., Li, B., Smith, N.A., Peng, W., Sun, W., Toner, M.J., Kress, B.T., Wang, L., Benraiss, A., et al. (2014). Neuronal transgene expression in dominant-negative SNARE mice. J. Neurosci. Off. J. Soc. Neurosci. *34*, 16594–16604.

Fuller, P.M., Gooley, J.J., and Saper, C.B. (2006). Neurobiology of the Sleep-Wake Cycle: Sleep Architecture, Circadian Regulation, and Regulatory Feedback. J. Biol. Rhythms *21*, 482–493.

Fuller, P.M., Fuller, P., Sherman, D., Pedersen, N.P., Saper, C.B., and Lu, J. (2011). Reassessment of the structural basis of the ascending arousal system. J. Comp. Neurol. *519*, 933–956.

Funato, H., Miyoshi, C., Fujiyama, T., Kanda, T., Sato, M., Wang, Z., Ma, J., Nakane, S., Tomita, J., Ikkyu, A., et al. (2016). Forward-genetics analysis of sleep in randomly mutagenized mice. Nature *advance online publication*.

Gallopin, T., Luppi, P.-H., Cauli, B., Urade, Y., Rossier, J., Hayaishi, O., Lambolez, B., and Fort, P. (2005). The endogenous somnogen adenosine excites a subset of sleep-promoting neurons via A2A receptors in the ventrolateral preoptic nucleus. Neuroscience *134*, 1377–1390.

Gao, Q., Liu, L., Chen, Y., Li, H., Yang, L., Wang, Y., and Qian, Q. (2015). Synaptosome-related (SNARE) genes and their interactions contribute to the susceptibility and working memory of attention-deficit/hyperactivity disorder in males. Prog. Neuropsychopharmacol. Biol. Psychiatry *57*, 132–139.

Gerashchenko, D., Wisor, J.P., Burns, D., Reh, R.K., Shiromani, P.J., Sakurai, T., Iglesia, H.O. de la, and Kilduff, T.S. (2008). Identification of a population of sleep-active cerebral cortex neurons. Proc. Natl. Acad. Sci. *105*, 10227–10232.

Girardeau, G., Benchenane, K., Wiener, S.I., Buzsáki, G., and Zugaro, M.B. (2009). Selective suppression of hippocampal ripples impairs spatial memory. Nat. Neurosci. *12*, 1222–1223.

Glenn, L.L., and Steriade, M. (1982). Discharge rate and excitability of cortically projecting intralaminar thalamic neurons during waking and sleep states. J. Neurosci. Off. J. Soc. Neurosci. *2*, 1387–1404.

Golan, N., Shahar, E., Ravid, S., and Pillar, G. (2004). Sleep disorders and daytime sleepiness in children with attention-deficit/hyperactive disorder. Sleep *27*, 261–266.

Gong, H., McGinty, D., Guzman-Marin, R., Chew, K.-T., Stewart, D., and Szymusiak, R. (2004). Activation of c-fos in GABAergic neurones in the preoptic area during sleep and in response to sleep deprivation. J. Physiol. *556*, 935–946.

Gottesmann, C. (1996). The transition from slow-wave sleep to paradoxical sleep: evolving facts and concepts of the neurophysiological processes underlying the intermediate stage of sleep. Neurosci. Biobehav. Rev. *20*, 367–387.

Gottesmann, C. (2011). The Involvement of Noradrenaline in Rapid Eye Movement Sleep Mentation. Front. Neurol. *2*.

Guarnieri, B., Adorni, F., Musicco, M., Appollonio, I., Bonanni, E., Caffarra, P., Caltagirone, C., Cerroni, G., Concari, L., Cosentino, F.I.I., et al. (2012). Prevalence of sleep disturbances in mild cognitive impairment and dementing disorders: a multicenter Italian clinical cross-sectional study on 431 patients. Dement. Geriatr. Cogn. Disord. *33*, 50–58.

Guillaumin, M.C.C., McKillop, L.E., Cui, N., Fisher, S.P., Foster, R.G., de Vos, M., Peirson, S.N., Achermann, P., and Vyazovskiy, V.V. (2018). Cortical region–specific sleep homeostasis in mice: effects of time of day and waking experience. Sleep.

Gutknecht, L., Kriegebaum, C., Waider, J., Schmitt, A., and Lesch, K.-P. (2009). Spatio-temporal expression of tryptophan hydroxylase isoforms in murine and human brain: convergent data from Tph2 knockout mice. Eur. Neuropsychopharmacol. J. Eur. Coll. Neuropsychopharmacol. *19*, 266–282.

Guzowski, J.F., Lyford, G.L., Stevenson, G.D., Houston, F.P., McGaugh, J.L., Worley, P.F., and Barnes, C.A. (2000). Inhibition of Activity-Dependent Arc Protein Expression in the Rat Hippocampus Impairs the Maintenance of Long-Term Potentiation and the Consolidation of Long-Term Memory. J. Neurosci. *20*, 3993–4001.

Halassa, M.M., Florian, C., Fellin, T., Munoz, J.R., Lee, S.-Y., Abel, T., Haydon, P.G., and Frank, M.G. (2009). Astrocytic modulation of sleep homeostasis and cognitive consequences of sleep loss. Neuron *61*, 213–219.

Hambrecht-Wiedbusch, V.S., Mitchell, M.F., Firn, K.A., Baghdoyan, H.A., and Lydic, R. (2014). Benzodiazepine Site Agonists Differentially Alter Acetylcholine Release in Rat Amygdala. Anesth. Analg. *118*, 1293–1300.

Hankins, M.W., Peirson, S.N., and Foster, R.G. (2008). Melanopsin: an exciting photopigment. Trends Neurosci. *31*, 27–36.

Hars, B., and Hennevin, E. (1983). Reminder abolishes impairment of learning induced by paradoxical sleep retardation. Physiol. Behav. *30*, 831–836.

Hassani, O.K., Lee, M.G., Henny, P., and Jones, B.E. (2009a). Discharge profiles of identified GABAergic in comparison to cholinergic and putative glutamatergic basal forebrain neurons across the sleep-wake cycle. J. Neurosci. Off. J. Soc. Neurosci. *29*, 11828–11840.

Hassani, O.K., Lee, M.G., and Jones, B.E. (2009b). Melanin-concentrating hormone neurons discharge in a reciprocal manner to orexin neurons across the sleep-wake cycle. Proc. Natl. Acad. Sci. U. S. A. *106*, 2418–2422.

Hastoy, B., Scotti, P.A., Milochau, A., Fezoua-Boubegtiten, Z., Rodas, J., Megret, R., Desbat, B., Laguerre, M., Castano, S., Perrais, D., et al. (2017). A Central Small Amino Acid in the VAMP2 Transmembrane Domain Regulates the Fusion Pore in Exocytosis. Sci. Rep. *7*, 2835.

Hayashi, Y., Kashiwagi, M., Yasuda, K., Ando, R., Kanuka, M., Sakai, K., and Itohara, S. (2015). Cells of a common developmental origin regulate REM/non-REM sleep and wakefulness in mice. Science *350*, 957–961.

Heise, I.R. (2015). Characterisation of ENU induced mutations affecting sleep/wake behaviour in mice. PhD thesis. Mammalian Genetics Unit - Medical Research Council Harwell - The Open University.

Heroux, N.A., Osborne, B.F., Miller, L.A., Kawan, M., Buban, K.N., Rosen, J.B., and Stanton, M.E. (2018). Differential expression of the immediate early genes c-Fos, Arc, Egr-1, and Npas4 during long-term memory formation in the context preexposure facilitation effect (CPFE). Neurobiol. Learn. Mem. *147*, 128–138.

Herring, B.E., Xie, Z., Marks, J., and Fox, A.P. (2009). Isoflurane inhibits the neurotransmitter release machinery. J. Neurophysiol. *102*, 1265–1273.

Herring, B.E., McMillan, K., Pike, C.M., Marks, J., Fox, A.P., and Xie, Z. (2011). Etomidate and propofol inhibit the neurotransmitter release machinery at different sites. J. Physiol. *589*, 1103–1115.

Hess, E.J., Jinnah, H.A., Kozak, C.A., and Wilson, M.C. (1992). Spontaneous locomotor hyperactivity in a mouse mutant with a deletion including the Snap gene on chromosome 2. J. Neurosci. Off. J. Soc. Neurosci. *12*, 2865–2874.

Hinard, V., Mikhail, C., Pradervand, S., Curie, T., Houtkooper, R.H., Auwerx, J., Franken, P., and Tafti, M. (2012). Key electrophysiological, molecular, and metabolic signatures of sleep and wakefulness revealed in primary cortical cultures. J. Neurosci. Off. J. Soc. Neurosci. *32*, 12506–12517.

Hobson, J.A., Goin, O.B., and Goin, C.J. (1968). Electrographic correlates of behaviour in tree frogs. Nature *220*, 386–387.

Holland, P.M., Abramson, R.D., Watson, R., and Gelfand, D.H. (1991). Detection of specific polymerase chain reaction product by utilizing the 5'----3' exonuclease activity of Thermus aquaticus DNA polymerase. Proc. Natl. Acad. Sci. U. S. A. *88*, 7276–7280.

Holth, J.K., Mahan, T.E., Robinson, G.O., Rocha, A., and Holtzman, D.M. (2017). Altered sleep and EEG power in the P301S Tau transgenic mouse model. Ann. Clin. Transl. Neurol. *4*, 180–190.

Horne, J.A. (2000). REM sleep - by default? Neurosci. Biobehav. Rev. *24*, 777–797.

Horne, J.A., and McGrath, M.J. (1984). The consolidation hypothesis for REM sleep function: Stress and other confounding factors — A review. Biol. Psychol. *18*, 165–184.

Huber, R., Deboer, T., and Tobler, I. (2000a). Effects of sleep deprivation on sleep and sleep EEG in three mouse strains: empirical data and simulations. Brain Res. *857*, 8–19.

Huber, R., Deboer, T., and Tobler, I. (2000b). Topography of EEG dynamics after sleep deprivation in mice. J. Neurophysiol. *84*, 1888–1893.

Huber, R., Ghilardi, M.F., Massimini, M., and Tononi, G. (2004). Local sleep and learning. Nature *430*, 78–81.

Huber, R., Tononi, G., and Cirelli, C. (2007). Exploratory behavior, cortical BDNF expression, and sleep homeostasis. Sleep *30*, 129–139.

Hughes, S.W., and Crunelli, V. (2005). Thalamic mechanisms of EEG alpha rhythms and their pathological implications. Neurosci. Rev. J. Bringing Neurobiol. Neurol. Psychiatry *11*, 357–372.

Hughes, S., Jagannath, A., Hankins, M.W., Foster, R.G., and Peirson, S.N. (2015). Photic regulation of clock systems. Methods Enzymol. *552*, 125–143.

Hurst, J.L., and West, R.S. (2010). Taming anxiety in laboratory mice. Nat. Methods *7*, 825–826.

Hvolby, A. (2015). Associations of sleep disturbance with ADHD: implications for treatment. Atten. Deficit Hyperact. Disord. *7*, 1–18.

Inutsuka, A., and Yamanaka, A. (2013). The physiological role of orexin/hypocretin neurons in the regulation of sleep/wakefulness and neuroendocrine functions. Front. Endocrinol. *4*.

Ito, H., Yanase, M., Yamashita, A., Kitabatake, C., Hamada, A., Suhara, Y., Narita, M., Ikegami, D., Sakai, H., Yamazaki, M., et al. (2013). Analysis of sleep disorders under pain using an optogenetic tool: possible involvement of the activation of dorsal raphe nucleus-serotonergic neurons. Mol. Brain *6*, 59.

Ito, W., Komada, Y., Okajima, I., and Inoue, Y. (2017). Excessive daytime sleepiness in adults with possible attention deficit/hyperactivity disorder (ADHD): a web-based cross-sectional study. Sleep Med. *32*, 4–9.

Jennings, K.A., Loder, M.K., Sheward, W.J., Pei, Q., Deacon, R.M.J., Benson, M.A., Olverman, H.J., Hastie, N.D., Harmar, A.J., Shen, S., et al. (2006). Increased expression of the 5-HT transporter confers a low-anxiety phenotype linked to decreased 5-HT transmission. J. Neurosci. Off. J. Soc. Neurosci. *26*, 8955–8964.

Jewett, M.E., and Kronauer, R.E. (1999). Interactive mathematical models of subjective alertness and cognitive throughput in humans. J. Biol. Rhythms *14*, 588–597.

Joiner, W.J., Friedman, E.B., Hung, H.-T., Koh, K., Sowcik, M., Sehgal, A., and Kelz, M.B. (2013). Genetic and anatomical basis of the barrier separating wakefulness and anesthetic-induced unresponsiveness. PLoS Genet. *9*, e1003605.

Justice, J.B. (1993). Quantitative microdialysis of neurotransmitters. J. Neurosci. Methods *48*, 263–276.

Justice, M.J., Noveroske, J.K., Weber, J.S., Zheng, B., and Bradley, A. (1999). Mouse ENU mutagenesis. Hum. Mol. Genet. *8*, 1955–1963.

Kattler, null, Dijk, null, and Borbély, null (1994). Effect of unilateral somatosensory stimulation prior to sleep on the sleep EEG in humans. J. Sleep Res. *3*, 159–164.

Kenar, A.N.I., Ay, O.İ., Herken, H., and Erdal, M.E. (2014). Association of VAMP-2 and Syntaxin 1A Genes with Adult Attention Deficit Hyperactivity Disorder. Psychiatry Investig. *11*, 76–83.

Kilduff, T.S., Cauli, B., and Gerashchenko, D. (2011). Activation of cortical interneurons during sleep: an anatomical link to homeostatic sleep regulation? Trends Neurosci. *34*, 10–19.

Kirszenblat, L., and van Swinderen, B. (2015). The yin and yang of sleep and attention. Trends Neurosci. *38*, 776–786.

Klein, D.C., Moore, R.Y., and Reppert, S.M. (1991). Suprachiasmatic Nucleus: The Mind's Clock (Oxford University Press).

Konadhode, R.R., Pelluru, D., and Shiromani, P.J. (2016). Unihemispheric Sleep: An Enigma for Current Models of Sleep-Wake Regulation. Sleep *39*, 491–494.

Kopell, N., Ermentrout, G.B., Whittington, M.A., and Traub, R.D. (2000). Gamma rhythms and beta rhythms have different synchronization properties. Proc. Natl. Acad. Sci. U. S. A. *97*, 1867–1872.

Krishnan, K.S., and Nash, H.A. (1990). A genetic study of the anesthetic response: mutants of Drosophila melanogaster altered in sensitivity to halothane. Proc. Natl. Acad. Sci. U. S. A. *87*, 8632–8636.

Krueger, J. (2010). What exactly is it that sleeps? The evolution, regulation and organization of an emergent network property. Evol. Sleep Phylogenetic Funct. Perspect.

Krueger, J.M., Rector, D.M., Roy, S., Van Dongen, H.P.A., Belenky, G., and Panksepp, J. (2008). Sleep as a fundamental property of neuronal assemblies. Nat. Rev. Neurosci. *9*, 910–919.

Krueger, J.M., Frank, M.G., Wisor, J.P., and Roy, S. (2016). Sleep function: Toward elucidating an enigma. Sleep Med. Rev. *28*, 46–54.

Kurt, S., and Ehret, G. (2010). Auditory discrimination learning and knowledge transfer in mice depends on task difficulty. Proc. Natl. Acad. Sci. U. S. A. *107*, 8481–8485.

Laposky, A.D., Shelton, J., Bass, J., Dugovic, C., Perrino, N., and Turek, F.W. (2006). Altered sleep regulation in leptin-deficient mice. Am. J. Physiol. Regul. Integr. Comp. Physiol. *290*, R894-903.

Laposky, A.D., Bradley, M.A., Williams, D.L., Bass, J., and Turek, F.W. (2008). Sleep-wake regulation is altered in leptin-resistant (db/db) genetically obese and diabetic mice. Am. J. Physiol. Regul. Integr. Comp. Physiol. *295*, R2059-2066.

Lazar, A.S., Lazar, Z.I., and Dijk, D.-J. (2015). Circadian regulation of slow waves in human sleep: Topographical aspects. Neuroimage *116*, 123–134.

Leemburg, S., Vyazovskiy, V.V., Olcese, U., Bassetti, C.L., Tononi, G., and Cirelli, C. (2010). Sleep homeostasis in the rat is preserved during chronic sleep restriction. Proc. Natl. Acad. Sci. U. S. A. *107*, 15939–15944.

Lesburguères, E., Tsokas, P., Sacktor, T.C., and Fenton, A.A. (2017). The Object Context-place-location Paradigm for Testing Spatial Memory in Mice. Bio-Protoc. *7*.

Levene, H. (1960). Robust tests for equality of variances. In Contributions to Probability and Statistics: Essays in Honor of Harold Hotelling, (Stanford, CA: Stanford University Press), pp. 278–292.

Li, S.K., Zhu, D., Gaisano, H.Y., and Brubaker, P.L. (2014). Role of vesicle-associated membrane protein 2 in exocytosis of glucagon-like peptide-1 from the murine intestinal L cell. Diabetologia *57*, 809–818.

Liebsch, G., Montkowski, A., Holsboer, F., and Landgraf, R. (1998). Behavioural profiles of two Wistar rat lines selectively bred for high or low anxiety-related behaviour. Behav. Brain Res. *94*, 301–310.

Lin, L., Faraco, J., Li, R., Kadotani, H., Rogers, W., Lin, X., Qiu, X., de Jong, P.J., Nishino, S., and Mignot, E. (1999). The sleep disorder canine narcolepsy is caused by a mutation in the hypocretin (orexin) receptor 2 gene. Cell *98*, 365–376.

Lipp, H.P., and Wolfer, D.P. (1998). Genetically modified mice and cognition. Curr. Opin. Neurobiol. *8*, 272–280.

Liu, S., Liu, Q., Tabuchi, M., and Wu, M.N. (2016). Sleep Drive Is Encoded by Neural Plastic Changes in a Dedicated Circuit. Cell *165*, 1347–1360.

Lu, J., Bjorkum, A.A., Xu, M., Gaus, S.E., Shiromani, P.J., and Saper, C.B. (2002). Selective Activation of the Extended Ventrolateral Preoptic Nucleus during Rapid Eye Movement Sleep. J. Neurosci. *22*, 4568–4576.

Lu, J., Sherman, D., Devor, M., and Saper, C.B. (2006). A putative flip-flop switch for control of REM sleep. Nature *441*, 589–594.

Lubow, R.E. (1989). Latent Inhibition and Conditioned Attention Theory (New York, NY, US: Cambridge University Press).

Lukatch, H.S., and MacIver, B.M. (1996). Synaptic Mechanisms of Thiopental-induced Alterations in Synchronized Cortical Activity. Anesthesiol. J. Am. Soc. Anesthesiol. *84*, 1425–1434.

Luppi, P.-H., Clement, O., Sapin, E., Peyron, C., Gervasoni, D., Léger, L., and Fort, P. (2012). Brainstem mechanisms of paradoxical (REM) sleep generation. Pflugers Arch. *463*, 43–52.

Lvamin, O.I., Oleksenko, A.I., Polyakova, I.G., and Mukhametov, L.M. (1996). Paradoxical sleep in northern fur seals in water and on land.

Lydic, R., and Baghdoyan, H.A. (2008). Acetylcholine modulates sleep and wakefulness: A synaptic perspective. Neurochem. Sleep Wakefulness 109–143.

Ma, S., Allocca, G., Ong-Pålsson, E.K.E., Singleton, C.E., Hawkes, D., McDougall, S.J., Williams, S.J., Bathgate, R.A.D., and Gundlach, A.L. (2017). Nucleus incertus promotes cortical desynchronization and behavioral arousal. Brain Struct. Funct. *222*, 515–537.

Ma, S., Hangya, B., Leonard, C.S., Wisden, W., and Gundlach, A.L. (2018). Dual-transmitter systems regulating arousal, attention, learning and memory. Neurosci. Biobehav. Rev. *85*, 21–33.

Mackiewicz, M., Paigen, B., Naidoo, N., and Pack, A.I. (2008). Analysis of the QTL for sleep homeostasis in mice: Homer1a is a likely candidate. Physiol. Genomics *33*, 91–99.

Malek, Z.S., Dardente, H., Pevet, P., and Raison, S. (2005). Tissue-specific expression of tryptophan hydroxylase mRNAs in the rat midbrain: anatomical evidence and daily profiles. Eur. J. Neurosci. *22*, 895–901.

Maret, S., Franken, P., Dauvilliers, Y., Ghyselinck, N.B., Chambon, P., and Tafti, M. (2005). Retinoic acid signaling affects cortical synchrony during sleep. Science *310*, 111–113.

Markwald, R.R., Melanson, E.L., Smith, M.R., Higgins, J., Perreault, L., Eckel, R.H., and Wright, K.P. (2013). Impact of insufficient sleep on total daily energy expenditure, food intake, and weight gain. Proc. Natl. Acad. Sci. U. S. A. *110*, 5695–5700.

Massimini, M., Huber, R., Ferrarelli, F., Hill, S., and Tononi, G. (2004). The sleep slow oscillation as a traveling wave. J. Neurosci. Off. J. Soc. Neurosci. *24*, 6862–6870.

Matsumoto, M., Togashi, H., Yoshioka, M., Morii, K., Hirokami, M., Tochihara, M., Ikeda, T., Saito, Y., and Saito, H. (1991). Significant correlation between cerebrospinal fluid and brain levels of norepinephrine, serotonin and acetylcholine in anesthetized rats. Life Sci. *48*, 823–829.

McCarley, R.W., and Hobson, J.A. (1975). Neuronal excitability modulation over the sleep cycle: a structural and mathematical model. Science *189*, 58–60.

McCarley, R.W., and Massaquoi, S.G. (1986). A limit cycle mathematical model of the REM sleep oscillator system. Am. J. Physiol. *251*, R1011-1029.

McGregor, R., and Siegel, J.M. (2010). Illuminating the locus coeruleus: control of posture and arousal. Nat. Neurosci. *13*, 1448–1449.

McShane, B.B., Galante, R.J., Jensen, S.T., Naidoo, N., Pack, A.I., and Wyner, A. (2010). Characterization of the bout durations of sleep and wakefulness. J. Neurosci. Methods *193*, 321–333.

Meiser, J., Weindl, D., and Hiller, K. (2013). Complexity of dopamine metabolism. Cell Commun. Signal. CCS *11*, 34.

Mendez, M., Gross, K.W., Glenn, S.T., Garvin, J.L., and Carretero, O.A. (2011). Vesicle-associated Membrane Protein-2 (VAMP2) Mediates cAMP-stimulated Renin Release in Mouse Juxtaglomerular Cells. J. Biol. Chem. *286*, 28608–28618.

Merica, H., and Fortune, R.D. (2004). State transitions between wake and sleep, and within the ultradian cycle, with focus on the link to neuronal activity. Sleep Med. Rev. *8*, 473–485.

Minatohara, K., Akiyoshi, M., and Okuno, H. (2016). Role of Immediate-Early Genes in Synaptic Plasticity and Neuronal Ensembles Underlying the Memory Trace. Front. Mol. Neurosci. *8*.

Mistlberger, R.E., Bergmann, B.M., Waldenar, W., and Rechtschaffen, A. (1983). Recovery sleep following sleep deprivation in intact and suprachiasmatic nuclei-lesioned rats. Sleep *6*, 217–233.

Mongrain, V., and Franken, P. (2013). Genetic interaction between circadian and homeostatic regulation of sleep. In The Genetic Basis of Sleep and Sleep Disorders, Ed. Paul Shaw, Mehdi Tafti and Michael Thorpy, (Cambridge: Cambridge University Press), pp. 147–161.

Monti, J.M., and Jantos, H. (2008). The roles of dopamine and serotonin, and of their receptors, in regulating sleep and waking. Prog. Brain Res. *172*, 625–646.

Moore-Ede, M., FM, S., and Fuller, C. (1982). The Clocks That Time Us: Physiology of the Circadian Timing System.

Mukovski, M., Chauvette, S., Timofeev, I., and Volgushev, M. (2007). Detection of active and silent states in neocortical neurons from the field potential signal during slow-wave sleep. Cereb. Cortex N. Y. N 1991 *17*, 400–414.

Müller, H.K., Kragballe, M., Fjorback, A.W., and Wiborg, O. (2014). Differential regulation of the serotonin transporter by vesicle-associated membrane protein 2 in cells of neuronal versus non-neuronal origin. PloS One *9*, e97540.

Mumby, D.G., Gaskin, S., Glenn, M.J., Schramek, T.E., and Lehmann, H. (2002). Hippocampal damage and exploratory preferences in rats: memory for objects, places, and contexts. Learn. Mem. Cold Spring Harb. N *9*, 49–57.

Murphy, D.L., and Lesch, K.-P. (2008). Targeting the murine serotonin transporter: insights into human neurobiology. Nat. Rev. Neurosci. *9*, 85–96.

Murphy, M., Huber, R., Esser, S., Riedner, B.A., Massimini, M., Ferrarelli, F., Ghilardi, M.F., and Tononi, G. (2011). The cortical topography of local sleep. Curr. Top. Med. Chem. *11*, 2438–2446.

Myöhänen, T.T., Schendzielorz, N., and Männistö, P.T. (2010). Distribution of catechol-O-methyltransferase (COMT) proteins and enzymatic activities in wild-type and soluble COMT deficient mice. J. Neurochem. *113*, 1632–1643.

Neckelmann, D., and Ursin, R. (1993). Sleep stages and EEG power spectrum in relation to acoustical stimulus arousal threshold in the rat. Sleep *16*, 467–477.

Némoz-Gaillard, E., Bosshard, A., Regazzi, R., Bernard, C., Cuber, J.C., Takahashi, M., Catsicas, S., Chayvialle, J.A., and Abello, J. (1998). Expression of SNARE proteins in enteroendocrine cell lines and functional role of tetanus toxin-sensitive proteins in cholecystokinin release. FEBS Lett. *425*, 66–70.

Nir, Y., Vyazovskiy, V.V., Cirelli, C., Banks, M.I., and Tononi, G. (2015). Auditory Responses and Stimulus-Specific Adaptation in Rat Auditory Cortex are Preserved Across NREM and REM Sleep. Cereb. Cortex N. Y. NY *25*, 1362–1378.

Nolan, P.M., Hugill, A., and Cox, R.D. (2002). ENU mutagenesis in the mouse: application to human genetic disease. Brief. Funct. Genomic. Proteomic. *1*, 278–289.

Oades, R. (2010). The Role of Serotonin in Attention-Deficit Hyperactivity Disorder (ADHD). Handb. Behav. Neurosci. *21*, 565–584.

Oades, R.D. (2008). Dopamine-serotonin interactions in attention-deficit hyperactivity disorder (ADHD). Prog. Brain Res. *172*, 543–565.

Oaks, A.W., and Sidhu, A. (2011). Synuclein modulation of monoamine transporters. FEBS Lett. *585*, 1001–1006.

Oleksenko, A.I., Mukhametov, L.., Polyakova, I.., Supin, A.Y., and Kovalzon, V.M. (1992). Unihemispheric sleep deprivation in bottlenose dolphins. J. Sleep Res. *1*, 40–44.

Olson, A.L., Knight, J.B., and Pessin, J.E. (1997). Syntaxin 4, VAMP2, and/or VAMP3/cellubrevin are functional target membrane and vesicle SNAP receptors for insulin-stimulated GLUT4 translocation in adipocytes. Mol. Cell. Biol. *17*, 2425–2435.

Owens, J.A. (2009). A Clinical Overview of Sleep and Attention-Deficit/Hyperactivity Disorder in Children and Adolescents. J. Can. Acad. Child Adolesc. Psychiatry *18*, 92–102.

Page, D.T., Kuti, O.J., Prestia, C., and Sur, M. (2009). Haploinsufficiency for Pten and Serotonin transporter cooperatively influences brain size and social behavior. Proc. Natl. Acad. Sci. U. S. A. *106*, 1989–1994.

Pal, D., Lipinski, W.J., Walker, A.J., Turner, A.M., and Mashour, G.A. (2011). State-specific effects of sevoflurane anesthesia on sleep homeostasis: selective recovery of slow wave but not rapid eye movement sleep. Anesthesiology *114*, 302–310.

Palchykova, S., Winsky-Sommerer, R., Meerlo, P., Dürr, R., and Tobler, I. (2006). Sleep deprivation impairs object recognition in mice. Neurobiol. Learn. Mem. *85*, 263–271.

Pandi-Perumal, S.R., Srinivasan, V., Maestroni, G.J.M., Cardinali, D.P., Poeggeler, B., and Hardeland, R. (2006). Melatonin: Nature's most versatile biological signal? FEBS J. *273*, 2813–2838.

Pascual, O., Casper, K.B., Kubera, C., Zhang, J., Revilla-Sanchez, R., Sul, J.-Y., Takano, H., Moss, S.J., McCarthy, K., and Haydon, P.G. (2005). Astrocytic purinergic signaling coordinates synaptic networks. Science *310*, 113–116.

Patel, P.D., Pontrello, C., and Burke, S. (2004). Robust and tissue-specific expression of TPH2 versus TPH1 in rat raphe and pineal gland. Biol. Psychiatry *55*, 428–433.

Patti, C.L., Zanin, K.A., Sanday, L., Kameda, S.R., Fernandes-Santos, L., Fernandes, H.A., Andersen, M.L., Tufik, S., and Frussa-Filho, R. (2010). Effects of Sleep Deprivation on Memory in Mice: Role of State-Dependent Learning. Sleep *33*, 1669–1679.

Peyron, C., Faraco, J., Rogers, W., Ripley, B., Overeem, S., Charnay, Y., Nevsimalova, S., Aldrich, M., Reynolds, D., Albin, R., et al. (2000). A mutation in a case of early onset narcolepsy and a generalized absence of hypocretin peptides in human narcoleptic brains. Nat. Med. *6*, 991–997.

Phillips, A.J.K., Robinson, P.A., and Klerman, E.B. (2013). Arousal state feedback as a potential physiological generator of the ultradian REM/NREM sleep cycle. J. Theor. Biol. *319*, 75–87.

Piazza, P.V., Rougé-Pont, F., Deminière, J.M., Kharoubi, M., Le Moal, M., and Simon, H. (1991). Dopaminergic activity is reduced in the prefrontal cortex and increased in the nucleus accumbens of rats predisposed to develop amphetamine self-administration. Brain Res. *567*, 169–174.

Picchioni, D., Pixa, M.L., Fukunaga, M., Carr, W.S., Horovitz, S.G., Braun, A.R., and Duyn, J.H. (2014). Decreased connectivity between the thalamus and the neocortex during human nonrapid eye movement sleep. Sleep *37*, 387–397.

Pietraszek, M.H., Takada, Y., Yan, D., Urano, T., Serizawa, K., and Takada, A. (1992). Relationship between serotonergic measures in periphery and the brain of mouse. Life Sci. *51*, 75–82.

Pimentel, D., Donlea, J.M., Talbot, C.B., Song, S.M., Thurston, A.J.F., and Miesenböck, G. (2016). Operation of a homeostatic sleep switch. Nature *536*, 333–337.

Pirone, L., Smaldone, G., Esposito, C., Balasco, N., Petoukhov, M.V., Spilotros, A., Svergun, D.I., Di Gaetano, S., Vitagliano, L., and Pedone, E.M. (2016). Proteins involved in sleep homeostasis: Biophysical characterization of INC and its partners. Biochimie *131*, 106–114.

Poe, G.R., Walsh, C.M., and Bjorness, T.E. (2010). Cognitive Neuroscience of Sleep. Prog. Brain Res. *185*, 1–19.

Poirier, M.A., Xiao, W., Macosko, J.C., Chan, C., Shin, Y.K., and Bennett, M.K. (1998). The synaptic SNARE complex is a parallel four-stranded helical bundle. Nat. Struct. Biol. *5*, 765–769.

Porkka-Heiskanen, T., Strecker, R.E., Thakkar, M., Bjorkum, A.A., Greene, R.W., and McCarley, R.W. (1997). Adenosine: a mediator of the sleep-inducing effects of prolonged wakefulness. Science *276*, 1265–1268.

Portas, C.M., Bjorvatn, B., Fagerland, S., Grønli, J., Mundal, V., Sørensen, E., and Ursin, R. (1998). On-line detection of extracellular levels of serotonin in dorsal raphe nucleus and frontal cortex over the sleep/wake cycle in the freely moving rat. Neuroscience *83*, 807–814.

Preitner, N., Damiola, F., Lopez-Molina, L., Zakany, J., Duboule, D., Albrecht, U., and Schibler, U. (2002). The orphan nuclear receptor REV-ERBalpha controls circadian transcription within the positive limb of the mammalian circadian oscillator. Cell *110*, 251–260.

Prince, J. (2008). Catecholamine dysfunction in attention-deficit/hyperactivity disorder: an update. J. Clin. Psychopharmacol. *28*, S39-45.

Prince, T.-M., and Abel, T. (2013). The impact of sleep loss on hippocampal function. Learn. Mem. *20*, 558–569.

Provencio, I., Rodriguez, I.R., Jiang, G., Hayes, W.P., Moreira, E.F., and Rollag, M.D. (2000). A Novel Human Opsin in the Inner Retina. J. Neurosci. *20*, 600–605.

Puentes-Mestril, C., and Aton, S.J. (2017). Linking Network Activity to Synaptic Plasticity during Sleep: Hypotheses and Recent Data. Front. Neural Circuits *11*.

Qiu, M.-H., Chen, M.C., and Lu, J. (2015). Cortical neuronal activity does not regulate sleep homeostasis. Neuroscience *297*, 211–218.

Quwailid, M.M., Hugill, A., Dear, N., Vizor, L., Wells, S., Horner, E., Fuller, S., Weedon, J., McMath, H., Woodman, P., et al. (2004). A gene-driven ENU-based approach to generating an allelic series in any gene. Mamm. Genome Off. J. Int. Mamm. Genome Soc. *15*, 585–591.

Rajaratnam, S.M., and Arendt, J. (2001). Health in a 24-h society. Lancet Lond. Engl. *358*, 999–1005.

Ramakrishnan, N.A., Drescher, M.J., and Drescher, D.G. (2012). The SNARE complex in neuronal and sensory cells. Mol. Cell. Neurosci. *50*, 58–69.

Raptis, A., Torrejón-Escribano, B., Gómez de Aranda, I., and Blasi, J. (2005). Distribution of synaptobrevin/VAMP 1 and 2 in rat brain. J. Chem. Neuroanat. *30*, 201–211.

Rasch, B., and Born, J. (2013). About sleep's role in memory. Physiol. Rev. *93*, 681–766.

Rasch, B., and Born, J. (2015). In search of a role of REM sleep in memory formation. Neurobiol. Learn. Mem. *122*, 1–3.

Rasch, B., Pommer, J., Diekelmann, S., and Born, J. (2009). Pharmacological REM sleep suppression paradoxically improves rather than impairs skill memory. Nat. Neurosci. *12*, 396–397.

Ravassard, P., Hamieh, A.M., Malleret, G., and Salin, P.-A. (2015). Paradoxical sleep: A vigilance state to gate long-term brain plasticity? Neurobiol. Learn. Mem. *122*, 4–10.

Rechtschaffen, A., Hauri, P., and Zeitlin, M. (1966). Auditory awakening thresholds in REM and NREM sleep stages. Percept. Mot. Skills *22*, 927–942.

Regazzi, R., Wollheim, C.B., Lang, J., Theler, J.M., Rossetto, O., Montecucco, C., Sadoul, K., Weller, U., Palmer, M., and Thorens, B. (1995). VAMP-2 and cellubrevin are expressed in pancreatic beta-cells and are essential for Ca(2+)-but not for GTP gamma S-induced insulin secretion. EMBO J. *14*, 2723–2730.

Reppert, S.M., and Weaver, D.R. (2002). Coordination of circadian timing in mammals. Nature *418*, 935–941.

Rimmele, U., and Tambini, A. (2015). Sleep, Sleep Alterations, Stress—Combined Effects on Memory? Sleep *38*, 1835–1836.

Robinson, T.E., Kramis, R.C., and Vanderwolf, C.H. (1977). Two types of cerebral activation during active sleep: relations to behavior. Brain Res. *124*, 544–549.

Rodriguiz, R.M., and Wetsel, W.C. (2006). Assessments of Cognitive Deficits in Mutant Mice. In Animal Models of Cognitive Impairment, E.D. Levin, and J.J. Buccafusco, eds. (Boca Raton (FL): CRC Press/Taylor & Francis), p.

Roffwarg, H.P., Muzio, J.N., and Dement, W.C. (1966). Ontogenetic development of the human sleep-dream cycle. Science *152*, 604–619.

Rosenmund, C., and Stevens, C.F. (1996). Definition of the readily releasable pool of vesicles at hippocampal synapses. Neuron *16*, 1197–1207.

Rosenwasser, A.M. (2009). Functional neuroanatomy of sleep and circadian rhythms. Brain Res. Rev. *61*, 281–306.

Roumis, D.K., and Frank, L.M. (2015). Hippocampal sharp-wave ripples in waking and sleeping states. Curr. Opin. Neurobiol. *35*, 6–12.

Rozov, S.V., Zant, J.C., Gurevicius, K., Porkka-Heiskanen, T., and Panula, P. (2016). Altered Electroencephalographic Activity Associated with Changes in the Sleep-Wakefulness Cycle of C57BL/6J Mice in Response to a Photoperiod Shortening. Front. Behav. Neurosci. *10*.

Rusterholz, T., and Achermann, P. (2011). Topographical aspects in the dynamics of sleep homeostasis in young men: individual patterns. BMC Neurosci. *12*, 84.

Rusterholz, T., Dürr, R., and Achermann, P. (2010). Inter-individual differences in the dynamics of sleep homeostasis. Sleep *33*, 491–498.

Sanchez-Vives, M.V., and Mattia, M. (2014). Slow wave activity as the default mode of the cerebral cortex. Arch. Ital. Biol. *152*, 147–155.

Sanders, M.J., Wiltgen, B.J., and Fanselow, M.S. (2003). The place of the hippocampus in fear conditioning. Eur. J. Pharmacol. *463*, 217–223.

Sanderson, D.J., Hindley, E., Smeaton, E., Denny, N., Taylor, A., Barkus, C., Sprengel, R., Seeburg, P.H., and Bannerman, D.M. (2011). Deletion of the GluA1 AMPA receptor subunit impairs recency-dependent object recognition memory. Learn. Mem. *18*, 181–190.

Saper, C.B., Chou, T.C., and Scammell, T.E. (2001). The sleep switch: hypothalamic control of sleep and wakefulness. Trends Neurosci. *24*, 726–731.

Saper, C.B., Fuller, P.M., Pedersen, N.P., Lu, J., and Scammell, T.E. (2010). Sleep state switching. Neuron *68*, 1023–1042.

Scammell, T.E., Arrigoni, E., and Lipton, J.O. (2017). Neural Circuitry of Wakefulness and Sleep. Neuron *93*, 747–765.

Scharf, M.T., Naidoo, N., Zimmerman, J.E., and Pack, A.I. (2008). The energy hypothesis of sleep revisited. Prog. Neurobiol. *86*, 264–280.

Scheller, R.H. (2013). In search of the molecular mechanism of intracellular membrane fusion and neurotransmitter release. Nat. Med. *19*, 1232–1235.

Schmidt, D., Roznoski, M., and Ebert, M.H. (1990). Qualitative and quantitative high performance liquid chromatographic analysis of monoamine neurotransmitters and metabolites in cerebrospinal fluid and brain tissue using reductive electrochemical detection. Biomed. Chromatogr. BMC *4*, 215–220.

Schoch, S., Deák, F., Königstorfer, A., Mozhayeva, M., Sara, Y., Südhof, T.C., and Kavalali, E.T. (2001). SNARE function analyzed in synaptobrevin/VAMP knockout mice. Science *294*, 1117–1122.

Schöne, C., and Burdakov, D. (2017). Orexin/Hypocretin and Organizing Principles for a Diversity of Wake-Promoting Neurons in the Brain. Curr. Top. Behav. Neurosci. *33*, 51–74.

Schwierin, B., Achermann, P., Deboer, T., Oleksenko, A., Borbély, A.A., and Tobler, I. (1999). Regional differences in the dynamics of the cortical EEG in the rat after sleep deprivation. Clin. Neurophysiol. Off. J. Int. Fed. Clin. Neurophysiol. *110*, 869–875.

Seidner, G., Robinson, J.E., Wu, M., Worden, K., Masek, P., Roberts, S.W., Keene, A.C., and Joiner, W.J. (2015). Identification of Neurons with a Privileged Role in Sleep Homeostasis in Drosophila melanogaster. Curr. Biol. CB *25*, 2928–2938.

Sestakova, N., Puzserova, A., Kluknavsky, M., and Bernatova, I. (2013). Determination of motor activity and anxiety-related behaviour in rodents: methodological aspects and role of nitric oxide. Interdiscip. Toxicol. *6*, 126–135.

Sherin, J.E., Shiromani, P.J., McCarley, R.W., and Saper, C.B. (1996). Activation of ventrolateral preoptic neurons during sleep. Science *271*, 216–219.

Shirvalkar, P., and Bahar, A.S. (2009). The multiple origins and laminar topography of the hippocampal theta rhythm. J. Neurosci. Off. J. Soc. Neurosci. *29*, 7111–7113.

Sidhu, A., Laruelle, M., and Vernier, P. (2003). Dopamine Receptors and Transporters: Function, Imaging and Clinical Implication, Second Edition (CRC Press).

Siegel, J.M. (2005). Clues to the functions of mammalian sleep. Nature *437*, 1264–1271.

Sitaraman, D., Aso, Y., Jin, X., Chen, N., Felix, M., Rubin, G.M., and Nitabach, M.N. (2015). Propagation of Homeostatic Sleep Signals by Segregated Synaptic Microcircuits of the Drosophila Mushroom Body. Curr. Biol. CB *25*, 2915–2927.

Skeberdis, V.A., Lan, J., Zheng, X., Zukin, R.S., and Bennett, M.V. (2001). Insulin promotes rapid delivery of N-methyl-D- aspartate receptors to the cell surface by exocytosis. Proc. Natl. Acad. Sci. U. S. A. *98*, 3561–3566.

Smith, C. (1995). Sleep states and memory processes. Behav. Brain Res. *69*, 137–145.

Söllner, T., Whiteheart, S.W., Brunner, M., Erdjument-Bromage, H., Geromanos, S., Tempst, P., and Rothman, J.E. (1993). SNAP receptors implicated in vesicle targeting and fusion. Nature *362*, 318–324.

Stein, A., Weber, G., Wahl, M.C., and Jahn, R. (2009). Helical extension of the neuronal SNARE complex into the membrane. Nature *460*, 525–528.

Steriade, M. (2006). Grouping of brain rhythms in corticothalamic systems. Neuroscience *137*, 1087–1106.

Steriade, M.M., and McCarley, R.W. (2005). Brain Control of Wakefulness and Sleep (Springer US).

Steriade, M., McCormick, D.A., and Sejnowski, T.J. (1993a). Thalamocortical oscillations in the sleeping and aroused brain. Science *262*, 679–685.

Steriade, M., Nuñez, A., and Amzica, F. (1993b). Intracellular analysis of relations between the slow (< 1 Hz) neocortical oscillation and other sleep rhythms of the electroencephalogram. J. Neurosci. Off. J. Soc. Neurosci. *13*, 3266–3283.

Steriade, M., Timofeev, I., and Grenier, F. (2001). Natural waking and sleep states: a view from inside neocortical neurons. J. Neurophysiol. *85*, 1969–1985.

Stickgold, R. (2013). Parsing the role of sleep in memory processing. Curr. Opin. Neurobiol. *23*, 847–853.

Stickgold, R., and Walker, M.P. (2013). Sleep-dependent memory triage: evolving generalization through selective processing. Nat. Neurosci. *16*, 139–145.

Strijkstra, A.M., Beersma, D.G.M., Drayer, B., Halbesma, N., and Daan, S. (2003). Subjective sleepiness correlates negatively with global alpha (8-12 Hz) and positively with central frontal theta (4-8 Hz) frequencies in the human resting awake electroencephalogram. Neurosci. Lett. *340*, 17–20.

Südhof, T.C. (1995). The synaptic vesicle cycle: a cascade of protein-protein interactions. Nature *375*, 645–653.

Südhof, T.C. (2013). Neurotransmitter Release: The Last Millisecond in the Life of a Synaptic Vesicle. Neuron *80*, 675–690.

Sunyer, B., Patil, S., Höger, H., and Lubec, G. (2007). Barnes maze, a useful task to assess spatial reference memory in the mice.

Szabadi, E. (2006). Drugs for sleep disorders: mechanisms and therapeutic prospects. Br. J. Clin. Pharmacol. *61*, 761–766.

Szentirmai, É., Kapás, L., Sun, Y., Smith, R.G., and Krueger, J.M. (2010). Restricted feeding-induced sleep, activity, and body temperature changes in normal and preproghrelin-deficient mice. Am. J. Physiol. - Regul. Integr. Comp. Physiol. *298*, R467–R477.

Szymusiak, R., and McGinty, D. (2008). Hypothalamic regulation of sleep and arousal. Ann. N. Y. Acad. Sci. *1129*, 275–286.

Tafti, M., and Franken, P. (2002). Invited review: genetic dissection of sleep. J. Appl. Physiol. Bethesda Md 1985 *92*, 1339–1347.

Tafti, M., Franken, P., Kitahama, K., Malafosse, A., Jouvet, M., and Valatx, J.L. (1997). Localization of candidate genomic regions influencing paradoxical sleep in mice. Neuroreport *8*, 3755–3758.

Tafti, M., Petit, B., Chollet, D., Neidhart, E., de Bilbao, F., Kiss, J.Z., Wood, P.A., and Franken, P. (2003). Deficiency in short-chain fatty acid beta-oxidation affects theta oscillations during sleep. Nat. Genet. *34*, 320–325.

Tam, S.K.E., Hasan, S., Hughes, S., Hankins, M.W., Foster, R.G., Bannerman, D.M., and Peirson, S.N. (2016). Modulation of recognition memory performance by light requires both melanopsin and classical photoreceptors. Proc. R. Soc. B Biol. Sci. *283*.

Taylor, A., Steinberg, J., and Webber, C. (2015). Duplications in ADHD patients harbour neurobehavioural genes that are co-expressed with genes associated with hyperactivity in the mouse. Am. J. Med. Genet. *168*, 97–107.

Thannickal, T.C., Moore, R.Y., Nienhuis, R., Ramanathan, L., Gulyani, S., Aldrich, M., Cornford, M., and Siegel, J.M. (2000). Reduced number of hypocretin neurons in human narcolepsy. Neuron *27*, 469–474.

Thurmond, D.C. (2013). Regulation of Insulin Action and Insulin Secretion by SNARE-Mediated Vesicle Exocytosis (Landes Bioscience).

Tobler, I. (1995). Is sleep fundamentally different between mammalian species? Behav. Brain Res. *69*, 35–41.

Tobler, I., and Borbély, A.A. (1986). Sleep EEG in the rat as a function of prior waking. Electroencephalogr. Clin. Neurophysiol. *64*, 74–76.

Tobler, I., and Borbély, A.A. (1990). Effects of 20-min forced locomotion on sleep and EEG spectra of the rat. (Pontenagel Press), pp. 102–105.

Tobler, null, Franken, null, Trachsel, null, and Borbély, null (1992). Models of sleep regulation in mammals. J. Sleep Res. *1*, 125–127.

Tobler, I., Borbély, A.A., and Groos, G. (1983). The effect of sleep deprivation on sleep in rats with suprachiasmatic lesions. Neurosci. Lett. *42*, 49–54.

Tononi, G., and Cirelli, C. (2003). Sleep and synaptic homeostasis: a hypothesis. Brain Res. Bull. *62*, 143–150.

Tononi, G., and Cirelli, C. (2006). Sleep function and synaptic homeostasis. Sleep Med. Rev. *10*, 49–62.

Tononi, G., and Cirelli, C. (2014). Sleep and the price of plasticity: from synaptic and cellular homeostasis to memory consolidation and integration. Neuron *81*, 12–34.

Tononi, G., and Cirelli, C. (2016). Sleep and Synaptic Down-Selection. In Micro-, Meso- and Macro-Dynamics of the Brain, G. Buzsáki, and Y. Christen, eds. (Cham (CH): Springer), p.

Toth, L.A., Tolley, E.A., and Krueger, J.M. (1993). Sleep as a prognostic indicator during infectious disease in rabbits. Proc. Soc. Exp. Biol. Med. Soc. Exp. Biol. Med. N. Y. N *203*, 179–192.

Trachsel, L., Tobler, I., Achermann, P., and Borbély, A.A. (1991). Sleep continuity and the REM-nonREM cycle in the rat under baseline conditions and after sleep deprivation. Physiol. Behav. *49*, 575–580.

Tsunematsu, T., Kilduff, T.S., Boyden, E.S., Takahashi, S., Tominaga, M., and Yamanaka, A. (2011). Acute optogenetic silencing of orexin/hypocretin neurons induces slow-wave sleep in mice. J. Neurosci. Off. J. Soc. Neurosci. *31*, 10529–10539.

Tung, A., Szafran, M.J., Bluhm, B., and Mendelson, W.B. (2002). Sleep deprivation potentiates the onset and duration of loss of righting reflex induced by propofol and isoflurane. Anesthesiology *97*, 906–911.

Ursin, R. (2002). Serotonin and sleep. Sleep Med. Rev. *6*, 55–69.

Vanini, G., Watson, C.J., Lydic, R., and Baghdoyan, H.A. (2008). γ-Aminobutyric Acid–mediated Neurotransmission in the Pontine Reticular Formation Modulates Hypnosis, Immobility, and Breathing during Isoflurane Anesthesia. Anesthesiol. J. Am. Soc. Anesthesiol. *109*, 978–988.

Vassalli, A., and Dijk, D.-J. (2009). Sleep function: current questions and new approaches. Eur. J. Neurosci. *29*, 1830–1841.

Vassalli, A., and Franken, P. (2017). Hypocretin (orexin) is critical in sustaining theta/gamma-rich waking behaviors that drive sleep need. Proc. Natl. Acad. Sci. U. S. A. *114*, E5464–E5473.

Vogel-Ciernia, A., and Wood, M.A. (2014). Examining Object Location and Object Recognition Memory in Mice. Curr. Protoc. Neurosci. Editor. Board Jacqueline N Crawley Al *69*, 8.31.1-8.31.17.

Vujovic, N., Gooley, J.J., Jhou, T.C., and Saper, C.B. (2015). Projections from the subparaventricular zone define four channels of output from the circadian timing system. J. Comp. Neurol. *523*, 2714–2737.

Vyazovskiy, V.V. (2015). Sleep, recovery, and metaregulation: explaining the benefits of sleep. Nat. Sci. Sleep *7*, 171–184.

Vyazovskiy, V.V., and Tobler, I. (2005a). Theta activity in the waking EEG is a marker of sleep propensity in the rat. Brain Res. *1050*, 64–71.

Vyazovskiy, V.V., and Tobler, I. (2005b). Regional differences in NREM sleep slow-wave activity in mice with congenital callosal dysgenesis. J. Sleep Res. *14*, 299–304.

Vyazovskiy, V.V., and Tobler, I. (2008). Handedness leads to interhemispheric EEG asymmetry during sleep in the rat. J. Neurophysiol. *99*, 969–975.

Vyazovskiy, V.V., and Tobler, I. (2012). The temporal structure of behaviour and sleep homeostasis. PloS One *7*, e50677.

Vyazovskiy, V.V., Borbély, A.A., and Tobler, I. (2002). Interhemispheric sleep EEG asymmetry in the rat is enhanced by sleep deprivation. J. Neurophysiol. *88*, 2280–2286.

Vyazovskiy, V.V., Achermann, P., Borbély, A.A., and Tobler, I. (2004). The dynamics of spindles and EEG slow-wave activity in NREM sleep in mice. Arch. Ital. Biol. *142*, 511–523.

Vyazovskiy, V.V., Ruijgrok, G., Deboer, T., and Tobler, I. (2006). Running wheel accessibility affects the regional electroencephalogram during sleep in mice. Cereb. Cortex N. Y. N 1991 *16*, 328–336.

Vyazovskiy, V.V., Achermann, P., and Tobler, I. (2007). Sleep homeostasis in the rat in the light and dark period. Brain Res. Bull. *74*, 37–44.

Vyazovskiy, V.V., Olcese, U., Lazimy, Y.M., Faraguna, U., Esser, S.K., Williams, J.C., Cirelli, C., and Tononi, G. (2009). Cortical firing and sleep homeostasis. Neuron *63*, 865–878.

Vyazovskiy, V.V., Olcese, U., Hanlon, E.C., Nir, Y., Cirelli, C., and Tononi, G. (2011a). Local sleep in awake rats. Nature *472*, 443–447.

Vyazovskiy, V.V., Cirelli, C., and Tononi, G. (2011b). Electrophysiological correlates of sleep homeostasis in freely behaving rats. Prog. Brain Res. *193*, 17–38.

Vyazovskiy, V.V., Walton, M.E., Peirson, S.N., and Bannerman, D.M. (2017). Sleep homeostasis, habits and habituation. Curr. Opin. Neurobiol. *44*, 202–211.

Watson, C.J., Soto-Calderon, H., Lydic, R., and Baghdoyan, H.A. (2008). Pontine reticular formation (PnO) administration of hypocretin-1 increases PnO GABA levels and wakefulness. Sleep *31*, 453–464.

Watson, C.J., Baghdoyan, H.A., and Lydic, R. (2010). Neuropharmacology of Sleep and Wakefulness. Sleep Med. Clin. *5*, 513–528.

Werth, E., and Borbély, A.A. (1995). Recording the sleep EEG with periorbital skin electrodes. Electroencephalogr. Clin. Neurophysiol. *94*, 406–413.

Werth, E., Achermann, P., and Borbély, A.A. (1996a). Brain topography of the human sleep EEG: antero-posterior shifts of spectral power. Neuroreport *8*, 123–127.

Werth, E., Dijk, D.J., Achermann, P., and Borbely, A.A. (1996b). Dynamics of the sleep EEG after an early evening nap: experimental data and simulations. Am. J. Physiol. - Regul. Integr. Comp. Physiol. *271*, R501–R510.

Werth, E., Achermann, P., and Borbély, A.A. (1997). Fronto-occipital EEG power gradients in human sleep. J. Sleep Res. *6*, 102–112.

Werth, E., Achermann, P., and Borbély, A.A. (1998). Regional differences in the sleep EEG: Functional implications. Sleep *21(Suppl)*, 207.

Wetherell, J.R., Fosbraey, P., and French, M.C. (1989). A Comparison of the Distribution of Neurotransmitters in Brain Regions of the Rat and Guinea-Pig Using a Chemiluminescent Method and HPLC with Electrochemical Detection. J. Neurochem. *53*, 1519–1526.

Wheeler, M.B., Sheu, L., Ghai, M., Bouquillon, A., Grondin, G., Weller, U., Beaudoin, A.R., Bennett, M.K., Trimble, W.S., and Gaisano, H.Y. (1996). Characterization of SNARE protein expression in beta cell lines and pancreatic islets. Endocrinology *137*, 1340–1348.

White, R.B., and Thomas, M.G. (2012). Moving beyond tyrosine hydroxylase to define dopaminergic neurons for use in cell replacement therapies for Parkinson's disease. CNS Neurol. Disord. Drug Targets *11*, 340–349.

Winrow, C.J., Williams, D.L., Kasarskis, A., Millstein, J., Laposky, A.D., Yang, H.S., Mrazek, K., Zhou, L., Owens, J.R., Radzicki, D., et al. (2009). Uncovering the Genetic Landscape for Multiple Sleep-Wake Traits. PLOS ONE *4*, e5161.

Wisor, J.P., Nishino, S., Sora, I., Uhl, G.H., Mignot, E., and Edgar, D.M. (2001). Dopaminergic role in stimulant-induced wakefulness. J. Neurosci. Off. J. Soc. Neurosci. *21*, 1787–1794.

Wulff, K., Gatti, S., Wettstein, J.G., and Foster, R.G. (2010). Sleep and circadian rhythm disruption in psychiatric and neurodegenerative disease. Nat. Rev. Neurosci. *11*, 589–599.

Wyatt, R.J., Karoum, F., and Casanova, M.F. (1995). Decreased DOPAC in the anterior cingulate cortex of individuals with schizophrenia. Biol. Psychiatry *38*, 4–12.

Xi, M.C., Morales, F.R., and Chase, M.H. (1999). Evidence that wakefulness and REM sleep are controlled by a GABAergic pontine mechanism. J. Neurophysiol. *82*, 2015–2019.

Xie, L., Kang, H., Xu, Q., Chen, M.J., Liao, Y., Thiyagarajan, M., O'Donnell, J., Christensen, D.J., Nicholson, C., Iliff, J.J., et al. (2013a). Sleep drives metabolite clearance from the adult brain. Science *342*, 373–377.

Xie, Z., McMillan, K., Pike, C.M., Cahill, A.L., Herring, B.E., Wang, Q., and Fox, A.P. (2013b). Interaction of anesthetics with neurotransmitter release machinery proteins. J. Neurophysiol. *109*, 758–767.

Xu, M., Chung, S., Zhang, S., Zhong, P., Ma, C., Chang, W.-C., Weissbourd, B., Sakai, N., Luo, L., Nishino, S., et al. (2015). Basal forebrain circuit for sleep-wake control. Nat. Neurosci. *18*, 1641–1647.

Yu, X., Zecharia, A., Zhang, Z., Yang, Q., Yustos, R., Jager, P., Vyssotski, A.L., Maywood, E.S., Chesham, J.E., Ma, Y., et al. (2014). Circadian factor BMAL1 in histaminergic neurons regulates sleep architecture. Curr. Biol. CB *24*, 2838–2844.

Zahniser, N.R., and Doolen, S. (2001). Chronic and acute regulation of Na+/Cl- -dependent neurotransmitter transporters: drugs, substrates, presynaptic receptors, and signaling systems. Pharmacol. Ther. *92*, 21–55.

Zavada, A., Strijkstra, A.M., Boerema, A.S., Daan, S., and Beersma, D.G.M. (2009). Evidence for differential human slow-wave activity regulation across the brain. J. Sleep Res. *18*, 3–10.

Zhang, Z., Ferretti, V., Güntan, İ., Moro, A., Steinberg, E.A., Ye, Z., Zecharia, A.Y., Yu, X., Vyssotski, A.L., Brickley, S.G., et al. (2015). Neuronal ensembles sufficient for recovery sleep and the sedative actions of α2 adrenergic agonists. Nat. Neurosci. *18*, 553–561.

Zhao, W.-Q., Chen, H., Quon, M.J., and Alkon, D.L. (2004). Insulin and the insulin receptor in experimental models of learning and memory. Eur. J. Pharmacol. *490*, 71–81.

Zimprich, A., Garrett, L., Deussing, J.M., Wotjak, C.T., Fuchs, H., Gailus-Durner, V., de Angelis, M.H., Wurst, W., and Hölter, S.M. (2014). A robust and reliable non-invasive test for stress responsivity in mice. Front. Behav. Neurosci. *8*.

Zwaka, H., Bartels, R., Gora, J., Franck, V., Culo, A., Götsch, M., and Menzel, R. (2015). Context odor presentation during sleep enhances memory in honeybees. Curr. Biol. CB *25*, 2869–2874.